AD NUMBER
AD392072
CLASSIFICATION CHANGES
TO: **UNCLASSIFIED**
FROM: **CONFIDENTIAL**
LIMITATION CHANGES
TO: **Approved for public release; distribution is unlimited.**
FROM: **Distribution authorized to U.S. Gov't. agencies and their contractors; Administrative/Operational Use; AUG 1968. Other requests shall be referred to Air Force Rocket Propulsion Lab., Edwards AFB, CA.**
AUTHORITY
31 Aug 1980, DoDD 5200.10 ; AFRPL ltr 5 Feb 1986

SECURITY MARKING

The classified or limited status of this report applies to each page, unless otherwise marked.
Separate page printouts MUST be marked accordingly.

THIS DOCUMENT CONTAINS INFORMATION AFFECTING THE NATIONAL DEFENSE OF THE UNITED STATES WITHIN THE MEANING OF THE ESPIONAGE LAWS, TITLE 18, U.S.C., SECTIONS 793 AND 794. THE TRANSMISSION OR THE REVELATION OF ITS CONTENTS IN ANY MANNER TO AN UNAUTHORIZED PERSON IS PROHIBITED BY LAW.

NOTICE: When government or other drawings, specifications or other data are used for any purpose other than in connection with a definitely related government procurement operation, the U. S. Government thereby incurs no responsibility, nor any obligation whatsoever; and the fact that the Government may have formulated, furnished, or in any way supplied the said drawings, specifications, or other data is not to be regarded by implication or otherwise as in any manner licensing the holder or any other person or corporation, or conveying any rights or permission to manufacture, use or sell any patented invention that may in any way be related thereto.

CONFIDENTIAL

(UNCLASSIFIED TITLE)

ACOUSTIC LINERS FOR STORABLE PROPELLANT ROCKET CHAMBERS - PHASE II

FINAL REPORT

G. D. Garrison, Program Manager
Pratt & Whitney Aircraft
Division of United Aircraft Corporation
Florida Research and Development Center

August 1968

Prepared for
Air Force Rocket Propulsion Laboratory
Air Force Systems Command
United States Air Force
Edwards Air Force Base, California

Pratt & Whitney Aircraft DIVISION OF UNITED AIRCRAFT CORPORATION
FLORIDA RESEARCH AND DEVELOPMENT CENTER
BOX 2691, WEST PALM BEACH, FLORIDA 33402

CONFIDENTIAL

Printed in the United States of America

Pratt & Whitney Aircraft
AFRPL-TR-68-118

PATENT SECRECY NOTICE

Material in this publication relating to

LAMINATED CHAMBER COOLING MEANS

CONFIDENTIAL

reveals subject matter contained in U.S. Patent Application Serial No. 319,047 entitled "High Pressure Rocket and Cooling Means," which has been placed under Secrecy Order issued by the Commissioner of Patents. This Secrecy Order has been modified by a SECURITY REQUIREMENTS PERMIT.

A Secrecy Order Prohibits publication or disclosure of the invention, or any material information with respect thereto. It is separate and distinct, and has nothing to do with the classification of Government contracts.

By statute, violation of a Secrecy Order is punishable by a fine not to exceed $10,000 and/or imprisonment for not more than two years.

A SECURITY REQUIREMENTS PERMIT authorizes disclosure of the invention or any material information with respect thereto, to the extent set forth by the security requirements of the Government contract which imposes the highest security classification on the subject matter of the application, except that export is prohibited.

Disclosure of this invention or any material information with respect thereto is prohibited except by written consent of the Commissioner of Patents or as authorized by the permit.

The foregoing does not in any way lessen responsibility for the security of the subject matter as imposed by any Government contract or the provisions of the existing laws relating to espionage and national security.

CONFIDENTIAL

(UNCLASSIFIED TITLE)

ACOUSTIC LINERS FOR STORABLE PROPELLANT ROCKET CHAMBERS - PHASE II

FINAL REPORT

Prepared Under
Contract AFO4(611)-11387
For
Air Force Rocket Propulsion Laboratory
Air Force Systems Command
United States Air Force
Edwards Air Force Base, California

PATENT SECRECY NOTICE

PORTIONS OF THIS DOCUMENT CONTAIN SUBJECT MATTER COVERED BY A U.S. PATENT OFFICE SECRECY ORDER WITH MODIFYING SECURITY REQUIREMENTS PERMIT. HANDLING SHALL BE IN ACCORDANCE WITH THE PERMIT AS DESCRIBED ON PAGE A AND INDICATED HEREIN. VIOLATORS MAY BE SUBJECT TO THE PENALTIES PRESCRIBED BY, TITLE 35, U. S. C. (1952), SECTIONS 182 AND 186.

IN ADDITION TO SECURITY REQUIREMENTS WHICH MUST BE MET, THIS DOCUMENT IS SUBJECT TO SPECIAL EXPORT CONTROLS AND EACH TRANSMITTAL TO FOREIGN GOVERNMENTS OR FOREIGN NATIONALS MAY BE MADE ONLY WITH PRIOR APPROVAL OF AFRPL (RPPR/STINFO), EDWARDS, CALIFORNIA 93523.

THIS REPORT IS CLASSIFIED CONFIDENTIAL TO PREVENT UNAUTHORIZED DISCLOSURE OF A RELATIONSHIP BETWEEN TWO OR MORE ITEMS AND TO PROTECT A COMPILATION OF INFORMATION AND A COMPLETE ANALYSIS OF THE SUBJECT. ALL INDIVIDUAL PARAGRAPHS CONTAINED IN THIS REPORT ARE UNCLASSIFIED.

Pratt & Whitney Aircraft DIVISION OF UNITED AIRCRAFT CORPORATION
FLORIDA RESEARCH AND DEVELOPMENT CENTER
BOX 2691, WEST PALM BEACH, FLORIDA 33402

FOREWORD

This report is submitted in compliance with the requirements of Contract AF 04(611)-11387, and presents the results of work accomplished under the Phase II portion of the program. All work was performed during the period 28 March 1967 through 31 May 1968.

The Air Force Project No. is 3058. The Program Structure is A3B2. The Pratt & Whitney Aircraft Control No. is PWA FR-2812.

The Air Force Project Officer is Mr. T. J. Fanciullo. The following personnel of Pratt & Whitney Aircraft contributed to the technical effort and preparation of the report: N. Bohn, P.L. Russell, and G.L. Parsons. The Pratt & Whitney Aircraft Program Manager was Mr. G.D. Garrison.

This report is classified Confidential to prevent unauthorized disclosure of a relationship between two or more items and to protect a compilation of information and a complete analysis of the subject. All individual paragraphs are unclassified.

This report contains no classified information extracted from other classified documents.

This technical report has been reviewed and is approved.

T. J. Fanciullo
AF Project Officer, RPRRC

UNCLASSIFIED ABSTRACT

This report describes the work performed under Phase II of Contract AF 04(611)-11387, Evaluation of Acoustic Liners for Rocket Chambers. The Phase II work consisted of three inter-related tasks: (1) the establishment and testing of a theory and design procedure for nonresonant absorbers; (2) the evaluation of the effects on liner performance of coolant flow through and/or past the liner apertures; and (3) the evaluation of ablative liners.

The types of cooled liners that were studied were transpiration (wafer and porous types), film-cooled, and ablative liners. Impedance data were obtained on transpiration and ablative-type liner samples and the results applied to liner design theory. Rocket test programs were conducted using film-cooled liners and a wafer liner at nominal chamber pressures of 200 and 800 psia; individual resonators and dual-open area ablative liners were tested at 200-psia chamber pressure. In addition, uncooled steel liners were tested to obtain data to support the ablative liner program. Propellants were N_2O_4/N_2H_4-UDMH (50-50 blend).

The film-cooled liners demonstrated stable combustion when no cooling and low cooling flows were used, but the combustion became progressively more unstable as cooling flow was increased. The wafer liner provided stable operation when no cooling was used but combustion was extremely unstable when hydrogen cooling was introduced. The test results show that when the chamber or liner wall is cooled externally with a film layer, or transpirationally, combustion stability varied inversely with the coolant flowrate. A dual-open area (parallel array) ablative liner was effective in suppressing combustion oscillations but an ablative liner with individual resonators failed to stabilize combustion.

From the results of this program it was concluded that nonresonant absorbers are not as effective in suppressing combustion oscillations as are resonant absorbers and it is recommended that ablative or regenerative cooling be used in conjunction with an acoustic liner rather than external wall cooling.

CONTENTS

SECTION		PAGE
	ILLUSTRATIONS	vi
	TABLES	xiii
	NOMENCLATURE	xiv
I	INTRODUCTION	1
	A. Task 1 - Special Report	1
	B. Task 2 - Aperture Shape Experiment	2
	C. Task 3 - Uncooled Liner Test Program	2
II	SUMMARY OF ACCOMPLISHMENTS	5
	A. Baseline Tests	5
	B. Film-Cooled Liner Program	5
	C. Ablative Liner Evaluation	6
	D. Transpiration-Cooled Liner Program	7
III	BASELINE TESTS	11
	A. High Pressure Baseline Tests	11
	B. Low Pressure Baseline Tests	15
IV	FILM-COOLED LINER PROGRAM	17
	A. Low Pressure Film-Cooled Liner Program	17
	B. High Pressure Film-Cooled Liner Program	23
	C. Conclusions	35
	D. Recommendations	37/38
V	ABLATIVE LINER PROGRAM	39
	A. Technical Discussion	39
VI	TRANSPIRATION-COOLED LINER PROGRAM	69
	A. Rigimesh Liner	69
	B. Wafer Liner	81
	C. Uncooled Tests	99
	D. Analysis of Results	99
VII	CONCLUSIONS AND RECOMMENDATIONS	103
	A. Conclusions	103
	B. Recommendations	104
VIII	REFERENCES	105/106
	APPENDIX A - Wide Band Liner Program	107
	APPENDIX B - Liner Test Data	113
	APPENDIX C - Fabrication Drawings	171
	DISTRIBUTION LIST	211

ILLUSTRATIONS

FIGURE		PAGE
1	Full-Length Solid Uncooled Liner.	13
2	High Pressure Baseline Instability Data	13
3	Film-Cooled Nozzle.	14
4	Fundamental Instability Modes in a 12-in. Chamber . . .	15
5	Amplitudes over 10% of Chamber Pressure - 200-psi Baseline Tests.	16
6	Effects of Aperture Combustion Gas Temperature - 200-psi Film-Cooled Liner	18
7	Absorption Characteristics of 200-psia Film-Cooled Liner for 500 ft/sec Flow Past Apertures.	19
8	200-psi One-Half Chamber Length Steel Liner	20
9	200-psi One-Half Chamber Length Steel Liner	20
10	Graph-I-Tite G-90 Nozzle Throat Insert.	21
11	Sketch of the 200-psi Film-Cooled Liner Assembly. . . .	21
12	Sketch of the 200-psi Film-Cooled Liner Assembly. . . .	22
13	200-psi Film-Cooled Liner After Test No. 57.01.	26
14	Closeup of 200-psi Film-Cooled Liner After Test No. 57.01	26
15	High-Speed Oscillograph for 200-psi Film-Cooled Liner - Test No. 54.01.	27
16	High-Speed Oscillograph for Stable Portion of Test No. 55.01.	27
17	High-Speed Oscillograph for Unstable Portion of Test No. 55.01.	28
18	High-Speed Oscillograph for 200-psi Film-Cooled Liner - Test No. 56.01.	28
19	High-Speed Oscillograph for 200-psi Film-Cooled Liner - Test No. 57.01.	29
20	Liner Cavity Temperature as a Function of Time and Coolant Flow for Test No. 54.01	29
21	High-Speed Oscillograph for Pulsed Tests of 200-psi Film-Cooled Liner - Test No. 75.01.	30
22	High-Speed Oscillograph for Pulsed Tests of 200-psi Film-Cooled Liner - Test No. 76.01.	30
23	High-Speed Oscillograph for Pulsed Tests of 200-psi Film-Cooled Liner - Test No. 79.01.	31
24	Coolant Flowrate vs First Tangential Mode Amplitude for the 200-psi Film-Cooled Liner Tests	31

ILLUSTRATIONS (Continued)

FIGURE		PAGE
25	Coolant Flowrate vs Third Tangential Mode Amplitude for the 200-psi Film-Cooled Liner Tests.	32
26	Coolant Flowrate vs First Radial Mode Amplitude for the 200-psi Film-Cooled Liner Tests.	32
27	1000-psi Film-Cooled Liner Assembly.	33
28	N_2O_4/Aerozine 1000-psi Film-Cooled Liner	34
29	Maximum Amplitudes for Tests No. 89.01 Through 91.01 as a Function of Film-Coolant Flowrate (Confidential) .	35
30	Absorption Characteristics of 1000-psia Ablative Liner.	40
31	Theoretical Absorbing Characteristics of Ablative Liner, Corrected for an Array.	41
32	Ablative Liner Configuration	41
33	One-Half Chamber Length, 200-psi Ablative Acoustic Liner.	42
34	200-psi Ablative Liner Test Configuration.	44
35	Solid Refrasil Ablative Liner.	45
36	Impedance Tube Sample-Cavity Side of 200-psi Ablative Liner Individual Resonator Configuration	45
37	Individual Resonator Impedance Tube Analysis	46
38	Theoretical Absorption Characteristics of 200-psia Ablative Liner	47
39	200-psia Ablative Liner Cavity Temperature - Test No. 72.01	49
40	Individual Resonator Ablative Acoustic Liner After Test No. 72.01	49
41	Ablative Solid Liner After Test No. 72.01.	50
42	Calculated Absorption Coefficient vs Frequency: 200-psi Ablative Individual Resonator Acoustic Liner .	52
43	Peak-to-Peak Amplitude vs Firing Time for Individual Resonator Ablative Liner.	53
44	Peak-to-Peak Amplitude vs Firing Time for Individual Resonator Ablative Liner.	53
45	200-psia Ablative Liner Section Post-Test No. 101.01	54
46	Kistler Model 615-A Transducer and Uncooled Adaptor Assembly	55
47	Reworked Pattern of Stainless Steel Liner.	60

ILLUSTRATIONS (Continued)

FIGURE		PAGE
48	Absorption Characteristics of Individual Resonator Steel Liner	60
49	Parallel Array Steel Liner Post-Test No. 113.01	62
50	200-psia Ablative Liner Design	62
51	Dual Open Area 200-psi Ablative Liner, Test No. 117.01	64
52	Dual Open Area Ablative Liner Post-Test No. 118.01	65
53	Dual Open Area Uncooled Liner Post-Test No. 122.01	65
54	Absorption of Reworked Steel Liner	66
55	Rigimesh Absorbing Liner	69
56	Transpiration Liner Cooling Requirements	71
57	45-scfm Rigimesh Sample	72
58	Low-Frequency Impedance Tube	73
59	Impedance Tube Data for 45-scfm Rigimesh Sample - 0 to 8 psi ΔP Across Sample at 146 db Total	73
60	2000- and 300-scfm Rigimesh Samples in Series with 45-scfm Rigimesh Sample	74
61	Impedance Tube Data for 300- and 45-scfm Rigimesh Samples in Series	74
62	Impedance Tube Data for 2000- and 45-scfm Rigimesh Samples in Series - 146 db Total	76
63	Zero Flow Impedance Tube Data for Rigimesh Samples - 146 db Total	76
64	Constant $\lambda/(t + L)$ Illustration for Extrapolation of Impedance Tube Data to Liner Design	77
65	Zero Flow Impedance Tube Data for Rigimesh at 151 db Total - L = 0.100	79
66	Zero Flow Impedance Tube Data for 56 Rayl Rigimesh Sample at 151 db Total	79
67	Absorption Coefficient vs Frequency: 140 Rayl Sample, t = 0.040 in. at 151 db Total	80
68	Copper Wafers Used to Fabricate Cooled Thrust Chambers (Confidential)	82
69	Wafer Chamber Plate (Confidential)	82
70	Parallel Resonator Array	83
71	Arbitrarily Shaped Resonator	83
72	Absorption vs Frequency for Wafer Samples	84

ILLUSTRATIONS (Continued)

FIGURE		PAGE
48	Absorption Characteristics of Individual Resonator Steel Liner.	60
49	Parallel Array Steel Liner Post-Test No. 113.01. . . .	62
50	200-psia Ablative Liner Design	62
51	Dual Open Area 200-psi Ablative Liner, Test No. 117.01	64
52	Dual Open Area Ablative Liner Post-Test No. 118.01 . .	65
53	Dual Open Area Uncooled Liner Post-Test No. 122.01 . .	65
54	Absorption of Reworked Steel Liner	66
55	Rigimesh Absorbing Liner	69
56	Transpiration Liner Cooling Requirements	71
57	45-scfm Rigimesh Sample.	72
58	Low-Frequency Impedance Tube	73
59	Impedance Tube Data for 45-scfm Rigimesh Sample - 0 to 8 psi ΔP Across Sample at 146 db Total.	73
60	2000- and 300-scfm Rigimesh Samples in Series with 45-scfm Rigimesh Sample.	74
61	Impedance Tube Data for 300- and 45-scfm Rigimesh Samples in Series.	74
62	Impedance Tube Data for 2000- and 45-scfm Rigimesh Samples in Series - 146 db Total	76
63	Zero Flow Impedance Tube Data for Rigimesh Samples - 146 db Total	76
64	Constant $\lambda/(t + L)$ Illustration for Extrapolation of Impedance Tube Data to Liner Design.	77
65	Zero Flow Impedance Tube Data for Rigimesh at 151 db Total - L = 0.100	79
66	Zero Flow Impedance Tube Data for 56 Rayl Rigimesh Sample at 151 db Total	79
67	Absorption Coefficient vs Frequency: 140 Rayl Sample, t = 0.040 in. at 151 db Total.	80
68	Copper Wafers Used to Fabricate Cooled Thrust Chambers (Confidential).	82
69	Wafer Chamber Plate (Confidential).	82
70	Parallel Resonator Array	83
71	Arbitrarily Shaped Resonator	83
72	Absorption vs Frequency for Wafer Samples.	84

ILLUSTRATIONS (Continued)

FIGURE		PAGE
73	Individual Resonators of Equal Volume.	85
74	Absorption vs Number of Resonators for Constant Resonator Size and Incidence Area.	85
75	Absorption vs Frequency for Different Numbers of Resonators	86
76	Wafer Liner Cold Flow Test Sample.	87
77	Simulated Wafer Liner Sample Flow-Through Test Results.	88
78	Wafer Coolant Slot Section	88
79	Theoretical Absorption vs Frequency Diagram for 200-psi Wafer Liner.	90
80	Theoretical Absorption vs Frequency Diagram for 800-psi Wafer Liner.	90
81	Acoustic Wafer Plate	91
82	Wafer Liner Assembly	92
83	Half-Chamber Length Wafer Liner - Pretest.	92
84	Half-Chamber Length Wafer Liner Closeup - Pretest. . .	93
85	Predominant Frequencies of Instability Wafer Liner - Low Pressure Tests	95
86	Oscillograph of Kistler Pressure Levels for Test No. 92.09.	95
87	Predominant Frequencies of Instability - Wafer Liner High Pressure Tests.	98
88	Wafer Liner at End of Test Sequence.	98
89	Wafer Liner Closeup at End of Test Sequence.	99
90	Wafer Liner Absorption Characteristics with No Coolant.	101/102
91	Absorption Characteristics of Uncooled Steel Liner . .	108
92	High Frequency Data Comparison	109
93	Gas Sampling Schematic Molecular Weight Measurement. .	110
94	Location Schematic of Kistler Dynamic Pressure Transducers.	113
95	Pressure Amplitude Data for Solid Liner Baseline Test No. 66.01	116
96	Pressure Amplitude Data for Solid Liner Baseline Test No. 68.01	117
97	Pressure Amplitude Data for Solid Liner Baseline Test No. 81.01	118

ILLUSTRATIONS (Continued)

FIGURE		PAGE
98	Pressure Amplitude Data for Solid Liner Baseline Test No. 82.01	119
99	Pressure Amplitude Data for Solid Liner Baseline Test No. 83.01	120
100	Pressure Amplitude Data for Solid Liner Baseline Test No. 84.01	121
101	Pressure Amplitude Data for Solid Liner Baseline Test No. 86.01	122
102	Pressure Amplitude Data for Solid Liner Baseline Test No. 114.01	123
103	Pressure Amplitude Data for Solid Liner Baseline Test No. 115.01	124
104	Pressure Amplitude Data for Film-Cooled Liner Test No. 54.01	125
105	Pressure Amplitude Data for Film-Cooled Liner Test No. 55.01 (Stable)	126
106	Pressure Amplitude Data for Film-Cooled Liner Test No. 55.01 (Unstable)	127
107	Pressure Amplitude Data for Film-Cooled Liner Test No. 56.01	128
108	Pressure Amplitude Data for Film-Cooled Liner Test No. 57.01	129
109	Pressure Amplitude Data for Film-Cooled Liner Test No. 75.01	130
110	Pressure Amplitude Data for Film-Cooled Liner Test No. 76.01	131
111	Pressure Amplitude Data for Film-Cooled Liner Test No. 79.01	132
112	Pressure Amplitude Data for Film-Cooled Liner Test No. 88.01	133
113	Pressure Amplitude Data for Film-Cooled Liner Test No. 89.01	134
114	Pressure Amplitude Data for Film-Cooled Liner Test No. 89.01	135
115	Pressure Amplitude Data for Film-Cooled Liner Test No. 90.01	136
116	Pressure Amplitude Data for Film-Cooled Liner Test No. 91.01	137
117	Pressure Amplitude Data for Ablative Liner Test No. 58.01	138

ILLUSTRATIONS (Continued)

FIGURE		PAGE
118	Pressure Amplitude Data for Ablative Liner Test No. 59.01	139
119	Pressure Amplitude Data for Ablative Liner Test No. 61.01	140
120	Pressure Amplitude Data for Ablative Liner Test No. 69.01	141
121	Pressure Amplitude Data for Ablative Liner Test No. 72.01	142
122	Pressure Amplitude Data for Ablative Liner Test No. 72.01	143
123	Pressure Amplitude Data for Ablative Liner Test No. 72.01	144
124	Pressure Amplitude Data for Ablative Liner Test No. 100.01.	145
125	Pressure Amplitude Data for Individual Resonator Steel Liner Test No. 104.01.	146
126	Pressure Amplitude Data for Individual Resonator Steel Liner Test No. 105.01.	147
127	Pressure Amplitude Data for Individual Resonator Steel Liner Test No. 106.01.	148
128	Pressure Amplitude Data for Individual Resonator Steel Liner Test No. 107.01.	149
129	Pressure Amplitude Data for Parallel Array Steel Liner Test No. 110.01.	150
130	Pressure Amplitude Data for Parallel Array Steel Liner Test No. 111.01.	151
131	Pressure Amplitude Data for Parallel Array Steel Liner Test No. 112.01.	152
132	Pressure Amplitude Data for Parallel Array Steel Liner Test No. 112.01.	153
133	Pressure Amplitude Data for Parallel Array Steel Liner Test No. 113.01.	154
134	Pressure Amplitude Data for Parallel Array Ablative Liner Test No. 118.01.	155
135	Pressure Amplitude Data for Dual Open Area Steel Liner Test No. 121.01.	156
136	Pressure Amplitude Data for Dual Open Area Steel Liner Test No. 122.01.	157
137	Pressure Amplitude Data for Wafer Liner Test No. 92.09	158

ILLUSTRATIONS (Continued)

FIGURE		PAGE
138	Pressure Amplitude Data for Wafer Liner Test No. 93.01	159
139	Pressure Amplitude Data for Wafer Liner Test No. 94.01	160
140	Pressure Amplitude Data for Wafer Liner Test No. 95.01	161
141	Pressure Amplitude Data for Wafer Liner Test No. 96.03	162
142	Pressure Amplitude Data for Wafer Liner Test No. 97.02	163
143	Pressure Amplitude Data for Wafer Liner Test No. 98.01	164
144	Pressure Amplitude Data for Wafer Liner Test No. 125.01.	165
145	Pressure Amplitude Data for Wafer Liner Test No. 126.01.	166
146	Pressure Amplitude Data for Wafer Liner Test No. 128.01.	167
147	Pressure Amplitude Data for Wide Band Liner Test No. 123.01.	168
148	Pressure Amplitude Data for Wide Band Liner Test No. 124.01.	169/170

The only classified items in this report are figures 29, 68, and 69 on pages 35 and 82.

TABLES

TABLE		PAGE
I	Solid Liner Data.	12
II	Film-Cooled Liner Design Data	19
III	200-psi Film-Cooled Liner	24
IV	1000-psi Film-Cooled Liner Design Data.	33
V	Film-Cooled Liner Tests	36
VI	Ablative Liner Tests.	43
VII	Ablative Liner Tests.	48
VIII	Ablative Liner Tests.	51
IX	Individual Resonator Steel Liner Tests.	56
X	Parallel Array Steel Liner.	61
XI	Dual Open Area Ablative Liner Tests	63
XII	Dual Open Area Steel Liner Tests.	67/68
XIII	Perturbation Data for Wafer Liner Tests	96

NOMENCLATURE

Symbol	Description	Units
C	Sonic Velocity	ft/sec
C_p	Specific heat at constant pressure	Btu/lb_m-°R
D_c	Backing cavity diameter for an individual resonator	in.
D_H	Aperture Hydraulic Diameter	in.
D_o	Aperture Diameter	in.
Hz	Frequency (Hertz)	cycles/sec
h_B	Convective wall film coefficient	$Btu/in.^2$-°R-sec
L	Liner Backing depth	in.
P_c	Chamber pressure	psia
Q	Transferred heat	Btu/sec
SPL	Incident Sound pressure level	db (re 0.002 microbar)
T_a	Liner aperture gas temperature	°R
T_c	Temperature of combustion	°R
T_i	Inlet temperature	°R
T_s	Static temperature	°R
T_w	Wall temperature	°R
t	Liner thickness	in.
V	Cavity volume	$in.^3$
V_p	Velocity past liner apertures	ft/sec
V_t	Velocity through liner apertures	ft/sec
$\dot{w}$	Coolant flow rate	lb_m/sec
α	Absorption coefficient	
r	Mixture ratio	
Z	Specific acoustic impedance	
θ	Specific flow resistance	
λ	Wave length	in.
μ	Viscosity	lb_m/ft-sec
χ	Specific acoustic reactance	
ρ	Density	lb_m/ft^3
σ	Liner open area ratio or percent	

SECTION I
INTRODUCTION

Work under Contract AF04(611)-11387 was initiated in March 1966. The program is divided into two phases; Phase I concerns resonant liner design information and Phase II efforts are directed toward the application of nonresonant and ablative liners to rocket combustion chambers. For the purposes of this work, nonresonant absorbers are defined as (1) liners of configurations other than arrays of Helmholtz-type resonators or (2) arrays of resonators that do not exhibit a well-defined frequency of resonance due to compromises in the design from cooling, structural or other considerations.

The objectives of the program are:

Phase I - Resonant Liner Program

1. Publication of a comprehensive absorbing liner design manual for use by all members of the technical community.
2. The determination of a method of relating odd hole shapes (that may be necessary from cooling considerations) to the round holes used in Helmholtz resonator analysis.
3. Definition of the amount and location of acoustic absorption required for stable combustion in a rocket motor burning N_2O_4/50% N_2H_4-50% UDMH (A-50) propellants.

Phase II - Nonresonant Liner Program

4. Establishment and testing of a theory and design procedure for nonresonant absorbers.
5. Evaluation of the effects on liner performance of coolant flow through and/or past the liner apertures.
6. Evaluation of ablative liners in storable propellant motors.

In this report, only the Phase II program is discussed in detail. The Phase I accomplishments, which have been described in a separate report (see Reference 1), are summarized in the following paragraphs.

A. TASK 1 - SPECIAL REPORT

At the beginning of the Phase I effort, a Special Report (Reference 2) was published. The purpose of the Special Report was to present both the basic principles and practical considerations of absorbing liner theory and to outline the techniques used in designing resonant liners for rocket engines. Included in the report was a listing of a computer program for use in the design of absorbing liners and a set of curves illustrating the effects of geometric variables on liner performance. The state-of-the-art of the suppression of combustion instability in rocket engines with absorbing devices has evolved from work accomplished at Pratt & Whitney Aircraft. Practical liner design information derived from this work was included as guidance.

B. TASK 2 - APERTURE SHAPE EXPERIMENT

No analytical technique was known for predicting the acoustical characteristics of resonant liners with noncircular apertures operating at nonlinear incident sound pressures, i.e., sound pressure levels above 140 db*; therefore, an experiment was performed with the objective of developing such a technique. Samples with apertures in the shape of rectangles, ellipses, and crosses were used in a standard impedance measuring device. For control purposes, data were also obtained from samples with circular apertures. Ten different resonator assemblies were used and each was tested at frequencies ranging from 800 to 2000 Hz. Determined from the data were the components of acoustic impedance, resistance and reactance, as well as the absorption coefficient, resonant frequency, and effective length of the aperture gas. Correlations were obtained in the form of empirical equations expressing the effective length and the specific acoustic resistance as a function of aperture area, hydraulic diameter, and the sample open area ratio. To demonstrate the validity of the empirical equations, theoretical values of absorption coefficient were computed and compared with the experimental data. Finally, a set of sample calculations was prepared to illustrate the application of the new theory.

C. TASK 3 - UNCOOLED LINER TEST PROGRAM

The objective of the uncooled liner test program was to determine experimentally the amount and location of acoustic absorption necessary to prevent combustion instability in a rocket motor burning N_2O_4/A-50. Tests were conducted to determine the minimum effective absorption coefficient, which were followed by tests of shorter liners in two different locations. All tests were preceded by baseline tests (no absorbing liner) of the combustor. A total of 45 firings were made. Nominal mixture ratios were 1.2 and 2; nominal chamber pressures were 100, 200, and 1000 psia.

The test motor consisted of a triplet impinging injector and an outer pressure shell in which both solid and perforated liner sections could be installed. Chamber pressure was varied by changing the uncooled nozzle section. Liners with open area ratios varying from 0 to 5.7% were used. An acoustic analysis was performed so that the absorption coefficient for a given liner and particular test condition would be known. Five dynamic pressure transducers were installed in the chamber to measure the pressure oscillations throughout each test. Other instrumentation included thermocouples to measure the gas temperatures in the liner apertures and backing cavity. A pulse gun containing four explosive charges was used to cause nonlinear pressure perturbations.

*In this report all pressures expressed in decibel (db) units are based on a reference pressure of 0.0002 microbar.

From the baseline test data, it was determined that the motor was inherently unstable at chamber pressures of 100 and 200 psia. The greatest peak-to-peak pressure amplitude occurred at a frequency corresponding to that of the second tangential mode; however, amplitudes greater than ± 5% of the mean chamber pressure occurred at frequencies from 2000 to 4800 Hz. No baseline data were obtained at a chamber pressure of 1000 and a mixture ratio of 2. Erroneous preliminary data from tests at the same pressure and a mixture ratio of 1.2 indicated that the motor was violently unstable; therefore, baseline tests at the higher mixture ratio were omitted to preclude possible injector damage.

To determine the amount of absorption necessary for stable operation of the motor, several full chamber-length liners, each designed for a different absorption coefficient, were tested at chamber pressures of 100 and 200 psia. All liners with absorption coefficients of 17%, based on the mean chamber velocity, damped the combustion process so that the resulting peak-to-peak pressure amplitudes were less than ± 5% of the mean chamber pressure. Partial-length liners of 1/8, 1/4, and 1/2 the chamber length were tested next; each liner was installed so that the upstream edge was at the injector face plane. One-half and quarter-length liners with absorption coefficients of 23% were found to be as effective as full-length liners for suppressing instability; however, one-eighth length liners with the same absorption coefficient would not consistently produce stable combustion.

The quarter-length liner that had proven effective in the previous tests was installed in a position three inches downstream from the injector face. The resulting peak-to-peak pressure amplitudes were more than twice as high as those recorded with the liner installed next to the injector.

Final analysis of the data from the 1000-psia chamber pressure firings showed that all tests at a mixture ratio of 1.2 were stable. The tests of the quarter-length liner at a mixture ratio of 2 were marginally stable, and pressure amplitudes varied from 2 to 12% of the mean chamber pressure. Results from the 1000-psia test series were considered inconclusive, and it was recommended that additional data be obtained during Phase II of the program.

The average temperature of the gas in the liner apertures and cavities was found to be approximately 2000°R. Higher average temperatures resulted (1) when combustion was unstable and (2) during the testing of the liners with the higher open area ratios.

An analysis of the combustion perturbation data showed that the liners significantly improved the ability of the system for damping the nonlinear pressure pulses, but as the absorption coefficient of the liner was increased above 17%, little additional improvement was noted.

SECTION II
SUMMARY OF ACCOMPLISHMENTS

A. BASELINE TESTS

At the end of the Phase I efforts it was concluded that the baseline stability characteristics of the test motor (Reference 1) had not been adequately defined at a nominal chamber pressure of 1000 psia and a mixture ratio of 2. It was recommended that additional firings with no liner be conducted during the Phase II program.

The firings were conducted early in the Phase II program. Analysis of the data showed no pressure oscillations greater than $\pm 5\%$ of chamber pressure were present at any particular frequency within the range of the instrumentation, 1 to 5 kHz. After consultation with the AFRPL Project Engineer it was decided to conduct additional firings and attempt to induce sustained, high amplitude instability in the test motor by (1) increasing the charge size in the tangentially mounted pulse gun, (2) reducing the chamber pressure to 800 psia, and (3) installing a thermally detonated nondirectional bomb on the injector face. Five additional baseline firings were made. Although the amplitudes of the instability levels were not significantly increased, it was concluded that the motor was sufficiently unstable at high chamber pressures to allow improvements in the stability characteristics through the use of acoustic liners to be noted.

B. FILM-COOLED LINER PROGRAM

For many applications of acoustic liners in rocket chambers, the most practical or simplest scheme to provide thermal protection for the liner assembly is film cooling. The concept has not been extensively used, however, because it was not known what effect, if any, the coolant would have on the acoustic characteristics of the liner. To investigate the effect, the film-cooled liner program was undertaken. Two liners were designed, one each for operation at a chamber pressure of 800 and 200 psia, so that with no film-coolant flow the absorption coefficients would be high enough to suppress combustion instability. The effectiveness of the liners was determined by conducting firings with three different A-50 coolant flowrates and with no coolant.

When operating with no coolant at a chamber pressure of 200 psia, the liner successfully suppressed the combustion instability. With coolant, the motor was less stable and with the exception of two tests the amplitude of the resulting pressure oscillations was found to be inversely proportional to the coolant flowrate. In addition, with coolant it was noted that results of tests could not be repeated, e.g., a rerun of an unstable test would be stable.

At higher chamber pressures, nominally 800 psia, the tests were all stable, i.e., no instability with pressure amplitudes greater than 10% of chamber pressure were measured. As in the 200 psia tests, the ampli-

tude of the oscillations was inversely proportional to the coolant flow-rate.

From the results of the experiment it was concluded that the successful application of film-cooled acoustic liners is extremely difficult because of the tendency of the fuel film to burn at the surface of the liner which causes the cavity gas temperatures to rise, thereby reducing the liner absorption coefficients.

C. ABLATIVE LINER EVALUATION

This portion of the effort was an evaluation of the effectiveness of ablative liners for suppressing combustion instability in storable propellant motors. The initial ablative liner was one-half chamber length, and was fabricated with an individual resonator configuration. Using the Phase I results as criteria, the liner theoretically had enough total absorption to suppress all modes of instability in the frequency range of interest, i.e., 1000 to 5000 Hz; however, all firings conducted with this liner were unstable. The initial reasons considered for the poor liner performance were (1) the basic theory used in the design analysis was not accurate for individual resonators, and (2) prerun purge gases (GN_2) trapped in the resonators caused poor absorption characteristics.

After the first series of hot firings, an impedance tube sample with an individual resonator configuration was fabricated and tested; analysis of results indicated that the basic theory used was correct. The liner absorption coefficients were then computed assuming nitrogen purge gas filled the resonator cavities. The theory predicted that combustion would be stable if the purge gases reached a temperature of 2000°R during the firing; for ambient temperature purge gases, combustion would have been unstable at frequencies greater than 2400 Hz.

To allow the cavity gases to become heated, a second series of tests was conducted using the ablative liner with the initial RCC* abort sample time increased. The tests were all unstable even though data indicated that the liner design temperature had been reached. Thus, the reasons for the failure of the liner to suppress the combustion instability of the system were not yet known. The following possibilities were considered:

1. Outgassing from ablative resins had been trapped in the resonators cavities

2. Not enough total absorption (not enough resonators) was present near the injector face.

A series of tests was conducted using a hot-gas-sampling system to record the molecular weight of the gases in the resonator cavities. Analysis of the results showed that the outgassing from the ablative liner should provide stable motor operation at high frequencies (4500 Hz), but provide marginal effectiveness at the design frequency (2200 Hz). The uncertainty

*RCC - Rough Combustion Cutoff, see Reference 1 for a complete description of this device.

due to the ablative outgassing during the firing was eliminated by fabricating and testing an uncooled steel liner with a configuration identical to the ablative liner. The steel liner also failed to suppress all the combustion oscillations occurring at frequencies of 5000 Hz or less; hence, it was concluded that not enough total absorption was present.

To obtain higher total absorption, the individual cavity liner design was abandoned and the liner was designed with a parallel array of resonators, even though the liner strength was compromised. The steel liner was reworked into the parallel array configuration and fired. The test data showed that increasing the total absorption reduced the pressure oscillations to less than 10% of chamber pressure at all frequencies less than 5000 Hz; however, at higher frequencies where the liner absorption was relatively low, high amplitude instability was present.

To provide stable operation over the frequency range of 1000 to 10,000 Hz, the reworked steel liner, which was a one-half chamber length assembly, was machined to increase the open area ratio of half of the parallel array pockets. The results from the dual-open area liner tests indicated that not enough total absorption was present above 5000 Hz.

A two-part full-chamber length, dual-open-area ablative liner was then fabricated and three firings were made. The motor was stable throughout each test; however, the upstream half of the liner failed structurally during the third test. Inspection of the motor revealed that failure of the liner occurred in the plane of the upstream Kistler ports near the injector. Apparently, the structural integrity of the liner had been compromised by the insertion of several Kistler holes at the same axial location.

D. TRANSPIRATION-COOLED LINER PROGRAM

The purpose of the transpiration-cooled liner program was to establish and test a design procedure for this class of nonresonant absorber. Original plans called for transpiration-cooled liners to be constructed of Rigimesh material and/or copper wafers and experimentally evaluated in a hot-firing test series. The type of acoustic analysis necessary for the design of a Rigimesh liner is considerably different than that required for a wafer liner; hence, concurrent efforts toward the development of each type of liner were initiated at the beginning of the Phase II program. A summary of the work performed is given in the following paragraphs.

1. Rigimesh Liner Analysis

Gaseous hydrogen was to be used to cool the transpiration liners. The amount of hydrogen flow necessary to keep the Rigimesh surface below a temperature of 1500°R was computed from a simple heat balance. Additional calculations showed that a high density Rigimesh material would be required to ensure that the coolant would be uniformly dispersed over the liner surface.

Phase I results indicated that a liner with absorption coefficients of at least 17% at frequencies greater than 2 kHz would suppress the combustion instability in the motor to be used for the transpiration-liner evaluation tests. The absorption coefficients of porous materials cannot be predicted from theoretical considerations alone; therefore, impedance tube experiments were conducted and the data used to determine the absorption coefficients of candidate Rigimesh samples.

The absorption coefficients of high density samples were found to be poor. In an attempt to improve the coefficients, a series arrangement of Rigimesh samples was fabricated and evaluated. The arrangement consisted of a high density sample separated from a low density Rigimesh facing by a resonator cavity. The addition of the low density facing and cavity in front of the high density material was found to improve the absorption coefficients of the assembly; however, no combination of cavity depths and facing density could be found that would produce adequate absorption characteristics for the existing test motor. A new pressure shell to accommodate the much larger cavity volumes would be necessary.

After consulting the AFRPL Project Engineer it was decided that the fabrication of a new pressure shell was not warranted; thus, further efforts in the development of a Rigimesh liner were abandoned. It is recommended that research devoted to the hot firing evaluation of Rigimesh liner suppression characteristics be continued using a test motor more suitable than was available under the present program. The recommendation is made although cooling flow degrades combustion stability, as was shown in the film-cooled liner tests and the wafer liner tests. However, the effect of cooling flow on the performance of a Rigimesh liner should be less noticeable than on film-cooled or wafer transpiration liners because of the relatively low velocity of flow through a Rigimesh liner.

2. Wafer Liner

The design of a transpiration-cooled wafer-type acoustic liner must incorporate a means of suppressing combustion instability without sacrificing cooling ability. The first design considered for evaluation was an adaptation of the existing wafer concept by the addition of individual cavities into each coolant slot. Analysis based on cold-flow impedance tests showed that the use of individual resonators severely limited the amount of absorption that could be obtained with a wafer chamber; the concept, therefore, was abandoned and attempts to design a liner more like a conventional resonator array (i.e., with a common cavity for all apertures) were begun.

The acoustic properties of a wafer-type liner with a common cavity volume had never been previously investigated. Therefore, a wafer sample was constructed and tested in the cold-flow impedance tube facility. The primary objective of such cold-flow testing was to investigate the acoustic characteristics of a wafer-liner design under known conditions and to establish a prediction theory using the experimental results as a basis.

Using the prediction theory, a parametric study was conducted to find a design that would theoretically stabilize the combustion process in the test motor. In addition, a heat transfer analysis was performed to determine the coolant flowrate necessary to keep the chamber surfaces below 1000°R.

A wafer chamber, which consisted of 29 Nickel 200 plates, was designed and fabricated. Sufficient instrumentation was installed so that the dynamic pressures and cavity gas temperatures could be measured during firings at nominal chamber pressures of 200 and 800 psia.

Seven firings were made using gaseous hydrogen as coolant, followed by four 2-second firings with no coolant. Although combustion during three of the cooled tests was stable, it was not possible to repeat the tests and duplicate results. All of the uncooled wafer tests were stable except for one low pressure test during which pressure amplitudes greater than ±5% of chamber pressure were recorded at frequencies greater than 6 kHz.

Analysis of the data showed that the presence of the gaseous hydrogen caused the motor to be more unstable at high chamber pressure than with no liner installed or with no coolant flowing through the wafer chamber. Possible reasons for the failure of the cooled wafer chamber to suppress the combustion instability are presented in Section VI.

SECTION III
BASELINE TESTS

The first step in a program to evaluate the performance of acoustic liners in a particular rocket motor is the conducting of baseline tests. These tests yield the basic stability characteristics of a rocket motor with no liner installed. The specific information obtained from baseline tests is the frequency at which instability occurs and the magnitude of oscillations at these frequencies. Once these data have been accumulated, acoustic liners can be designed to suppress the combustion instability over the range of frequencies required. Baseline tests were conducted at a nominal chamber pressure of 800 psia and mixture ratio of 2.0; in addition tests were repeated at 200 psia and a mixture ratio of 2.0 to determine if a change in the basic stability characteristics of the rocket motor had occurred since the Phase I baseline tests were conducted.

A. HIGH PRESSURE BASELINE TESTS

Eleven baseline tests were conducted at elevated chamber pressures. Table I contains pertinent test data as well as perturbation analysis for the high pressure baseline tests. A full length solid uncooled liner was used for the tests* (figure 1). All amplitudes over 20 psi are shown in figure 2. The nozzle was film cooled by flowing water through rows of slots at four axial locations (figure 3). The same nozzle was used for all of the high pressure tests. Kistler dynamic pressure transducers were mounted on the chamber wall to measure the amplitudes and frequencies of the various instability modes existing in the chamber. A sufficient number of transducers was used so that organized instability modes could be identified by the relative amplitude outputs from the transducers.

The first three tests (65.01 through 67.01) did not reach the design chamber pressure of 800 psia because of an incorrect setting in the frequency to direct current converter between the oxidizer flow meter and the digital tape recorder. The necessary corrections were made prior to test No. 68.01. Test No. 68.01 was conducted with no nozzle coolant and was pulsed with 6, 9, 12, and 15 grain PETN explosive charges. The frequency amplitude data indicated that although instability modes did exist at 3800 Hz and 4700 Hz, none of the amplitudes was greater than 66 psi, peak-to-peak in the 1000 to 5000 Hz frequency range. The test was considered to be stable since none of the amplitudes at a particular frequency was over ± 5% of mean chamber pressure, the figure that represents the criterion for an unstable test.

*See Phase I final report, Reference 1, for a description of test facility.

Table I. Solid Liner Data

Test No.	Test Duration - sec	Mixture Ratio	Chamber Pressure - psia	Combustion Efficiency, η_{c^*}-%	Perturbation Amplitude - P/P as % of P_c	Decay Time - msec	Time Perturbation Initiated After Ignition - sec	Comments
65.01	1.95	0.891	675		16.6	20	1.32 1.39	Low P_c because of incorrect oxidizer converter card. Instability buildup from 50 to 90 psi P/P total amplitude in 40 msec. Instability continued for remainder of test with 50-130 psi P/P total amplitude.
66.01	1.96	0.97	630		44.1 25.4	30	0.83 0.92	Initiated high frequency that continued for remainder of test. 7:00 "A" plane Kistler levels: 28 psi P/P at 2200 Hz, 120 psi P/P at 3600 Hz, 40 psi P/P at 4500 Hz.
67.01	1.95	1.00	675		44.5 41.5	8 25	0.61 1.00 1.20	6 grain PETN explosive charge from tangential pulse gun. Instability built to 136 psi total amplitude. Amplitude existed for remainder of test varying between 35 and 135 psi P/P total amplitude.
68.01	1.96	2.13	903	98.4	21.0 10.6	15	0.71 0.75	Total amplitude 50 to 190 psi P/P for remainder of test. 3:00 "A" plane steady-state instability levels: 30 psi P/P at 3750 Hz, 70 psi P/P at 4700 Hz.
80.01	0.74							Burnwire abort, incomplete test
81.01	1.47	2.04	747	93.1	32.2 24.1 18.1	6 8 5	0.62 0.70 0.72	High Chamber pressure abort (faulty pressure switch). 3:00 "A" plane Kistler levels: 58 psi P/P at 2200 Hz, 27 psi P/P at 2800 Hz.
82.01	1.23	2.01	797	95.2	28.2	10	0.66	High chamber pressure abort (faulty pressure switch). Highest levels on 3:00 "A" plane: 77 psi P/P at 2250 Hz.
83.01	1.94	2.00	775	94.4	23.3	20	0.81	3:00 "A" plane Kistler levels: 72.5 psi P/P at 2250 Hz, 31.5 psi P/P at 2900 Hz, and 27 psi P/P at 4650 Hz. Several 1 cycle pops over 200 psi P/P.
84.01	1.94	2.05	813	97.0	44.9 20.3	10 15	0.70 1.21	Caused by 50 grain pulse gun. 3:00 "A" plane levels: 27 psi P/P at 2200 Hz.
85.01	1.72	2.09	782	94.5				Pops of around 300 psi decayed to about 15 psi every 40 to 70 msec, 12 times throughout test; probably caused by cycling of fuel control valve because of high gain setting. Nozzle damage was apparent and 4 Kistler transducers were burned.
86.01	1.72	1.96	768	94.2	25.4 30.3	10	0.50 0.60	Initiated high frequency instability that continued for remainder of test. 12:00 "A" plane Kistler levels: 42 psi P/P at 4600 Hz and 21 psi P/P at 5000 Hz.

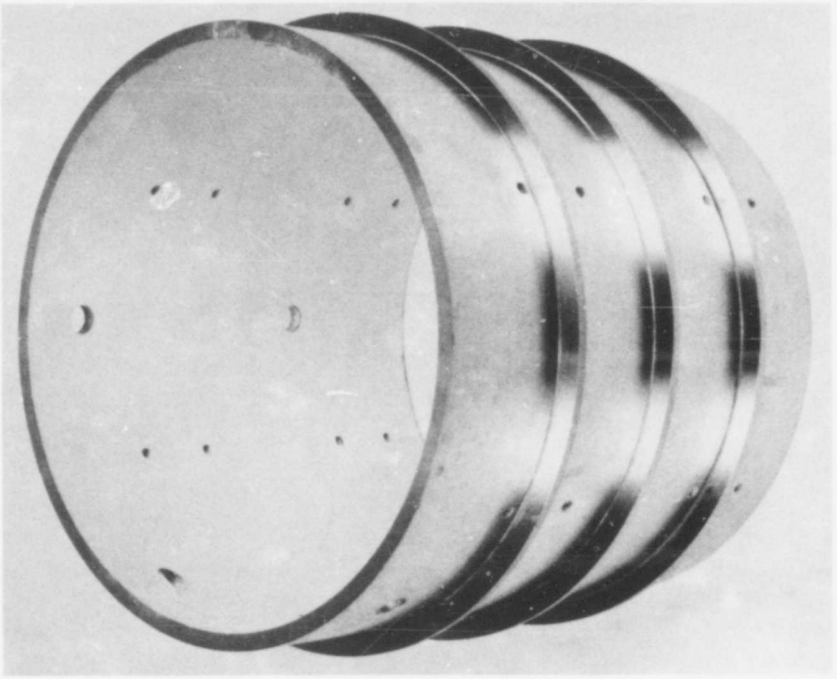

Figure 1. Full-Length Solid Uncooled Liner FE 63903

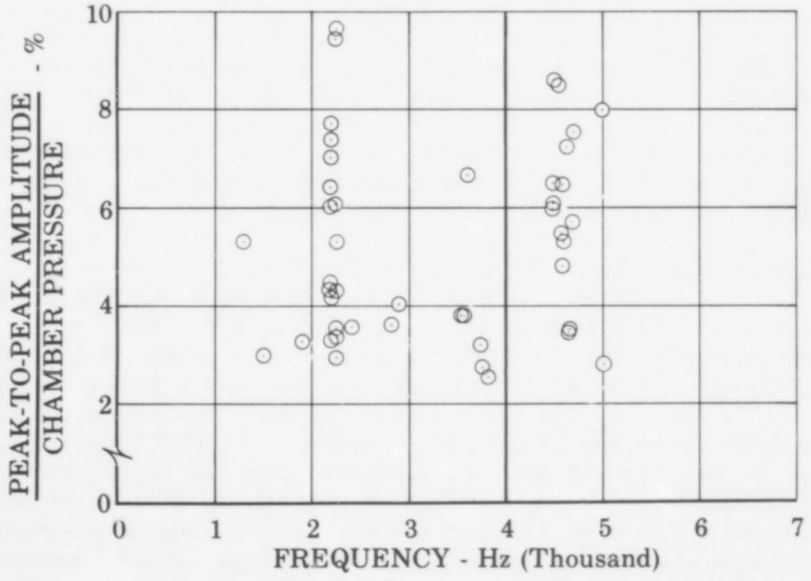

Figure 2. High Pressure Baseline Instability Data FD 24198A

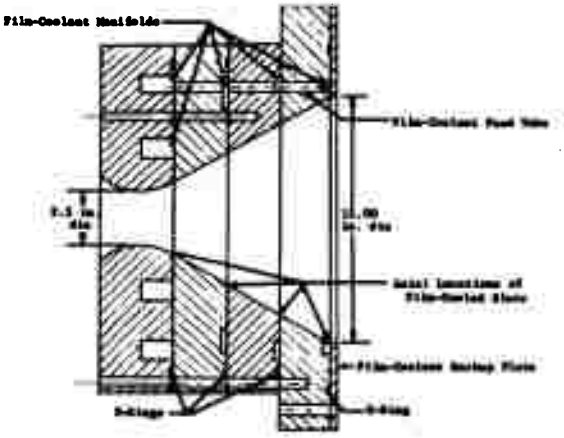

Figure 3. Film-Cooled Nozzle FD 23111

The highest amplitudes for tests No. 81.01 and 82.01 occurred at about 2200 Hz, but were less than ± 5% of mean chamber pressure. The remaining four tests (83.01 through 86.01) were bombed with explosive charges to induce high amplitude instability. Tangentially injected C-4 explosive of 27 and 50 grains were used in tests No. 83.01 and 84.01, respectively. Thermally detonated bombs containing 50 grains of C-4 explosive were fastened to the injector face for tests No. 85.01 and 86.01. As with the unbombed tests, no amplitude over ± 5% of chamber pressure was produced. The tangential pulses did not produce pressure perturbations with amplitudes greater than those caused by spontaneous pops (maximum 195 psi peak-to-peak). Both the pulse gun perturbations and the spontaneous pops were damped, in every instance, within 20 msec. The effects on stability of the nondirectional bomb are unknown, because the instant of detonation in either test No. 85.01 or test No. 86.01 could not be determined.

Although no sustained high amplitude instability existed during the high pressure baseline tests, enough instability was present for lined and unlined combustion chamber test data comparison.

Since the nozzle was film cooled with water for most of the 800-psi baseline tests, the c* efficiency values are only approximate, because the actual nozzle flow area for combustion gases is unknown. The c* efficiency values for the 800-psi film-cooled liner tests (Section IV) and the 800-psi wafer liner tests (Section VI) are also approximate, inasmuch as the same film-cooled nozzle was used for those programs as for the 800-psi baseline liner test program. Perhaps the efficiency of a test motor that has a film-cooled nozzle could be better approximated by an analysis of the frequencies at which high amplitude instabilities occur. Figure 4 contains information on the frequencies at which several organized modes of instability exist in a 12-in. chamber. A sonic velocity of about 4000 ft/sec corresponds to an efficiency of 100%. An efficiency of 90% would then occur when the sonic velocity is 3600 ft/sec. If two or more of the pure modes shown exist in the chamber,

the c^* efficiency can be approximated in this manner. If only one frequency of oscillation is present in the chamber, the mode may be very difficult to determine, e.g., both the first radial and the third tangential modes can occur at 4700 Hz, the first radial mode when the η_{c^*} efficiency is 96%, and the third tangential mode when the efficiency is 88%. However, if another pure mode exists in the chamber (such as at 2250 Hz, a possible first tangential mode), the sonic velocity is more clearly determined and the 4700 Hz instability is shown to correspond to the first radial mode of oscillation and an efficiency of 96%.

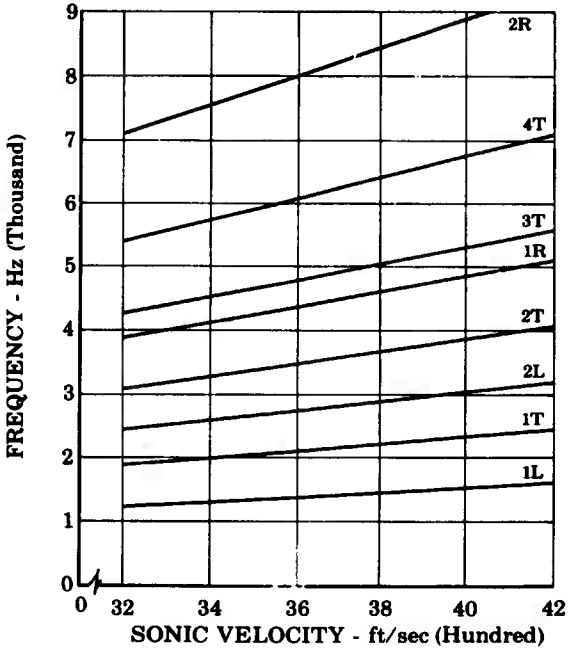

Figure 4. Fundamental Instability Modes in a 12-in. Chamber FD 24199A

B. LOW PRESSURE BASELINE TESTS

Two baseline tests, tests No. 114.01 and 115.01, were conducted at a nominal chamber pressure of 200 psia and mixture ratio of 2.0. The tests were conducted to determine if a change of the stability characteristics of the motor had occurred since the Phase I baseline program. The Phase I baseline test at 200 psia and a mixture ratio of 2.0 produced pressure oscillations of greater than 20% of chamber pressure at 2800 Hz and 4900 Hz corresponding in frequency to the second longitudinal and third tangential instability modes. Frequencies over 5000 Hz were not recorded because of the amplification of signal that occurred over 5000 Hz (see Reference 1).

Helium bleed transducers were used for tests No. 114.01 and 115.01 and frequencies were recorded up to 10,000 Hz. Amplitudes over 10% of chamber pressure for the tests are shown in figure 5. The predominant modes of instability for test No. 114.01 were at 2350 Hz, 4700 Hz and 6250 Hz. The amplitudes at the 2 highest frequencies exceeded 25% of chamber pressure. The only frequency at which an amplitude over 10% of chamber pressure occurred during test No. 115.01 was 3650 Hz. Several other amplitudes over 5% of chamber pressure were recorded.

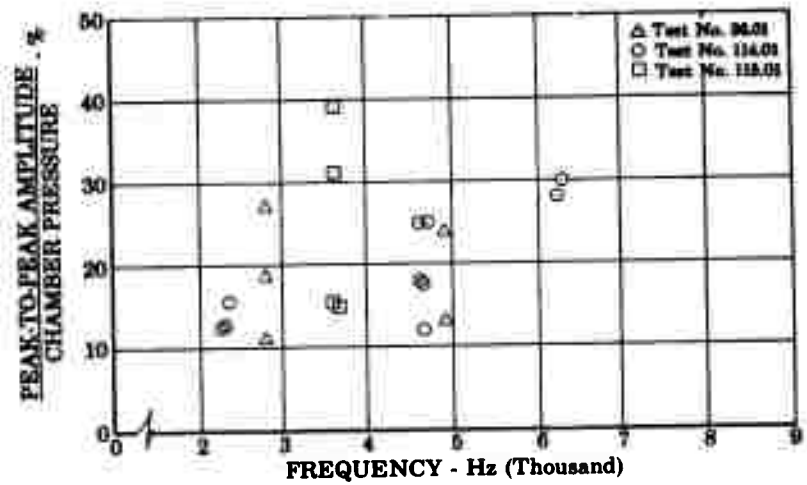

Figure 5. Amplitudes over 10% of Chamber Pressure - 200-psi Baseline Tests

FD 24197A

SECTION IV
FILM-COOLED LINER PROGRAM

Film cooling is a basic method of cooling the walls of rocket chambers; this method is often used when other requirements preclude regenerative and transpiration cooling. The principal advantages of film cooling over other cooling techniques are its simplicity of design and fabrication. In addition, when other cooling methods are not feasible, film cooling can be used in conjunction with an ablative chamber.

The design of an effective acoustic liner depends to a large degree on the ability to predict the liner aperture gas properties. These gas properties - sonic velocity, density, and viscosity - can be closely approximated when no cooling is used, but are difficult to assess when external wall cooling is used. The liner design is further complicated because the film coolant manifold must be placed near the injector, thereby eliminating the use of an acoustic liner in the chamber section most sensitive to combustion instability. Because of the inability to forecast liner gas properties when film cooling was used, liners for this experiment were designed for no coolant flow using the computer program of Reference 2. Then, test programs were run at two chamber pressures with a range of coolant flows, so that the effects of the flow on liner effectiveness could be evaluated. The 200- and 800- psi film-cooled liner programs are discussed in detail in the following paragraphs.

A. LOW PRESSURE FILM-COOLED LINER PROGRAM

1. Heat Transfer

Heat balance equations were used to determine the amount of Aerozine-50 required to film cool the N_2O_4/Aerozine-50 engine. The liner wall convective film coefficient (h_B) was computed using the Bartz closed-form equation (Reference 3). The cooling rate required to cool the wall to a given temperature was calculated by equating the heat supplied to the liner wall by combustion and the heat absorbing capacity of the coolant. The coolant rate was calculated at 1000 psi assuming constant specific heat.

$$Q_{combustion} = h_B A\ (T_c - T_w)$$
$$Q_{combustion} = Q_{coolant}$$
$$Q_{coolant} = \dot{w} C_p\ (T_s - T_i)$$
$$h_B A\ (T_c - T_w) = \dot{w} C_p\ (T_s - T_i)$$
$$\dot{w} = h_B A\ (T_c - T_w)/C_p\ (T_s - T_i)$$

The required coolant flowrate of Aerozine-50 for a one-half chamber-length liner was 1.5 lb_m/sec. Phase I tests demonstrated one-half chamber-length liners to be as effective as full chamber-length liners for reducing combustion instability in this particular motor.

2. Liner Design

The liner was designed for no coolant flow because of the difficulty in determining the liner aperture gas properties when film cooling was used. At least three coolant rates were to be used to establish a trend of the effects of film cooling on the effectiveness of the acoustic liner to suppress combustion oscillations. Each time a change is made in the flowrate, changes also occur in the overall mixture ratio, flow velocity past the liner apertures, as well as the aperture gas viscosity and density. The liner apertures most probably contain a mixture of combustion gases and unburned Aerozine-50 during hot testing, the percentages of which cannot be evaluated. That the liner design curve can be radically changed with only a change in the liner aperture temperature is illustrated in figure 6, if the apertures contain only combustion gases.

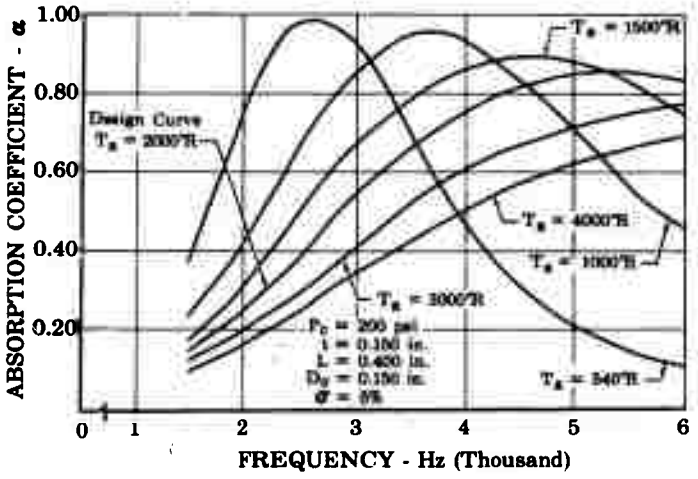

Figure 6. Effects of Aperture Combustion Gas Temperature - 200-psi Film-Cooled Liner FD 24200A

The design-point data for the 200-psia film-cooled liner are given in table II. The liner design curve is shown in figure 7.

3. Hardware

The 200-psi one-half chamber length steel liner is shown in figures 8 and 9. The coolant was supplied to the chamber by a manifold near the injector. The coolant was supplied by 120 0.021-in.-diameter holes, drilled circumferentially about 1 in. downstream of the injector face. The first inch of the liner was cooled by 36 0.021-in.-diameter holes, which exit near the injector face. The remainder of the chamber was made up of a solid ablative liner. The nozzle employed a graphite insert, figure 10, that acted as a heat resistance shield. The insert was held

in place by a steel nozzle cutout and a steel backup plate. A sketch of the 200-psi film-cooled liner is shown in figure 11 and a sketch of the liner inserted in the chamber is shown in figure 12.

Table II. Film-Cooled Liner Design Data

Chamber pressure, psia	200
Mixture ratio	2
Aperture gas temperature, °R	2000
Aperture gas viscosity, $lb_m/ft\text{-}sec$	2.87×10^{-5}
Aperture gas sonic velocity, ft/sec	2340
Flow velocity past apertures, ft/sec	500
Liner Dimensions	
Thickness, in.	0.150
Backing distance, in.	0.400
Aperture diameter, in.	0.150
Open area ratio, %	5.0

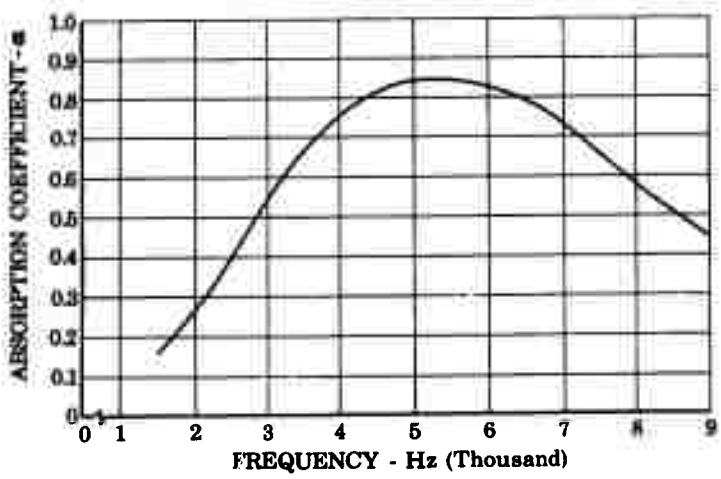

Figure 7. Absorption Characteristics of 200-psia Film-Cooled Liner for 500-ft/sec Flow Past Apertures FD 20796A

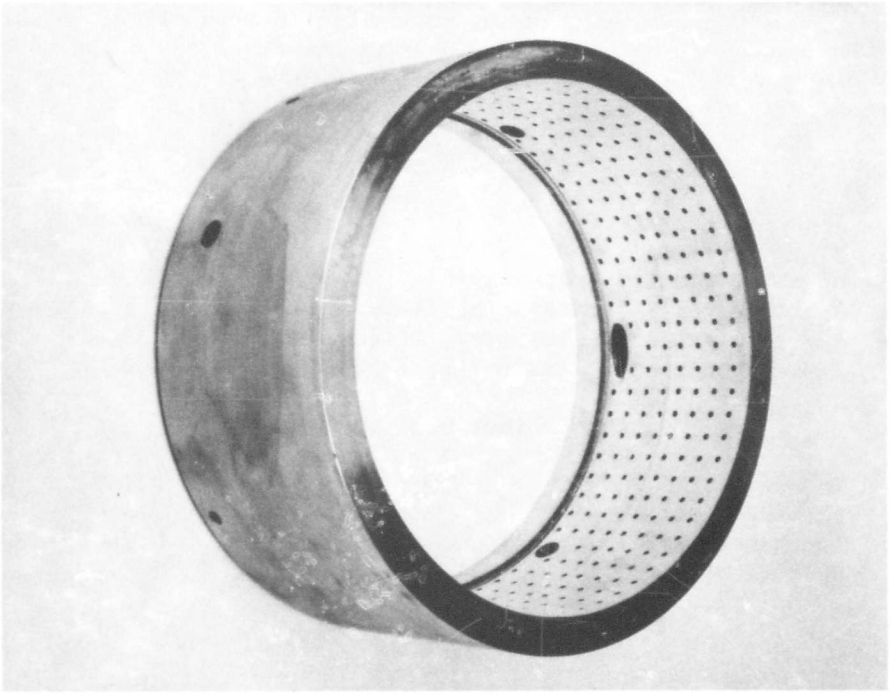

Figure 8. 200-psi One-Half Chamber Length Steel Liner FE 70879

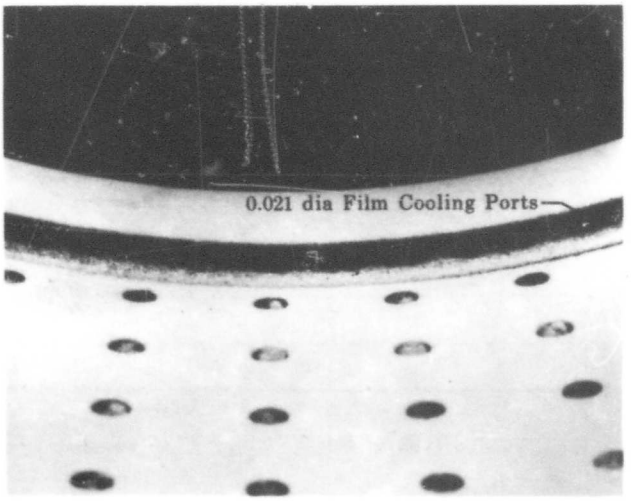

Figure 9. 200-psi One-Half Chamber Length Steel Liner FD 22238

Figure 10. Graph-I-Tite* G-90 Nozzle Throat Insert FE 70877

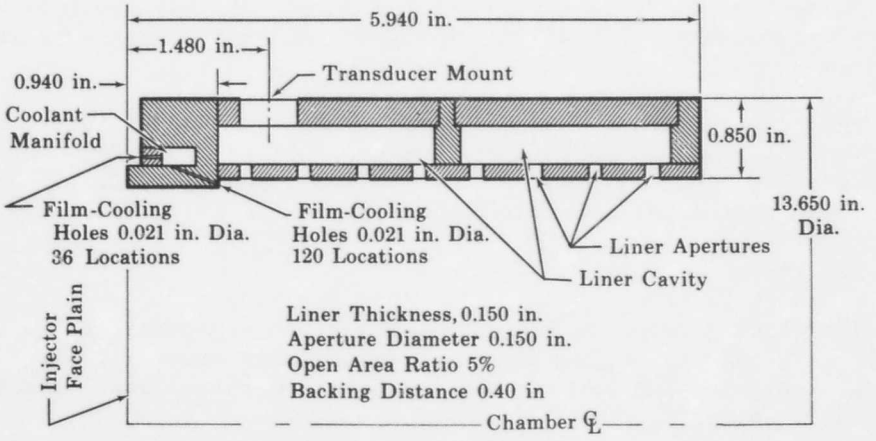

Figure 11. Sketch of the 200-psi Film-Cooled Liner Assembly FD 20795

* Registered Trademark of Carborundum Co., Graphite Products Division, Sanborn, New York.

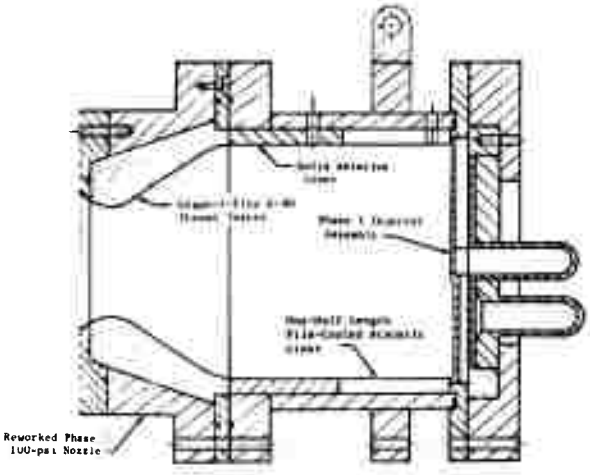

Figure 12. Sketch of the 200-psi Film-Cooled Liner Assembly FD 25015

Four Kistler dynamic pressure transducers were used to monitor instability. Three were located in the A plane 1.600 in. from the injector at the 12:00, 3:00, and 7:00 o'clock angular orientations. The fourth transducer was located in the B plane 7.700 in. from the injector at the 12:00 o'clock position. This transducer was in the solid ablative section of the chamber. Because some amplification of the transducer signal occurs at high frequencies, all frequencies over 5000 Hz were filtered out of the system before they were recorded on tape.

The rough combustion cutoff device, used in Phase I tests, was modified to only analyze frequencies between 1000 and 5000 Hz. The range of 1000 to 5000 Hz covers instabilities between the first longitudinal and the third tangential modes of the chamber.

4. Hot Tests

The planned sequence included tests at three nominal coolant flowrates (2.5, 2.0, and 1.5 lb_m/sec) and a baseline test with no coolant flow. The stable tests were to be repeated and pulsed with explosive charges to drive the motor unstable.

Seventeen tests were conducted on the one-half chamber length, 200-psi film-cooled acoustic liner (see table III for summary).

The first eight tests (tests No. 46.01 through 53.01) were not considered valid because the design point chamber pressure and/or mixture ratio were not attained. The design point deviations were a result of

high fuel flow caused by an incorrect fuel control valve setting. The controller was set for total fuel flow (cooling flow plus injector flow) rather than for injector flow. Also, the oxidizer control valve was insensitive to oscillations in oxidizer inlet pressure. When the run tank pressure was reduced, the possibility of cavitation across the oxidizer control valve was eliminated and the control valve operated correctly. All test stand deviations were corrected before test No. 54.01. Tests No. 54.01 through 57.01 were valid unpulsed tests. Test No. 54.01 (2.34 lb_m/sec coolant flow) was unstable with the highest levels at 2100 Hz, and instability levels over 20% of chamber pressure were recorded at 4300 and 4800 Hz. The frequencies correspond to the first tangential, first radial and third tangential modes, respectively. Test No. 55.01 (1.92 lb_m/sec coolant flow) was alternately stable and unstable. The unstable portions of the test lasted from 0.110 to 0.460 sec with the highest levels occurring at 2150 Hz. Tests No. 56.01 (1.40 lb_m/sec coolant flow) and 57.01 (no coolant) were very stable, but the liner was badly burned during test No. 57.01 (figures 13 and 14). It is interesting to note that no instability occurred in spite of the burned liner. Relative instability levels from high speed oscillographs for tests No. 54.01 through 57.01 are shown in figures 15 through 19. The liner cavity temperature as a function of time and coolant flow for tests No. 54.01 through 57.01 is shown in figure 20.

A second film-cooled liner, identical to the one described, was fabricated and used for pulsed tests No. 75.01 through 79.01. Test No. 75.01 (1.92 lb_m/sec coolant flow) was stable except for several combustion pops. Tests No. 76.01 through 79.01 were all conducted at a nominal coolant rate of 1.50 lb_m/sec. No amplitude analysis was made on test No. 77.01 because of the brevity of the test, nor was an amplitude analysis made for 78.01 because the tape deck did not function properly. Tests No. 76.01 and 79.01 had first tangential amplitudes up to 30% of chamber pressure (see figures 21 through 23). Figures 24 through 26 show instability data for the 200 psi tests at the first tangential, third tangential, and first radial modes, respectively. Tests No. 56.01 (1.4 lb_m/sec coolant) 57.01 (no coolant) and 75.01 (1.97 lb_m/sec coolant) were not included in the analysis because they had no steady-state instability. The results indicate combustion stability to be inversely proportional to flowrate. The first radial and third tangential mode amplitudes were greater than 12% of chamber pressure only when the coolant rate was high (2.34 lb_m/sec). The first tangential mode had the highest amplitudes and also followed the trend of lower levels with lower coolant rates.

B. HIGH PRESSURE FILM-COOLED LINER PROGRAM

1. Liner Design

An acoustic analysis of the 1000-psi film-cooled liner revealed that, for the particular input conditions, high absorption and wide frequency bandwidth characteristics were difficult to obtain with a single resonator configuration. Therefore, a liner with two different resonators was designed (figure 27). The design point data for the 1000-psi film-cooled liner are given in table IV. The liner design curve, which is shown in figure 28, provides at least 25% absorption through the frequency range of 2000 to 4400 Hz.

Table III. 200-psi Film-Cooled Liner

Test No.	Test Duration - sec	Injector Mixture Ratio	Fuel Cooling Rate - lb_m/sec	Overall Mixture Ratio	Chamber Pressure - psia	Combustion Efficiency η_{c^*} - % Based on Total Flow	Perturbation Amplitude - P/P as % of P_c	Decay Time - msec	Time Perturbation Initiated After Ignition - sec	Comments
46.01	2.94	1.58	3.35	1.22	228	95.7	26.3	13	0.64	Overall instability levels were about 8 psi P/P.
47.01	0.74						24.5	50	0.62	High P_c abort-pressure switch faulty: design chamber pressure not reached.
48.01	4.01	1.58	3.42	1.22	226	94.9	27.4		2.91	Instability continued until end of test at about 2100 Hz and 20 to 60 psi overall.
49.01	2.61	1.64	2.65	1.32	225	97.2	30.2	30	0.69	High frequency instability for most of test between 30 to 70 psi total amplitude.
50.01	0.77						32.8	50	0.62	High cavity temperature abort (1500 R): chamber pressure maximum was 146.7 psia.
51.01	2.48	1.64	3.34	1.26	228	97.1	33.4	10	0.67	
							24.2	12	0.69	
							32.9		0.95	Instability continued until RCC abort: total levels up to 70 psi P/P.
52.01	No Test									Fuel run valve failed to open.
53.01	2.07	1.99	0	1.99	179	90.6	40.2		1.56	Instability continued until end of test: cavitation across oxidizer control valve may have caused instability.
54.01	1.19	2.03	2.34	1.60	198	93.6	40.3		1.07	Initiated instability that lasted until RCC abort: 3:00 "A" plane Kistler levels: 140 psi P/P at 2100 Hz, 40 psi P/P at 4300 Hz, 96 psi P/P at 4800 Hz.
55.01	5.59	1.99	1.92	1.63	204	95.6	49.0	30	1.12	
							40.2	40	1.94	
							17.7	85	2.14	
							41.2		3.25	High frequency instability continued for 0.360 sec.
							49.0		3.80	High frequency instability continued for 0.130 sec.
							31.4		4.26	High frequency instability continued for 0.110 sec.
							23.6		4.90	High frequency instability continued for 0.460 sec.
										Test was alternately stable and unstable. several one-cycle pops up to 50 psi occurred throughout test; 3:00 "A" plane levels during unstable portions of test: 164 psi P/P at 2150 Hz, 24 psi P/P at 4400 Hz, 25 psi P/P at 5050 Hz.
56.01	5.88	2.00	1.40	1.73	203	96.6	49.0	6	0.59	
							36.8	5	0.69	
							41.2	40	0.79	6 to 15 psi total P/P amplitude for remainder of test: stable test.
57.01	2.94	2.00	0	2.00	196	99.5	53.0	100	0.71	Remainder of test was stable with 6 to 12 psi P/P total amplitude.

Table III. 200-psi Film-Cooled Liner (Continued)

Test No.	Test Duration - sec	Injector Mixture Ratio	Fuel Cooling Rate - lb_m/sec	Overall Mixture Ratio	Chamber Pressure - psia	Combustion Efficiency η_c^* - % Based on Total Flow	Perturbation Amplitude - P/P as % of P_c	Decay Time - msec	Time Perturbation Initiated After Ignition - sec	Comments
75.01	7.8	2.02	1.97	1.65	185	85.1	25.9	10	0.94	
							52.4	10	1.01	6 grain tangentially directed pulse gun charge.
							46.4	9	1.25	
							22.7	7	1.55	
							73.0	25	2.02	Caused by 9 grain explosive charge.
							71.3	13	3.02	Caused by 12 grain explosive charge.
							17.3	5	3.58	
							51.8	10	3.80	
							62.1	10	4.02	Caused by 15 grain explosive charge.
							35.1	5	4.73	
										Extremely stable test: no steady-state instability.
76.01	1.45	2.01	1.52	1.72	192	90.5	22.4	8	0.63	
							39.1	15	1.01	Caused by 6 grain pulse gun charge.
							38.1		1.32	Initiated high amplitude instability-RCC abort in 0.130 sec. Highest amplitude seen on 3:00 "A" plane Kistler: 56 psi P/P at 1900 Hz, 19 psi P/P at 2450 Hz, and 15 psi P/P at 4000 Hz.
77.01	1.03	2.03	1.48	1.74	191	90.8	53.4		1.01	High cavity temperature abort (set at 1700°R): may have been caused by explosive circuit. Test was very stable.
78.01	3.50	2.03	1.51	1.73	202	95.8				High cavity temperature abort: no Kistler data, tape recorder inoperative.
79.01	3.45	2.0	1.49	1.72	201	95.5	20.9	20	0.60	
							53.2		0.68	High level instability started and continued until high cavity temperature abort at 3.45 sec, 6 grain explosive charge at 2.0 sec hidden by steady-state instability. 3:00 "A" plane Kistler levels: 57.5 psi P/P at 2150 Hz, 21 psi P/P at 2800 Hz, 18 psi at 4300 Hz, and 18 psi P/P at 4950 Hz.

UNCLASSIFIED

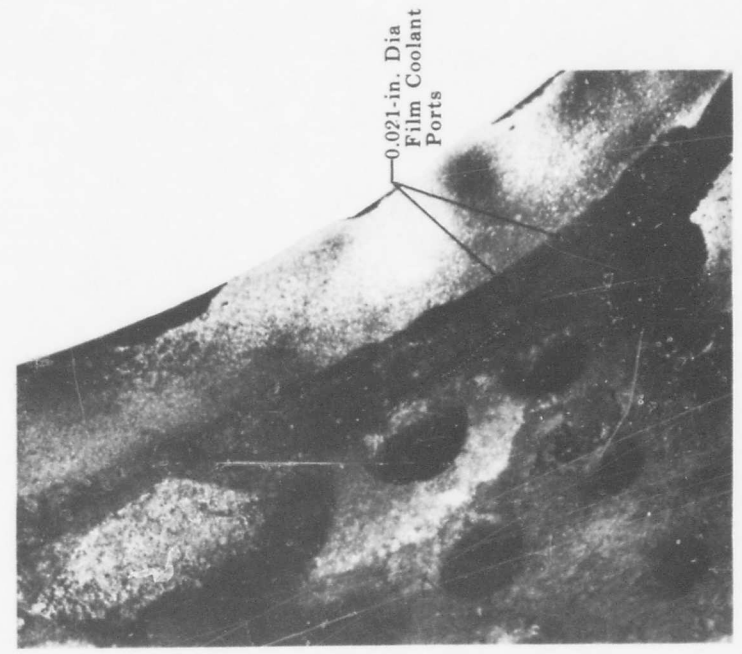

FD 23104

Figure 14. Closeup of 200-psi Film-Cooled Liner After Test No. 57.01

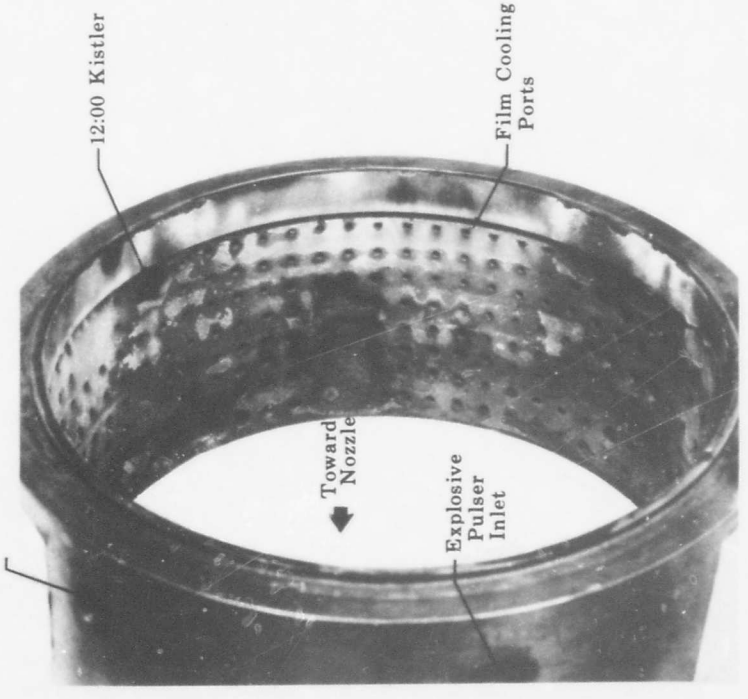

FD 23103

Figure 13. 200-psi Film-Cooled Liner After Test No. 57.01

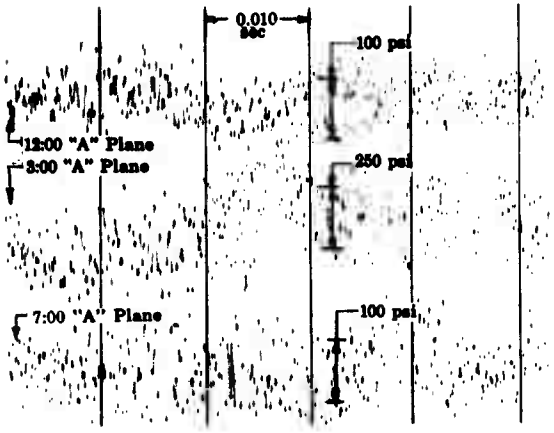

Figure 15. High-Speed Oscillograph for 200-psi Film-Cooled Liner - Test No. 54.01

FD 24216

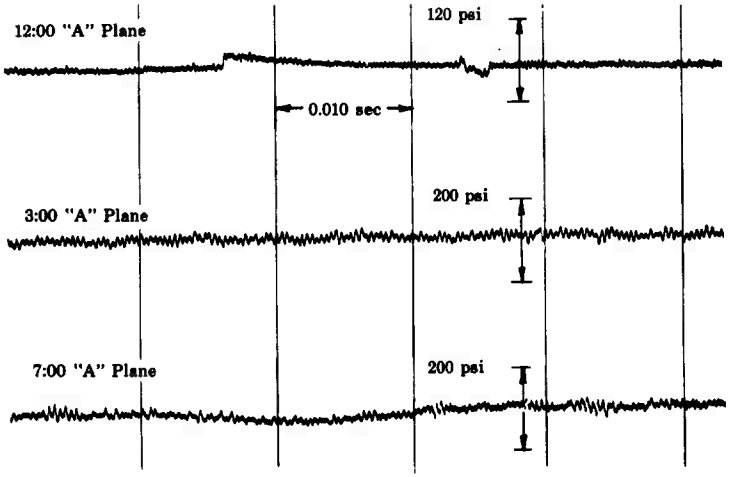

Figure 16. High-Speed Oscillograph for Stable Portion of Test No. 55.01

FD 24217

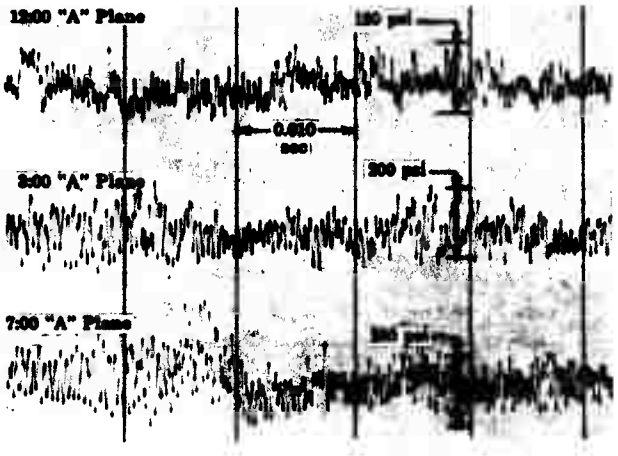

Figure 17. High-Speed Oscillograph for Unstable Portion of Test No. 55.01

FD 24218

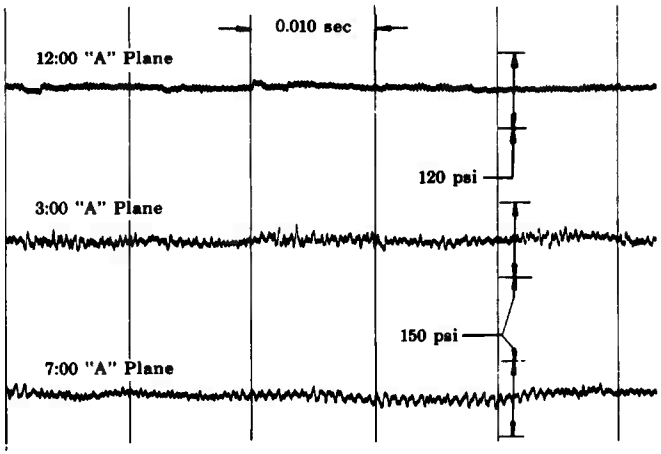

Figure 18. High-Speed Oscillograph for 200-psi Film-Cooled Liner - Test No. 56.01

FD 24219

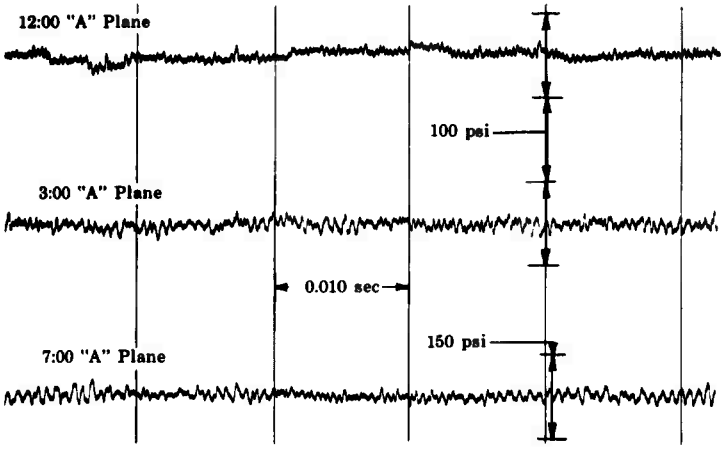

Figure 19. High-Speed Oscillograph for 200-psi Film-Cooled Liner - Test No. 57.01

FD 24220

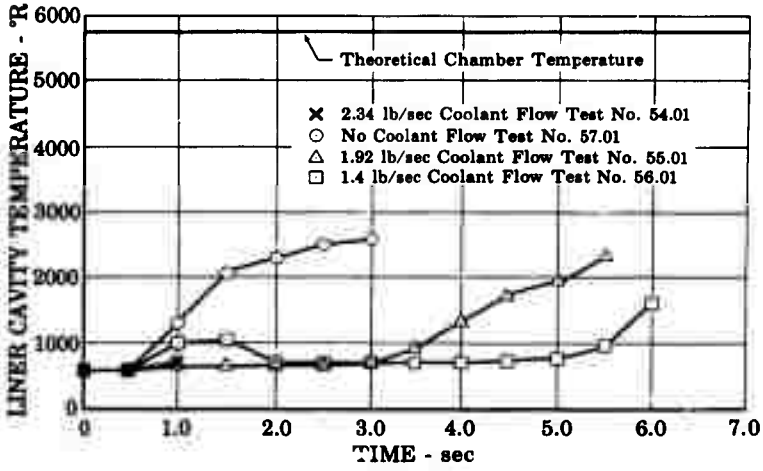

Figure 20. Liner Cavity Temperature as a Function of Time and Coolant Flow for Test No. 54.01

FD 24204

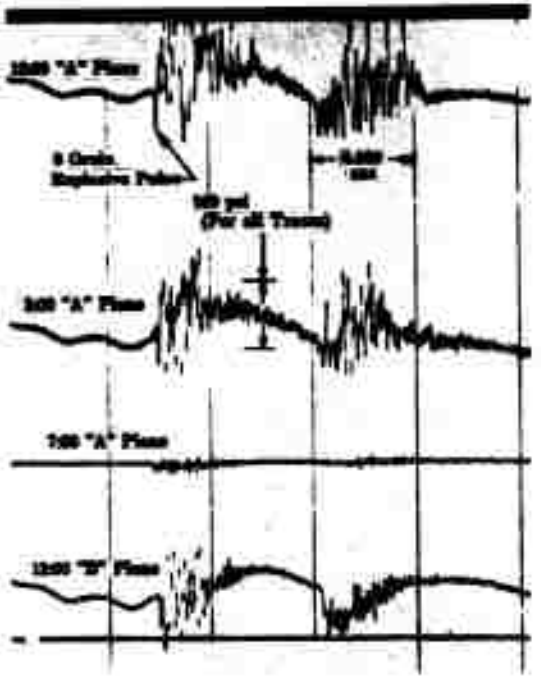

Figure 21. High-Speed Oscillograph for Pulsed Tests of 200-psi Film-Cooled Liner - Test No. 75.01

FD 24221

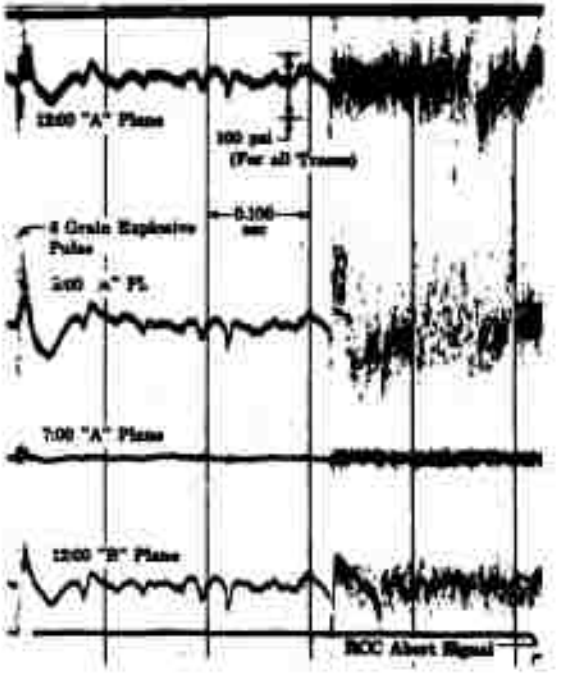

Figure 22. High-Speed Oscillograph for Pulsed Tests of 200-psi Film-Cooled Liner - Test No. 76.01

FD 24222

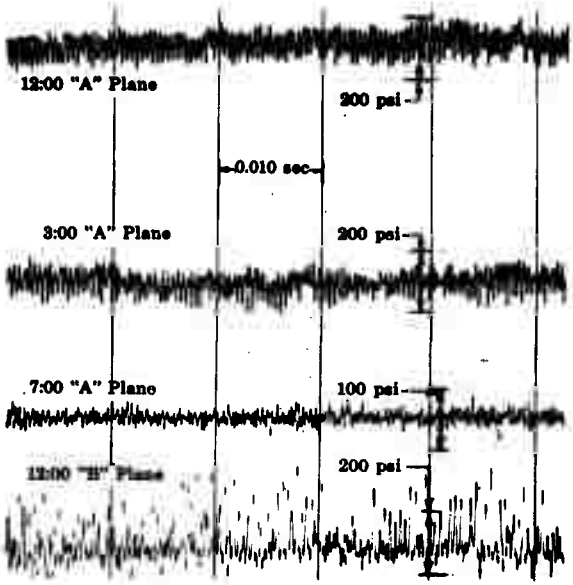

Figure 23. High-Speed Oscillograph for Pulsed Tests of 200-psi Film-Cooled Liner - Test No. 79.01

FD 24223

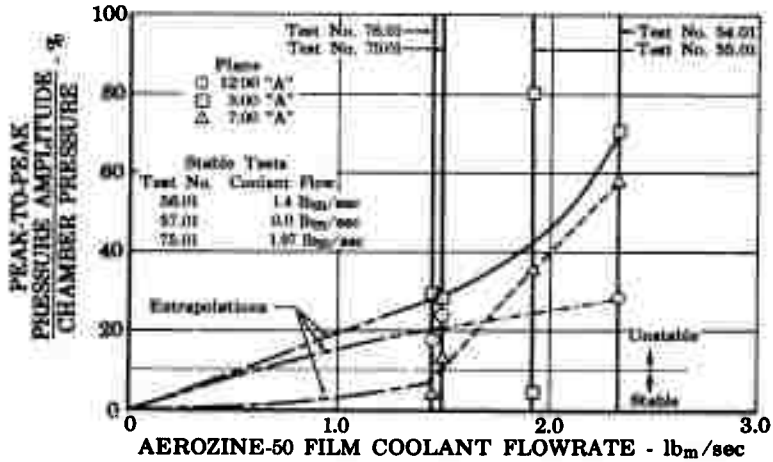

Figure 24. Coolant Flowrate vs First Tangential Mode Amplitude for the 200-psi Film-Cooled Liner Tests

FD 24201

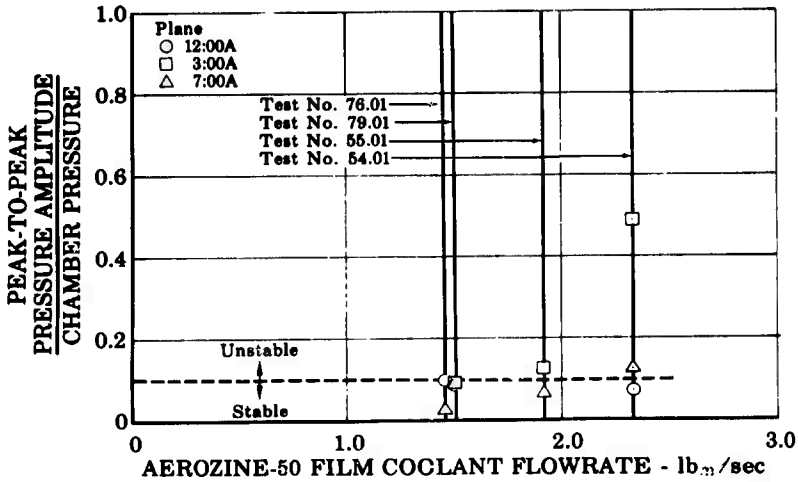

Figure 25. Coolant Flowrate vs Third Tangential Mode Amplitude for the 200-psi Film-Cooled Liner Tests

FD 24202

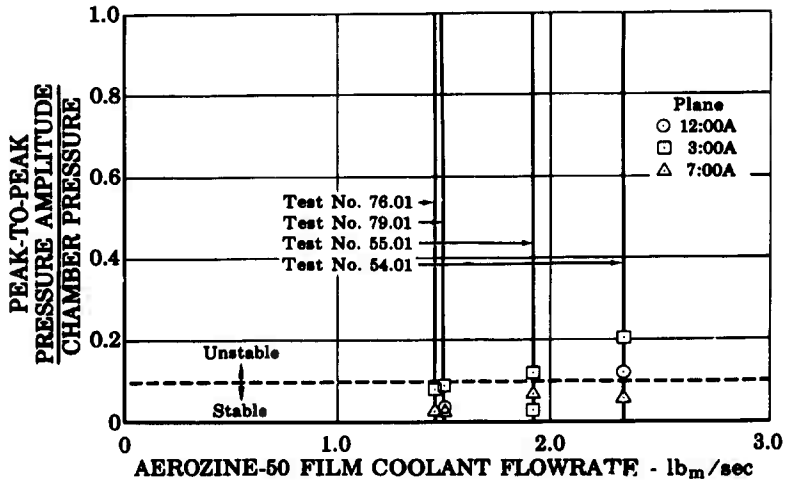

Figure 26. Coolant Flowrate vs First Radial Mode Amplitude for the 200-psi Film-Cooled Liner Tests

FD 24203

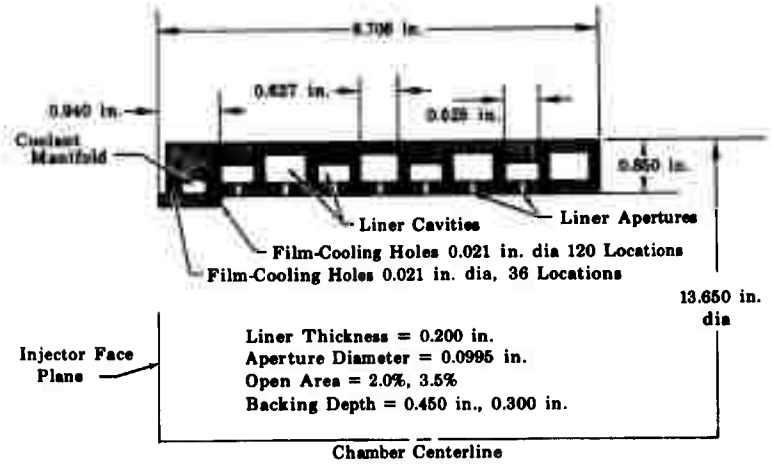

Figure 27. 1000-psi Film-Cooled Liner Assembly FD 22239

Table IV. 1000-psi Film-Cooled Liner Design Data

Chamber pressure, psia	1000
Mixture Ratio	2
Aperture Gas Temperature, °R	2000
Aperture Gas Density, lb_m/ft^3	1.05
Aperture Gas Viscosity, $lb_m/ft\text{-}sec$	2.92×10^5
Aperture Gas Sonic Velocity, ft/sec	2330
Liner Thickness, in.	0.200
Liner Backing Distance, in.	0.450, 0.300
Aperture Diameter, in.	0.0995
Open Area Ratio, %	2.0, 3.5

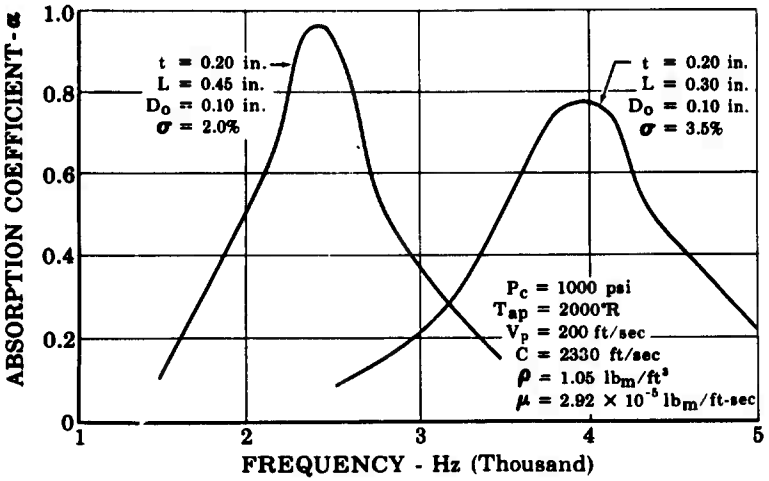

Figure 28. N_2O_4/Aerozine 1000-psi Film-Cooled Liner FD 22240A

2. Hot Tests

Five tests (tests No. 87.01 through 91.01) were made on the high pressure film-cooled liner at 900 psia. No Kistler data were recorded for test No. 87.01, and low chamber pressure occurred in test No. 88.01 because of a malfunction in the oxidizer system. Tests No. 89.01 through 91.01 were valid high pressure tests scheduled for a nominal chamber pressure of 800 psia. Deviations from that pressure were caused primarily by excessive water flow through the film-cooled nozzle. The excessive flow decreased the nozzle throat flow area and therefore increased the chamber pressure. The additional fuel flow used to cool the wall also increased the chamber pressure over the 800-psia setpoint.

The maximum amplitudes from tests No. 89.01 through 91.01 are plotted as a function of film-coolant flowrate in figure 29. The motor stability, as was also noted for the 200-psi film-cooled tests, was inversely proportional to the coolant flowrate. The highest amplitudes occurred at approximately 2200 Hz for each flowrate, although no amplitudes were over 10% of chamber pressure. Some instability occurred at about 4500 Hz, but the levels were less than 5% of chamber pressure. As in the baseline tests, most combustion pops were damped in 10-20 msec. Test No. 91.01 was aborted at 1.04 sec of test time by the hot gas leak abort. The pulse gun was damaged when the explosive detonated, causing a combustion gas leak through the pulser fitting in the chamber wall. The test summary for the high pressure film-cooled liner tests is shown in table V.

C. CONCLUSIONS

The 200-psi film-cooled liner demonstrated stable combustion when no cooling was used, but combustion became progressively more unstable as the cooling rate was increased. This effect was especially pronounced at the first tangential mode, but was also notable at the first radial and third tangential modes. The 1R and 3T mode amplitudes were over 12% of chamber pressure only when the cooling rate was high (2.34 lb_m/sec). All of the stable tests were characterized by low liner cavity temperatures (600° to 900°R) while high cavity temperatures occurred during unstable operation. The decrease in the liner absorption coefficient at low frequencies with an increase in the cavity temperature is shown in figure 6. The N_2O_4/A-50 propellant combination exhibits a tendency for uneven burning; i.e., localized unburned propellants mix and burn rapidly, resulting in combustion pops or spontaneous, high-magnitude, overpressures when compared to steady-state chamber pressure. The combustion pops can promote instability by disrupting the film layer on the liner wall, thus causing the liner aperture temperature to rise. The liner absorption is lowered and if the aperture temperature remains high, subsequent pops can initiate high-level steady-state instability. In addition, the disruption of the film layer by multiple pops occurring in rapid succession promotes instability because the film layer becomes free to burn. The result is high localized heat fluxes and a susceptibility to the initiation of the transverse modes of instability.

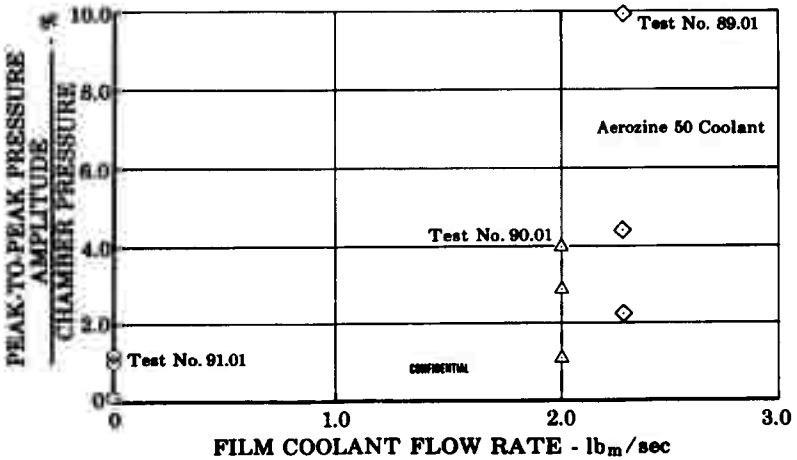

(U) Figure 29. Maximum Amplitudes for Tests No. 89.01 Through 91.01 as a Function of Film-Coolant Flowrate FDC 24941

Table V. Film-Cooled Liner Tests

Test No.	Test Duration - sec	Liner Type	Injector Mixture Ratio	Fuel Cooling Rate - lb_m/sec	Overall Mixture Ratio	Chamber Pressure - psia	Combustion Efficiency η_{c^*} - % Based on Total Flow	Perturbation Amplitude - P/P as % of P_c	Decay Time - msec	Time Perturbation Initiated After Ignition - sec	Comments
87.01	1.75	Film Cooled	1.982	2.99	1.42	887	93.2				Kistler tape inoperative.
88.01	1.72	Film Cooled	0.733	2.51	0.55	585					Low chamber pressure; insufficient oxidizer flow.
								10.6	10	1.01	Caused by pulse gun; 50 grains C-4 explosive. Very stable test.
89.01	1.72	Film Cooled	2.00	2.33	1.52	911	95.7	42.8	10	0.62	High frequency [illegible] initiated and continued to end of test.
								19.7	5	1.01	Caused by 50 grain C-4 explosive pulse gun. 12:00 "A" plane: 67.5 psi P/P at [illegible] Hz, only frequency apparent. Very low levels on 3:00 "B" plane Kistler. 7:00 "A" plane levels: 89 psi P/P at 2200 Hz, 34 psi P/P at 2800 Hz, 24 psi P/P at [illegible], and 39 psi P/P at 4000 Hz.
90.01	1.72	Film Cooled	1.98	1.96	1.57	900	92.5	65.1	15	1.01	Caused by 50 grain explosive pulse gun. 28 spontaneous pops were present varying in amplitude from 160 to 500 psi P/P; each was damped to less than 30 psi in 25 msec. Steady-state instability levels from 12:00 "A" plane Kistler: 21 psi P/P at 2100 Hz, 15 psi P/P at 2650 Hz.
91.01	1.04	Film Cooled	2.00	0.00	2.00	852	99.0	72.7	18	1.01	50 grain pulse gun. Test very stable. Gas leak abort occurred when pulser body ruptured.

D. RECOMMENDATIONS

It is suggested that whenever possible, chamber cooling techniques other than film cooling be considered when acoustic liners are required to suppress combustion instability. The aperture conditions are difficult to determine in a film-cooled liner because of the mixture of coolant and combustion gases in the liner apertures and cavities. Also, the film-cooling may induce instability when the film layer is disrupted and the coolant burns. If a regeneratively cooled liner were used, the absorption could be more accurately assessed because the aperture conditions could be more easily determined.

SECTION V
ABLATIVE LINER PROGRAM

A. TECHNICAL DISCUSSION

1. Liner Design

The ablative liner program was conducted to demonstrate the effectiveness of ablatively cooled acoustic liners for suppressing combustion instability in storable-propellant motors. Precharred Refrasil was selected as the ablative material. Refrasil, a product of the H. I. Thompson Fiber Glass Company, has in numerous tests withstood the heat fluxes and compatibility difficulties associated with N_2O_4/Aerozine-50 propellants. The ablation rate of this material was estimated by the manufacturer to be 0.001-inch per second. Since a total test duration of 200 seconds was planned, the minimum liner thickness of 0.20 inch was necessary for adequate ablation depth. Assuming a margin of safety of 2.0, the minimum thickness that could be considered for the aperture thickness was 0.40 inch. The total liner thickness, aperture thickness plus backing depth, was restricted to 0.85 inch since the Phase I pressure shell assembly was to be used. With the restrictions on the minimum and maximum total thickness in mind, the preliminary design data were generated for a chamber pressure of 1000 psia. The design point properties for the liner were as follows:

Chamber Pressure, psia	1000
Mixture Ratio	2.0
Aperture Gas Temperature, °R	2000
Aperture Gas Density, lb_m/ft^3	1.05
Aperture Gas Viscosity, lb_m/ft-sec	2.92×10^{-5}
Aperture Gas Sonic Velocity, ft/sec	2330
Velocity Past Apertures, ft/sec	100
Incident Pressure Amplitude, db	190

The results of the preliminary design data indicated that poor absorption characteristics would be obtained, i.e., the maximum absorption of 52% could be obtained with a very narrow frequency bandwidth (see figure 30). Thus, several resonator configurations would be necessary to absorb the instabilities over the frequency range of 1000 to 5000 Hz. Because of the difficulties in obtaining adequate absorption characteristics with the geometric restrictions placed on the liner, the operating chamber pressure was changed from 1000 to 200 psia. The change facilitated a more practical liner-design configuration at conditions more nearly representative of normal ablative chamber operation.

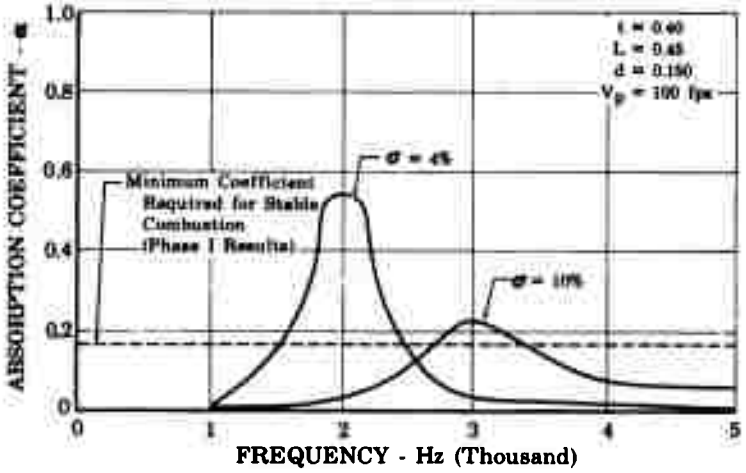

Figure 30. Absorption Characteristics of 1000-psia Ablative Liner FD 24797A

At the lower chamber pressure, a single resonator configuration theoretically would provide adequate absorption for stable motor operation based on Phase I criteria, i.e., minimum 17% absorption. To prevent structural failure of the liner when the liner ablates and to provide a configuration adaptable to a flightweight engine, an individual resonator pattern was recommended for the ablative liner design. Figure 31 shows the final design curve, and figures 32 and 33 show a dimensional sketch and a photograph of the liner, respectively. The design point properties for the 200-psia liner were as follows:

Chamber Pressure, psi	200
Mixture Ratio	2.0
Density, lb_m/ft^3	0.207
Gas Constant, $ft\text{-}lb_f/lb_m°R$	69.5
Ratio of Specific Heats	1.224
Viscosity, $lb_m/ft\text{-}sec$	2.87×10^{-5}
Incident Pressure Amplitude, db	190
Aperture Temperature, °R	2000
Aperture Sonic Velocity, ft/sec	2340
Velocity Past Apertures, ft/sec	500
Liner Thickness, in.	0.40
Backing Cavity Depth, in.	0.45
Backing Cavity Diameter, in.	0.66
Aperture Diameter, in.	0.125
Open Area Ratio, %	3.5
Number of Resonators	277

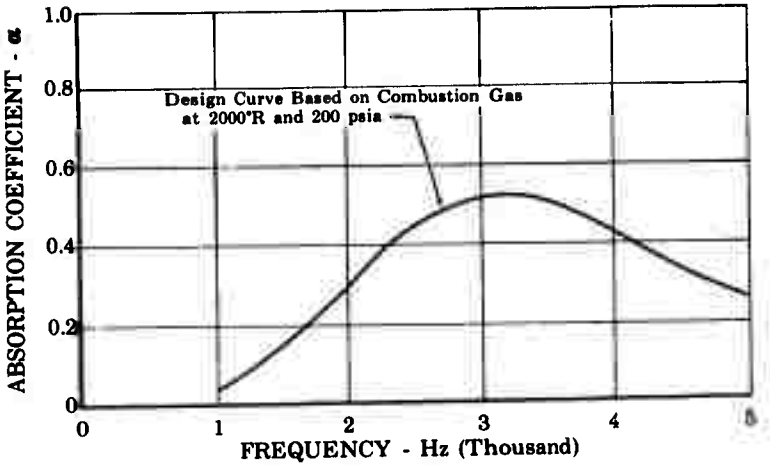

Figure 31. Theoretical Absorbing Characteristics of Ablative Liner, Corrected for an Array

FD 24767A

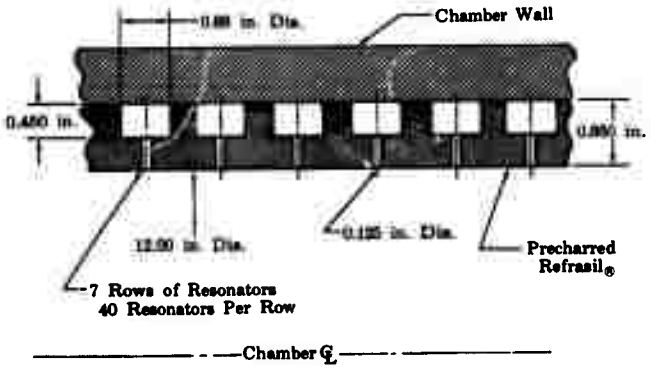

Figure 32. Ablative Liner Configuration

FD 20824A

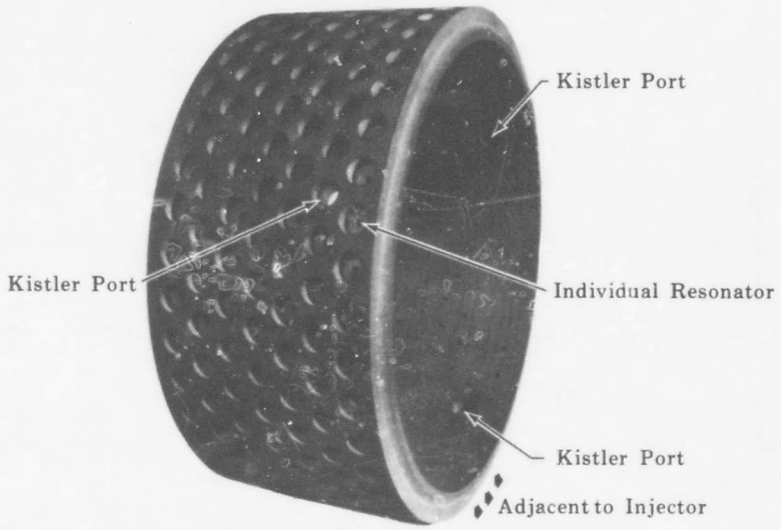

Figure 33. One-Half Chamber Length, 200-psi Ablative Acoustic Liner FD 23107

2. Individual Resonator Ablative Liner Tests

A sketch of the test configuration for the first series of firings is shown in figure 34. The half-chamber length acoustic liner was adjacent to the injector; the remainder of the chamber contained a solid Refrasil ablative liner (figure 35). The throat section of the nozzle was fabricated from Graph-I-Tite* G-90, which served as a heat resistant shield. The 100-psia nozzle from the Phase I program was reworked to hold the throat insert in place.

The first six tests (tests No. 58.01 through 63.01) were unstable; each was aborted by the rough combustion cutoff device that was set at 30 psi peak-to-peak amplitude for 0.100 second (see table VI for test summary). Combustion instability with peak-to-peak pressure amplitudes in excess of 70% of chamber pressure (140 psi) were recorded. The amplitude/frequency diagrams for each test are given in Appendix B. The oscillations occurred at frequencies that correspond to one or more of the first three tangential modes and/or the first radial mode (see figure 4). Even though the tests were all unstable, a post-test inspection of the hardware revealed no hardware damage or significant erosion of the ablative liners.

*Registered Trademark, see Page 21.

Table VI. Ablative Liner Tests

Test No.	Test Duration - sec	Injector Mixture Ratio	Chamber Pressure - psia	Combustion Efficiency, c* - %	Perturbation Amplitude - P/P as % of P_c	Decay Time - msec	Time Perturbation Initiated After Ignition - sec	Comments
58.1	1.10	2.02	181	93.9	73.0		0.96	Initiated high level instability that continued until the RCC abort at 1.10 sec. 12:00 "A" plane Kistler levels: 100 psi P/P at 2200 Hz, 200 psi P/P at 4500 Hz.
59.01	0.99	2.02	179	94.6	63.0 76.7	10	0.60 0.88	RCC abort in 0.11 sec.
60.01	0.78	2.11	174	94.5	77.7 79.9	7	0.65 0.70	Down to 80 psi P/P in 7 msec; RCC abort in 0.070 sec.
61.01	0.94	2.05	184	96.0	63.1 62.6		0.63 0.85	Down to 50 psi P/P in 15 msec. RCC abort in 0.090 sec. 12:00 "A" plane levels; 264 psi P/P at 2200 Hz, 176 psi P/P at 4450 Hz, 135 psi P/P at 4600 Hz. 3:00 "A" and 7:00 "A" plane Kistlers showed no levels over 50 psi P/P.
62.01	0.80	2.13	166	90.7	77.0 78.4	15	0.62 0.69	RCC abort in 0.110 sec; very unstable test.
63.01	0.82	2.00	175	95.2			0.72	RCC abort in 0.100 sec; very unstable test.

To determine the reason for the poor liner performance, the following tasks were initiated: (1) a study to determine the accuracy of the basic theory used in the computer design deck for the individual resonator configuration; and (2) a study to determine the effects on liner performance of nitrogen purge gases trapped in the resonator cavities.

To determine the accuracy of the theory used in the computer design deck, an impedance tube sample, which is shown in figure 36, was fabricated in physical dimensions identical to those of the ablative liner. Tests were conducted to compare the predicted absorption coefficient to the actual values determined from the impedance tube tests. The prediction curve was adjusted for the relationship between absorption and the number of equal volume resonators for the constant incident area that will be discussed in Section VI, page 85. The results of the impedance tube tests and the theoretical prediction curve on the calculation for a single Helmholtz resonator are shown in figure 37. Good agreement existed between the theoretical and experimental data, indicating that the basic theory used to calculate the performance of the ablative liner was correct.

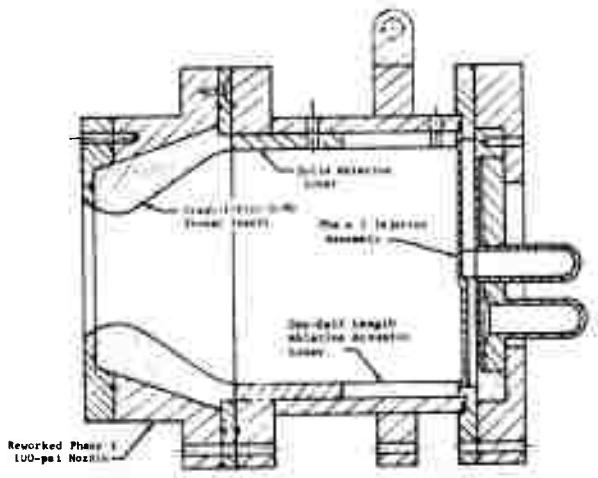

Figure 34. 200-psi Ablative Liner Test Configuration FD 25014

AD 392 072

AUTHORITY: AFRPL
ltrs 5 Feb 86

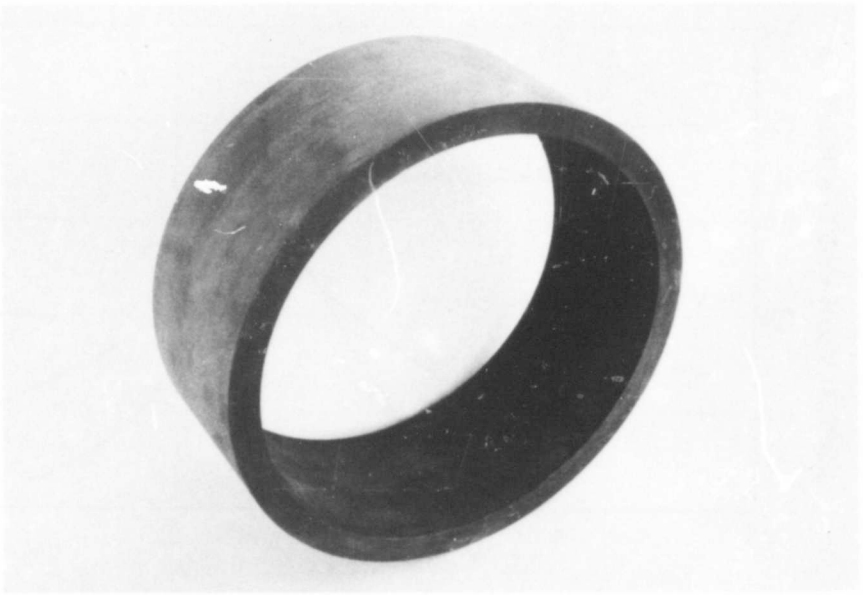

Figure 35. Solid Refrasil Ablative Liner FE 72384

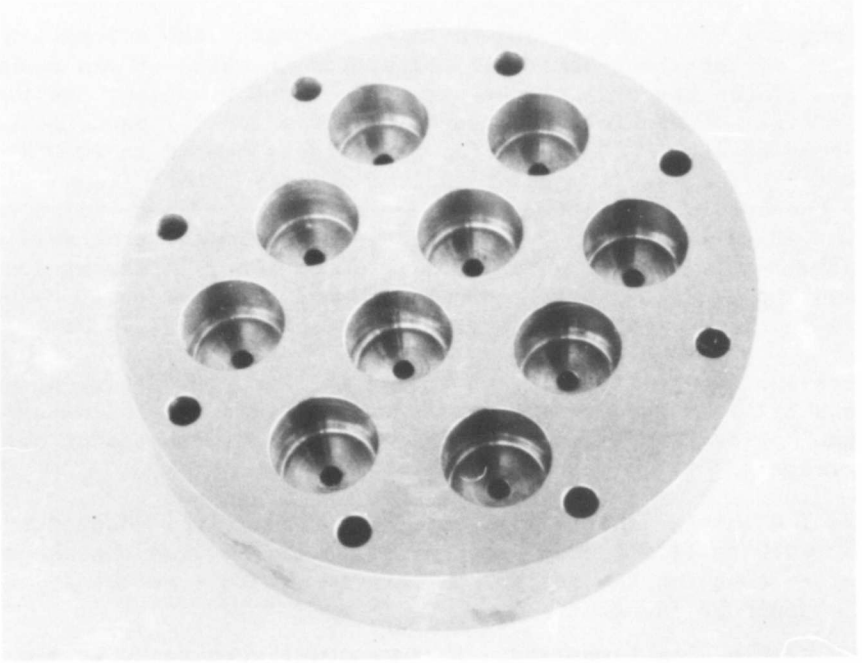

Figure 36. Impedance Tube Sample-Cavity Side of 200-psi Ablative Liner Individual Resonator Configuration FE 72382

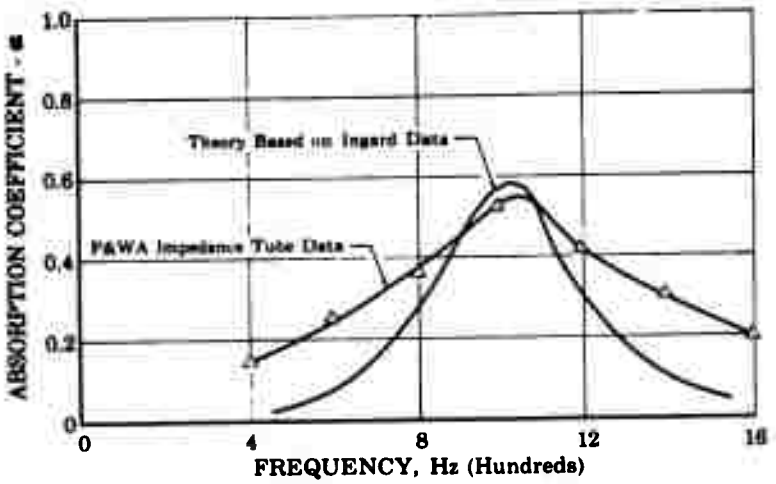

Figure 37. Individual Resonator Impedance Tube Analysis FD 24768

Since the basic theory proved to be accurate, the absorption characteristics of the liner were then calculated in which it was assumed that nitrogen prerun purge gases were trapped in the resonator cavities during the firings. Absorption values were obtained for (1) purge gases at ambient temperature (540°R), and (2) purge gases heated to 2000°R due to combustion. The results are shown in figure 38; this figure also includes the original ablative liner design curve. The calculations assuming hot purge gases trapped in the cavities indicated that sufficient absorption would be available, i.e., greater than 17% absorption; however, if the trapped purge gases remained at ambient temperature, combustion could have been unstable at frequencies greater than 2400 Hz.

To allow the cavity gas temperature to reach its design point and to ensure sufficient steady-state data for analysis, the following changes were made prior to the second series of individual resonator ablative liner tests:

1. The initial sample time for the RCC abort was changed from +0.0 to +1.0 second after ignition to increase the chance of reaching the design aperture temperature before an abort could be incurred.
2. Four cavity temperature thermocouples were added to measure the gas temperature at various liner locations.
3. The three Kistler transducer ports in the acoustic liner were enlarged to prevent possible wall-induced vibrations that could magnify the Kistler readout.

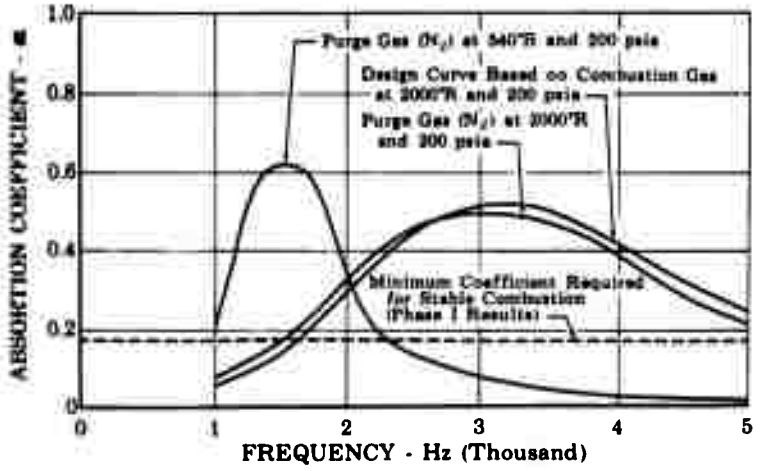

Figure 38. Theoretical Absorption Characteristics of 200-psia Ablative Liner FD 24786

Tests No. 69.01 through 71.01 were all unstable and were aborted by the rough combustion curoff device (see table VII for test summary). Prior to test No. 72.01, the RCC abort was changed from 30 to 50 psi peak-to-peak amplitude. The scheduled 15.0-second test was aborted after 8 seconds by the high temperature abort (set at 2200°R). Cavity temperature data from test No. 72.01, figure 39, indicate that the liner aperture design temperature was reached 2.0 to 2.5 seconds after ignition, thus, the motor should have exhibited stable operation at the first tangential and first radial modes.

The amplitude/frequency diagrams from three different portions of test No. 72.01 (see Appendix B) show that the motor was unstable at frequencies corresponding to the first tangential and/or the first radial modes. The post-test condition of the individual resonator liner and the solid liner are shown in figures 40 and 41, respectively.

Because of the poor liner performance, the following tasks were initiated to determine if the unstable operation of the ablative liner was caused by the presence of ablative by-products trapped in the resonator cavities of the liner:

1. An analytical study of the chemical process involved during the ablation of a phenolic liner
2. A test series with the liner using a hot-gas-sampling system to trap and identify the gases in the resonator cavities.

Table VII. Ablative Liner Tests

Test No.	Test Duration - sec	Injector Mixture Ratio	Chamber Pressure - psia	Combustion Efficiency, c* - %	Perturbation Amplitude - P/P as % of P_c	Decay Time - msec	Time Perturbation Initiated After Ignition - sec	Comments
69.01	1.82	2.00	175	87.3	91.2 80.0	5	0.50 0.73	Initiated high level instability that continued for remainder of test (Rcc abort). Highest levels on 12:00 "A" plane Kistler: 20 psi P/P at 2000 Hz, 20 psi P/P at 4050 Hz.
70.01	1.01	2.01	175	90.6	66.8 58.3	7	0.46 0.62	Initiated high level instability (60 to 80 psi P/P total) that lasted until RCC at 1.01 sec.
71.01	1.09	2.01	174	91.3	59.2 62.0	4	0.44 0.79	Initiated high level instability that continued until RCC abort at 1.09 sec. Levels were between 60 and 80 psi P/P total.
72.01	8.34	2.01	188	95.0	55.8 48.0	11	0.48 0.73	Initiated high frequency instability that continued until end of test aborted by high temperature. 12:00 "A" plane Kistler levels from Amp/Frequency plots: from 1.000 to 2.00 sec after ignition, 41 psi P/P at 4400 Hz; from 4.50 to 5.50 seconds after ignition, 14 psi P/P at 2150 Hz, 16 psi P/P at 2650 Hz, 35 psi P/P at 4350 Hz; from 7.00 to 8.00 seconds after ignition, 45 psi P/P at 2100 Hz, 21 psi P/P at 4400 Hz.

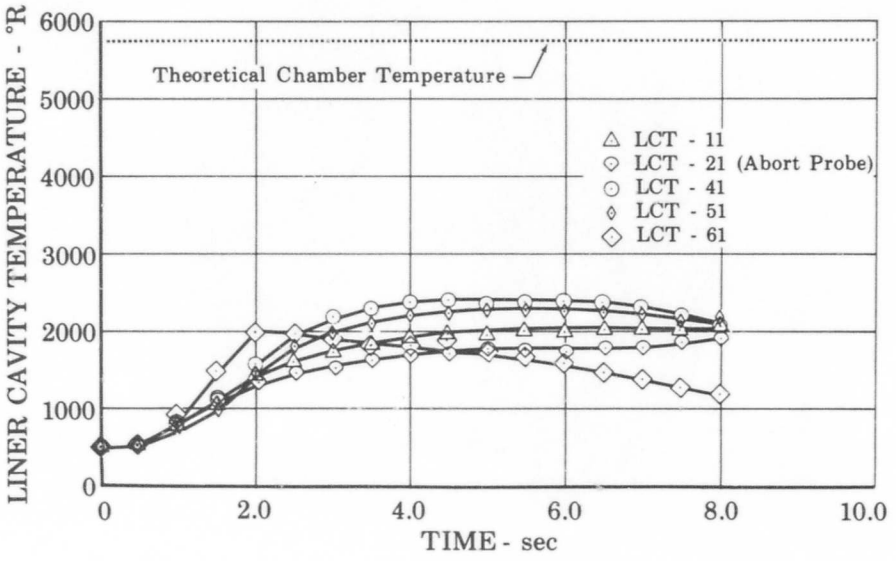

Figure 39. 200-psia Ablative Liner Cavity Temperature - Test No. 72.01 FD 24780

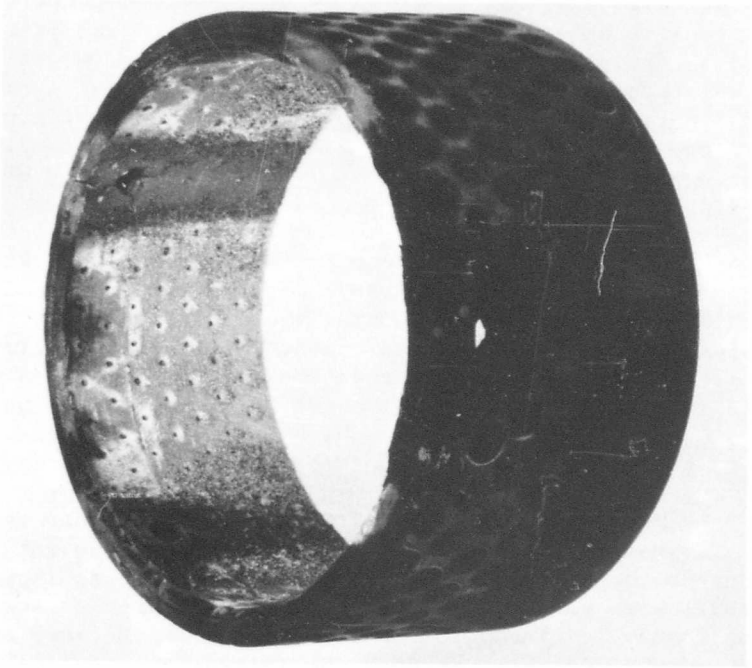

Figure 40. Individual Resonator Ablative Acoustic Liner After Test No. 72.01 FE 72742

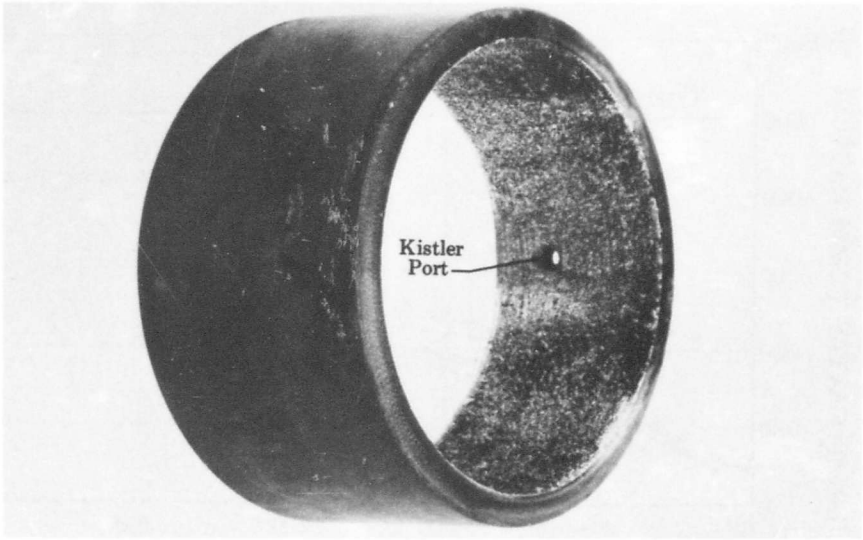

Figure 41. Ablative Solid Liner After Test No. 72.01 FD 23109

The analytical study was conducted to evaluate the properties of the gas in the acoustic apertures resulting from the chemical processes that are involved in the ablation of a phenolic liner. The investigation of these chemical processes was accomplished by studying the pyrolysis of an ablative liner, constructed of phenol-formaldehyde, while operating at a chamber pressure of 200 psia and a temperature of approximately 2000°R. The evolved gas was found to be composed primarily of hydrogen, carbon monoxide, methane, and water vapor.

Reference to a phase diagram for amorphous carbon indicated that under the aforementioned conditions any free carbon that might result from the reaction would exist in the solid state. The subsequent determination of the properties of the evolved gas was subject to the assumption that the free solid carbon generated by the reaction remained with the wall. The property of particular interest in the design of acoustic liners was the molecular weight of the evolved gas, which was determined to be approximately 13 for the conditions mentioned above.

A series of tests was conducted with the ablative liner using a hot-gas-sampling system to determine the average molecular weight of the gases in the resonator cavities during the firing. Three tests (No. 99.01 through 101.01) were conducted to accomplish this purpose (see table VIII for the test summary). The motor configuration was the same as for tests No. 69.01 through 72.01, but included the instrumentation for the molecular weight analysis. Appendix A includes a detailed description of the gas-analysis system.

Table VIII . Ablative Liner Tests

Test No.	Test Duration - sec	Injector Mixture Ratio	Chamber Pressure - psia	Combustion Efficiency, ηc^* - %	Cavity Gas Molecular Weight	Perturbation Amplitude - P/P as % of P_c	Decay Time - msec	Time Perturbation Initiated After Ignition - sec	Comments
99.01	2.94	2.02	182	91.6	13.4				Kistler tape operating incorrectly.
100.01	2.94	1.98	191	95.4	10.5	36.7	57	0.53	Initiated 20 psi high frequency instability that lasted 70 msec.
						33.5		0.64	Initiated high frequency instability that continued for remainder of test. Total amplitude was 20 to 40 psi P/P. Test was stable. 3:00 "A" plane levels: 12.5 psi P/P at 2150 Hz. There was no steady-state instability at any frequency on the 7:00 "A" plane Kistler. The 12:00 "B" plane Kistler in the solid liner half of the chamber had 28.5 psi P/P amplitude at 2150 Hz.
101.01	2.94	2.00	193	97.5	(N/A) - Not Available	32.6		0.54	Initiated high frequency instability that continued for remainder of test. Total levels, 30 to 50 psi P/P.

The gas analyzer data indicated that the gas in the cavities was of lower molecular weight than that of the combustion gases and varied from 10.5 to 13.4. Thus, the experimental value compared favorably with the theoretical values that were determined from the analytical investigation. The absorption characteristics of the ablative liner were then calculated for this molecular weight range (figure 42). The figure includes the original ablative liner design curve. All of the curves were corrected to account for the individual cavity configuration. The data show that the frequency at which maximum absorption occurred increased as the cavity molecular weight decreased. Thus, the liner with ablative outgassing in the resonator cavities had good theoretical absorption characteristics at frequencies near the first radial mode (4500 Hz) but had marginal stabilizing effects near the design frequency (2100 Hz).

The instability levels of all the ablative liner tests, in the form of peak-to-peak (P/P) pressure amplitudes for the first tangential and first radial modes are graphed as a function of firing time in figures 43 and 44. Although unstable operation (i.e., peak-to-peak amplitudes greater than 10% of chamber pressure or approximately 20 psi) existed for most of the 26.51 seconds of the liner's firing time, significant reductions in amplitudes occurred within the first 5.0 seconds. This reduction was believed to be the result of the formation of a char-layer on the liner ID. Figure 45 shows a section of the ablative liner after test No. 101.01.

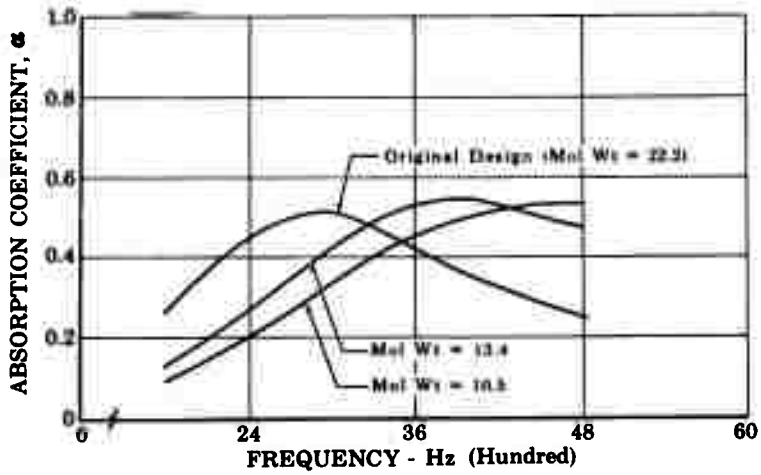

Figure 42. Calculated Absorption Coefficient vs Frequency: 200-psi Ablative Individual Resonator Acoustic Liner

FD 23749A

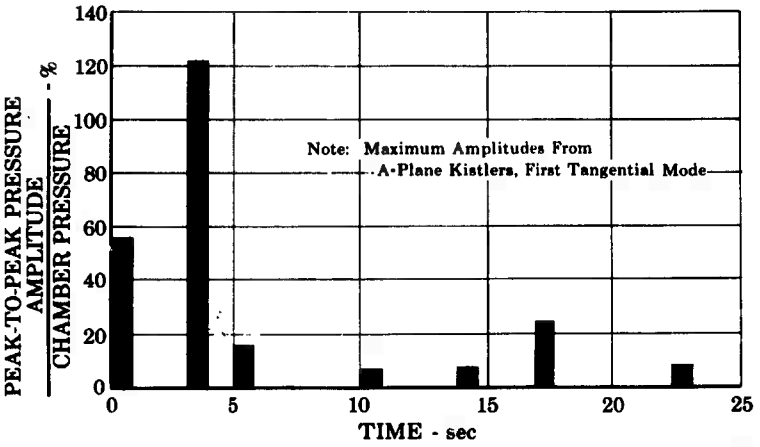

Figure 43. Peak-to-Peak Amplitude vs Firing Time for Individual Resonator Ablative Liner

FD 24787

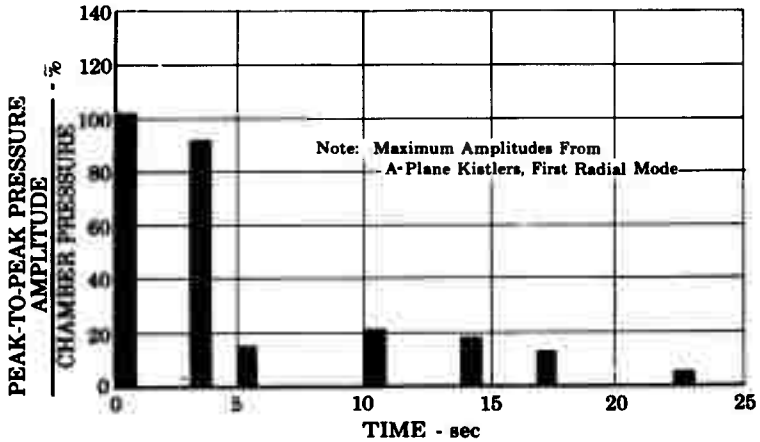

Figure 44. Peak-to-Peak Amplitude vs Firing Time for Individual Resonator Ablative Liner

FD 24788

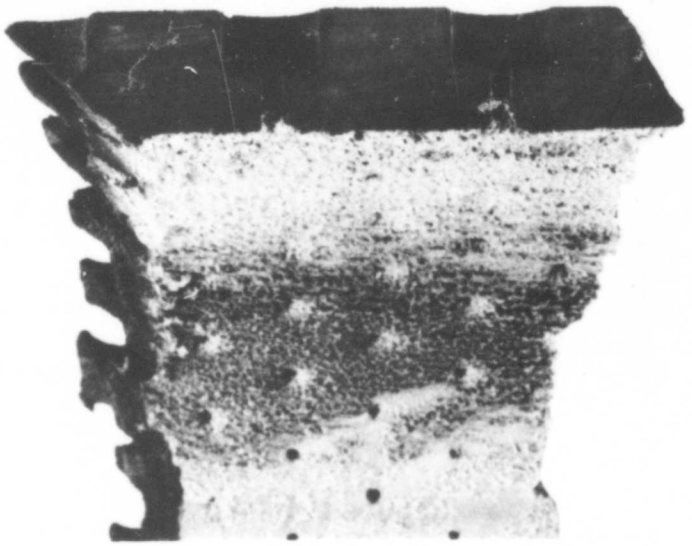

Figure 45. 200-psia Ablative Liner Section Post-Test No. 101.01 FE 76081

3. Individual Resonator Steel Liner Tests

To determine if the motor instability was due to the lack of sufficient total absorption near the injector face, an uncooled steel liner identical in geometric configuration to the ablative liner was fabricated and tested. For the test series, two improved helium bleed Kistler Model 615-A transducers were installed in the motor (see figure 46), in addition to the Kistler Model 601-A transducers used thus far in the program. The 615-A helium bleed transducer presented several advantages that included:

1. Higher frequency response that was almost three times that of an air or combustion gas-filled passage.
2. Better damping that resulted in less tendency for acoustic oscillations within the passage.
3. Gas cooling that maintained a constant temperature transducer environment

4. Thermal isolation from the severe combustion environment.
5. Clean passages that resulted in no fouling due to combustion deposits.

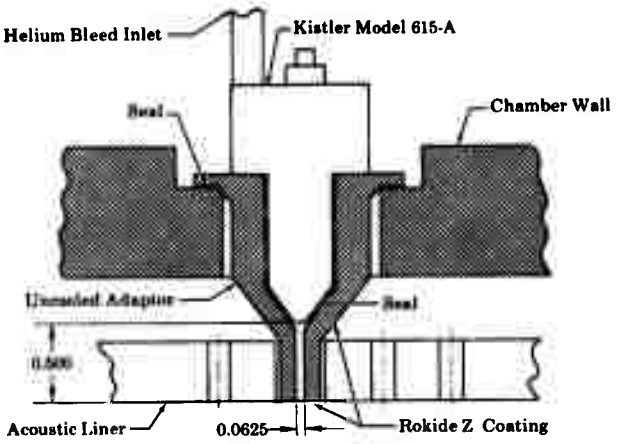

Figure 46. Kistler Model 615-A Transducer and Uncooled Adaptor Assembly FD 24841

Six tests (tests No. 102.01 through 107.01) were conducted with the liner (see table IX for test conditions). Since the first test was aborted by the rough combustion cutoff before sufficient stability data could be obtained, the RCC setting was changed from 50 to 100 psi P/P for 0.10 second for all the remaining tests. The test duration, which was originally set at 3.0 seconds, was changed to 1.50 seconds to prevent serious damage to the motor resulting from the increased allowable instability. Analysis of the test data indicates that peak-to-peak oscillations greater than 40% of chamber pressure occurred at a frequency of 4600 Hz (first radial mode). High amplitude oscillations up to 65% of chamber pressure were recorded at 6200 Hz, corresponding to the fourth tangential mode.

Table IX. Individual Resonator Steel Liner Tests

Test No.	Test Duration - Sec.	Injector Mixture Ratio	Chamber Pressure - psia	Combustion Efficiency, ηc^* - %	Comments
102.01	0.68	1.85	172	76	From 0.58 sec after start to RCC abort at 0.68 sec there was high frequency instability between 60 to 80 psi P/P total amplitude.
103.01	0.81	1.86	184	80.0	From 0.65 sec after start to high P_c abort at 0.81 sec there was high frequency instability between 60 to 80 psi P/P total amplitude.
104.01	1.47	1.93	192	97	From 0.53 sec after start to end of test there was high frequency instability between 60 to 80 psi P/P total amplitude.
105.01	1.47	1.91	196	98	From 0.51 sec to 0.81 sec after start there was high frequency instability between 20 to 60 P/P total amplitude; from 0.81 sec to end of test, high frequency instability between 60 to 80 psi P/P total amplitude.
106.01	1.47	1.94	194	97	From 0.45 sec after start to end of test there was high frequency instability between 60 to 80 psi P/P total amplitude.
107.01	1.47	1.91	189	96.8	From 0.49 sec after start to end of test there was high frequency instability between 60 to 80 psi P/P total amplitude.

Liner gas samples were taken during the test series to help determine the cause of instability of the ablative liner, i.e., whether it was caused by ablative outgassing, or simply from a lack of sufficient absorption. The samples were taken at 1.25 seconds after the start of the test. The results of the hot-gas-sample data indicate that the molecular weight decreased with each successive test in which data were obtained. The molecular weight of the samples varied from 17.2 to 5.2; however, a post-test inspection of the sampling system indicated that a solid residue was deposited in the one cc sample loop. This residue buildup caused a decrease in the trapped sample volume and effected a decrease in the sample molecular weight. A granular filter was placed in the sample system upstream of the sample loop to prevent any residue from reaching the loop.

The individual resonator steel liner design curve, figure 42, is corrected for a partial array using the factor developed in Section VI, as shown in figure 74. The liner should have provided stable operation since, from Phase I results, liners with absorption coefficients greater than 17% successfully damped combustion oscillations in the motor tested. However, these results were for a liner with a full array. Actually, the amount of absorption required to suppress combustion oscillations is unknown for liner configurations other than a full array. The full array liner may be more efficient than the individual resonator liner because of the interactions of instability waves in apertures adjacent to each other and the freedom of travel of the waves from one pressure zone to another in the liner backing cavity.

The unstable operation of the individual resonator steel liner indicated that the total absorption near the injector face was insufficient and that the amount of absorption required to eliminate instability is greater for individual resonators than for full resonator arrays.

4. Parallel Array Steel Liner Tests

Because of the uncooled steel liner results, the individual cavity liner design was abandoned and a liner was designed with a parallel array of resonators to obtain higher total absorption. The steel liner was reworked to increase the total absorption and another series of tests was conducted.

The parallel array was formed by grouping several of the individual resonators together. This was accomplished by removing material between the circular backing cavity volume of the resonators and then drilling additional apertures. Figure 47 is a sketch of the reworked configuration of the steel liner. Figure 48 shows a comparison between the total absorption coefficient versus frequency of the original steel liner and the parallel array steel liner.

Four tests (tests No. 110.01 through 113.01) were conducted on the parallel array steel liner. The test conditions are listed in table X. During the first test, the cavity gas temperature reached only 850°R

(design temperature was 2000°R); thus, the test duration for the remaining three tests was increased from 1.50 to 5.0 seconds. During the last two tests some erosion occurred around the Kistler ports and two of the helium bleed transducers were damaged. Figure 49 shows the post-test condition of the liner. Peak-to-peak (P/P) pressure amplitudes were less than 5% of chamber pressure for all frequencies below 5500 Hz; however, maximum pressure amplitudes of 30 psi P/P and 80 psi P/P occurred at 6200 and 7800 Hz respectively. It was concluded from frequency/pressure amplitude data that the operation of the motor was stabilized over the liner design frequency range of 1000 to 5000 Hz by increasing the total absorption near the injector face.

Since pressure peaks of 50% of chamber pressure occurred at 6200 Hz for the individual cavity steel liner, and pressure peaks of 80% and 60% of chamber pressure occurred at 7800 and 9250 Hz with the reworked steel liner, a series of frequency response tests were conducted to determine if the adaptors used with the helium bleed transducers were resonating at frequencies below 10,000 Hz; thus causing amplification of the pressure signals. An impedance tube sample simulating the adaptor was fabricated and tested in the P&WA high frequency impedance tube (Reference 4). The tests were conducted in a helium environment at sound pressure levels of 134 and 140 db (re 0.0002 microbar). Although the adaptor caused a 90-degree phase shift in the signal at 8400 Hz, no amplification of the input pressure signal was recorded. It was concluded that the signal to the helium bleed Kistler transducers would not be amplified because of the resonant effects that occurred in the helium-filled passages of the adaptor. Thus the frequency-amplitude data above 5000 Hz from the uncooled steel liner tests were valid. However, the lack of hardware damage during the tests indicates that instability occurring above 5000 Hz was less severe than for frequencies below 5000 Hz.

5. Dual Open Area Ablative Liner

A new full-length ablative liner with two parallel arrays of resonators was fabricated for the final series of firings conducted under the program. The parallel arrays were chosen to extend the absorption characteristics of the liner so that all modes of instability at frequencies up to 10,000 Hz would be suppressed. The design, figure 50, was full-chamber length (two half-chamber length liners) and consisted of 50 resonator arrays, with 5 rows along the length of the liners and 10 arrays per row. The arrays or pockets were each 33 deg of an arc wide and 1.500 inches long and were separated by axial and circumferential webs. Half of the 50 arrays consisted of 8 holes of 0.159-inch diameter each, which yielded a liner open area of 2.6%. The other 25 arrays consisted of 18 holes of 0.173-inch diameter each, for an open area of 7.0%. The dual open area design was necessary to provide high absorption over the frequency range of 1,000 to 10,000 Hz. The lower open area of 2.6% provided low frequency coverage and the higher open area of 7.0% provided high frequency coverage. The design point data for the liner was as follows:

Chamber pressure, psia	200
Mixture ratio	2.0
Gas sonic velocity in resonator, ft/sec	3370
Molecular weight of resonator gas	10.5
Velocity past apertures, ft/sec	500
Aperture gas temperature, ^{o}R	2000
Liner thickness, in.	0.325
Backing cavity depth, in.	0.525
Aperture diameters and open area ratios	0.153 in. open area 2.6% 0.185 in. open area 7.0%

Three tests (tests No. 116.01 through 118.01) were conducted on the parallel array ablative liner (see table XI for the test summary). The first test was aborted in 0.600 seconds because of an erroneous hot gas leak indication. Tests No. 117.01 and 118.01 were 3.0 seconds long as scheduled, with chamber pressure of 178 psia and mixture ratios of about 1.90. During each of these tests several combustion pops with amplitudes up to 250 psi peak-to-peak occurred (see figure 51). All of the pops were damped within 0.010 second and there was no steady-state instability. During test No. 118.01, the liner was broken into two large pieces in the plane of the Kistler adaptor holes in the liner (see figure 52). The precharred Refrasil liner, because of its low impact strength combined with the structural weakness at the Kistler ports, was probably broken by the pressure shock from the high level combustion pops.

6. Dual Open Area Steel Liner

The reworked steel liner was machined to increase the open area ratio of one-half of the parallel array pockets in an attempt to provide stable operation over the frequency range of 1000 to 10,000 Hz. The liner shown in figure 53 was altered to the dual open area configuration by enlarging the diameter of one-half of the apertures from 0.127 to 0.193 inch. Thus, the liner had 15 arrays of apertures with an open area of 3.8% and 15 with an open area of 8.0%. The absorption characteristics of the liner are shown in figure 54.

Four tests (tests No. 119.01 through 122.01) were conducted on the dual open area stainless steel liner (see table XII for test summary). Tests No. 119.01 and 120.01 were aborted by rough combustion. So that stability data could be obtained on the liner, the rough combustion cut-off device was filtered to be sensitive only to frequencies below 5000 Hz starting with test No. 121.01. Tests No. 121.01 and 122.01 were both 3.0 seconds long and exhibited no steady-state instability. Analysis of the data indicated that peak-to-peak pressure amplitudes were less than 10% of chamber pressure for all frequencies below 5000 Hz; however, a maximum pressure amplitude of 62% of chamber pressure occurred at the second radial mode, 7600 Hz.

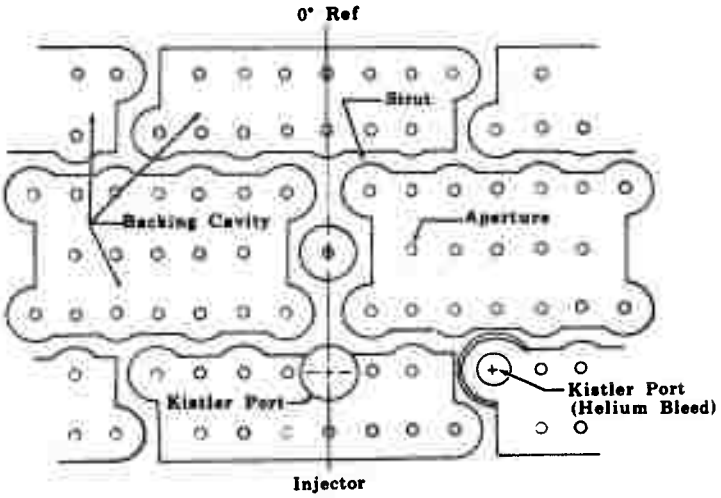

Figure 47. Reworked Pattern of Stainless Steel Liner

FD 24842

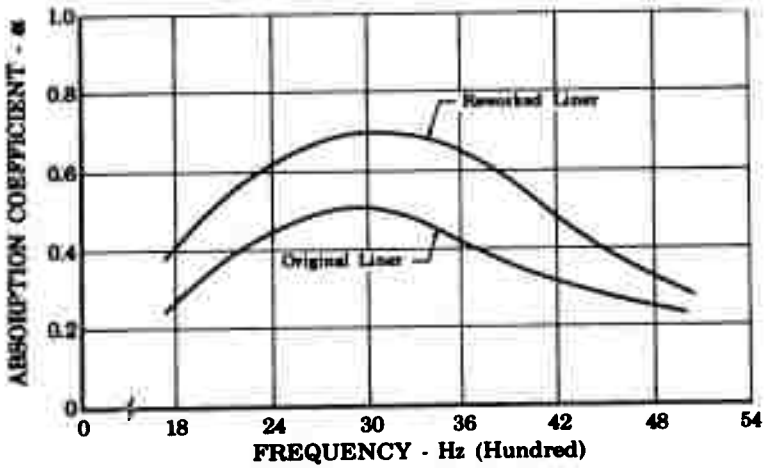

Figure 48. Absorption Characteristics of Individual Resonator Steel Liner

FD 24783

Table X. Parallel Array Steel Liner

Test No.	Test Duration - sec	Injector Mixture Ratio	Chamber Pressure - psia	Combustion Efficiency, c* - %	Perturbation Amplitude - P/P as % of P_c	Decay Time - msec	Time Perturbation Initiated After Ignition - sec	Comments
110.01	1.45	1.926	191	97.5	0.931		0.65	High frequency initiated high level instability at 6200 and 7200 Hz. RCC signal filtered out above 5000 Hz. Therefore, no abort occurred.
111.01	2.91	2.005	197	99.2	0.940		0.45	Initiated high level, high frequency instability at 6200 and 7800 Hz.
112.01	4.87	2.007	198	99.8	0.945	10	0.375	
					0.807	7	0.44	
					0.985	13	0.48	
					1.085		0.525	Initiated high frequency instability; no abort.
113.01	4.87	2.008	194	97.6	1.031		0.575	Initiated high frequency instability to end of test.

UNCLASSIFIED

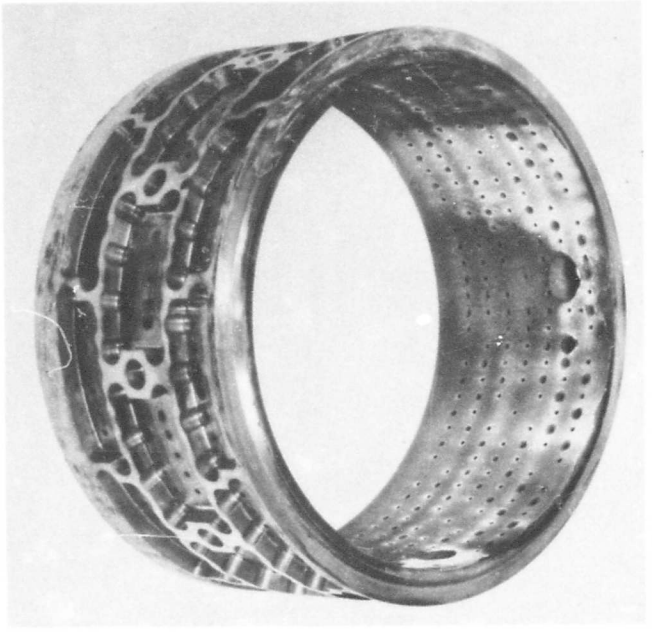

Figure 49. Parallel Array Steel Liner Post-Test No. 113.01 FE 76077

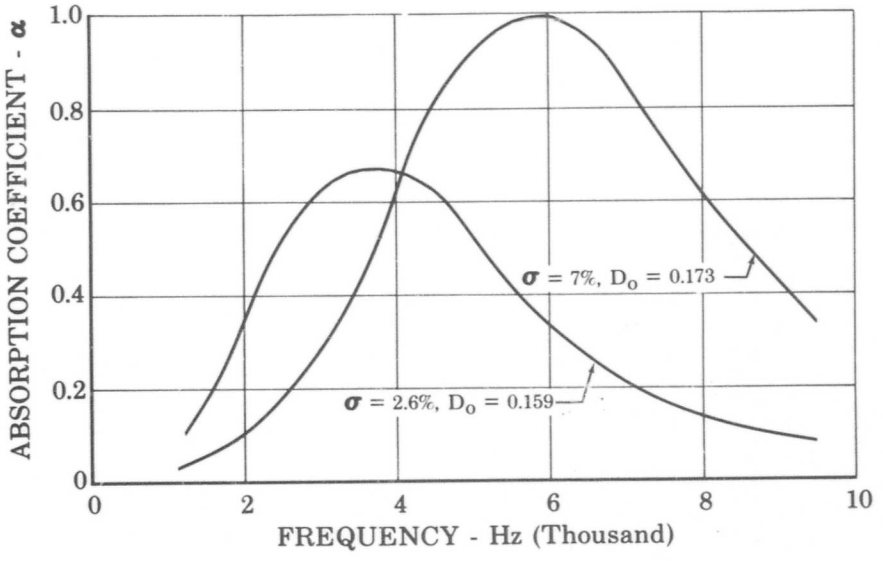

Figure 50. 200-psia Ablative Liner Design FD 24781

Table XI. Dual Open Area Ablative Liner Tests

Test No.	Test Duration - sec	Injector Mixture Ratio	Chamber Pressure - psia	Combustion Efficiency, c* - %	Perturbation Amplitude - P/P as % of P_c	Decay Time - msec	Time Perturbation Initiated After Ignition - sec	Comments
116.01	0.6				42	20	0.53	Gas leakwire abort caused by faulty connector.
117.01	3.0	1.89	178	93	65 68 70	10 5 4	0.45 0.54 0.62	Several pops of 50 to 70 psi amplitude. Most were damped to prepop levels within 10 msec. Steady-state levels were between 6 and 16 psi P/P.
118.01	3.0	1.91	178	92				Several pops 50 to 80 psi; all were damped within 15 msec. Steady-state levels were 4 to 14 psi P/P.

UNCLASSIFIED

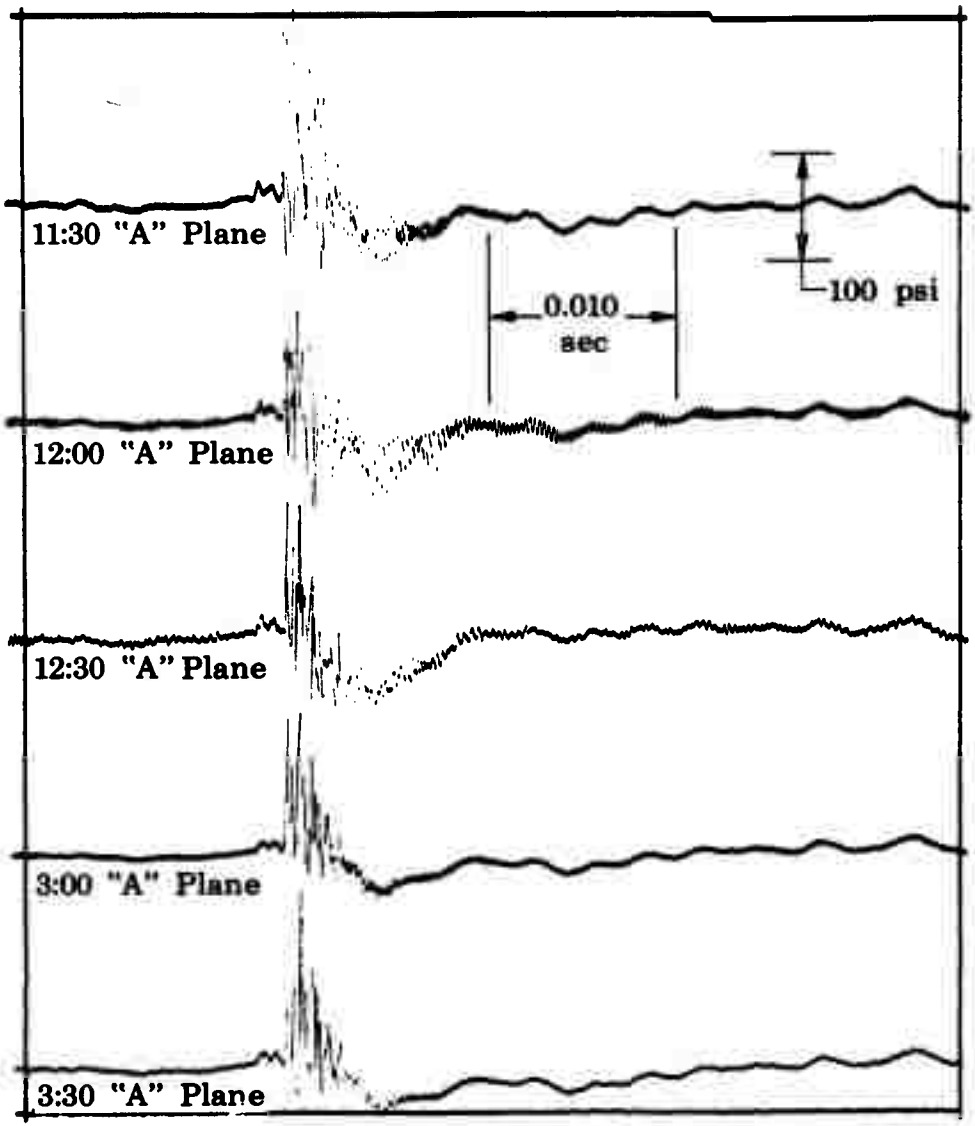

Figure 51. Dual Open Area 200-psi Ablative Liner, Test No. 117.01 FD 24769

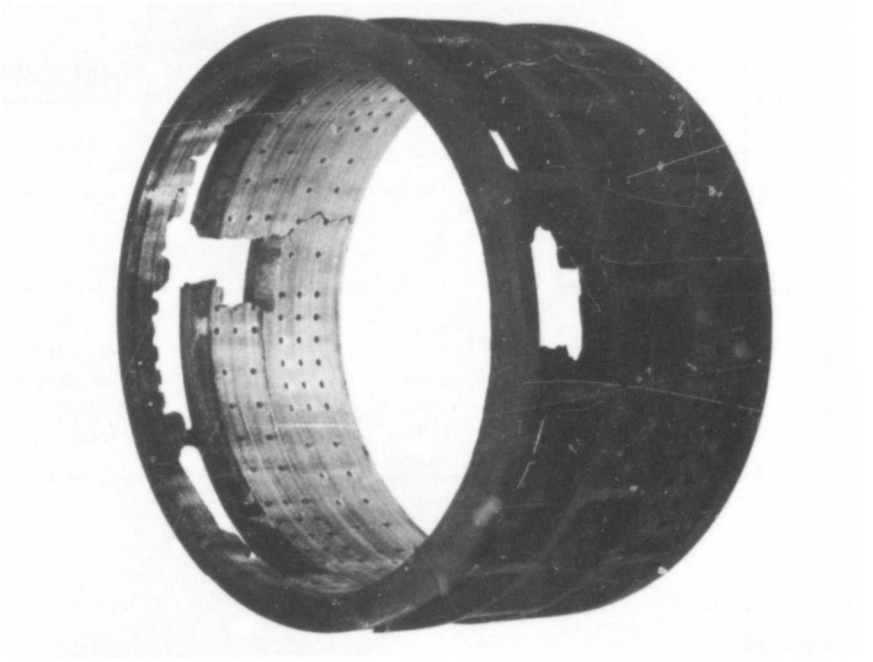

Figure 52. Dual Open Area Ablative Liner Post-Test No. 118.01 FE 77163

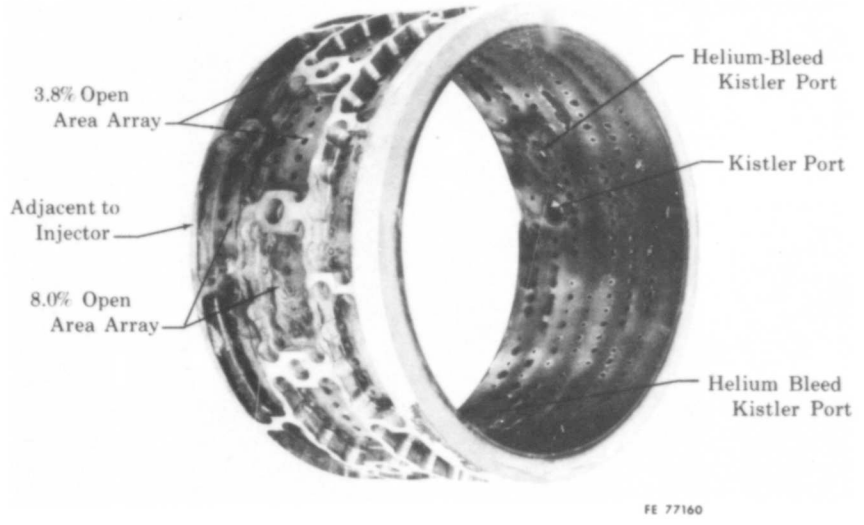

Figure 53. Dual Open Area Uncooled Liner Post-Test No. 122.01 FD 24785

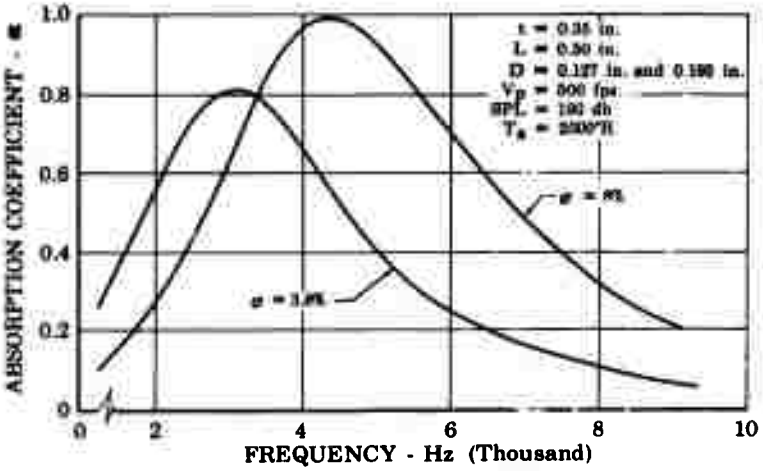

Figure 54. Absorption of Reworked Steel Liner FD 24782

A comparison of the design curves from the dual open area steel liner with the dual open area ablative liner indicates that the steel liner had approximately one-half the total absorption coefficient of the ablative liner at the second radial mode, i.e., 37 vs 71%. Since the ablative liner suppressed all of the instability in the motor, it was concluded from the data that the dual open area steel liner did not have enough total absorption to suppress the motor instability for the high frequency range.

Table XII. Dual Open Area Steel Liner Tests

Test No.	Test Duration - sec	Injector Mixture Ratio	Chamber Pressure - psia	Combustion Efficiency, c* - %	Perturbation Amplitude - P/P as % of P_c	Decay Time - msec	Time Perturbation Initiated After Ignition - sec	Comments
119.01	0.62						0.52	Spontaneous pop or about 70 psi initiated high frequency instability that ended with an RCC abort in 100 msec.
120.01	1.05	1.92	180	94	68	10	0.41	
					80	30	0.53	
					72	15	0.62	
					81	21	0.77	
					75		0.85	RCC abort in 0.270 sec.
121.01	3.00	1.91	174	89	70	5	1.14	
					96	8	1.52	
					94		1.56	High level instability pop at 0.130 sec.
					90	11	2.07	
					88		2.22	
122.01	3.00	1.90	184	95	70	10	0.55	1 to 5 Filter installed on test oscillograph and RCC starting with test 122.01.
					89	22	0.58	
					91	11	0.88	
					100	45	0.91	Steady-state levels less than 10 psi; very stable test.

SECTION VI
TRANSPIRATION-COOLED LINER PROGRAM

The heat fluxes experienced in rocket engine combustion chambers pose serious cooling problems to sound-absorbing liners. The traditional convectively cooled screech liner used in air-breathing applications would stand little chance of surviving the environment of a high pressure rocket chamber. On the other hand, the cooling techniques currently being experimented with for high pressure applications, such as the wafer-cooled chamber, may have only slight absorption capabilities. It was therefore necessary to accurately determine the absorption capabilities of candidate chamber surfaces in the presence of cooling flows and to attempt improvement of this capability where necessary.

Original plans for the program included the analysis, design, and hot firing of two different types of transpiration-cooled chambers: a nonresonant liner fabricated from a porous pressed-and-sintered material and a wafer-type chamber similar to those presently under development for high chamber pressure applications. The work performed in the design and evaluation of each type of liner is discussed in the following sections.

A. RIGIMESH LINER

The design of a nonresonant liner, such as the Rigimesh liner shown in figure 55, must be concerned with both the heat transfer and acoustic characteristics of the material. The cooling ability of the assembly is influenced primarily by the pressure drop and flowrate of coolant, while the acoustic characteristics are determined by the particle size and permeability of the wall material. To determine a workable set of the above parameters, a particular type of porous material was selected; then both a heat transfer and acoustic analysis were performed.

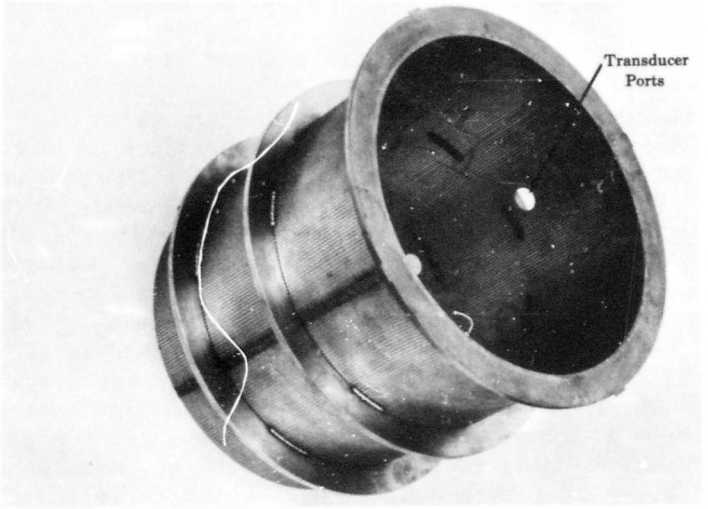

Figure 55. Rigimesh Absorbing Liner FD 9831

A review of product information files revealed several different types of porous materials, both ceramic and metals, that could have possibly been used for nonresonant liner applications. The particular material selected for this program, Rigimesh, manufactured by Aircraft Porous Media, Inc., was chosen because the particular method of fabrication, pressed-and-sintered wire mesh, produces a structure that has good strength and flow characteristics yet can still be machined and welded as a homogenous metal. In addition, Rigimesh can be fabricated so that a wide range of permeabilities and flow characteristics are available with several different base metals; therefore, the need to compromise a potential liner design because of propellant compatibility problems or flow requirements is unnecessary.

1. Technical Discussion

Heat balance equations were used to determine the amount of gaseous hydrogen flow required to transpiration-cool the N_2O_4/Aerozine-50 motor. The liner wall convective film coefficient (h_B) was computed using the Bartz closed-form equation (Reference 3). The cooling rate required to cool the wall to a given temperature was calculated by equating the heat supplied to the liner wall by combustion and the heat absorbing capacity of the coolant. That is

$$Q_{combustion}\ (Btu/hr) = Q_{coolant}\ (Btu/hr)$$
$$Q_{combustion} = h_B\, A(T_c - T_w)$$
$$Q_{coolant} = \dot{w}\, C_p\, (T_w - T_{in})$$

where

h_B = Bartz convective film coefficient - $Btu/ft^2\text{-}hr\text{-}^\circ R$
A = Liner surface area - ft^2
T_c = Combustion temperature - $^\circ R$
T_w = Liner wall temperature - $^\circ R$
$\dot{w}$ = Cooling required - lb_m/hr
C_p = Specific heat of coolant at constant pressure - $Btu/lb_m - ^\circ R$
T_{in} = Coolant inlet temperature - $^\circ R$

In this type of analysis two assumptions are made: (1) the coolant emerges from the porous wall at the same temperature as the surface and (2) the convective coefficient is not affected by the presence of the transpiration flow. The first assumption is reasonable for wall materials (such as Rigimesh), which act as efficient heat exchanging devices because of the high turbulence levels in the coolant passages. The second assumption, the use of the simple Bartz equation to predict the combustion gas heat transfer coefficient, is justifiable for the following reason. Heat transfer rates to the chamber walls, especially in the vicinity of the injector face, are strongly influenced by the primary injection flow patterns. None of the existing heat transfer theories attempts to consider the effect of the injection patterns on the wall coefficients; therefore, the choice of any one technique becomes arbitrary. The use of a more complex or sophisticated function in an attempt to account for the presence of the coolant would not necessarily reduce the uncertainty in the computation.

The results of the heat transfer analysis are shown in figure 56. If the liner wall is to be held to a temperature of 1500°R or less, a flowrate of at least 0.28 lb_m/sec of gaseous hydrogen is required. After the required coolant flow is estimated, the next step in the porous liner design is to select a material of the correct thickness and permeability so that good absorption coefficients can be obtained with the above flow of coolant passing through the pores of the structure. Hence, an analytical technique for predicting the acoustic characteristics of porous surfaces is desirable. Such a technique was developed under Contract NAS8-11038, Reference 5 . From the results of this work it was determined that the absorption coefficients of nonresonant materials can be calculated only with a prior knowledge of the structure factor. The structure factor used in the calculation of the material surface impedance is a function of the inner structure of the material through which the gas passes. Acoustically, it describes the increase in inertia caused by the motion of the fibers and the constrictions through which the sound wave must pass. Unfortunately, there is no absolute relation that can be used to analytically determine the structure factor of any given porous material. Empirical generalizations of data have been made, but the results are only approximate and cannot be used with any degree of confidence. Therefore, it is necessary to either assume the structure factor or measure the surface impedance of a nonresonant material before calculating the absorption coefficient.

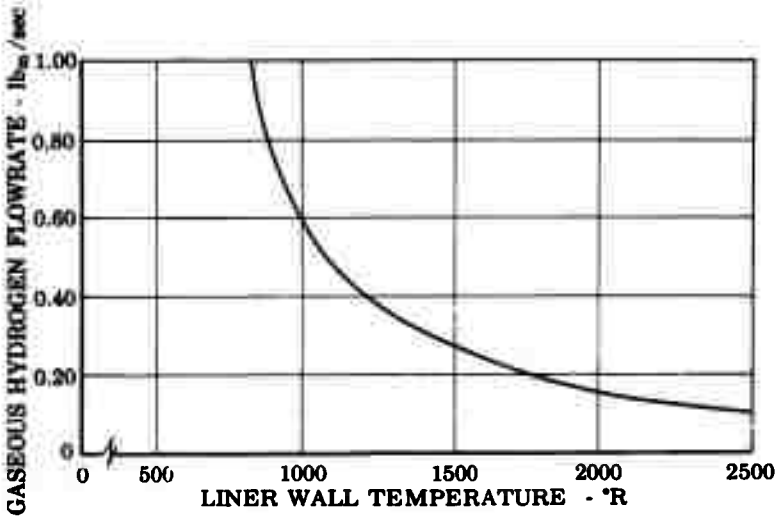

Figure 56. Transpiration Liner Cooling Requirements FD 24513

No data on the structure factor of the absorption coefficients of Rigimesh material were available, so a number of samples with various flowratings (permeabilities) and thicknesses was supplied by the manufacturer for testing in the P&WA impedance facility.

The pressure drop across the wall of a porous liner should be high to ensure that the flow distribution is uniform over the liner surface. In addition, with a low flowrate (such as that required for a liner in the 5K test motor) a high density, i.e., low flowrating, porous material must be used or the pressure drop across the wall becomes so minute that control of the coolant supply pressure becomes extremely critical.

Preliminary pressure drop calculations indicated that a Rigimesh wall with a flowrating of 45 scfm was necessary for flow control purposes; therefore, the high-density Rigimesh sample (45 scfm[1] and 0.250 in. thick shown in figure 57) was tested on the low-frequency impedance tube (figure 58) to determine if, in addition to flow control, the sample would yield high sound absorption. Tests were conducted both with zero flow and with flow-through (GN_2). As shown in figure 59, the sample was found to have poor absorption characteristics, and no effects of flow on absorption were discernible.

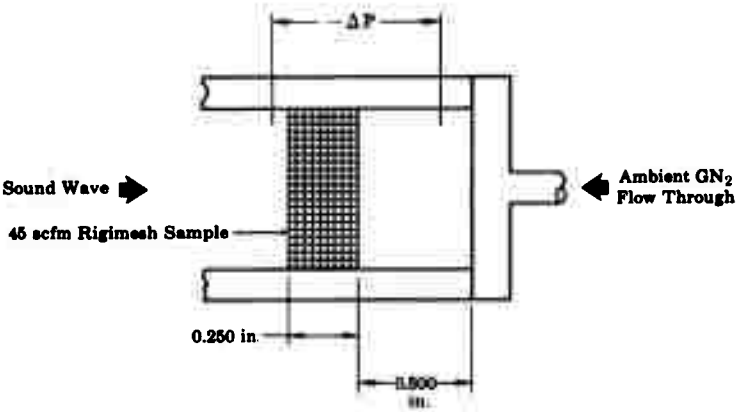

Figure 57. 45-scfm Rigimesh Sample FD 24514

In an attempt to improve the absorption coefficients, a 300-scfm Rigimesh sample, also 0.250 in. thick, was placed in series with the 45-scfm sample and tested (figure 60). Improvement in the absorption coefficients (figure 61) were noted over those of the 45-scfm sample by itself and, in addition, the absorption was found to vary inversely with the differential pressure across the sample.

[1]The standard cubic feet per minute of flow was rated with standard ambient air over a 1-ft^2 cross section with a differential pressure across the sample of 2 psi.

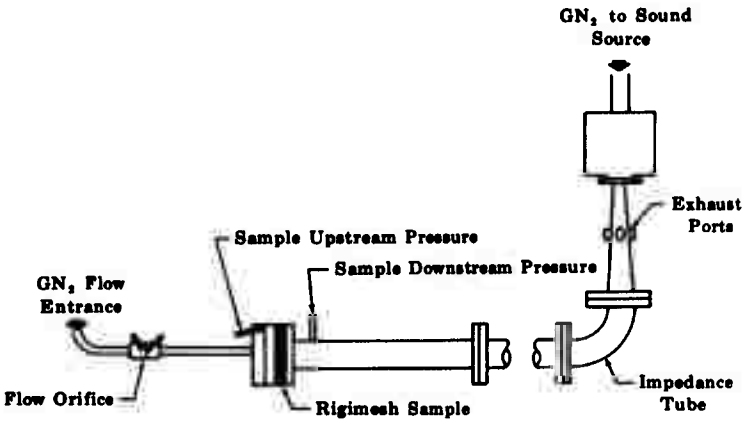

Figure 58. Low-Frequency Impedance Tube FD 22235

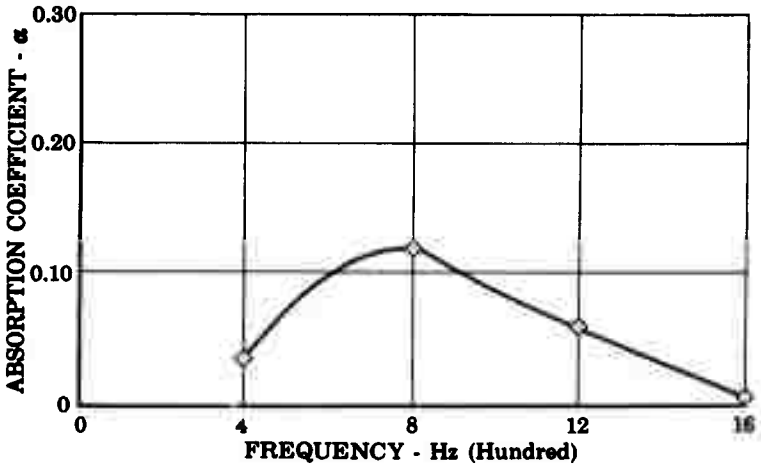

Figure 59. Impedance Tube Data for 45-scfm Rigimesh Sample - 0 to 8 psi ΔP Across Sample at 146 db Total FD 24515

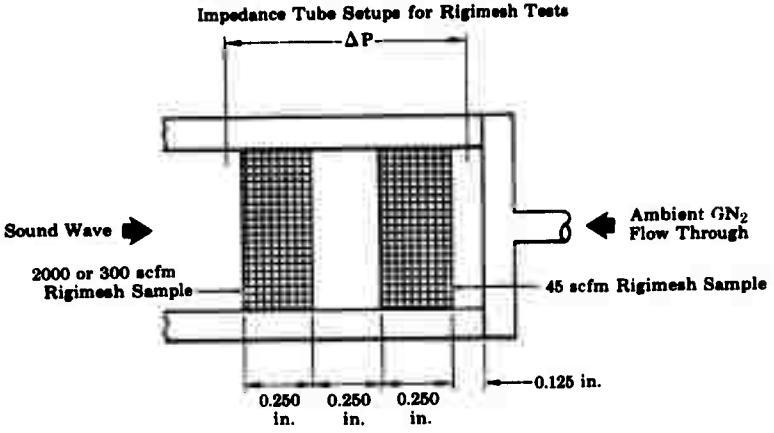

Figure 60. 2000- and 300-scfm Rigimesh Samples in Series with 45-scfm Rigimesh Sample

FD 24516

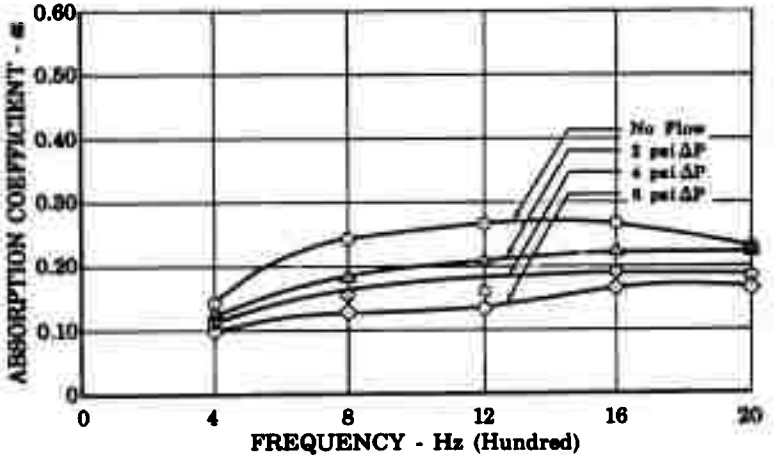

Figure 61. Impedance Tube Data for 300- and 45-scfm Rigimesh Samples in Series

FD 24517

A 2000-scfm Rigimesh sample was then tested in series with the 45-scfm sample to determine if further improvement in absorption would be effected. A vast improvement in absorption occurred over the first two configurations (figure 62). Figure 63 shows comparative zero flow data for the three different configurations.

The previous experiments have shown that a series arrangement of a high density sample and a low density sample can provide flow control as well as high absorption. There are limitations, however, in the data. The highest frequency tested was 2000 Hz; higher frequencies must be investigated for the design of a transpiration liner for hot tests since instabilities can occur at much higher frequencies. Also, the impedance tube absorption data taken in a gaseous nitrogen environment must be extrapolated to determine absorption values for hydrogen at the hot test temperatures and pressures.

The program consultant, Dr. Uno Ingard, suggested that the impedance tube data be extrapolated to actual hot test conditions by keeping the ratio of λ to $(t + L)$ constant, where λ is the wave length of the incident pressure wave and $(t + L)$ is the total thickness of the porous sample or liner (Rigimesh) and the backing cavity. Figure 64 illustrates the extrapolation of impedance tube data to hot test conditions. With this method, the same wave phase angle exists in the impedance tube sample assembly when tested with GH_2 and in the hot tests using hydrogen, so that theoretically the same absorption coefficients will be obtained. This theory is based on the following observation: if the incident sound pressure is in the linear regime, maximum absorption can be obtained with a given porous material when $(t + L) = \lambda/4$, because the maximum particle velocity occurs in the sample, therefore the maximum wave energy is dissipated. In the nonlinear regime (i.e., incident sound pressure levels higher than approximately 120 db), maximum absorption does not necessarily occur in a porous sample when $(t + L) = \lambda/4$ because of the complex turbulence patterns that exist within the interstices of the material; however, if the ratio of assembly to wave length for two different porous absorbers is the same, then for a given incident SPL the turbulence levels and thus the absorbing characteristics will be the same.

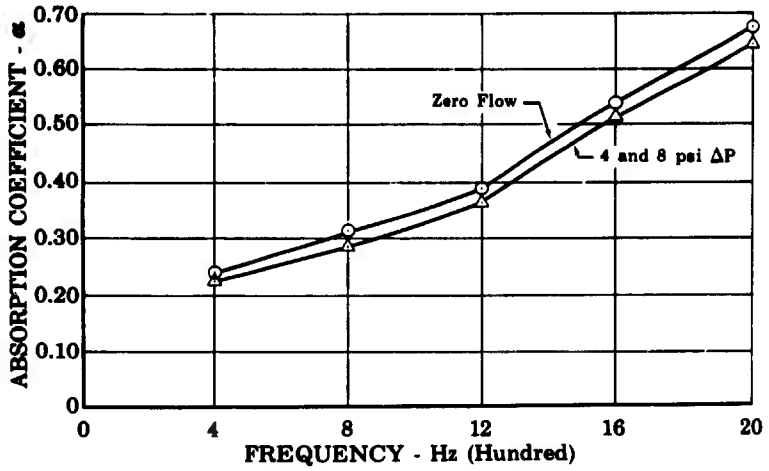

Figure 62. Impedance Tube Data for 2000- and 45-scfm Rigimesh Samples in Series - 146 db Total

FD 24518

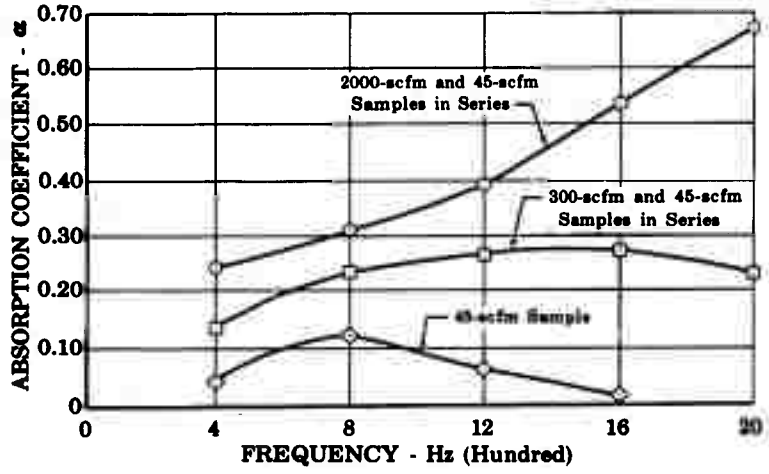

Figure 63. Zero Flow Impedance Tube Data for Rigimesh Samples - 146 db Total

FD 24519

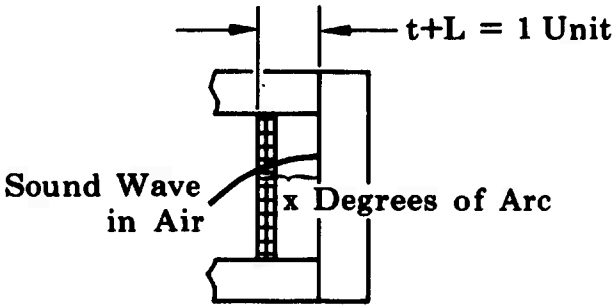

Cold Flow Impedance Tube Test Setup

Define λ Air = 1 Unit
(t+L) Air = 1 Unit
then λ GH_2 (1000 psia and 1500°R) = 6.4 Units
$\lambda/(t+L)$ Air = $\lambda/(t+L)$ GH_2
(t+L) GH_2 = 6.4 (t+L) Air

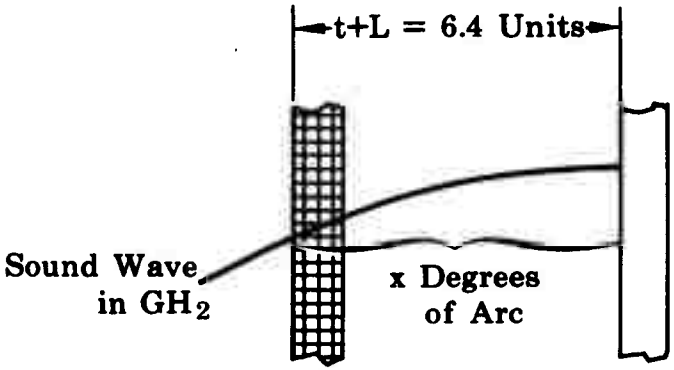

Equivalent Liner Design Applying Constant $\lambda/(t+L)$ Ratio

Figure 64. Constant $\lambda/(t + L)$ Illustration for Extrapolation of Impedance Tube Data to Liner Design

FD 24520

Using this technique it was found that the ratio of λ for hydrogen at 1500°R and a pressure of 1000 psia to that of nitrogen at ambient conditions is approximately 6.4 for any particular frequency. To maintain a constant $\lambda/(t + L)$ ratio, the thickness of the hydrogen-cooled porous liner and backing cavity must be 6.4 times larger than that of the sample assemblies used to obtain the basic impedance data.

To determine the nonlinear absorbing characteristics of Rigimesh at high frequencies, a number of samples described in the following table were tested in the P&WA high-frequency impedance tube facility (Reference 4) at frequencies up to 6000 Hz at a total sound pressure level of 151 db:

Sample No.	Rayls	Thickness - in.
1	5	0.0315
2	11	0.037
3	29	0.041
4	56	0.0315

Rayls are a measure of the permeability of Rigimesh samples, where:

$$\text{Rayls} = 2261.5 \ \Delta P/V$$

ΔP = Differential pressure across the sample - $lb_f/in.^2$

V = Flow velocity through the sample - ft/sec.

Figure 65 shows the absorption coefficients of the samples with a backing distance of 0.100 in. The sample with the highest resistance, 56 rayls, provided the best absorption values. This sample had a zero flow absorption of at least 17% at all frequencies between 3250 and 6000 Hz. (Phase I test results, Reference 1, showed that resonant liners with at least 17% absorption coefficients were necessary for stable operation of the test motor.) The 56-rayl sample was then tested with larger backings to determine if the absorption of the sample would be improved. The largest backing tested, 0.400 in., provided excellent absorption from about 2500 to 6000 Hz (figure 66).

Although the absorption of the 56-rayl sample was much better with a backing of 0.400 in. than with a backing of 0.100 in., the larger backing value is unrealistic because of physical size limitations in the pressure shell of the test motor, i.e., a total of only 0.850 in. is available between the liner inner diameter and the chamber inner diameter. This distance must accommodate a Rigimesh liner for absorption, a backing distance or annular gap, a high-density Rigimesh liner for flow control, and a thin annulus for coolant entry. Applying the extrapolation of impedance tube data to actual hot test conditions, the annular gap in the test motor that is equivalent to the impedance tube backing of 0.400 in.

is about 2.56 in. The impedance tests conducted with a 0.100-in. backing are more representative of a feasible design, since this distance only requires an equivalent backing distance of 0.640 in. in the test motor.

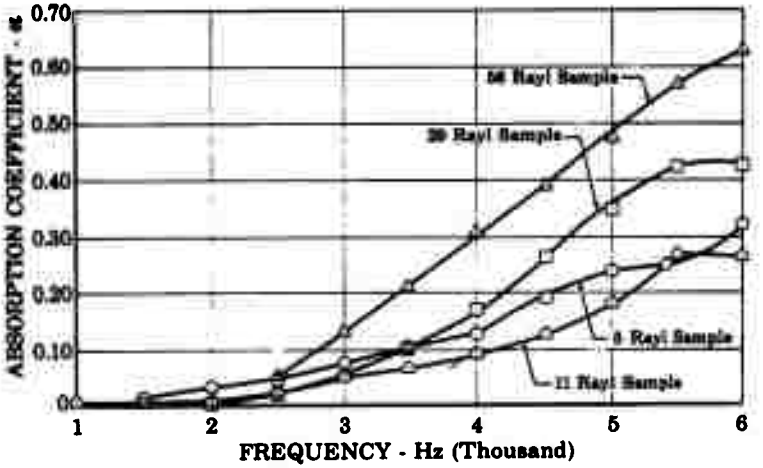

Figure 65. Zero Flow Impedance Tube Data for Rigimesh at 151 db Total - L = 0.100

FD 24542

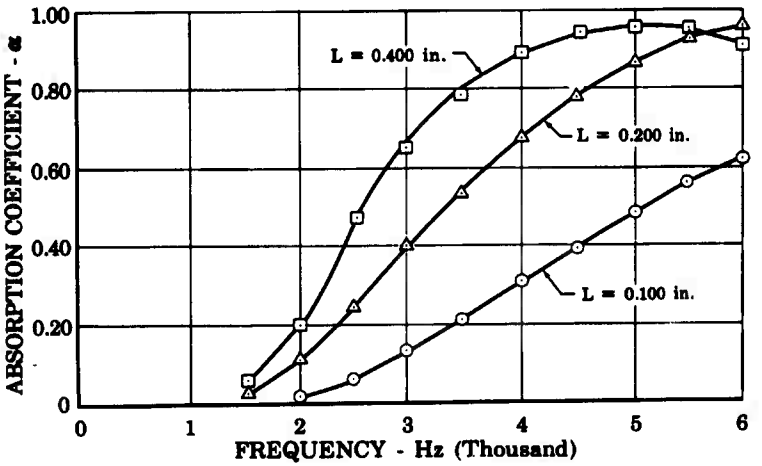

Figure 66. Zero Flow Impedance Tube Data for 56 Rayl Rigimesh Sample at 151 db Total

FD 24541

Additional Rigimesh samples of various flowratings and thicknesses were tested on the impedance tube in an attempt to find a porous facing that would provide adequate absorption, i.e., a coefficient of at least 17% over a range of frequencies from 2 to 5kHz, with backing cavity depths that could be utilized in the test motor. The data from the assembly that provided the best absorption, a 140-rayl sample that was tested with backing depths of 0.10 and 0.05 in., are shown in figure 67. As may be noted from the figure, the absorption of the best assembly failed to produce adequate absorption at frequencies less than 2500 Hz, the region where the most destructive mode of instability was known to occur in the test motor. Based on these results it was concluded that it would not be possible to fabricate a Rigimesh liner of the type necessary to suppress the combustion instability in the available 5K test motor. After consulting with the AFRPL Project Engineer it was decided that in view of the unrealistically large cavity depths that would be necessary the fabrication of a new test motor pressure shell to accommodate the Rigimesh liner was not warranted; thus, further efforts under this portion of the transpiration-cooled liner program were abandoned.

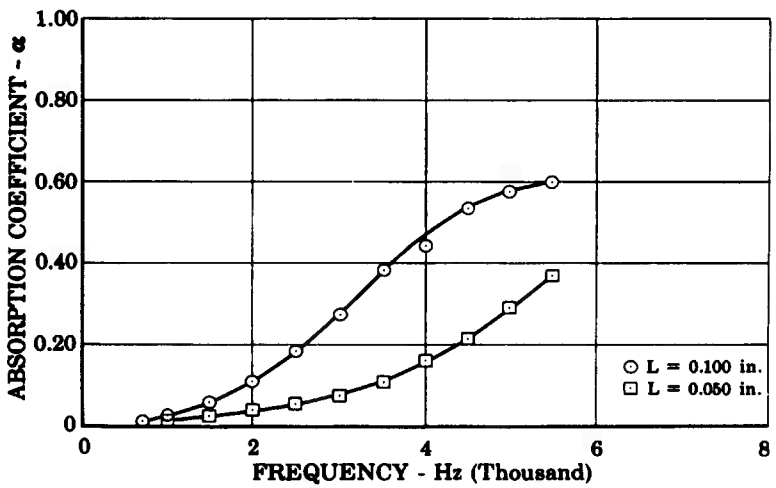

Figure 67. Absorption Coefficient vs Frequency: 140 Rayl Sample, t = 0.040 in. at 151 db Total FD 24525

2. Recommendation

The above decision does not intimate that Rigimesh or other porous materials are poor candidates for absorbing liner applications. For many rocket applications, e.g., where unlimited cavity volumes were available or in small motors in which the natural modes of instability occur at frequencies above 2500 Hz, the use of a Rigimesh liner would appear entirely feasible. For this reason it is recommended that the research devoted to the evaluation of porous liner suppression characteristics be continued using a test motor more suitable than was available for the present program.

B. WAFER LINER

The objective of the wafer chamber program was to determine experimentally the effectiveness of nonresonant wafer-type transpiration cooled acoustic liner for suppressing combustion instability in a rocket motor.

Analytical studies were first conducted to determine the feasibility of using a wafer-type combustion chamber cooled with gaseous hydrogen as an effective combustion instability suppressor; cold-flow impedance experiments were conducted to supply data for the analysis. Design techniques were developed from the studies and used in the design of test hardware. Tests were conducted with N_2O_4/Aerozine-50 propellants at nominal chamber pressures of 200 and 800 psi and sea level conditions.

1. Design Analysis

The predominant purpose of a wafer-type combustion chamber is to provide a method of primary cooling. The cooling principle is basically a transpiration-cooling scheme in that the coolant passes through the chamber wall, via coolant slots, into the hot combustion gas boundary layer with the effect of reducing heat flux to the wall. The coolant passages are slots etched or milled into the faces of plates, which are held in place by tie bolts or are brazed together. The wafer cooling method is efficient primarily because of the axial and circumferential uniformity of the wall coolant flow profile.

The design of a wafer-type acoustic liner must incorporate a means of suppressing combustion instability without sacrificing cooling abilities. Thus, it is necessary to attempt to optimize a particular design with regard to both acoustic and cooling performance. Unfortunately, compromises must be made to achieve a design that is functional in each area. For example, high coolant flow velocities are desirable for cooling considerations but detrimental to absorption characteristics; some tradeoff, therefore, is necessary.

Typical wafer plates are shown in figure 68. Coolant slots are cut into both sides of each plate so that the coolant enters the chamber tangentially. The wafer plates are stacked and held together with tie bolts to form a liner assembly. The initial concept of modifying wafer plate design, so that acoustic absorption would be obtained, simply involved the addition of circular cavities into each coolant slot as shown in figure 69. Each wafer plate would then represent a series of individual resonators. In a design such as this, each resonator is characterized by a particular aperture hydraulic diameter, thickness, and individual cavity volume. This type of configuration was desirable since so little modification to the proven wafer-chamber-cooling design was necessary.

To predict the absorption characteristics of a wafer chamber incorporating individual resonators, two problems had to be solved. The first concerned the ability to predict the absorption of a resonator with an irregular-shaped cavity volume, and the second was the ability to predict the absorption of resonators fewer in number from those found in array but possessing an equal incident area.

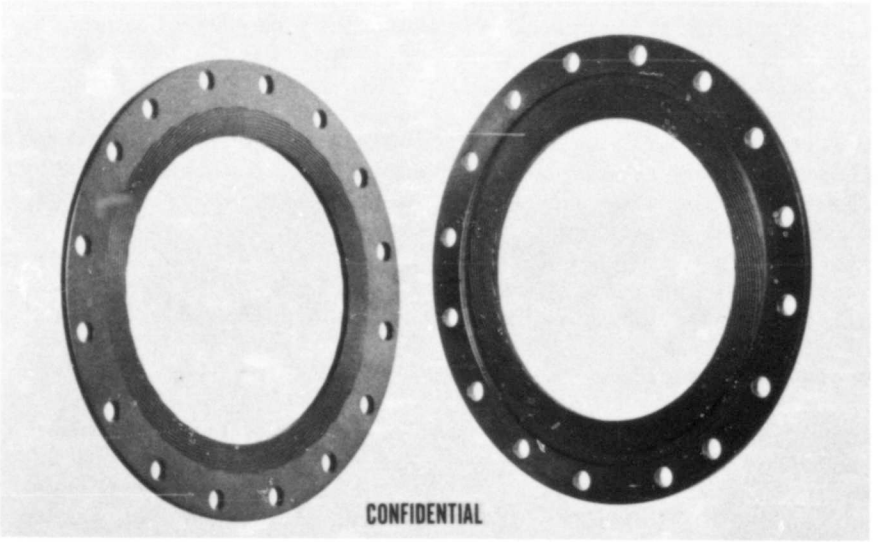

Figure 68. Copper Wafers Used to Fabricate Cooled Thrust Chamber FEC 35910

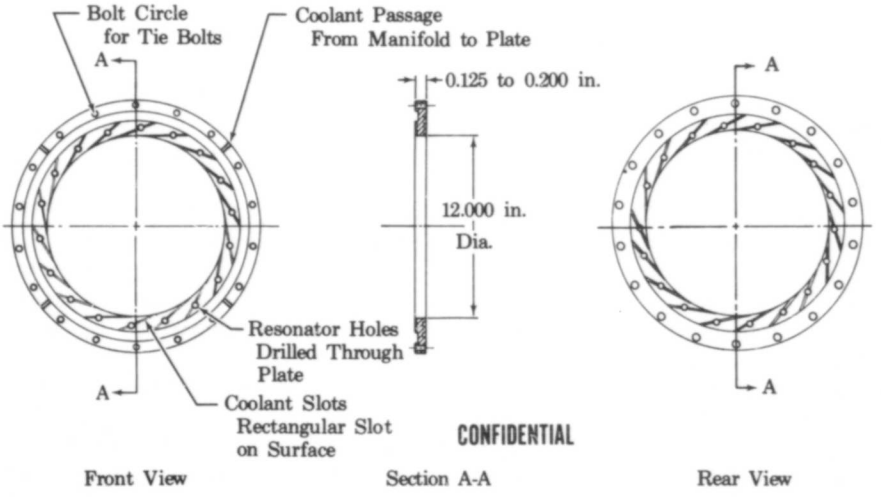

Figure 69. Wafer Chamber Plate FDC 19518

A conventional Helmholtz resonator array (figure 70) is a square geometrical pattern with each resonator defined in terms of aperture diameter, aperture thickness, backing distance, and open area ratio.

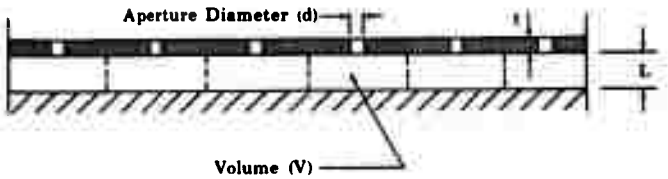

Figure 70. Parallel Resonator Array FD 20825

If σ is defined as the fraction of open hole area, then for an array of resonators:

$$\sigma = N \frac{\pi}{4} d^2 = N (A_1)$$

hence:

$$\frac{A_1}{V} = \frac{\sigma}{L}$$

$$\sigma = A_1/A_2$$

where:

N = Number of holes/unit area

d = Diameter of holes

A_1 = Cross-sectional area of a single aperture

A_2 = Cavity area for volume (V)

When an arbitrarily shaped cavity volume (see figure 71) is considered, some of the above terms cannot be defined. The configuration still has a certain aperture diameter and aperture thickness, but the backing distance and open area ratio have no meaning.

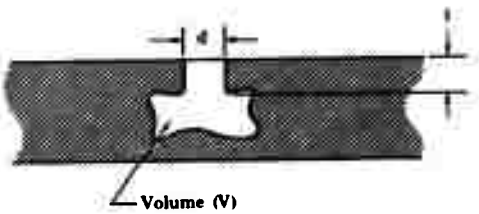

Figure 71. Arbitrarily Shaped Resonator FD 20826

To investigate the effects of arbitrarily shaped cavity volumes on the acoustic design theory, a series of experimental cold flow tests was conducted using the Pratt & Whitney Aircraft impedance tube facility (Reference 1). Two samples each with an equal number of individual resonators were tested. The aperture diameter, thickness, and cavity volume were the same for each resonator; however, one sample had cylindrical cavity volumes whereas the other sample had cavity shapes like those proposed for the preliminary wafer-liner design. Test results are shown in figure 72. Note that absorption coefficient values and, as expected, the resonant frequency are the same for each sample. It was therefore concluded that the proposed wafer-type resonator with the irregular-shaped cavity volume would have the same absorption characteristics as a conventional resonator, i.e., cavity contour has no effect on the ratio of absorbed-to-incident energy.

The initially proposed wafer-liner design would be comprised of a certain number of individual resonator assemblies spaced so that the incidence area was greater than that of the active area, i.e., the area backed by resonator cavities. A method exists, Reference 2 , for predicting the absorption of a resonator array in which the sum of cavity cross-sectional areas equals the incidence area, figure 70. However, no method was known for predicting absorption of an array when the sum of the cavity cross-sectional areas is less than the incidence area, figure 73.

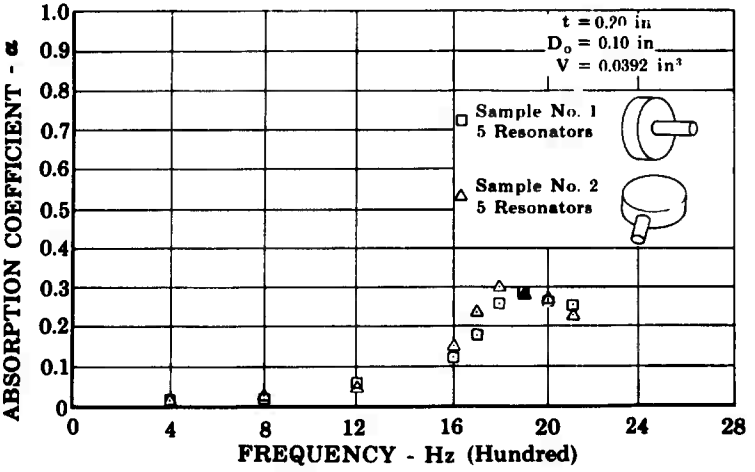

Figure 72. Absorption vs Frequency for Wafer Samples

FD 20828A

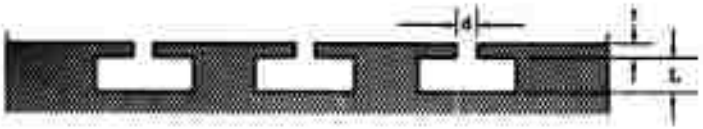

Figure 73. Individual Resonators of Equal Volume FD 20827

A series of experiments were conducted using the impedance tube to determine the relationship between absorption and the number of equal-volume resonators for a constant incidence area. The sample with cylindrical cavity volumes used in previous experiment was reworked so that the number of resonators within a constant incidence area could be varied. Results are shown in figures 74 and 75. From figure 74 it is evident that a nonlinear relationship exists between percentage of absorption obtained and the ratio of total cavity cross-sectional area to incidence area. The limit in figure 74 is represented by a conventional resonator array. In figure 75 the same comparison of results is made on an absorption versus frequency diagram. Note that the number of resonators has little effect on absorption at the lower frequencies.

From these results it was concluded that, to arrive at a suitable solution for predicting the absorption of an individual resonator wafer liner, the array prediction values may be used as an upper limit. The actual absorption for a number of resonators over a fixed incidence area, all other parameters constant, may then be determined from a diagram such as that shown in figure 74.

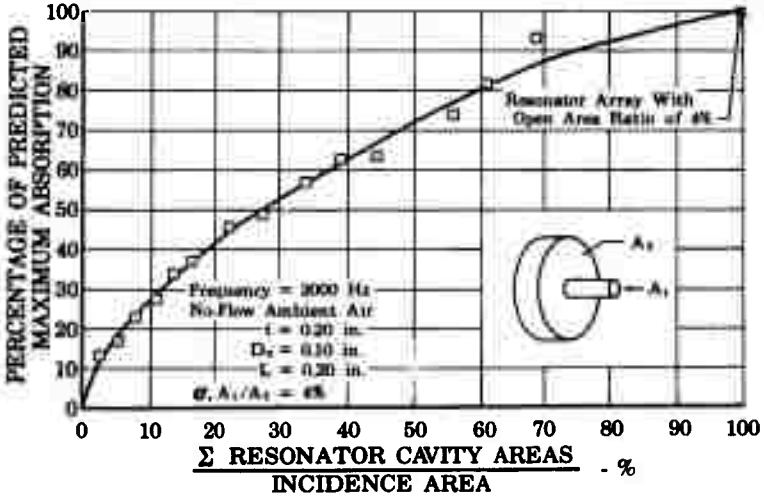

Figure 74. Absorption vs Number of Resonators for Constant Resonator Size and Incidence Area FD 20829A

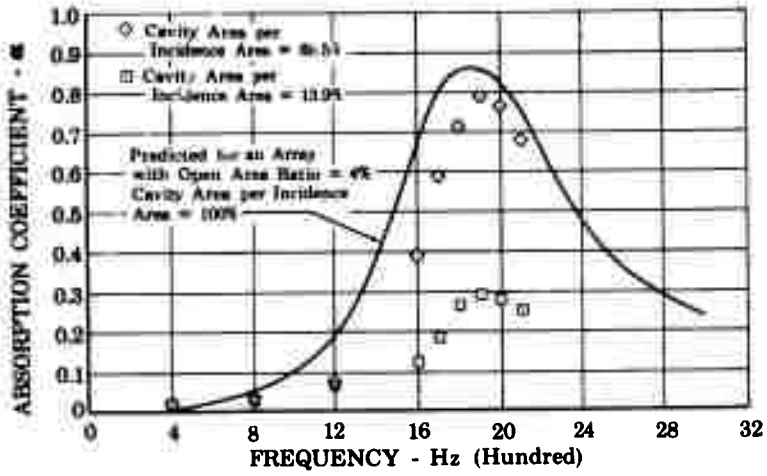

Figure 75. Absorption vs Frequency for Different Numbers of Resonators

FD 20830B

Methods have thus been established to confront the two main problems presented by the preliminary wafer design, i.e., the inability to predict absorption characteristics of the irregular-shaped cavity volume resonator and the nonarray individual resonator. However, it remained to be established whether the scheme would provide a sufficient amount of total absorption. To answer this question, a parameter study was conducted from which theoretical absorption curves were produced for planned test conditions. It was found that the use of an individual resonator design severely limited the useful range of open area ratio, liner thickness, and cavity volume and no combination that would produce adequate absorption characteristics could be found. Hence, the individual resonator concept was abandoned and efforts were made to design a liner using a concept more like a conventional resonator array.

The acoustic properties of a wafer-type liner with a common cavity volume had never been previously investigated. Therefore, to demonstrate experimentally the absorption characteristics of an array type wafer design, a sample was constructed and tested in the cold flow impedance tube facility. The standard resonator prediction method of Reference 1 was used to obtain a design that would produce good absorption characteristics over the range of frequencies for which the impedance tube could be operated. This design was used as a guide in constructing the wafer impedance sample. The primary objective of such cold flow testing was to investigate the acoustic characteristics of a wafer-liner design under known conditions and, if necessary, to establish a prediction theory using the experimental results as a basis.

The wafer liner facing sample constructed for cold flow tests is shown in figure 76. The experimental tests conducted with the wafer sample were made with GN_2 flow-through Mach numbers, the same as those expected with hydrogen coolant at full chamber pressure conditions in the test motor.

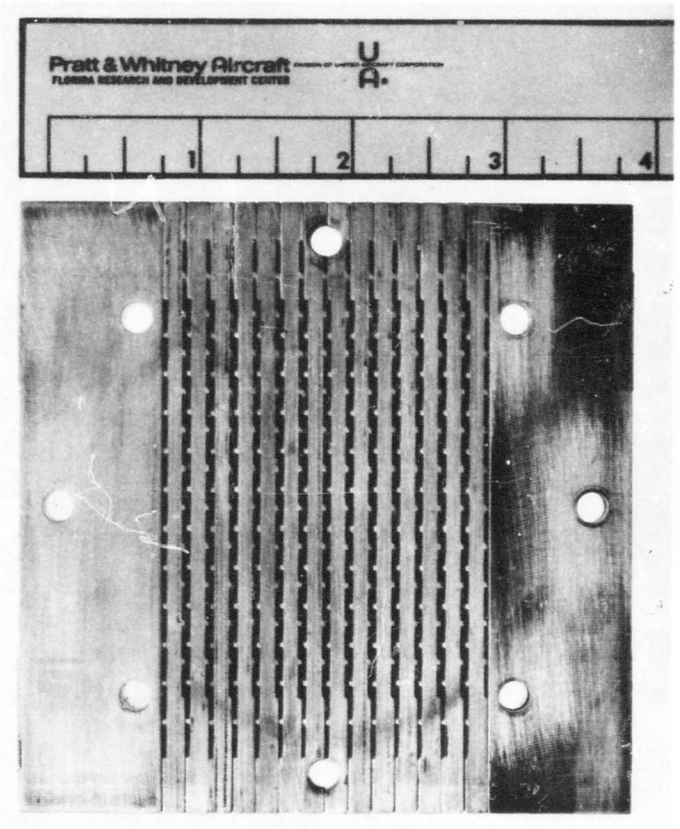

Figure 76. Wafer Liner Cold Flow Test Sample FE 70914

In figure 77 the experimental impedance tube results for one Mach number are shown. Also included in the figure is a theoretical curve based on the conventional Helmholtz resonator array with the same flow-through Mach number. The graph indicates a close agreement between theoretical and experimental absorption amplitudes and resonant frequencies. Theoretical absorption coefficients were calculated using the Helmholtz acoustic theory of Reference 2 , in which the resonator is described by a particular aperture diameter, aperture thickness, backing depth, and open area ratio. The only necessary modification to accommodate the wafer model was the use of the projected slot length T_B (see figure 78, instead of actual slot length T_A, for the aperture thickness. Such agreement between theory and experiment shows that the present acoustic design theory with the modification in the aperture thickness can be applied to the design of wafer-type acoustic arrays with a common cavity volume.

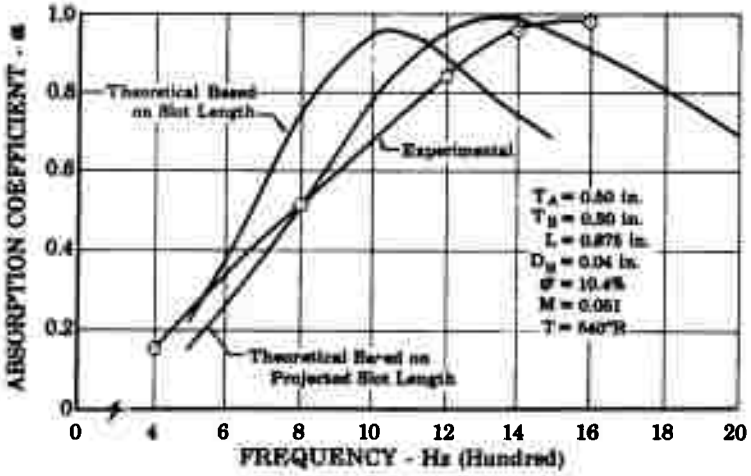

Figure 77. Simulated Wafer Liner Sample Flow-Through Test Results FD 24225A

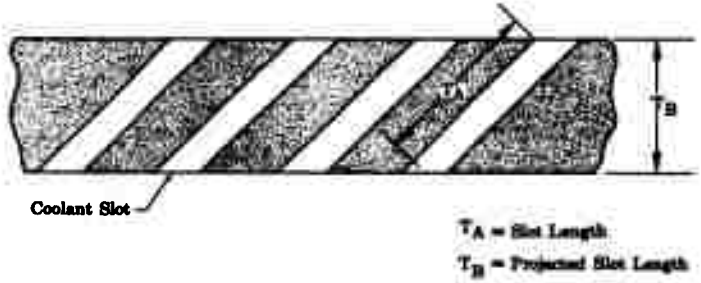

Figure 78. Wafer Coolant Slot Section FD 23106

Theoretical combustion properties were then determined for the conditions under which the N_2O_4/Aerozine-50 wafer chamber was to operate. A wall temperature operating range was selected based upon the properties of the wall material, Nickel 200. The particular material was chosen because it possessed good structural characteristics, high thermal conductivity, and is compatible with the propellants. Heat-balance equations were solved to determine the coolant flowrates necessary to maintain chamber wall temperatures within the established range, i.e., 540°R to 1200°R. This was determined by equating the heat supplied to the liner wall by combustion and the heat absorbing capacity of the gaseous hydrogen coolant. The heat transfer coefficients used to calculate the combustion side heat flux was computed using the Bartz equation (Reference 3). No attempt to modify the coefficient to account for the transpiration cooling was made. It was found that a minimum coolant flowrate of 0.62 lb_m/sec was necessary to maintain the combustion chamber wall at a temperature of less than 1000°R.

Gaseous hydrogen was used as the coolant because neither of the propellants was suitable for use as transpiration coolants. In addition, the cavity of a liner must contain a compressible gas so that the acoustic characteristics of the assembly can be utilized.

The final wafer-liner design was based on the results of a parametric study in which all the possible combinations of liner thickness, open area ratio, aperture hydraulic diameter, cavity volume, and flow-through velocity were considered. The digital computer program of Reference 2 was used to compute the absorption characteristics for each set of parameters. Tradeoffs among the independent variables were made so that a functional design could be obtained. A dimensional description of the liner that was selected from the results of the parametric study is given below:

Aperture hydraulic diameter	0.04 in.
Cavity backing depth	0.40 in.
Open area ratio	0.10
Slot length (actual)	0.60 in.
Slot length (projected)	0.40 in.
Overall liner length	6.45 in.

The theoretical absorption curves for the above liner are shown in figures 79 and 80. The wafer assembly was designed so that it filled the upstream half of the combustion chamber. A total of 29 individual wafer plates were used with coolant slots milled on both surfaces as shown in figure 81. The slots on a given plate surface were machined so that they would, upon assembly, cross the slots on the adjoining plate. The wafer liner assembly is shown in figure 82. Additional information concerning the wafer chamber can be obtained from the assembly and detail design drawings that appear in Appendix B. Photographs of the assembly are shown in figures 83 and 84.

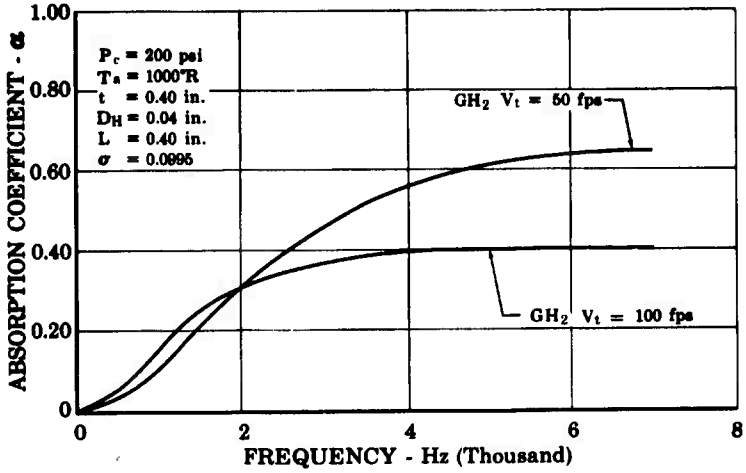

Figure 79. Theoretical Absorption vs Frequency Diagram for 200-psi Wafer Liner

FD 24205

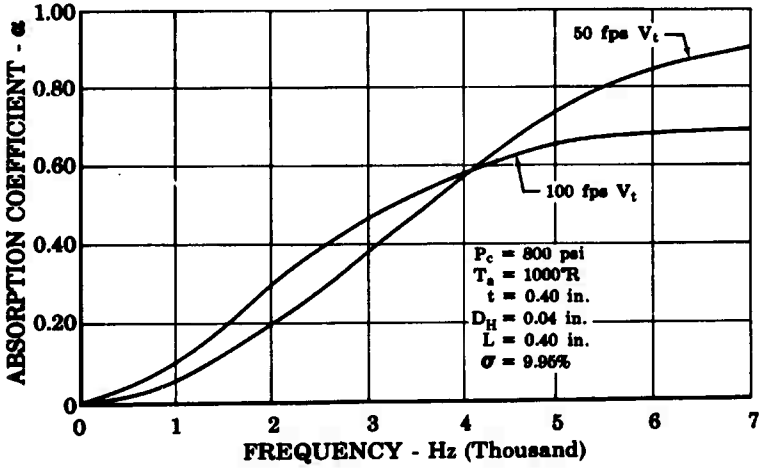

Figure 80. Theoretical Absorption vs Frequency Diagram for 800-psi Wafer Liner

FD 24206

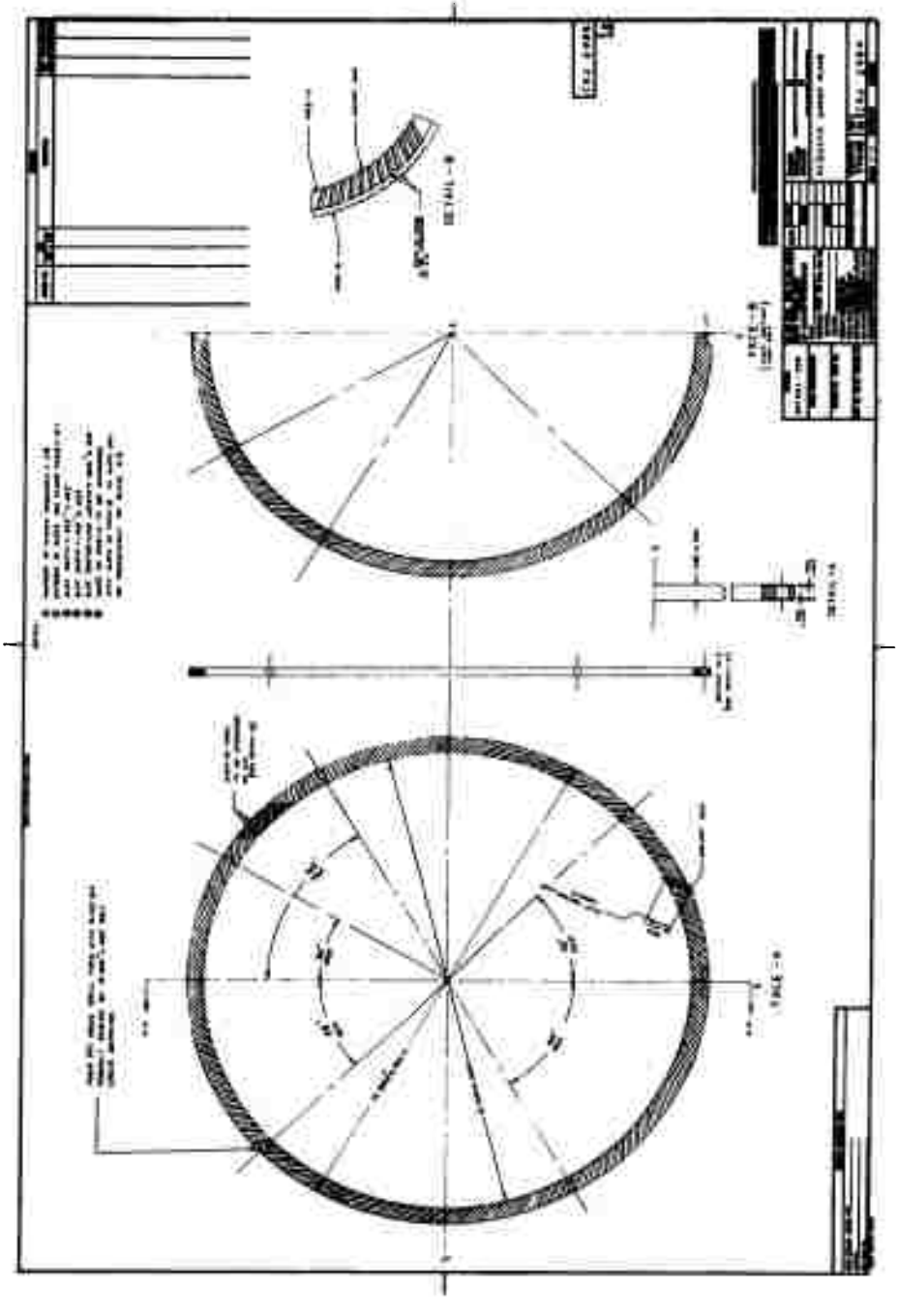

Figure 81. Acoustic Wafer Plate

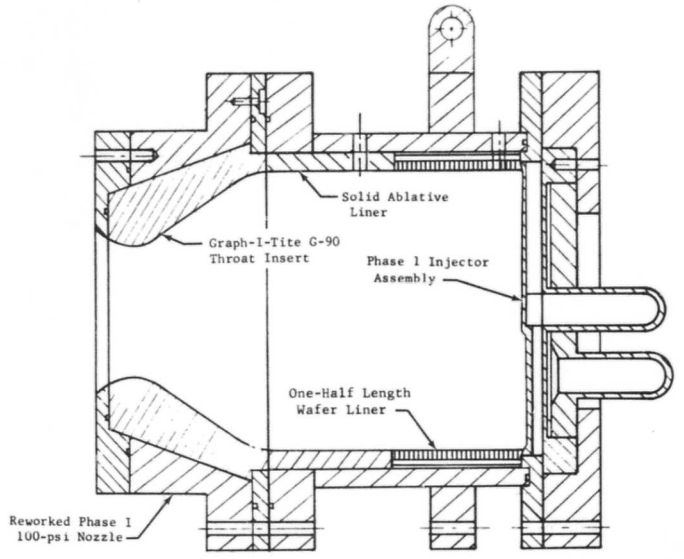

Figure 82. Wafer Liner Assembly FD 25016

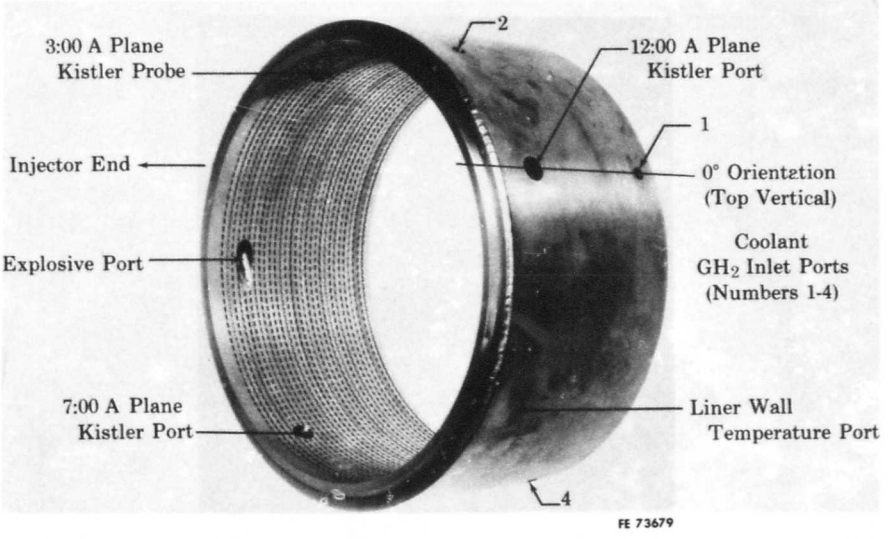

Figure 83. Half-Chamber Length Wafer Liner - Pretest FD 24207

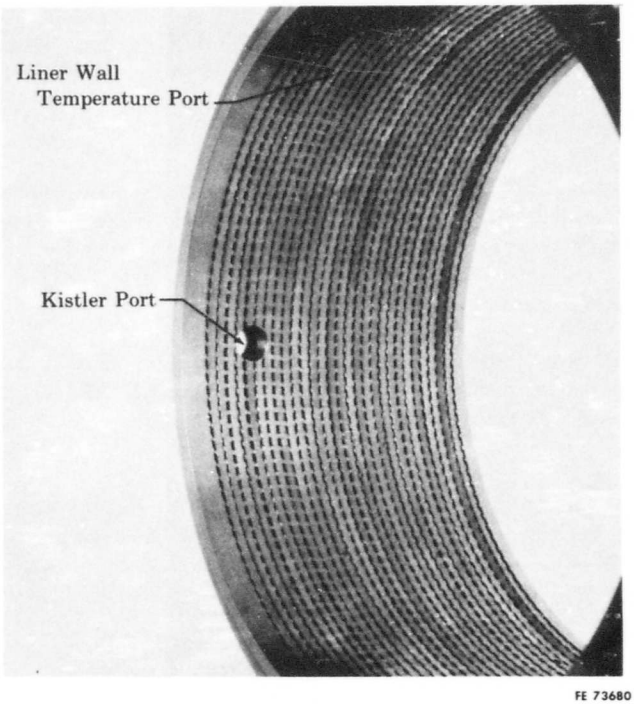

Figure 84. Half-Chamber Length Wafer Liner Closeup - Pretest FD 24208

2. Test Program

Seven firings were conducted utilizing the cooled wafer liner in the 5K thrust chamber. In each case gaseous hydrogen was used as the coolant, with coolant flowrates predetermined by a series of orifice calibrating cold flow tests. To eliminate the threat of high heat fluxes at the start of the test run and after shutdown, the coolant flowrate was allowed to reach steady-state conditions approximately 2.0 sec before startup and until 7.0 sec after shutdown. After the cooled test series was completed four additional firings with no coolant were made.

Dynamic pressure transducers were installed in the combustion chamber to measure the pressure oscillations throughout each test. The transducer type was the Kistler Instrument Corporation Model 603A dynamic pressure transducer. The specific axial and circumferential locations of the transducers within the wafer chamber were as follows:

A-Plane	12:00
A-Plane	3:00
A-Plane	7:00
B-Plane	12:00

A-Plane Kistlers were located 1.6 in. from the injector face and B-Plane Kistlers were located 7.7 in. from the injector face. Circumferential orientation in the combustion chamber is obtained by viewing toward the

injector face. Response tests conducted during the Phase I program, Reference 1 , demonstrated that no signal amplification caused by resonance of the gas in the transducer adapter should be expected at frequencies below 5000 Hz.

Thermocouple probes were installed so that the liner combustion-side surface temperatures and the liner cavity temperatures could be monitored during testing.

a. Preliminary Tests

Two preliminary tests (tests No. 92.09 and 93.01, see table XIII) were conducted at a nominal chamber pressure of 200 psia. Both tests were unstable and were aborted by the Rough Combustion Cutoff (RCC) systems.

The mass cooling flowrate during test No. 92.09 was 0.786 lb/sec and the maximum wall temperature was 850°R. The corresponding values for test No. 93.01 were 0.690 lb/sec and 980°R. Upon disassembly of the motor, no hardware damage or evidence of excessive heat transfer rates was found.

Amplitude/frequency diagrams for the two firings are presented in Appendix B. The data for the two firings are also presented in figure 85 with instability levels represented as percentages of nominal chamber pressure. From this chart the two predominant modes of instability are noted to occur in the 2100 Hz (first tangential) and the 4350 Hz (first radial) range. Instability levels are also noted to be less than 70% of chamber pressure, except for one transducer reading of 178% at the first tangential mode. A high speed oscillograph trace of the Kistler transducer pressure levels for test No. 92.09 is shown in figure 86; the 7:00 A-Plane transducer recorded the highest instability levels (total) and the 12:00 and 3:00 A-Plane traces showed only first tangential mode oscillations.

b. High Chamber Pressure Tests

Original plans for the high pressure test series included firings with coolant flows of 0.50, 0.65, and 0.80 lb_m/sec. Two firings were to be made with each flow; the first was to be a short duration (1.5 sec) firing for checkout purposes, followed by a test of 8 to 10 sec duration to demonstrate the steady-state heat transfer and stability characteristics of the wafer chamber. As shown in table XIII, the first high pressure test (test No. 94.01) was conducted with the highest coolant flowrate. Although some low amplitude (i.e., 10-20 psi) rough combustion appeared, it was damped within 100 msec and the remainder of the 1.47 sec firing was stable. Furthermore, no evidence of excessive heat transfer rates was evident in any of the thermocouple readings.

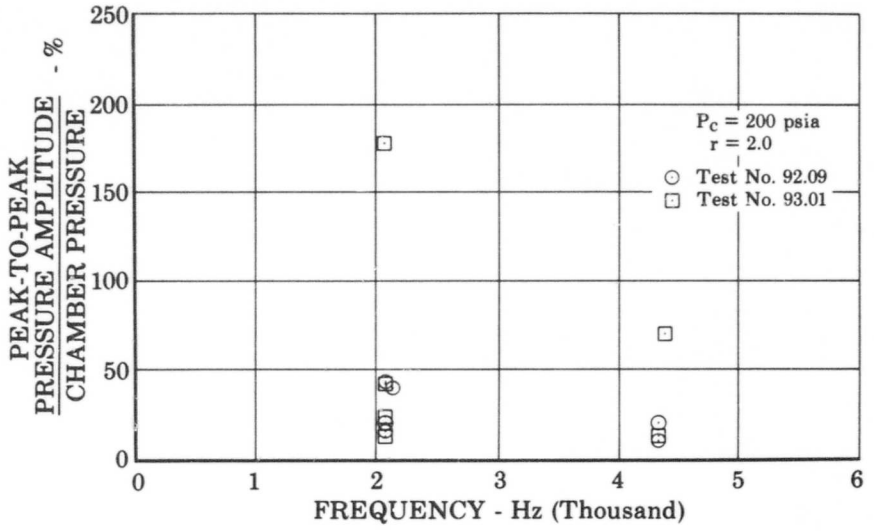

Figure 85. Predominant Frequencies of Instability Wafer Liner - Low Pressure Tests

FD 24209

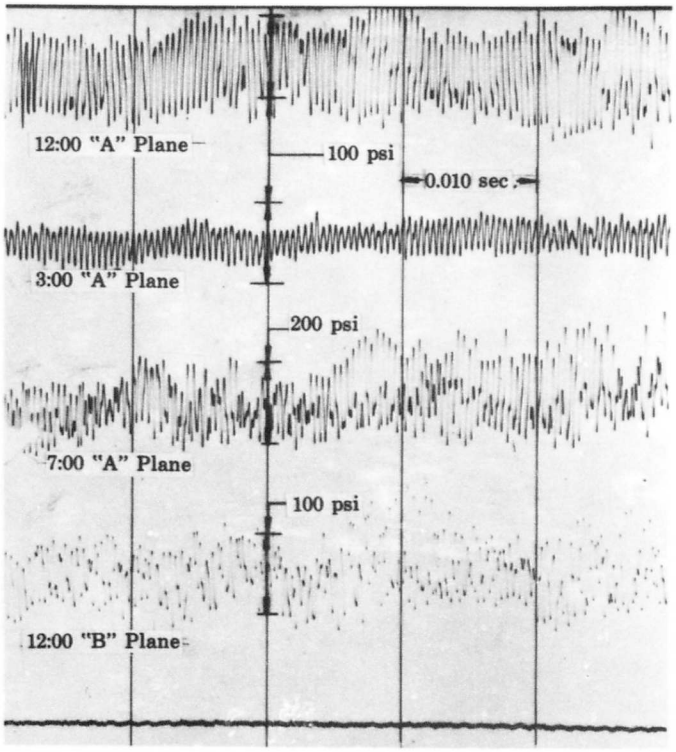

Figure 86. Oscillograph of Kistler Pressure Levels for Test No. 92.09

FD 24238

Table XIII. Perturbation Data for Wafer Liner Tests

Test No.	Test Duration - sec	Injector Mixture Ratio	Chamber Pressure - psia	Combustion Efficiency, η_{c^*}-%	Hydrogen Cooling Rate - lb_m/sec	Perturbation Amplitude - P/P as % of P_c	Decay Time - msec	Time Perturbation Initiated After Ignition, sec	Comments
92.09	1.03	1.99	206	94.5	0.79	58.3 46.1	10	0.43 0.93	Initiated high frequency instability that ended in RCC abort in 100 msec. 12:00 "A" plane levels: 80 psi P/P at 2150 Hz, 22 psi P/P at 4350 Hz. 3:00 "A" plane levels: 30 psi P/P at 2100 Hz.
93.01	0.73	1.88	190	97.0	0.69	65 7		0.60	40 to 140 psi amplitude (total) until RCC abort in 130 msec. 3:00 "A" plane levels: 78 psi P/P at 2100 Hz, 24 psi P/P at 4350 Hz.
94.01	1.47	2.05	896	98.0	0.79	10.6	6	0.70	Starts 10 to 20 psi total amplitude wave for 100 msec; remainder of test completely stable.
95.01	2.30	2.00	899	99.0	0.80	33.4 15.6	5	0.5? 0.89	Starts high frequency instability with total level of 30 to 150 psi P/P until RCC abort at 2.30 sec. 7:00 "A" plane levels: 68 psi P/P at 2200 Hz, 39.5 psi P/P at 2900 Hz.
96.03	1.50	1.96	840	93.0	0.54				No instability; high wall temperature abort (1500°R) at 1.50 sec.
97.02	1.04	..95	805	90.3	0.67	44.7 59.1	12 12	0.73 1.01	50 grain tangential pulse gun. Very stable test except for 2 pops. High wall temperature abort (1500°R).
98.01	1.27	1.94	840	96.0	0.67	33.9 53.6	10	0.83 0.98	High frequency instability for remainder of test; 50 psi P/P total for 150 msec, then 120 to 150 psi P/P total for 120 msec. RCC abort at 1.27 sec. 12:00 "A" plane levels: 126 psi P/P at 2250 Hz, 58 psi P/P at 2900 Hz, 78 psi P/P at 5000 Hz.
125.01	2.08	1.93	187	97.0	0.0				
126.01	2.02	1.95	172	84.0	0.0				
127.01	2.02	1.98	760	96.0	0.0				
128.01	2.00	1.98	744	94.0	0.0				

Attempts to repeat the test, (test No. 95.01) and obtain steady-state data were unsuccessful. Sustained instability with amplitudes greater than 100 psi occurred and the test was aborted after 2.3 sec by the RCC device. Again, no evidence of excessive heat transfer rates was present; therefore, a short deviation firing with the lowest coolant flow was conducted (test No. 96.03). Although this test was completely stable, the wall temperature thermocouples showed that additional coolant was required to maintain the combustion chamber surfaces at a temperature of 1500°R or less. The test was not repeated because a high wall temperature abort occurred just prior to the programed shutdown showing that the motor could not be operated for longer durations with that coolant flowrate.

The next two tests (tests No. 97.02 and 98.0) were conducted with a coolant flow of 0.67 lb_m/sec. Test No. 97.02 was stable for the first second after ignition and, in an attempt to induce instability, a 50-grain charge was fired in the tangential pulse gun. The resulting perturbation was damped within 12 msec, but the test was aborted before the programed shutdown when one of the wall thermocouples recorded a temperature exceeding 1500°R. Analysis of the data showed that the high temperature abort had been caused by an erroneous thermocouple signal and, unlike the previous test, the liner was sufficiently cooled. The test was repeated; however, combustion became spontaneously unstable at approximately 1-sec after ignition, and the RCC device aborted the test 0.3 sec later.

The amplitude/frequency diagrams from the high pressure firings are presented in Appendix B. In figure 87 a summary of the data from the two unstable tests is shown. No peak-to-peak pressure amplitudes exceeded 50% of chamber pressure, but four separate modes of instability were present. The modes correspond in frequency to the first tangential ($\approx$ 2200 Hz), the second longitudinal ($\approx$ 2900 Hz), the first radial ($\approx$ 4400 Hz), and the third tangential ($\approx$ 5000 Hz) modes. As may be noted in the above figure, the highest amplitudes occurred at the lowest frequency and the levels decreased with frequency increase; these results are reasonable since the absorption coefficient of the liner (see figure 80 is lowest at low frequencies and shows improvement with increasing frequency.

The instability modes presented in the amplitude/frequency diagrams are oscillatory in nature and characterized by a particular frequency. Natural disturbances other than the apparent modes also appeared in the dynamic pressure recordings. These aperiodic pressure perturbations (spikes or pops) cannot be classified as instability modes because of the lack of following pressure oscillations and an associated frequency. Table XIII contains pertinent data on these instantaneous pops, such as pressure amplitude and the decay period of the pressure disturbance.

As shown in figures 88 and 89, the area around the pulse gun entrance was found, upon disassembly of the motor, to be covered by a soot-like deposit, probably caused by the rapid burning of the C-4 explosive. Otherwise, the liner remained in excellent condition.

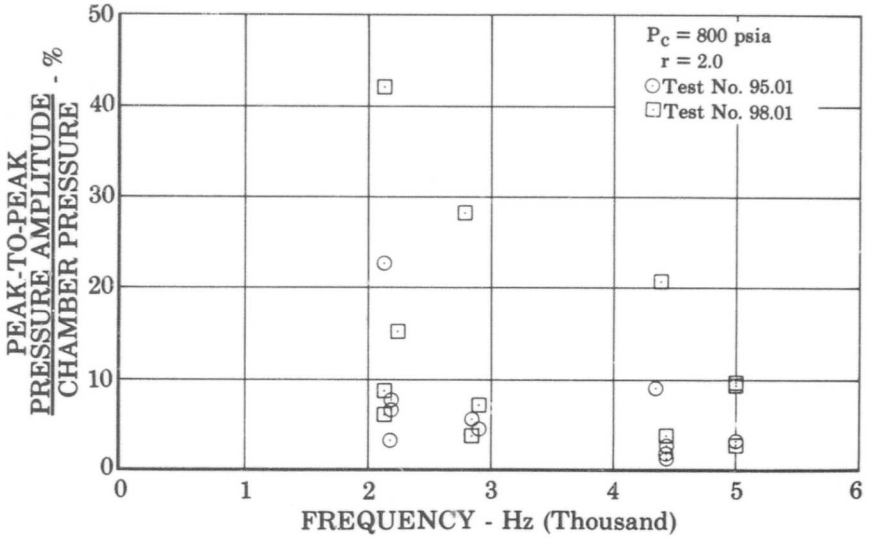

Figure 87. Predominant Frequencies of Instability - Wafer Liner High Pressure Tests

FD 24211

Figure 88. Wafer Liner at End of Test Sequence

FE 73900

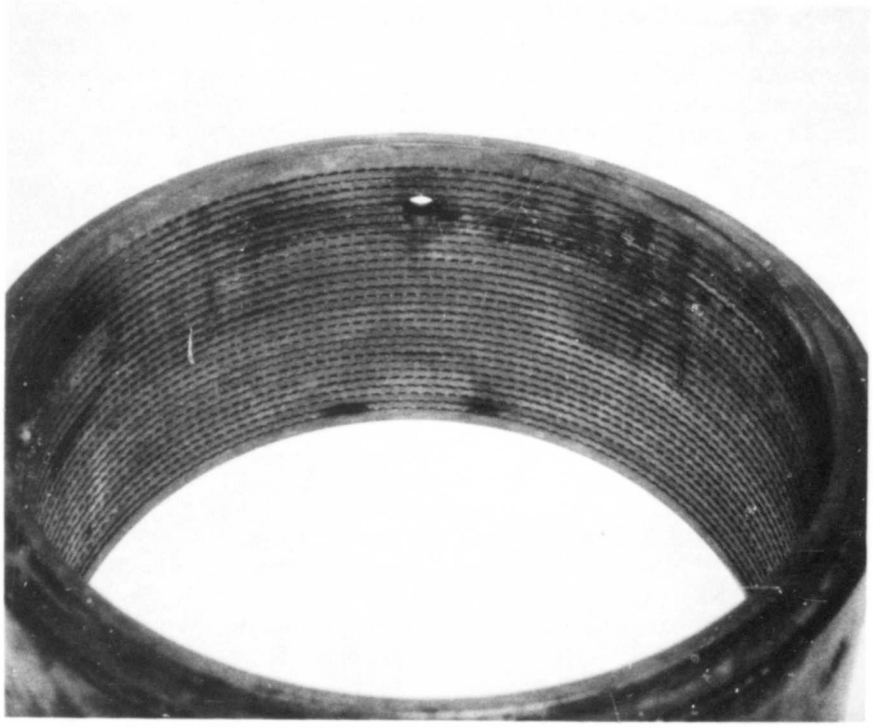

Figure 89. Wafer Liner Closeup at End of Test Sequence FE 73901

C. UNCOOLED TESTS

Analysis of the hydrogen-cooled wafer chamber data showed that the motor was more unstable at the higher chamber pressure than with no liner installed for no pressure amplitudes greater than ±5% of the mean chamber pressure were recorded during the baseline test series reported in Section III. Apparently the presence of the hydrogen caused the motor to be more unstable; therefore, the motor was reassembled and four additional tests were conducted to investigate the baseline characteristics of the wafer chamber with no coolant flow. The firings, which are listed as the last four tests in table XIII, were made at nominal chamber pressures of 200 and 800 psia; the duration of each firing was approximately 2 seconds.

The amplitude/frequency diagrams from the uncooled tests are presented in Appendix B. All four tests were stable in the frequency range from 1 to 5k Hz. Test No. 126.01, with a chamber pressure of 172 psi, was the only firing in which pressure amplitudes of greater than ±5% of the mean pressure were recorded and these occurred at extremely high frequencies, 7700 and 9200 Hz.

D. ANALYSIS OF RESULTS

The aperture temperatures measured throughout the test series were in reasonable agreement with the design point temperature of 1000°R; thus the coolant flow velocity through the liner would be approximately

50 to 100 ft/sec. For these conditions the results of the design analysis, figures 79 and 80, show that the liner has better than 30% absorption for all frequencies greater than 2000 Hz. From the results of the Phase I program, Reference 1 , it was concluded that all uncooled liners with at least 17% absorption stabilized the test motor so that the resulting pressure oscillations were less than 10% of chamber pressure. If the Phase I results are used as a criterion, all of the hydrogen cooled tests should have been stable.

Analysis and review of the wafer chamber design, test procedures, and test data failed to produce specific reason(s) for the unstable condition; hence, the cause of the poor liner performance, especially in view of the uncooled tests results, can only be attributed to the presence of the gaseous hydrogen coolant. The gas, upon exiting from the liner slots, mixes with the mainstream combustion gases and burns at the edge of the boundary layer. The resulting combustion zones in the transpiration-cooled motor are inevitably different from those that existed in the uncooled Phase I test motor; therefore, the amount of energy driving the instability and the amount of the absorption necessary to stabilize the system should also be different. In addition, comparisons of the instability data of figure 87 with the high pressure uncooled baseline data show that the P/P pressure amplitudes are greater than those measured with no hydrogen coolant. Thus, it is apparent that the gaseous hydrogen has changed the sensitive combustion zones so that the motor is more unstable than that of either the Phase I configuration or with no coolant flow.

The boundary layer combustion could also theoretically cause degradation of the absorption coefficients. This would be the net effect of the increased turbulence levels at the surface of the liner, which increase the acoustic resistance of the facing and thereby cause the liner absorption to be lower than if no combustion were present. A similar phenomenon is experienced by a resonator subjected to very high intensity sound waves or high Mach number flows at grazing incidence angles. Both cause extreme turbulence patterns in the vicinity of the resonator apertures and significant increases in the acoustic resistance. The absorption coefficient (α) is dependent on the acoustic resistance (θ), in the following manner:

$$\alpha = \frac{4\theta}{(\theta + 1)^2 + \chi^2}$$

where χ is the specific acoustic reactance.

In the presence of high turbulence the resistance becomes several orders of magnitude greater than either the reactance or unity which, as may be noted from the above equation, reduces the absorption coefficient to a value near zero.

The theoretical absorption coefficients for the uncooled wafer chamber computed for chamber pressures of 200 and 800 psia are shown in figure 90. These results show that the uncooled liner had enough absorption to cause the motor to be stable at both pressures. The reason for the high frequency instability in the one uncooled test is best explained by noting the results

reported in Reference 1 where it was found that at frequencies much greater than the resonant frequency of the acoustic liner, the design theory predicts higher coefficients than those determined from impedance measurements. A similar phenomenon would also be expected of the wafer liner theory. The 200-psia coefficients at frequencies greater than 6000 Hz would be significantly lower than those shown in figure 90, thereby permitting the high frequency instability to exist. Based on these results it is recommended that additional research be conducted to improve the absorbing liner theory in the high frequency, i.e. above resonance, high sound pressure level regime.

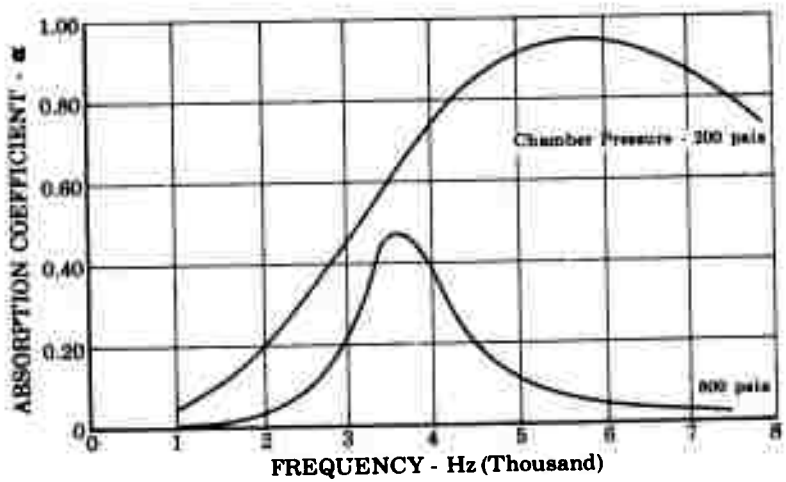

Figure 90. Wafer Liner Absorption Characteristics with No Coolant

FD 24770

SECTION VII
CONCLUSIONS AND RECOMMENDATIONS

From the results of the work discussed in this report the following conclusions and recommendations are made.

A. CONCLUSIONS

1. Ablative absorbing liners with individual resonators are not as effective for suppressing combustion instability as conventional liners, i.e., arrays of apertures with a common cavity, and with the same theoretical absorption characteristics.

2. The amount of damping of instability in the rocket motor tested was proportional to the total absorption of the liners used, i.e., the absorption coefficient multiplied by the percent of the total incidence area over which the absorption coefficient applies. Thus, a liner to be effective, must not only have a high absorption coefficient, but the coefficient must be applied over a sufficiently large percentage of the liner incident area. A liner is most effective when it is placed near the injector face, so that high total absorption near the injector is more important than high total absorption a few inches downstream of the injector.

3. The evolved gases from the decomposition of an ablative liner can cause significant changes in the liner absorption characteristics.

4. The properties of gases that will fill the cavities and apertures of an ablative liner can be predicted with sufficient accuracy for acoustic liner design purposes.

5. Parallel array ablative liners can be used to suppress combustion instability over extremely wide frequency ranges, i.e., between 2 and 10 kHz.

6. For the particular motor used in this program combustion instability that occurred at frequencies greater than 5500 Hz was much less detrimental to hardware components than the instability that occurred at lower frequencies.

7. Hydrogen transpiration cooling caused the test motor to be more unstable than when no coolant was used.

8. The effectiveness of film-cooled acoustic liners is inversely proportional to the Aerozine 50 coolant flowrate.

9. Nonresonant liners are less effective for suppressing combustion instability than resonant liners.

10. Liners with parallel arrays are more effective for suppressing instability over wide frequency ranges than liners with common cavities.

B. RECOMMENDATIONS

1. Acoustic liners with parallel arrays should be [illegible]n necessary to extend absorption bandwidth characteristic.
2. The properties used in the design analysis of ablative liners should be those of the gases given off by the hot wall material.
3. The acoustic liner design theory should be extended to include thrust chambers with combustion gas velocities of at least 2000 ft/sec.
4. The effectiveness of regeneratively cooled, flightweight acoustic liners should be demonstrated.
5. Basic research to improve the acoustic liner design theory in the high frequency, high SPL regime should be conducted.
6. Liners with single backing cavities should be used in preference to individual resonator liners because of their higher total absorption.

SECTION VIII
REFERENCES

1. "Acoustic Liners for Storable Propellant Rocket Chambers - Phase I Final Report," Pratt & Whitney Aircraft, AFRPL-TR-67-205, Contract AF04(611)-11387, 1 July 1967 (Confidential)

2. "Absorbing Liners for Rocket Combustion Chambers Theory and Design Techniques," Pratt & Whitney Aircraft, AFRPL-TR-66-234, August 1966, (Confidential)

3. Bartz, D. R., "A Simple Equation for Rapid Estimation of Rocket Nozzle Heat Transfer Coefficients," Jet Propulsion Laboratory, January 1957

4. "A Study of the Suppression of Combustion Oscillations With Mechanical Damping Devices," Final Report, PWA FR-2596, 20 November 1967

5. "A Study of the Suppression of Combustion Oscillations With Mechanical Damping Devices," Phase II Summary Report. PWA FR-1922, 15 July 1966.

APPENDIX A
WIDE BAND LINER PROGRAM

Phase I tests demonstrated that an acoustic liner with an absorption coefficient of 17% was effective in suppressing combustion instability below 5000 Hz in the N_2O_4/Aerozine-50 rocket motor tested. Because of amplification of the signal to the Kistler Model 601-A pressure transducer near the resonant frequency of the transducer adaptor passage, frequencies over 5000 Hz were not considered. Late in the Phase II test program, Kistler Model 615-A acceleration-compensated helium bleed pressure transducers were used because of the relatively high resonant frequency of the adaptor and because of the negligible gain in signal amplitude at resonance (see Section V).

Hot test data obtained from the 615-A transducers (tests No. 101.01 through 107.01) indicated that high amplitude instability had occurred at frequencies well over 5000 Hz. The data indicated that to effectively combat combustion instability, a liner must be designed over the frequency of 0 to 10,000 Hz. The liner computer design program was used to determine whether high theoretical absorption could be attained over the frequency range of 0 to 10,000 Hz. The liner design chosen, figure 91, had very high theoretical absorption over the frequency range of interest.

Liner design point data were

P_c	= 200 psia
r	= 2.0
C apertures	= 2330 fps
V_p	= 500 fps
T_a^P	= 2000°R
t	= 0.2 inch
L	= 0.650 inch
D_o	= 0.150 inch
σ	= 7.0%

Two tests (test No. 123.01 and 124.01) were conducted on the wide band liner at 200 psi. Both tests were very unstable with amplitudes of 66 psi peak-to-peak at 2100 Hz, and about 30 psi at 4200 Hz. High instability levels also occurred at 6400 Hz and 8600 Hz. Three Kistler transducers were used for each test. Helium bleed transducers (Model No. 615-A) were mounted in the 11:30 A plane location. Regular water-cooled Model 601-A transducers were inserted in the 12:00 A plane position. Model 601-A Kistlers mounted in short adaptors were used in the 12:30 A plane position. This transducer measured the wave amplitude incident on the chamber wall rather than on the liner wall.

A. CONCLUSIONS

The wide band liner failed to stabilize combustion in the N_2O_4/Aerozine-50 Rocket Motor, even though the theoretical absorption coefficient was high through the 0 to 10,000 Hz frequency range. High amplitude instability occurred at several frequencies from 2100 to 8600 Hz as the liner failed

to damp oscillations at any of the primary modes of instability. The wide band liner is a nonresonant liner, i.e., it does not exhibit a well-defined frequency of resonance. Most of the liners in the past were designed to suppress one or two modes of instability within a narrow frequency band (less than 3000 Hz). This enabled the designer to choose an absorption curve with a well-defined frequency of resonance because the instability modes to be damped were always near the resonant point. The wide frequency range over which instability occurred in the N_2O_4/Aerozine-50 Rocket Motor, required a liner design with either a relatively flat absorption curve or one with more than one resonant frequency (dual open area). The dual open area liner operated successfully (Section V), but the unstable wide band liner tests demonstrated the inability of a nonresonant liner to suppress combustion instability. Significant disagreement in the theoretical and experimental absorption coefficients of a resonant absorber at frequencies above resonance was demonstrated (Reference 4) with the aid of the P&WA impedance tube facility. The tests (see figure 92) demonstrated that the experimental absorption coefficient fell rapidly after the resonant frequency was reached, while the theoretical coefficient remained high. The same condition may have existed in the liner tested so that low absorption would result at frequencies over about 4000 Hz.

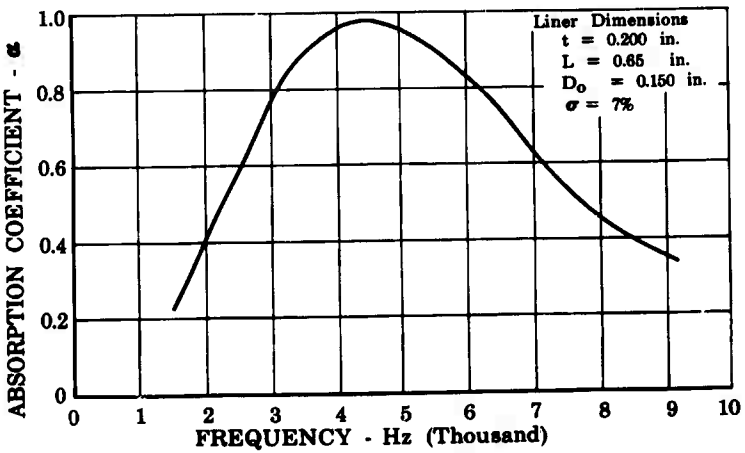

Figure 91. Absorption Characteristics of Uncooled Steel Liner

FD 24831A

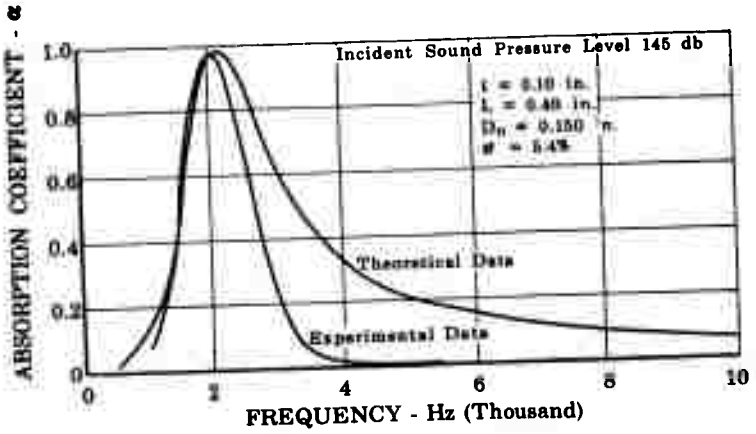

Figure 92. High Frequency Data Comparison FD 24832

B. RECOMMENDATIONS

The inability of the wide band liner to suppress combustion instability, despite its high theoretical absorption, illustrates the lack of knowledge of nonresonant liner operation and points out the need for further experimental and analytical effort in this area. The effort should include comparisons of theoretical and experimental absorption coefficients for a wide variety of nonresonant resonators. The absorption liner computer program should be amended and adjusted to reflect the experimental results. Liners should be designed based on the amended program and hot test series should be conducted to validate the design program.

Effort should be expended to accurately measure the parameters that are input to the design program, including liner aperture gas temperature, liner aperture gas viscosity, and the aperture gas composition. Perhaps the largest error in the liner design is the assumed sound pressure level incident on the liner wall. A means to accurately measure the incident sound pressure level during hot tests should be developed and the information gathered should be used as feedback to the design of efficient liners.

C. HOT GAS ANALYSIS SYSTEM

The gas analyzer system was used to determine the average molecular weight of the gases in the resonator cavities of an acoustic liner during a hot test. Figure 93 is a schematic of the gas sampling system.

UNCLASSIFIED

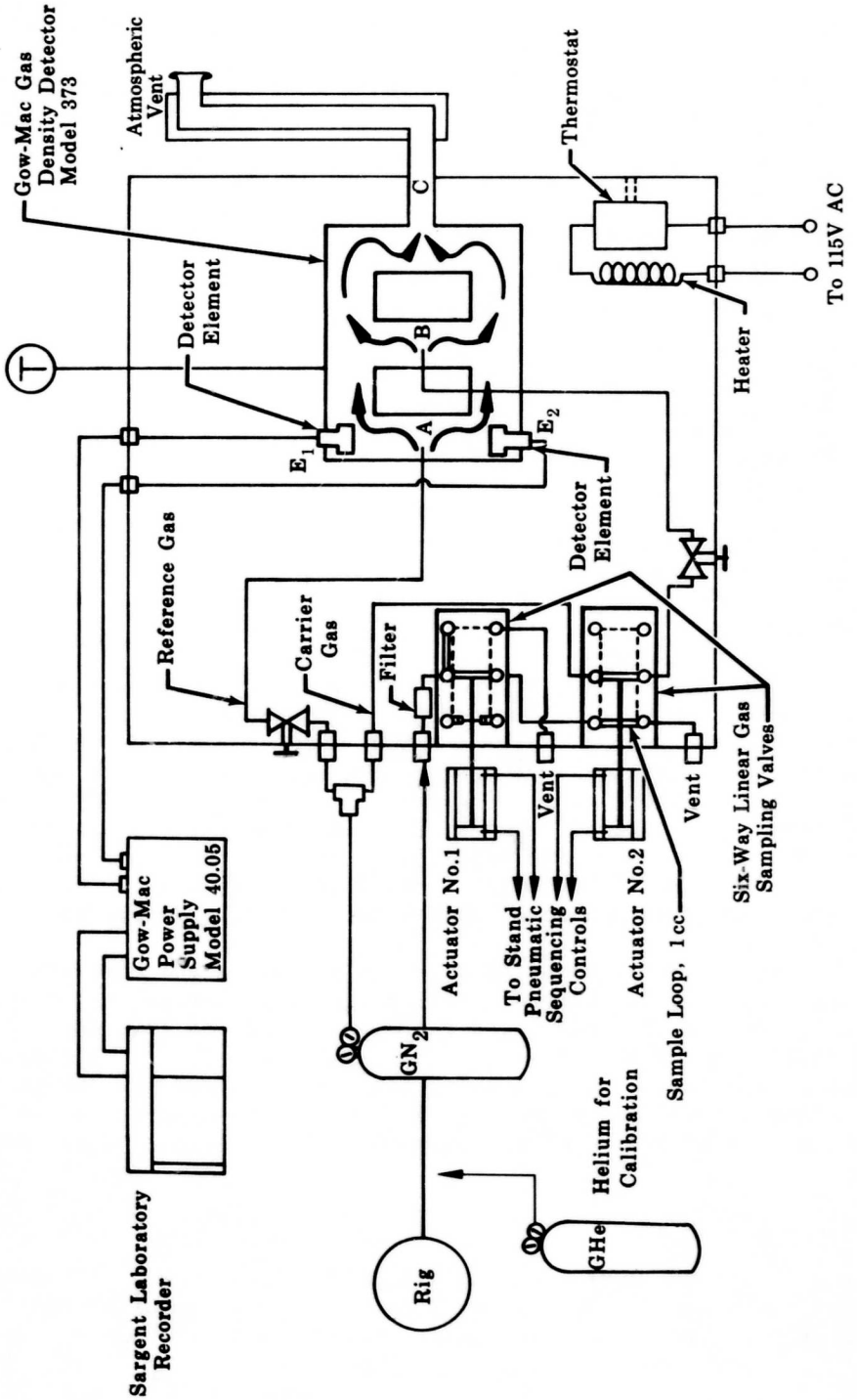

FD 24837

Figure 93. Gas Sampling Schematic Molecular Weight Measurement

UNCLASSIFIED

The procedure for determining the molecular weight is as follows.

The gas sample exits from the liner cavity forced by the rig chamber pressure to the 1st Varian Aerograph 6-way linear gas sampling valve. Actuator No. 1 closes at the desired sampling time and gas is allowed to drop to ambient pressure before actuator No. 2 closes (1.5 sec after No. 1 closes). The precise sample volume (1 cc) is injected into the nitrogen sample carrier flow to a Gow-Mac Gas Density Detector Model 373.

The Gow-Mac Density Detector detects changes in flow through the use of heated wire elements in a bridge circuit (E_1 and E_2). A reference gas (gaseous nitrogen) enters the detector (at A), splits into two streams, flows past the detector elements and exits to the atmosphere (at C). The sample enters the detector downstream of the heated elements (at B), splits into two streams, combines with the reference gas flow, and is discharged to the atmosphere.

When the sample gas is the same density as the reference gas, the detector bridge circuit is balanced. When a sample of different density is injected into the detector, the sample density causes a net upward or downward flow in the detector. This flow variation causes an imbalance in the bridge circuit, which is recorded on the Sargent Laboratory Recorder. The difference between the molecular weight of the sample gas and the reference gas is linear, for equal gas volumes, with the bridge output. The molecular weight of the sample is thus determined.

APPENDIX B
LINER TEST DATA

The pressure amplitude data for all representative tests are presented as a function of frequency in order by main report body section. Figure 94 serves as a guide to the angular and axial location of each Kistler transducer used during the Phase II test program. All Kistler adaptors were flush mounted with the liner internal diameter, except for the 12:30 and 2:00 A Plane Kistlers that were mounted in the liner cavity. A "dummy" probe is defined as a Kistler transducer that does not sense combustion chamber oscillations, but serves to measure vibration levels. This is done by mounting the Kistler transducer into an adaptor that does not have an aperture leading to the combustion zone.

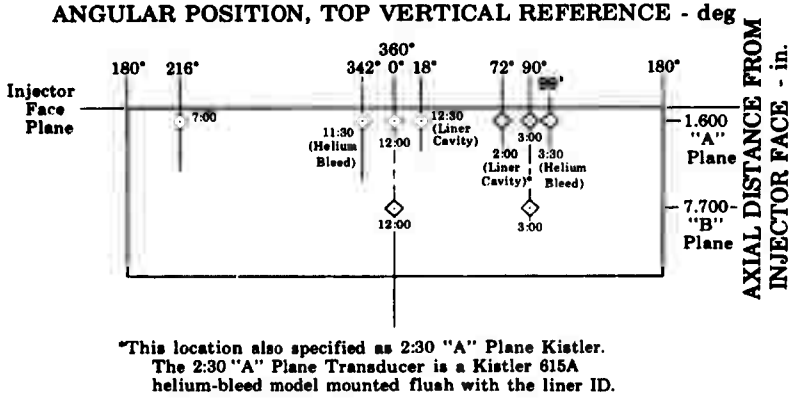

Figure 94. Location Schematic of Kistler Dynamic Pressure Transducers FD 24212

SOLID LINER BASELINE TESTS

Test Number	Chamber Pressure - psia	Test Duration - sec	Mixture Ratio	Frequency vs Amplitude Diagrams - Figure
66.01	630	1.96	0.97	95
68.01	903	1.96	2.13	96
81.01	747	1.47	2.04	97
82.01	797	1.23	2.01	98
83.01	775	1.94	2.00	99
84.01	813	1.94	2.05	100
86.01	768	1.72	1.96	101
114.01	191	1.47	1.94	102
115.01	190	1.47	1.95	103

FILM-COOLED LINER TESTS

Test Number	Chamber Pressure - psia	Test Duration - sec	Coolant Flowrate - lb_m/sec	Injector Mixture Ratio	Frequency vs Amplitude Diagrams - Figure
54.01	198	1.19	2.34	2.03	104
55.01	204	5.59	1.92	1.99	105 (Stable Portion)
55.01	204	5.59	1.92	1.99	106 (Unstable Portion)
56.01	203	5.88	1.40	2.00	107
57.01	196	2.94	0.00	2.00	108
75.01	185	7.80	1.97	2.02	109
76.01	192	1.45	1.52	2.01	110
79.01	201	3.45	1.49	2.00	111
88.01	585	1.72	2.51	0.73	112
89.01	911	1.72	2.33	2.00	113 and 114
90.01	900	1.72	1.96	1.98	115
91.01	852	1.04	0.00	2.00	116

ABLATIVE LINER TESTS

Test Number	Chamber Pressure - psia	Test Duration - sec	Mixture Ratio	Frequency vs Amplitude Diagrams - Figure
58.01	181	1.10	2.02	117
59.01	179	0.99	2.02	118
61.01	184	0.94	2.05	119
69.01	175	1.82	2.00	120
72.01	188	8.34	2.01	121,122,123
100.01	191	2.94	1.98	124

Test Number	Chamber Pressure - psia	Test Duration - sec	Mixture Ratio	Frequency Amplitude Diagrams - Figure
104.01 *	192	1.47	1.93	125
105.01 *	196	1.47	1.91	126
106.01 *	194	1.47	1.94	127
107.01 *	189	1.47	1.91	128
110.01 **	197	1.47	1.94	129
111.01 **	197	2.94	2.00	130
112.01 **	200	4.90	2.00	131 and 132
113.01 **	197	4.89	2.00	133
118.01 ***	178	3.00	1.91	134
121.01 ****	174	3.00	1.91	135
122.01 ****	184	3.00	1.90	136

WAFER LINER TESTS

Test Number	Chamber Pressure - psia	Test Duration - sec	Coolant Flowrate - lb_m/sec	Mixture Ratio	Frequency vs Amplitude Diagrams - Figure
92.09	206	1.03	0.786	1.99	137
93.01	190	0.73	0.690	1.88	138
94.01	896	1.47	0.785	2.05	139
95.01	899	2.30	0.800	2.00	140
96.03	840	1.50	0.535	1.96	141
97.02	805	1.04	0.665	1.95	142
98.01	840	1.27	0.665	1.94	143
125.01	187	2.08	0.0	1.93	144
126.01	172	2.02	0.0	1.95	145
128.01	744	2.00	0.0	1.98	146

WIDE BAND LINER TESTS

Test Number	Chamber Pressure - psia	Test Duration - sec	Mixture Ratio	Frequency vs Amplitude Diagrams - Figure
123.01	171	1.22	1.92	147
124.01	177	2.65	1.91	148

*Individual resonator steel liner
**Parallel array steel liner
***Parallel array ablative liner
****Dual open area steel liner

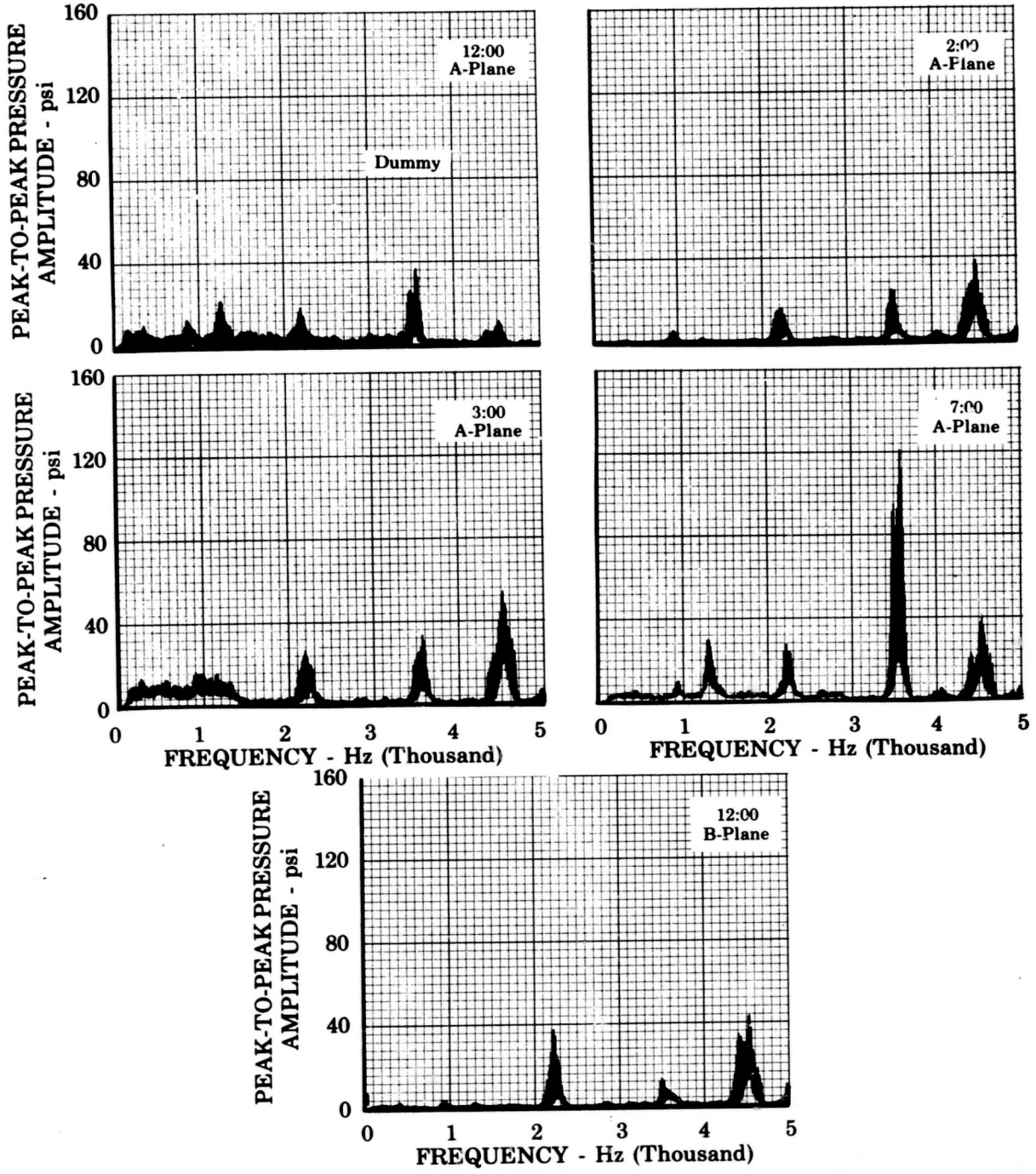

Figure 95. Pressure Amplitude Data for Solid Liner Baseline Test No. 66.01 FD 24595

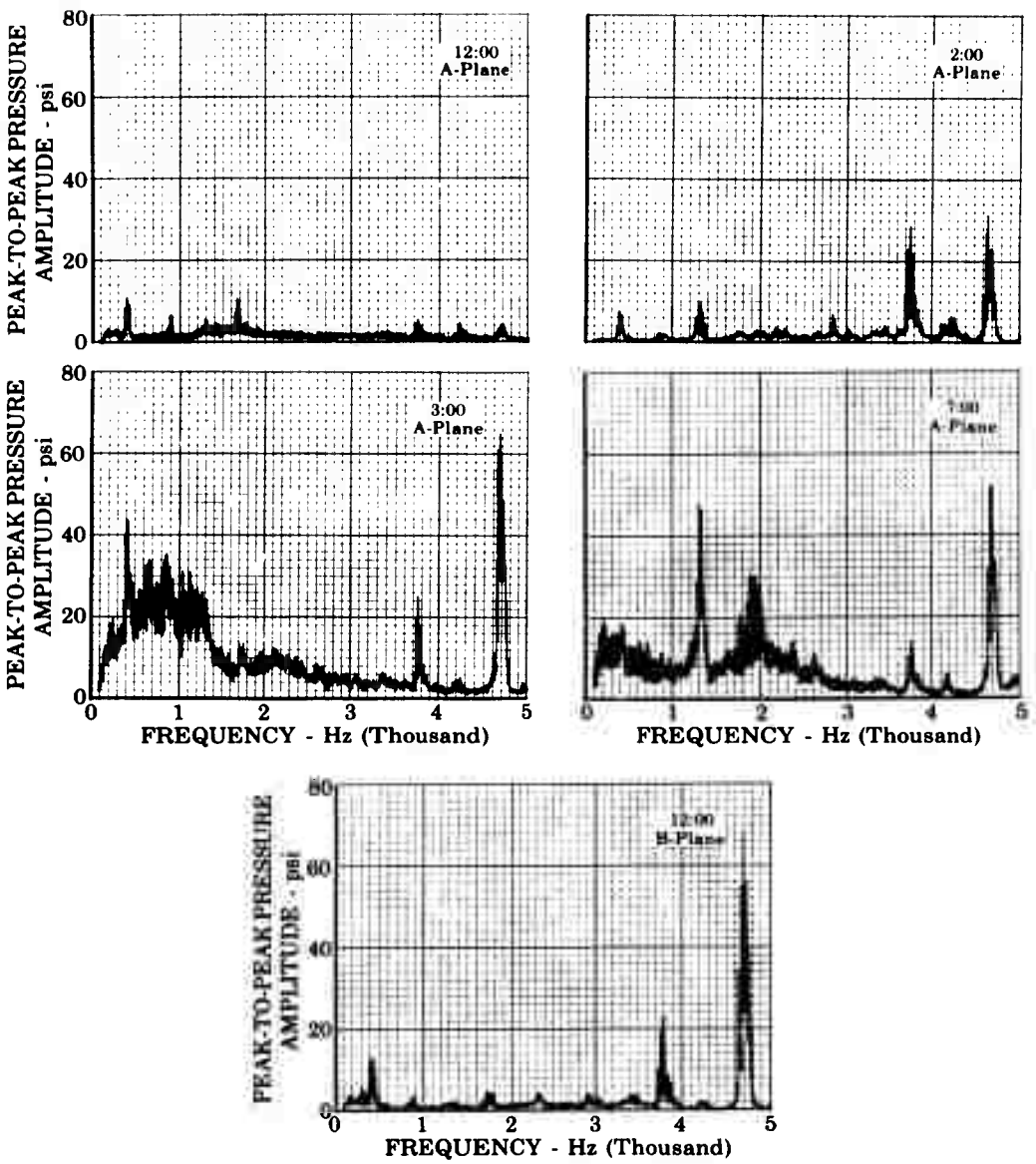

Figure 96. Pressure Amplitude Data for Solid Liner Baseline Test No. 68.01 FD 24604

UNCLASSIFIED

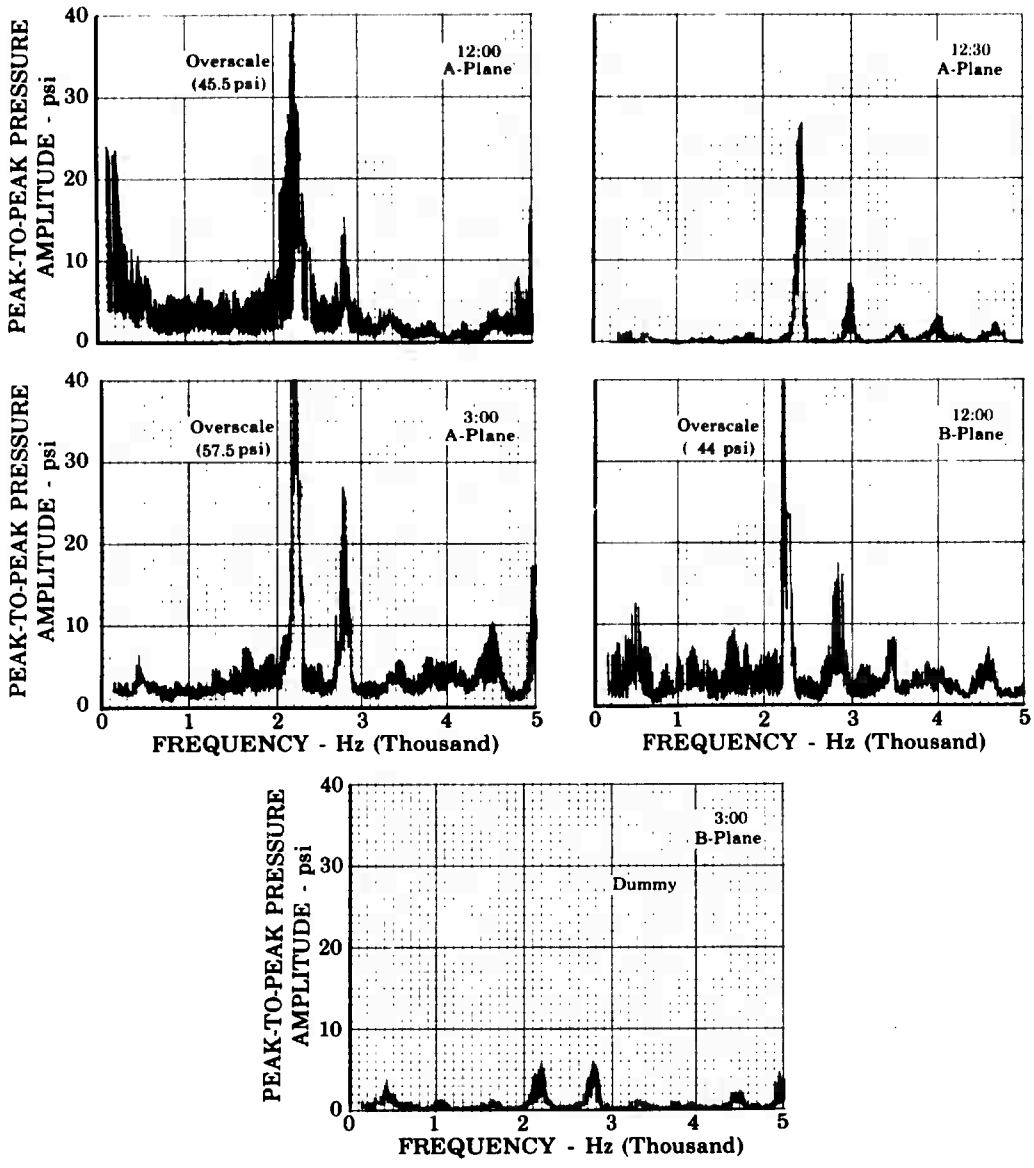

Figure 97. Pressure Amplitude Data for Solid Liner Baseline Test No. 81.01 FD 24600

UNCLASSIFIED

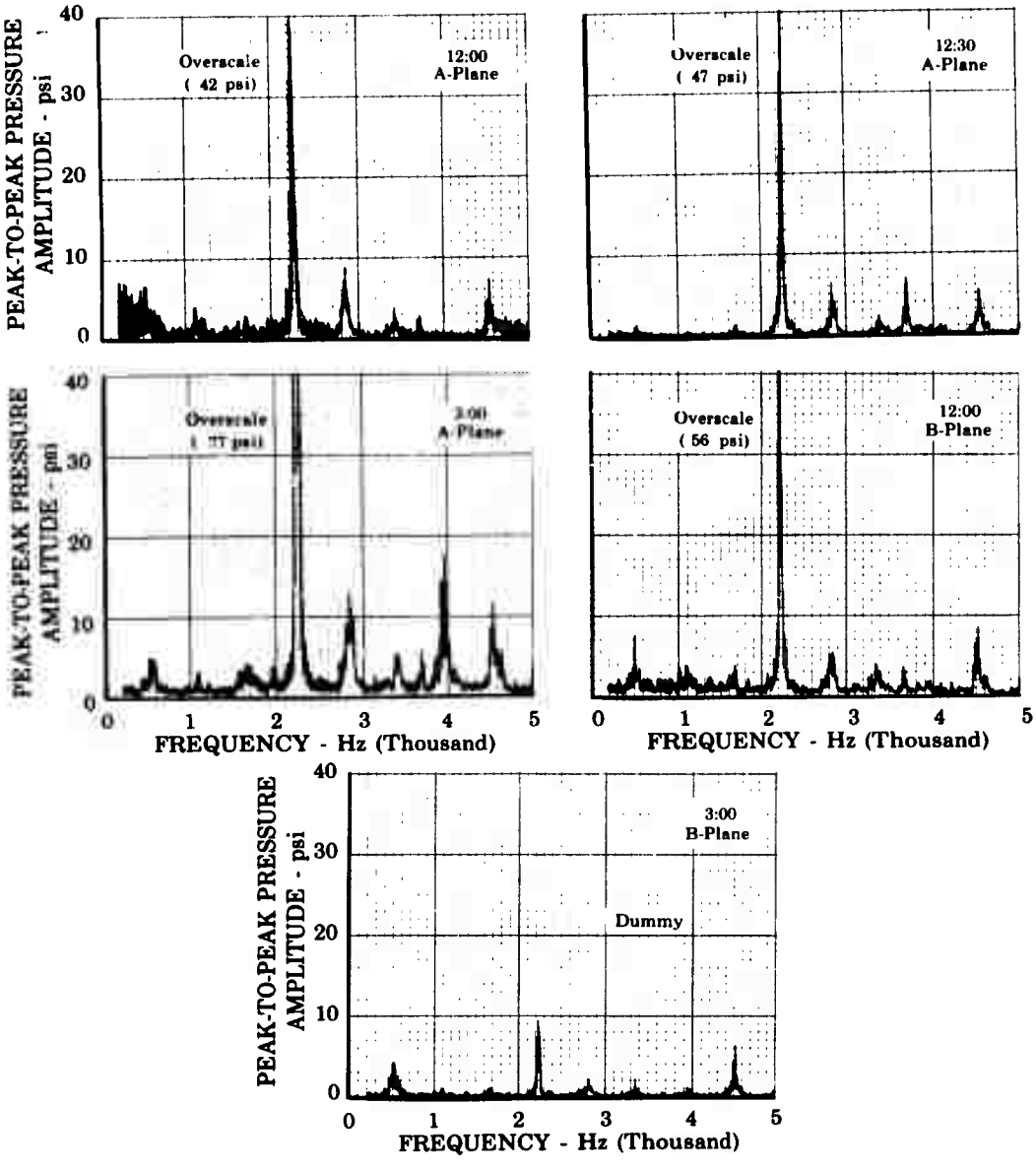

Figure 98. Pressure Amplitude Data for Solid Liner Baseline Test No. 82.01 FD 24592

UNCLASSIFIED

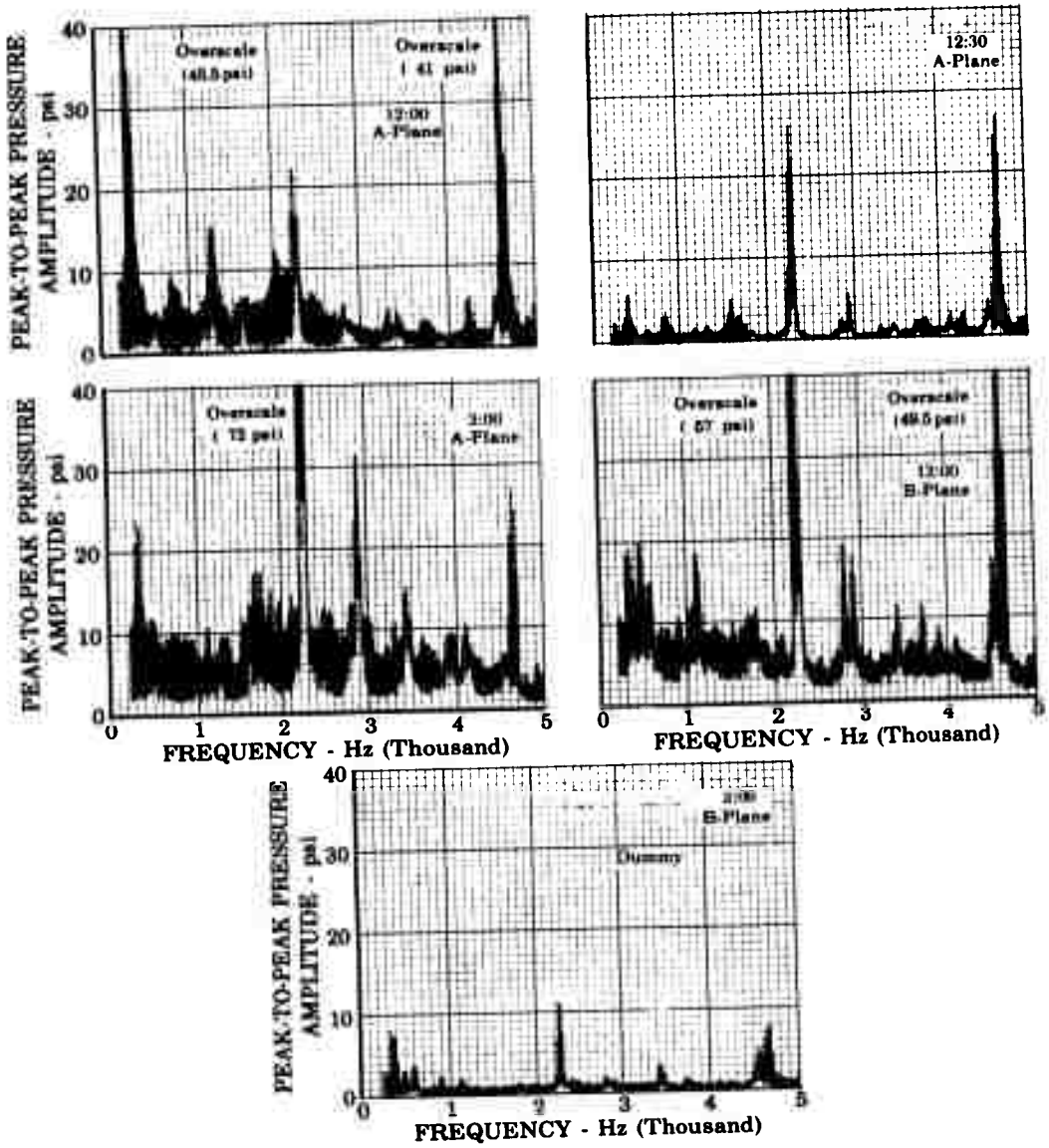

Figure 99. Pressure Amplitude Data for Solid Liner Baseline Test No. 83.01

FD 24593

UNCLASSIFIED

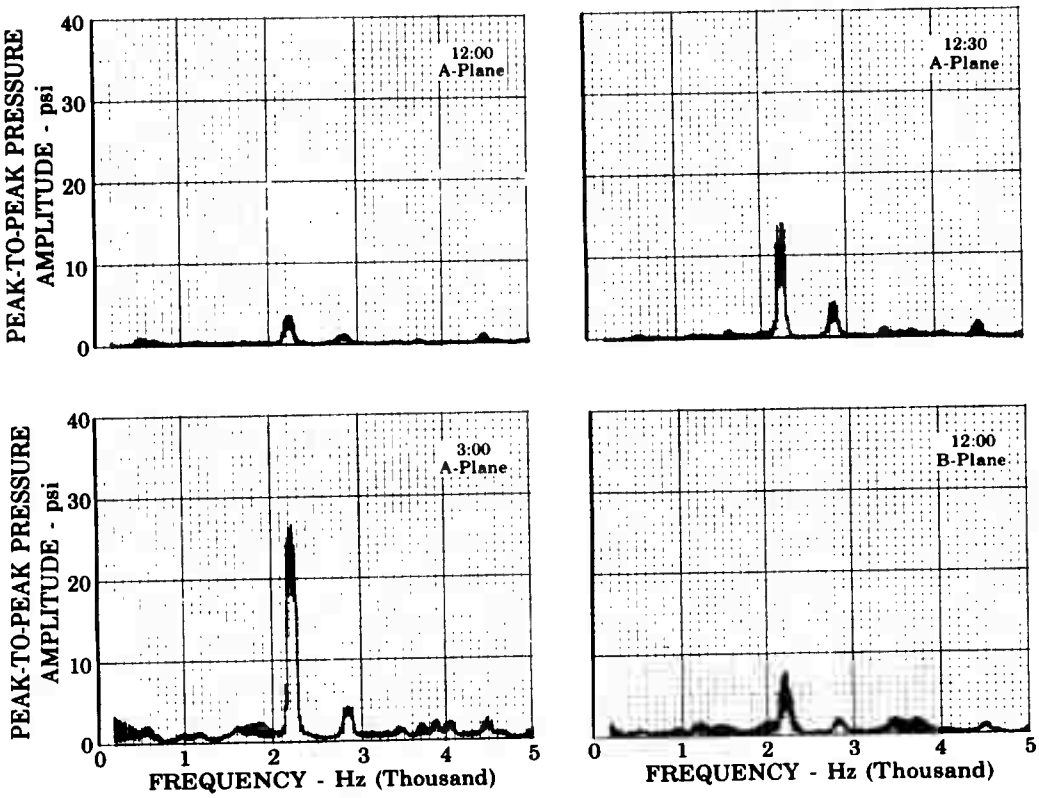

Figure 100. Pressure Amplitude Data for Solid Liner Baseline Test No. 84.01

FD 24591

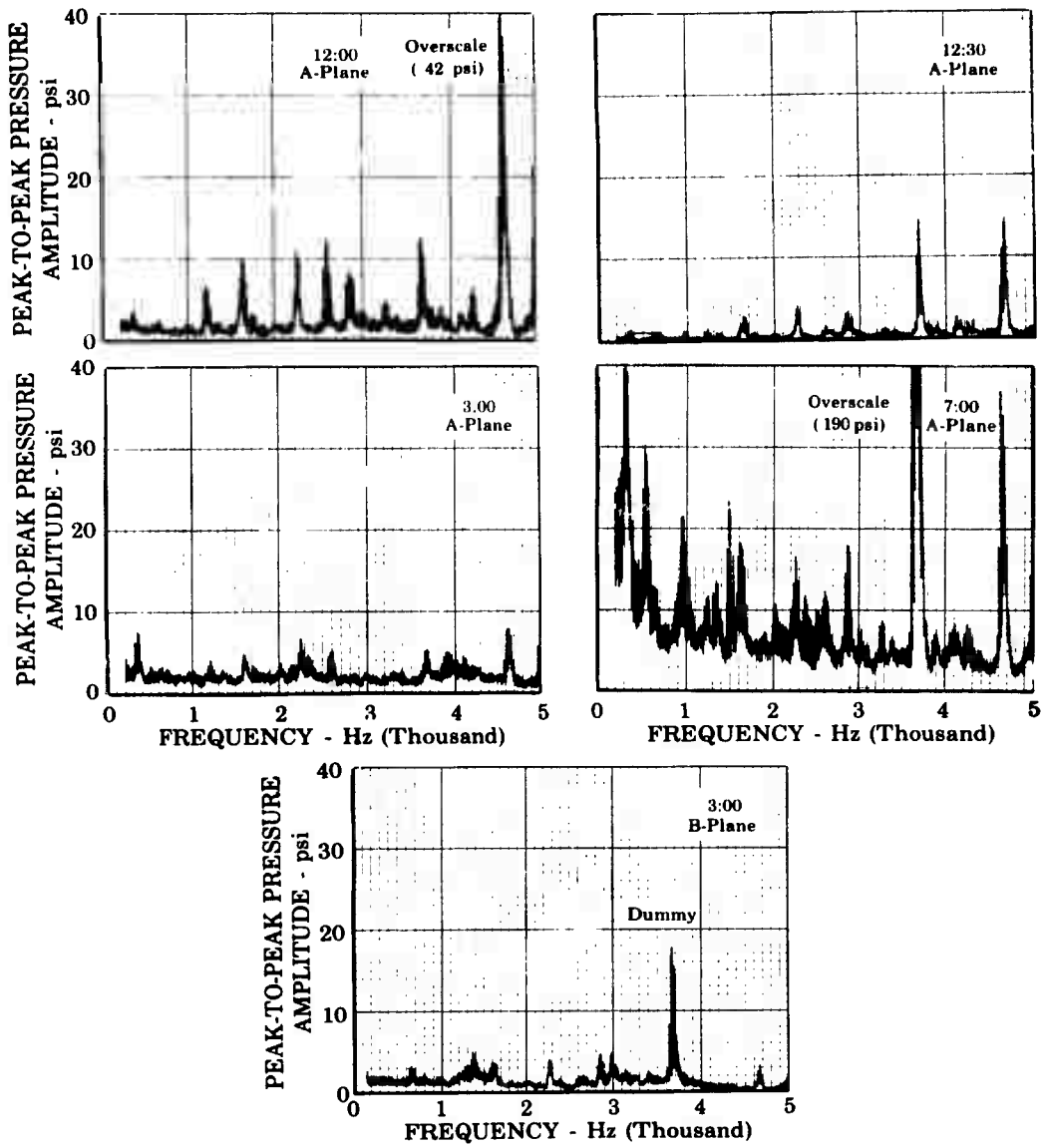

Figure 101. Pressure Amplitude Data for Solid Liner Baseline Test No. 86.01 FD 24599

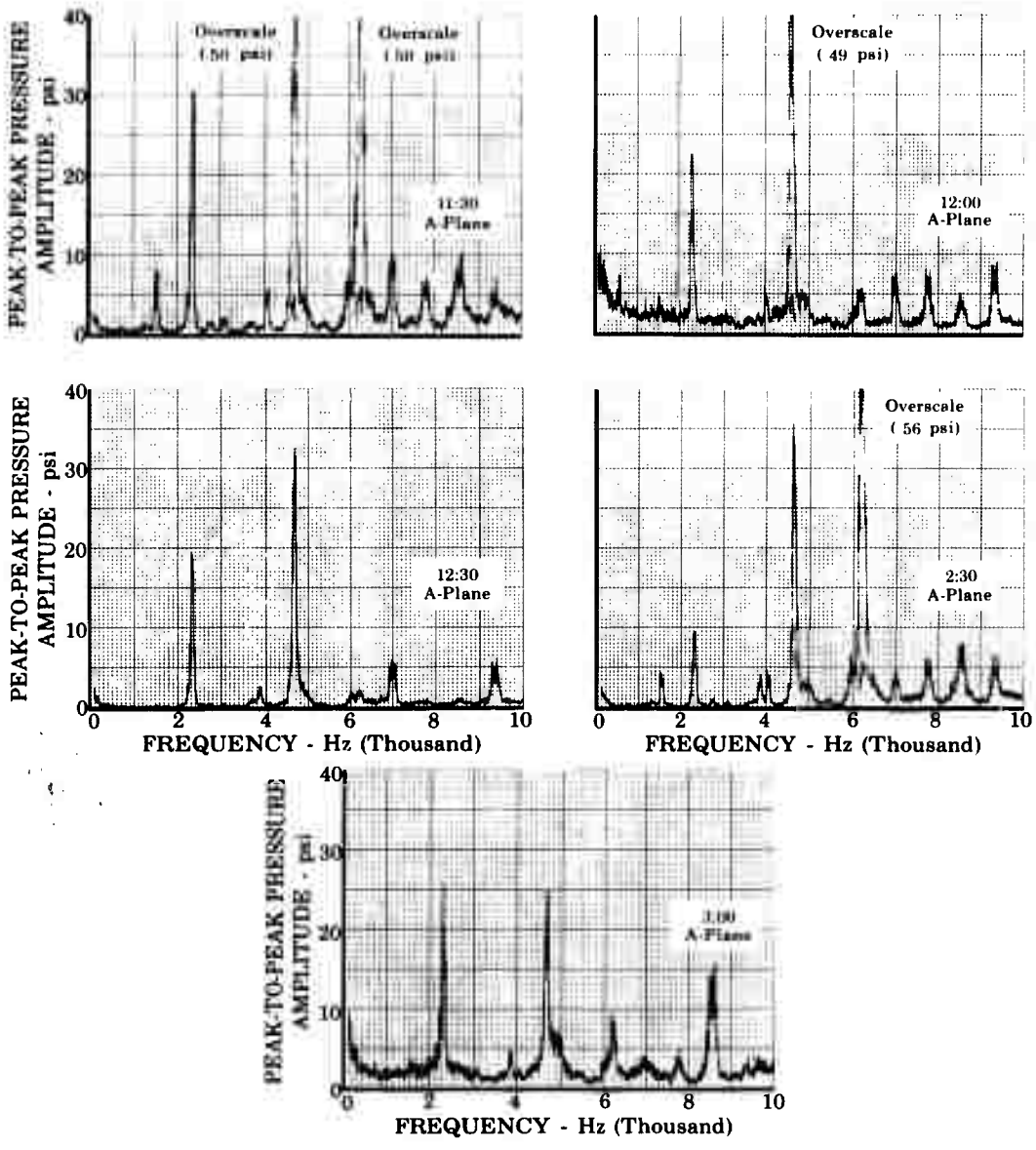

Figure 102. Pressure Amplitude Data for Solid Liner Baseline Test No. 114.01 FD 24632

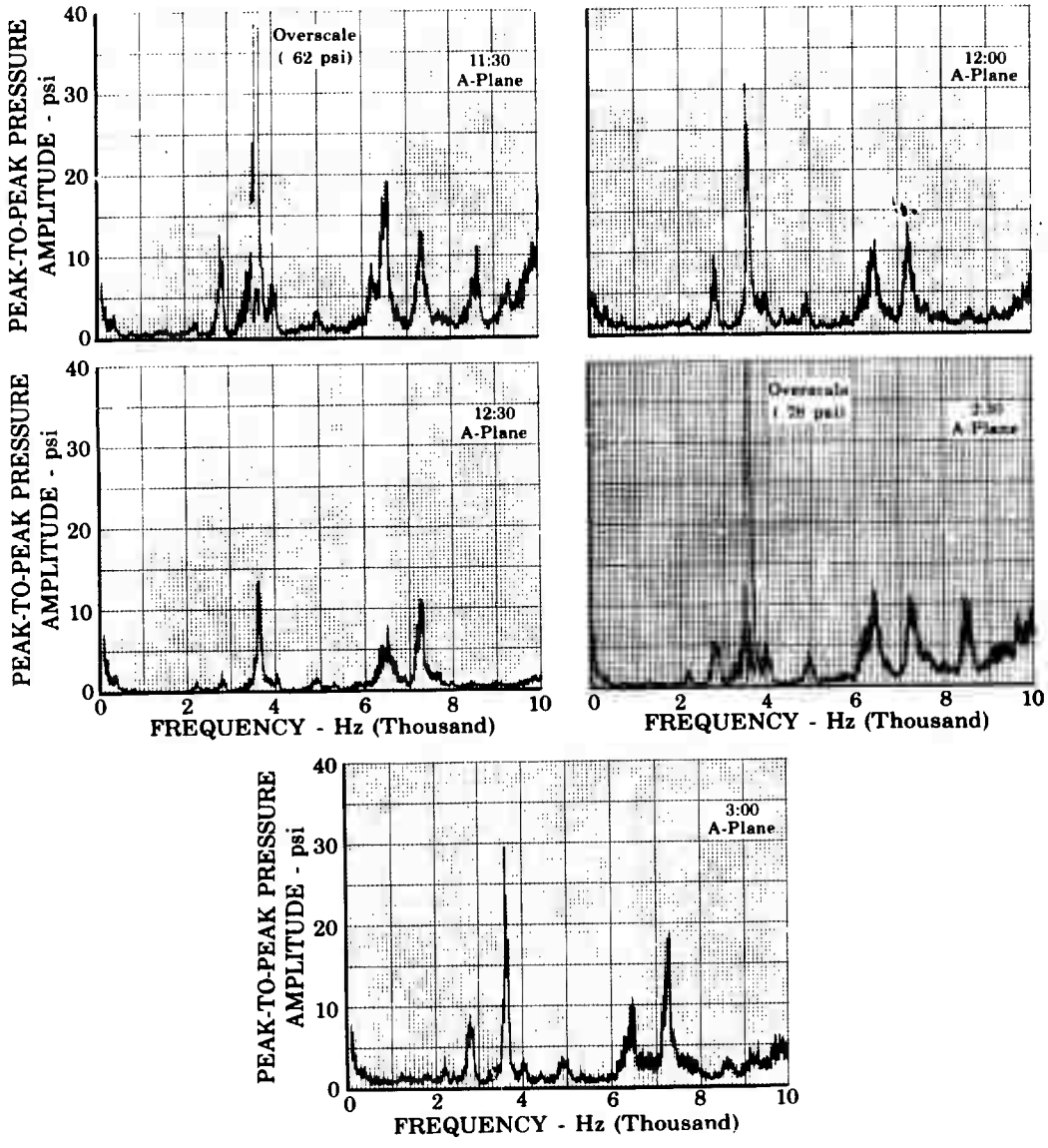

Figure 103. Pressure Amplitude Data for Solid Liner Baseline Test No. 115.01 FD 24633

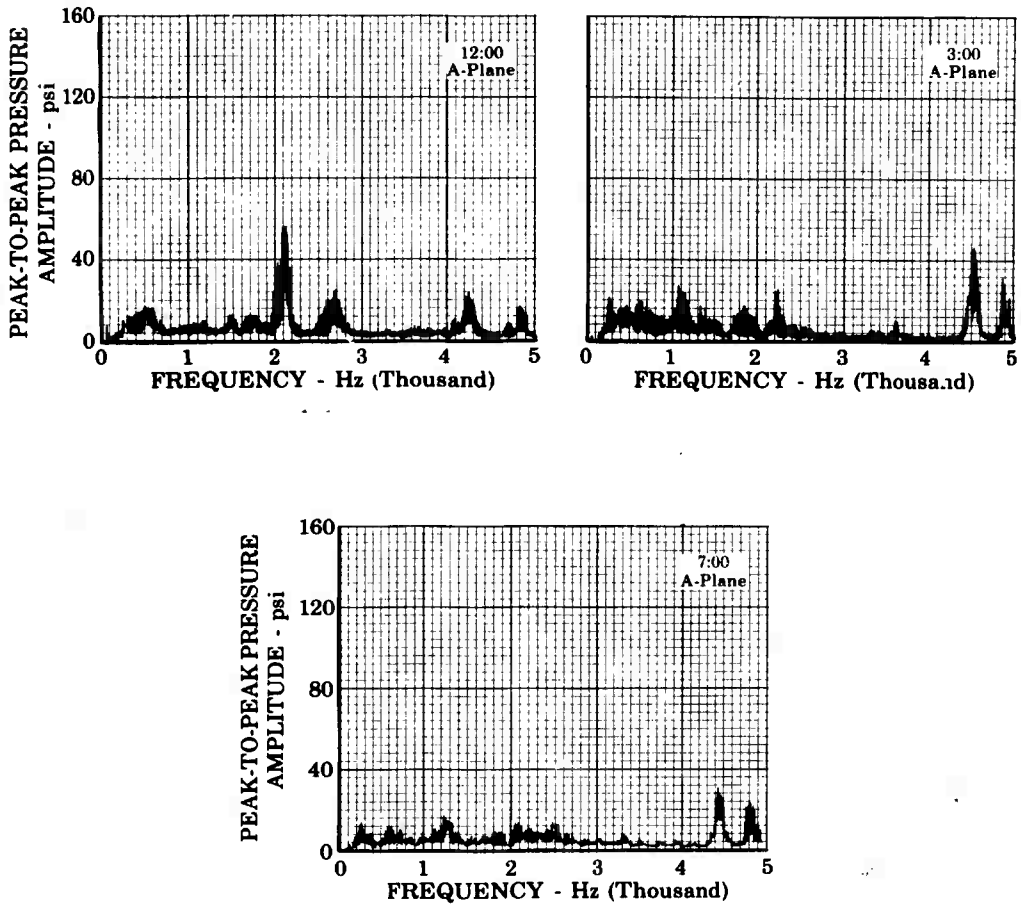

Figure 104. Pressure Amplitude Data for Film-Cooled Liner Test No. 54.01 FD 24607

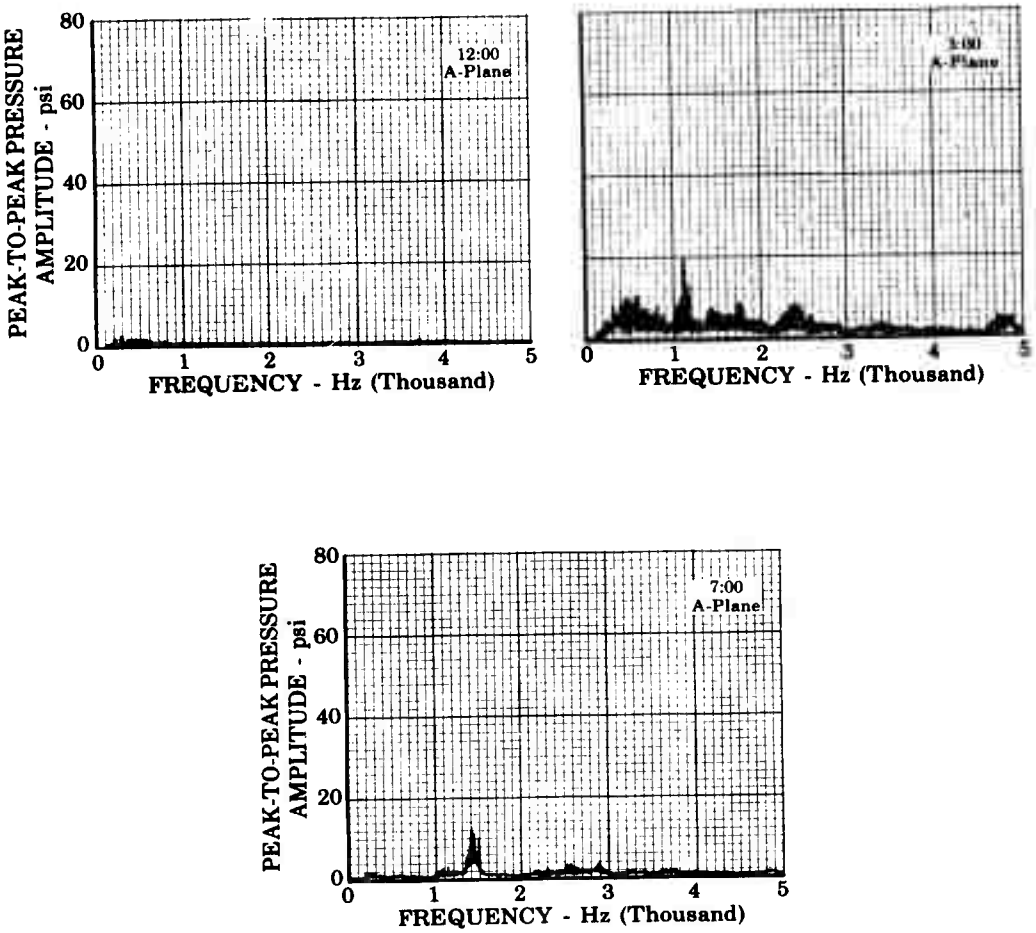

Figure 105. Pressure Amplitude Data for Film-Cooled Liner Test No. 55.01 (Stable) FD 24598

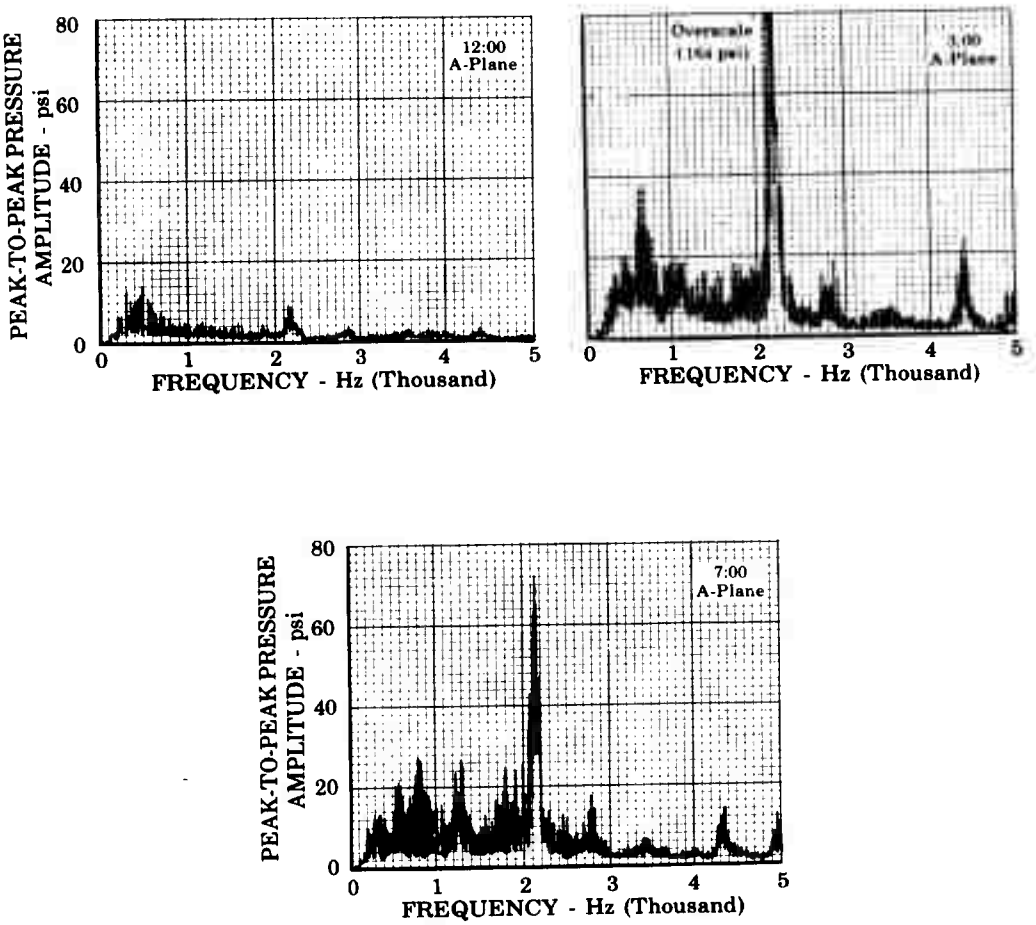

Figure 106. Pressure Amplitude Data for Film-Cooled Liner Test No. 55.01 (Unstable)

FD 24603

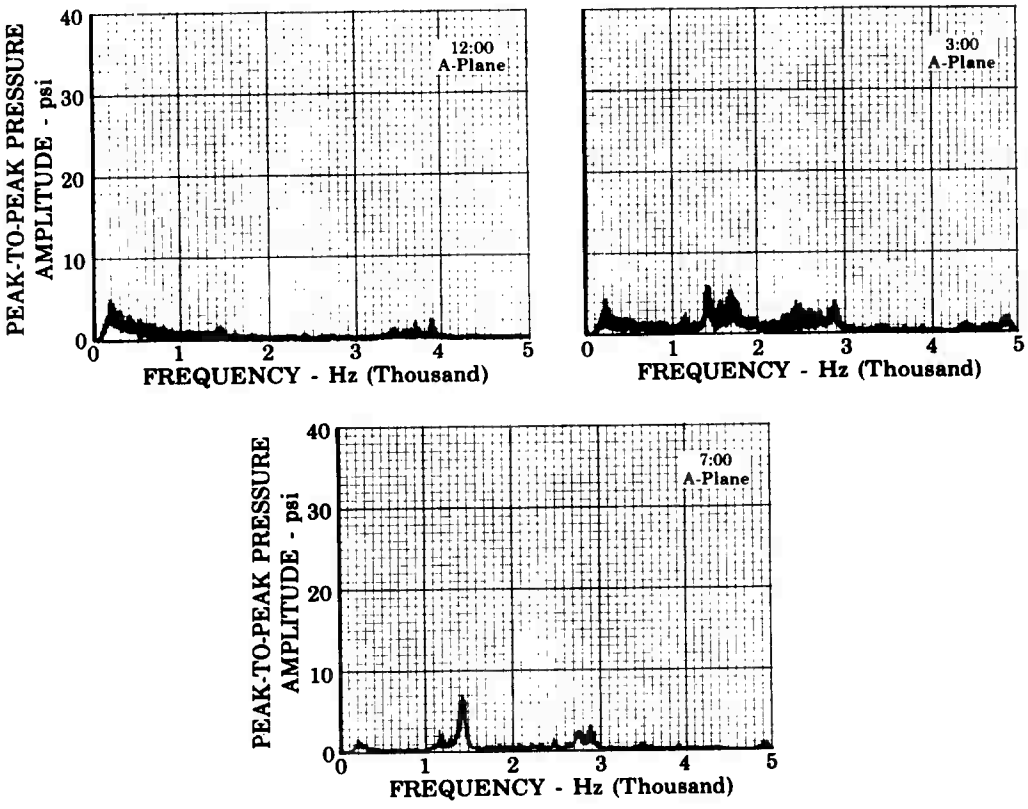

Figure 107. Pressure Amplitude Data for Film-Cooled Liner Test No. 56.01

FD 24596

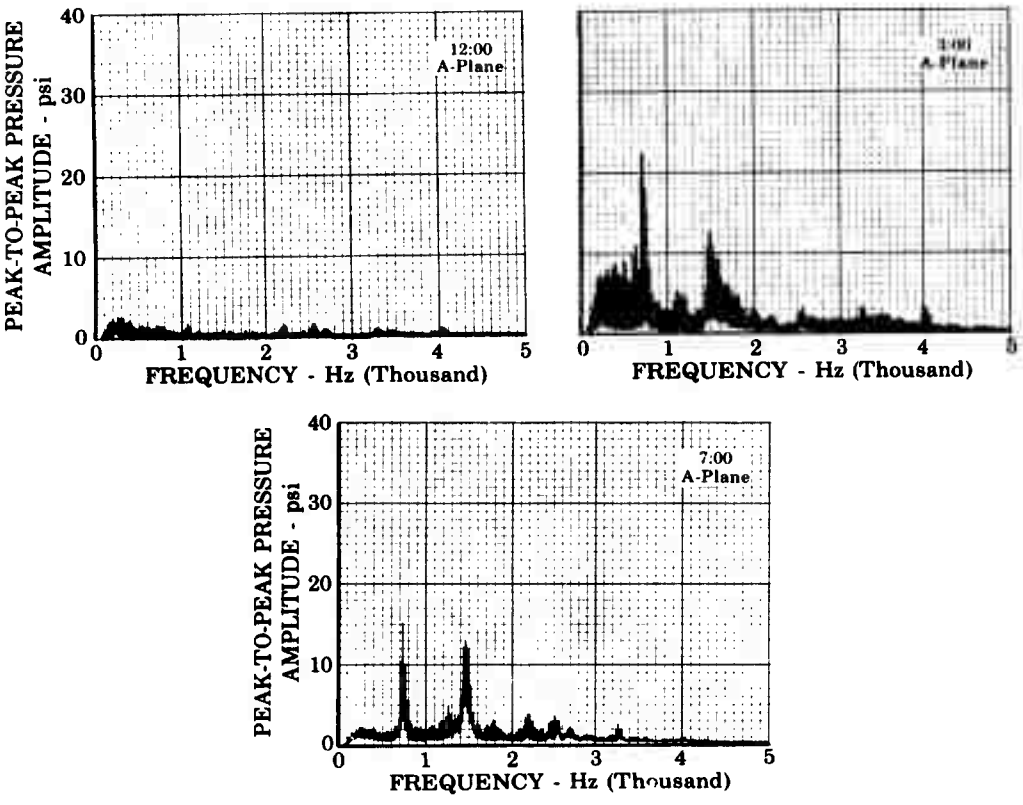

Figure 108. Pressure Amplitude Data for Film-Cooled Liner Test No. 57.01 FD 24597

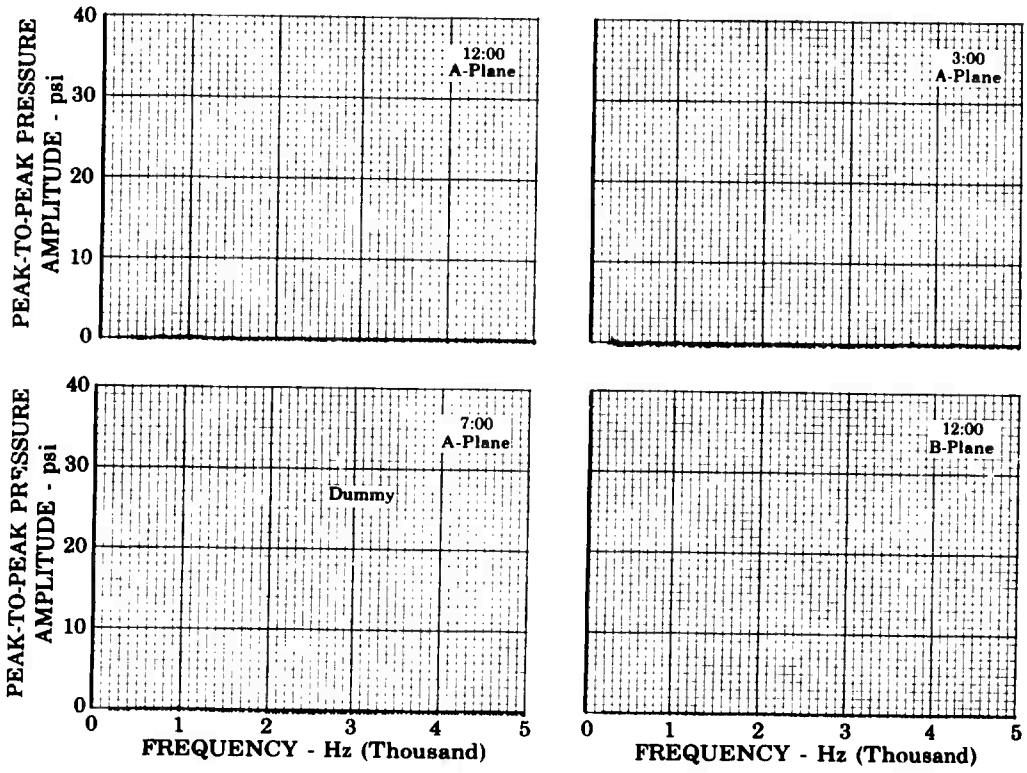

Figure 109. Pressure Amplitude Data for Film-Cooled Liner Test No. 75.01 FD 24605

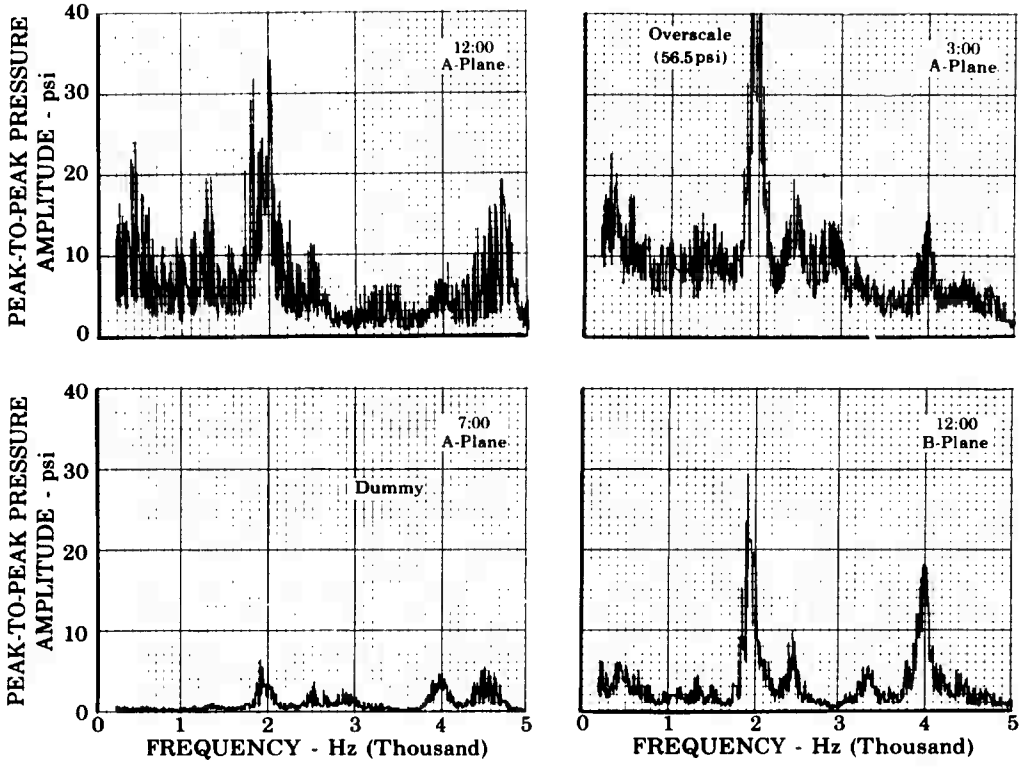

Figure 110. Pressure Amplitude Data for Film-Cooled Liner Test No. 76.01 FD 24606

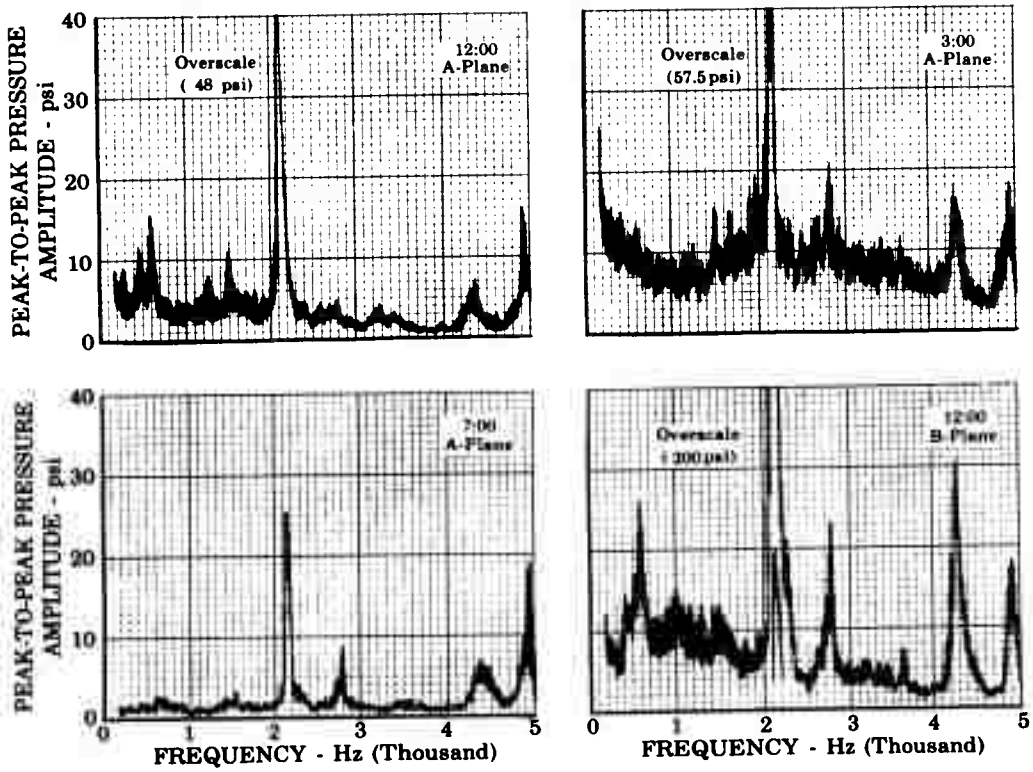

Figure 111. Pressure Amplitude Data for Film-Cooled Liner Test No. 79.01

FD 24594

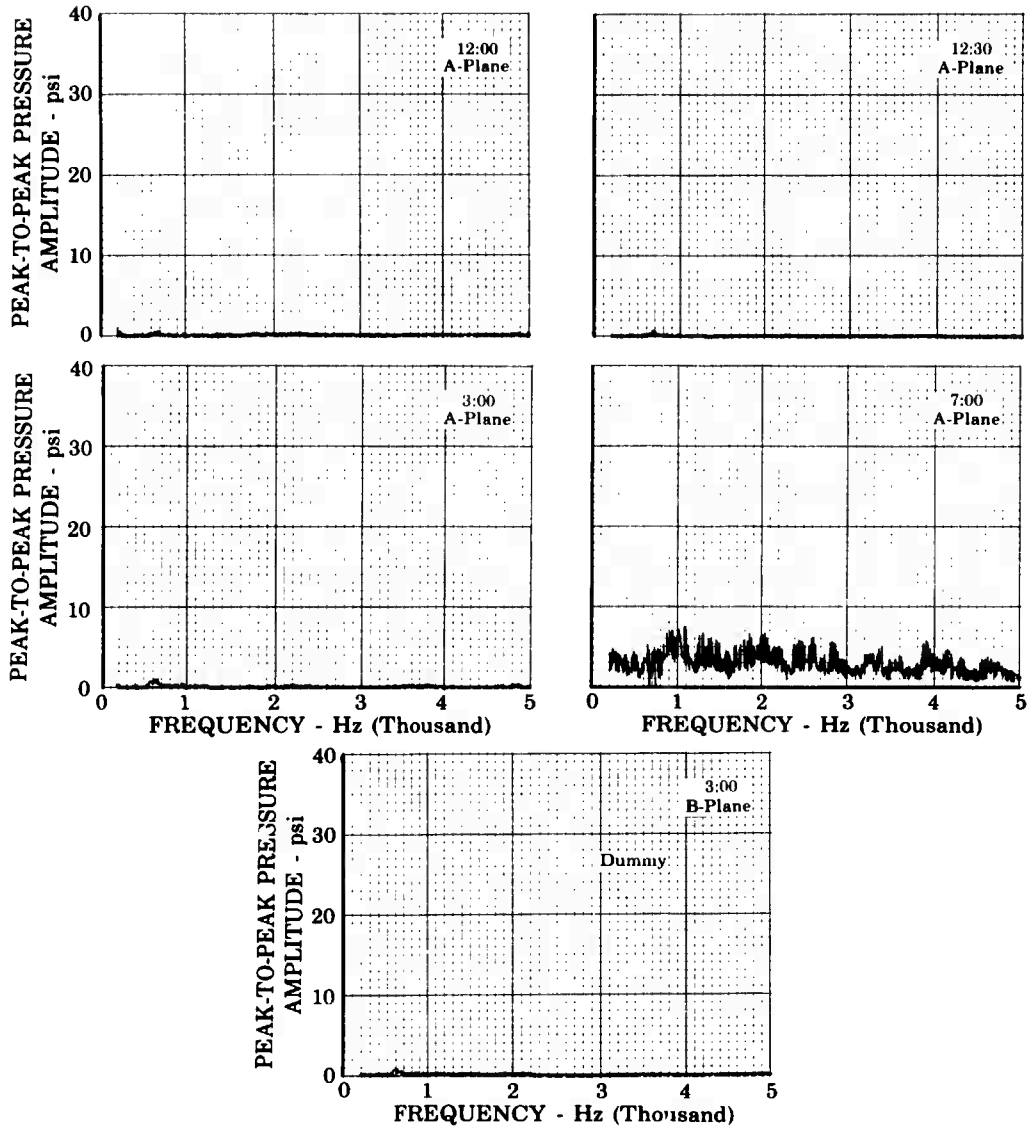

Figure 112. Pressure Amplitude Data for Film-Cooled Liner Test No. 88.01 FD 24611

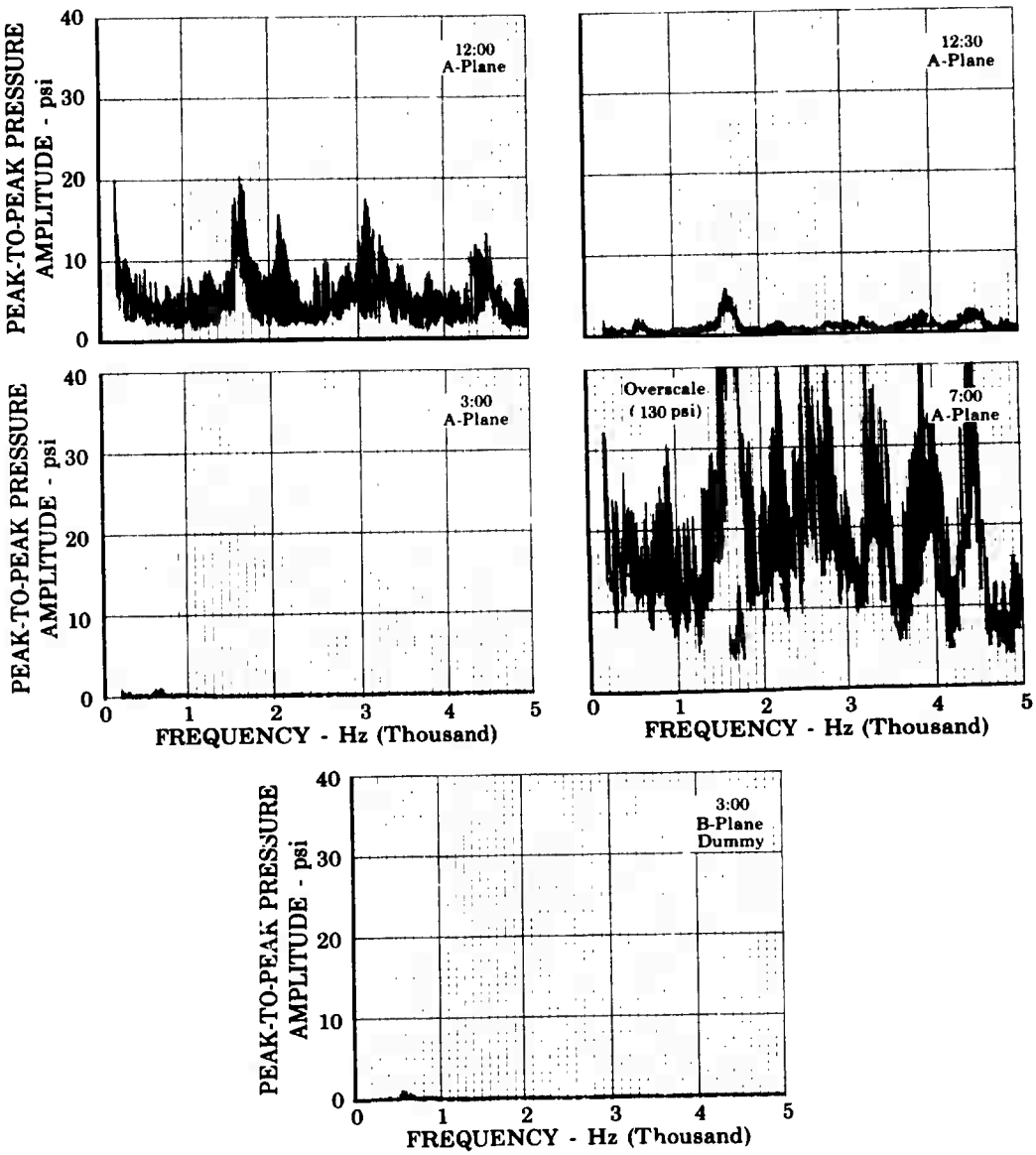

Figure 113. Pressure Amplitude Data for Film-Cooled Liner Test No. 89.01 FD 24608

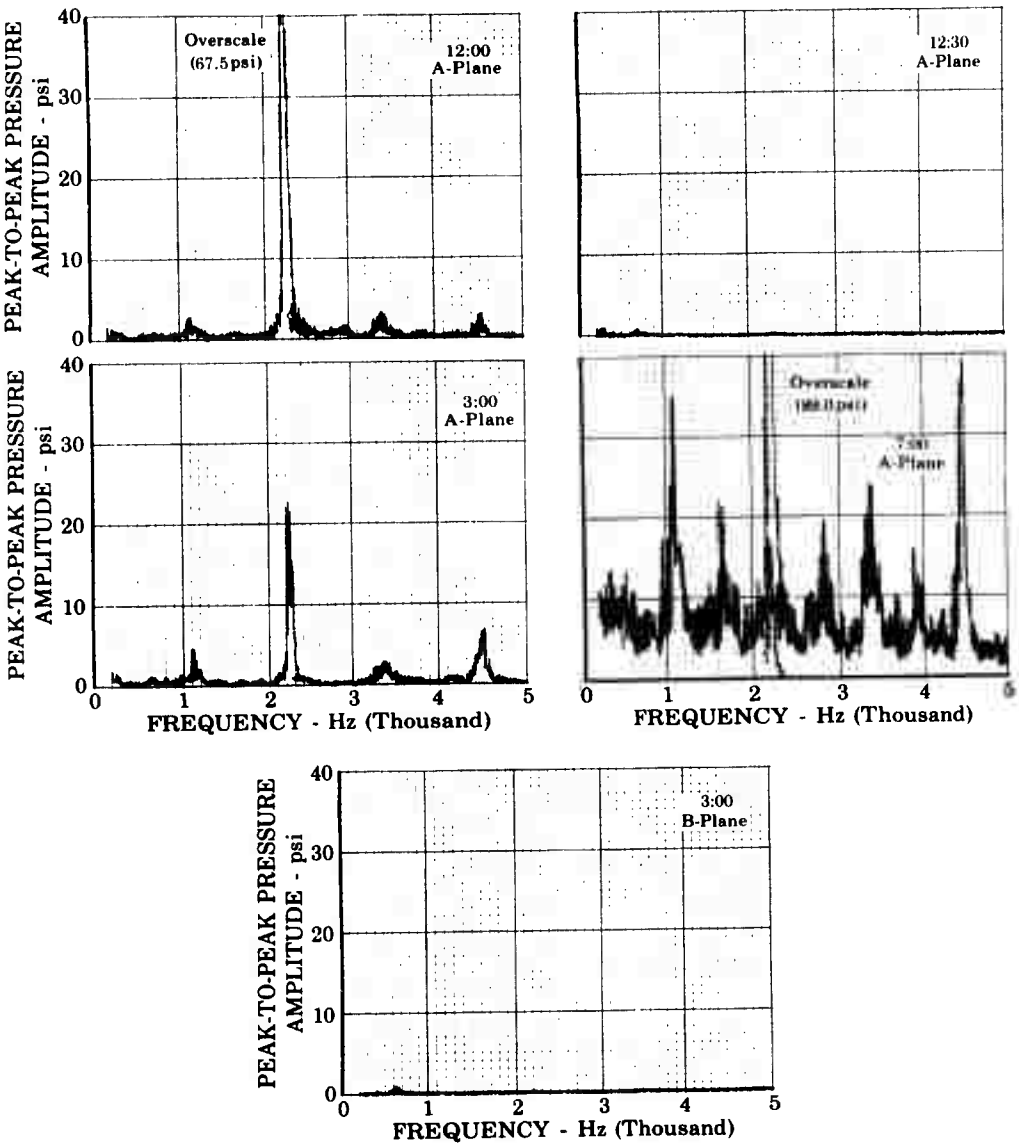

Figure 114. Pressure Amplitude Data for Film-Cooled Liner Test No. 89.01 FD 24828

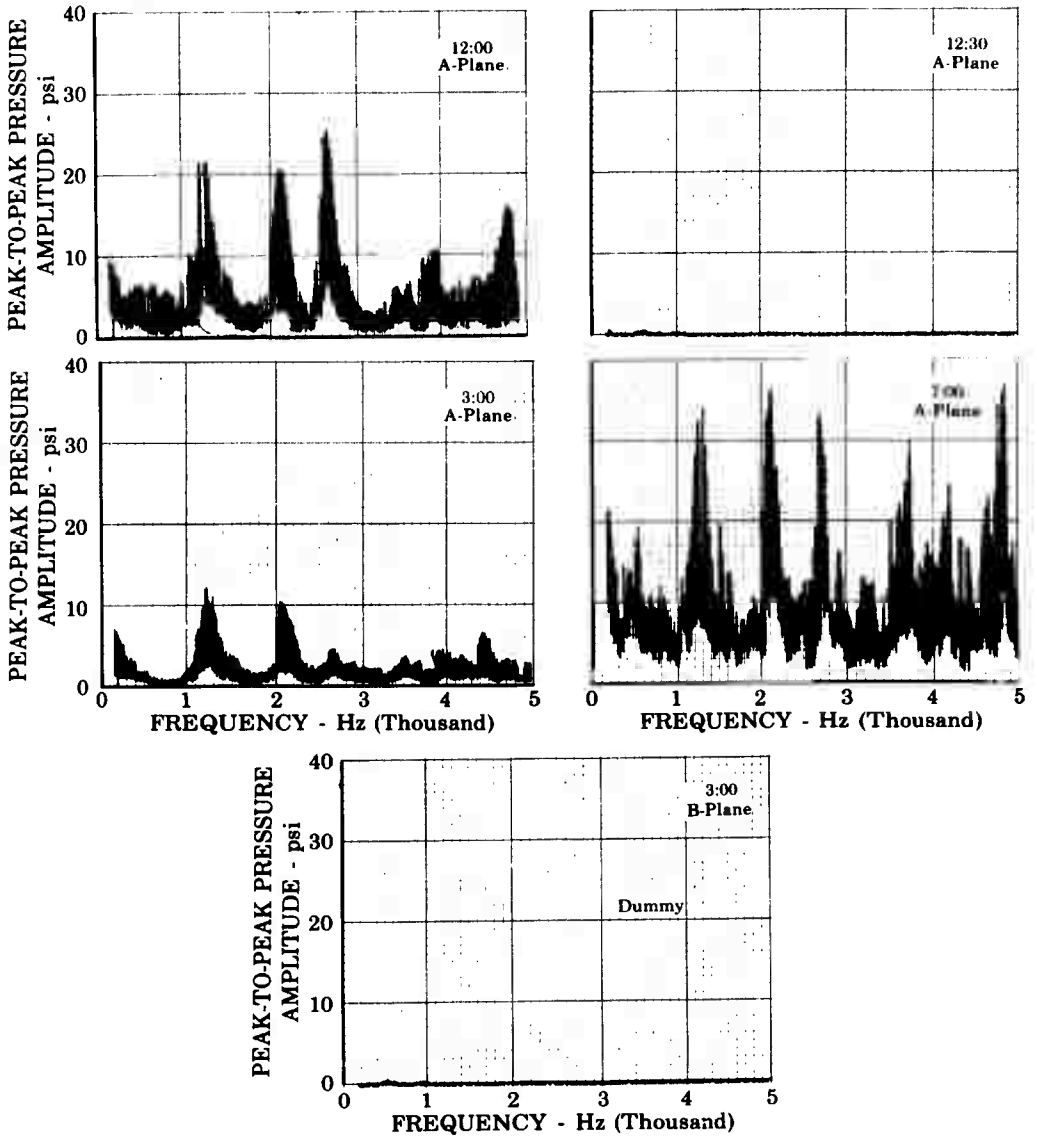

Figure 115. Pressure Amplitude Data for Film-Cooled Liner Test No. 90.01 FD 24609

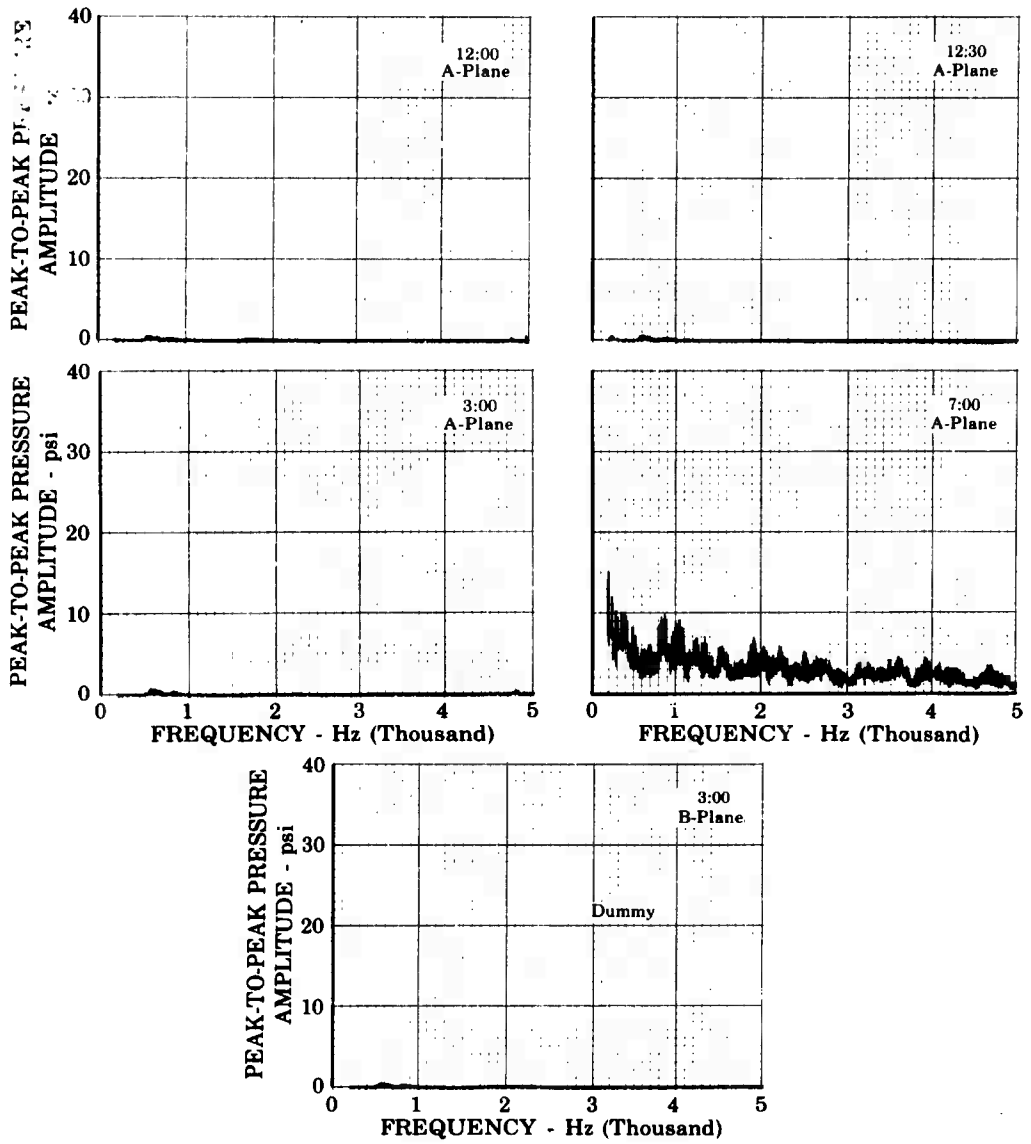

Figure 116. Pressure Amplitude Data for Film-Cooled Liner Test No. 91.01 FD 24610

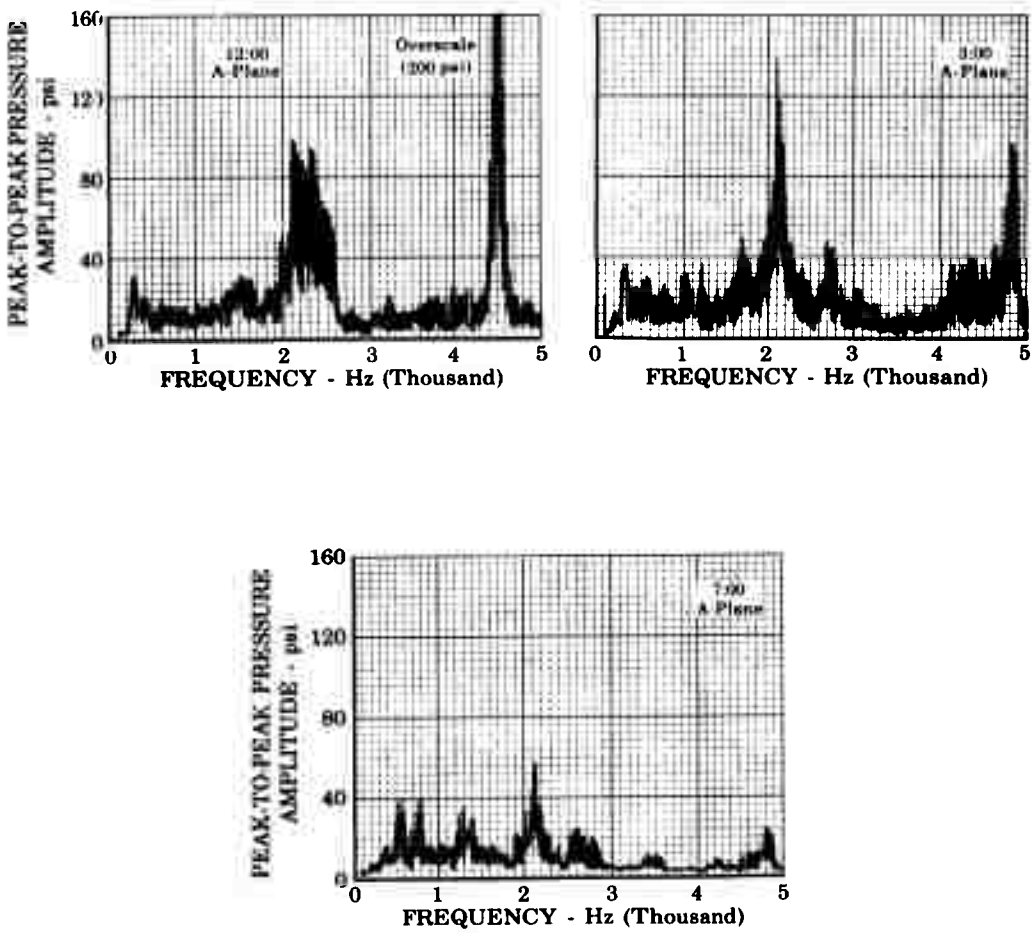

Figure 117. Pressure Amplitude Data for Ablative Liner Test No. 58.01 FD 24631

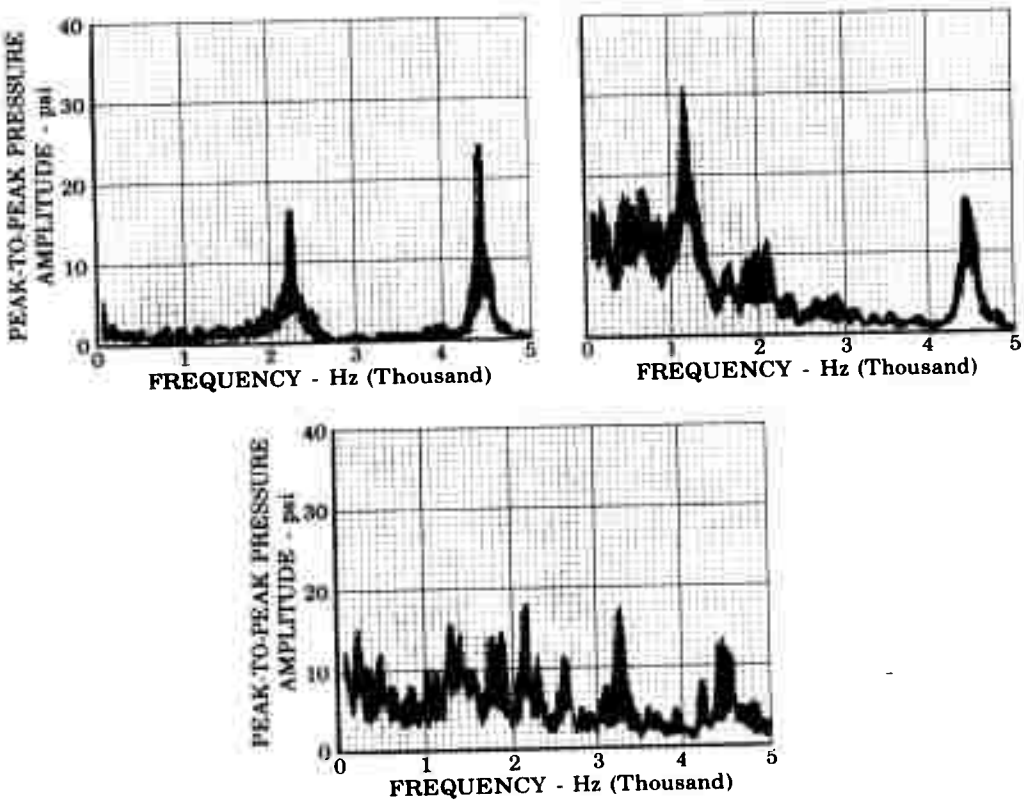

Figure 118. Pressure Amplitude Data for Ablative Liner Test No. 59.01 FD 24602

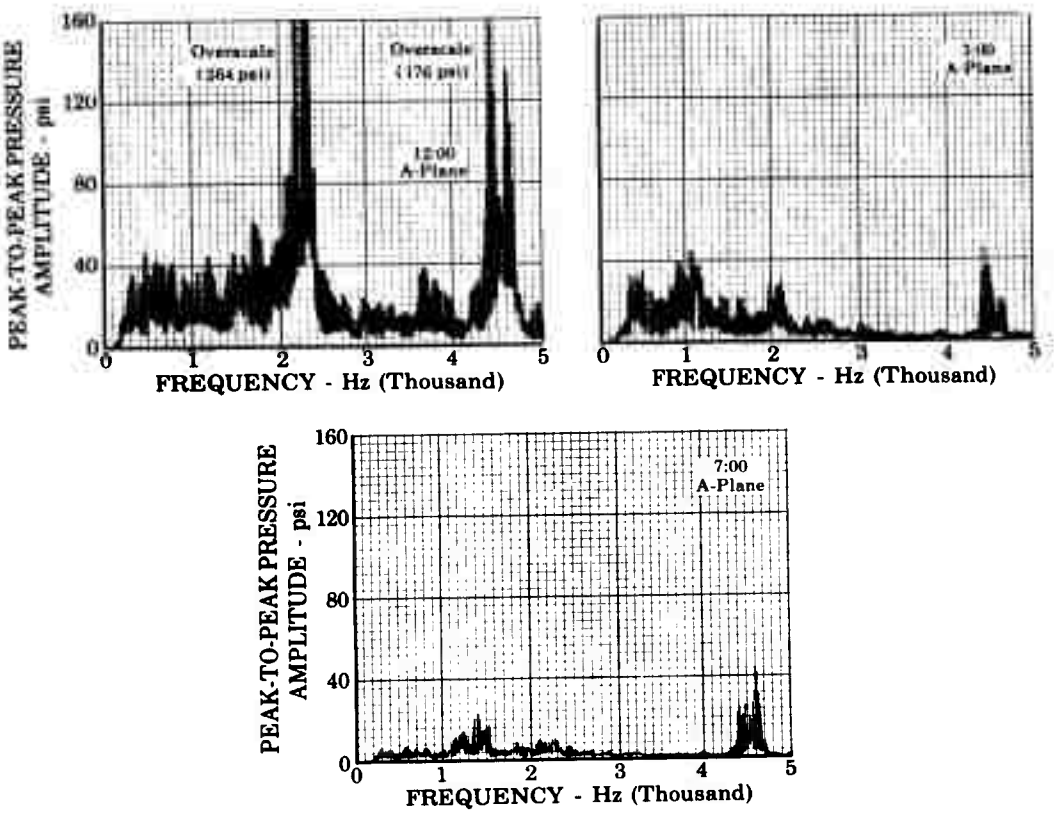

Figure 119. Pressure Amplitude Data for Ablative Liner Test No. 61.01 FD 24601

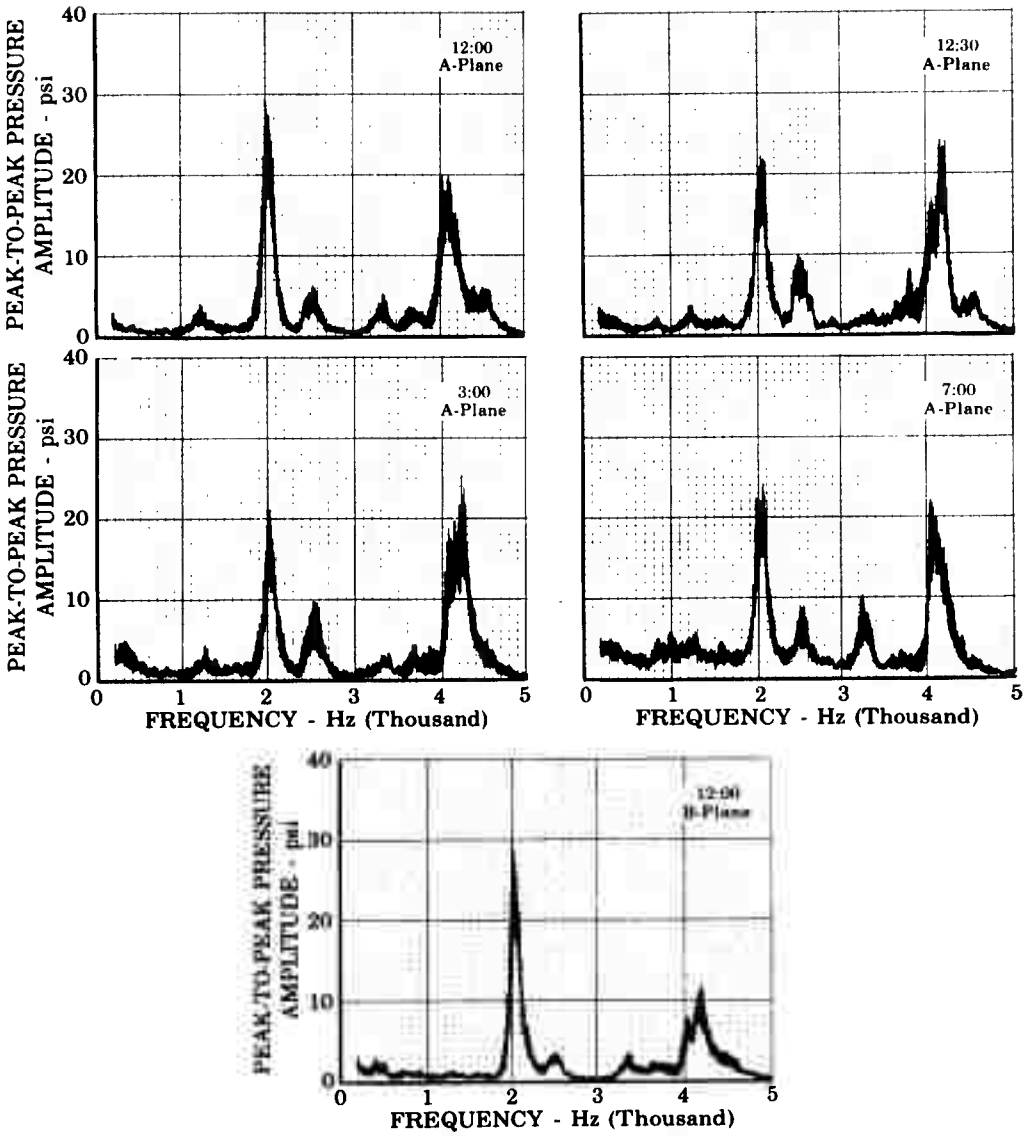

Figure 120. Pressure Amplitude Data for Ablative Liner Test No. 69.01 FD 24634

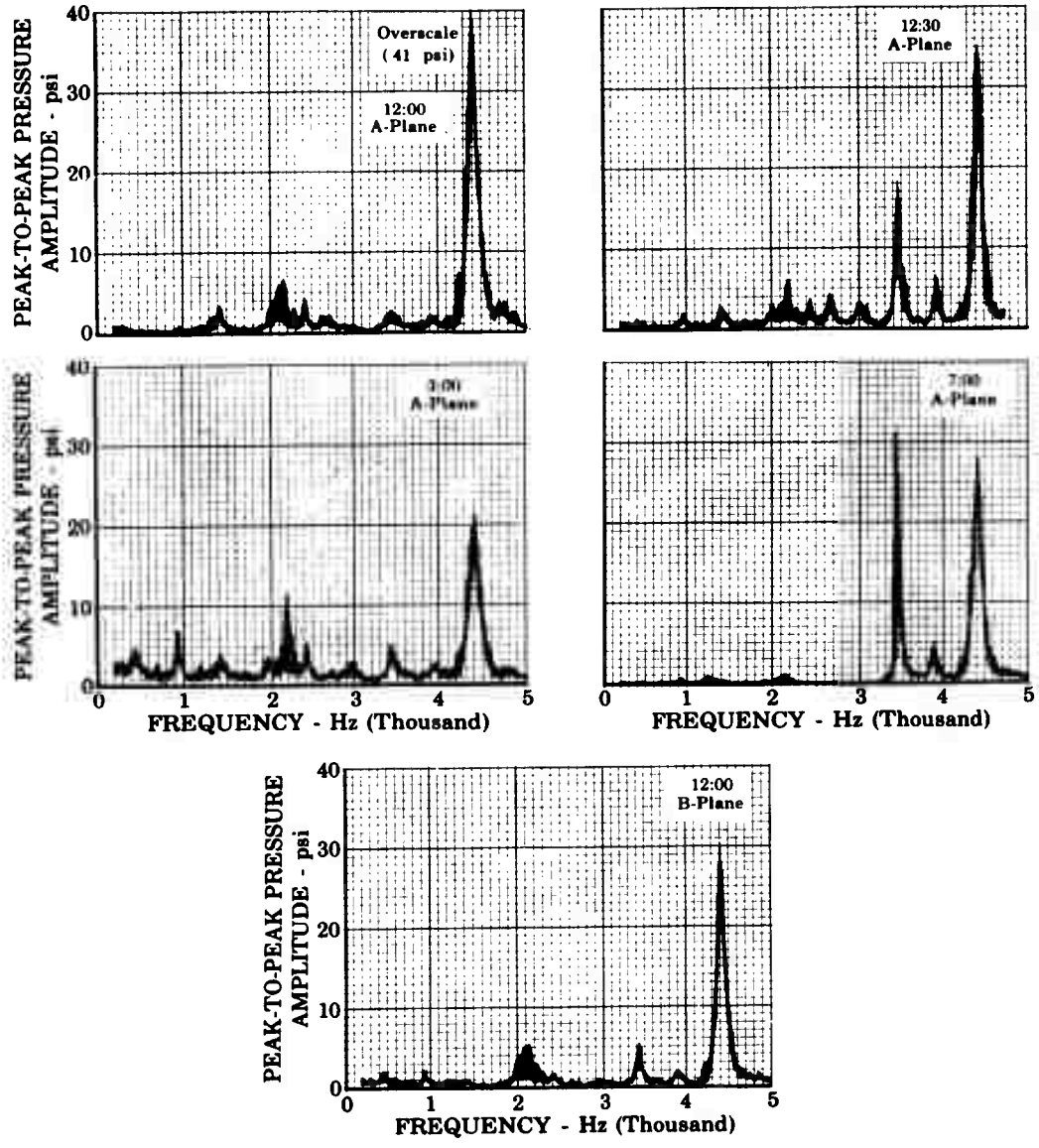

Figure 121. Pressure Amplitude Data for Ablative Liner Test No. 72.01 FD 24635

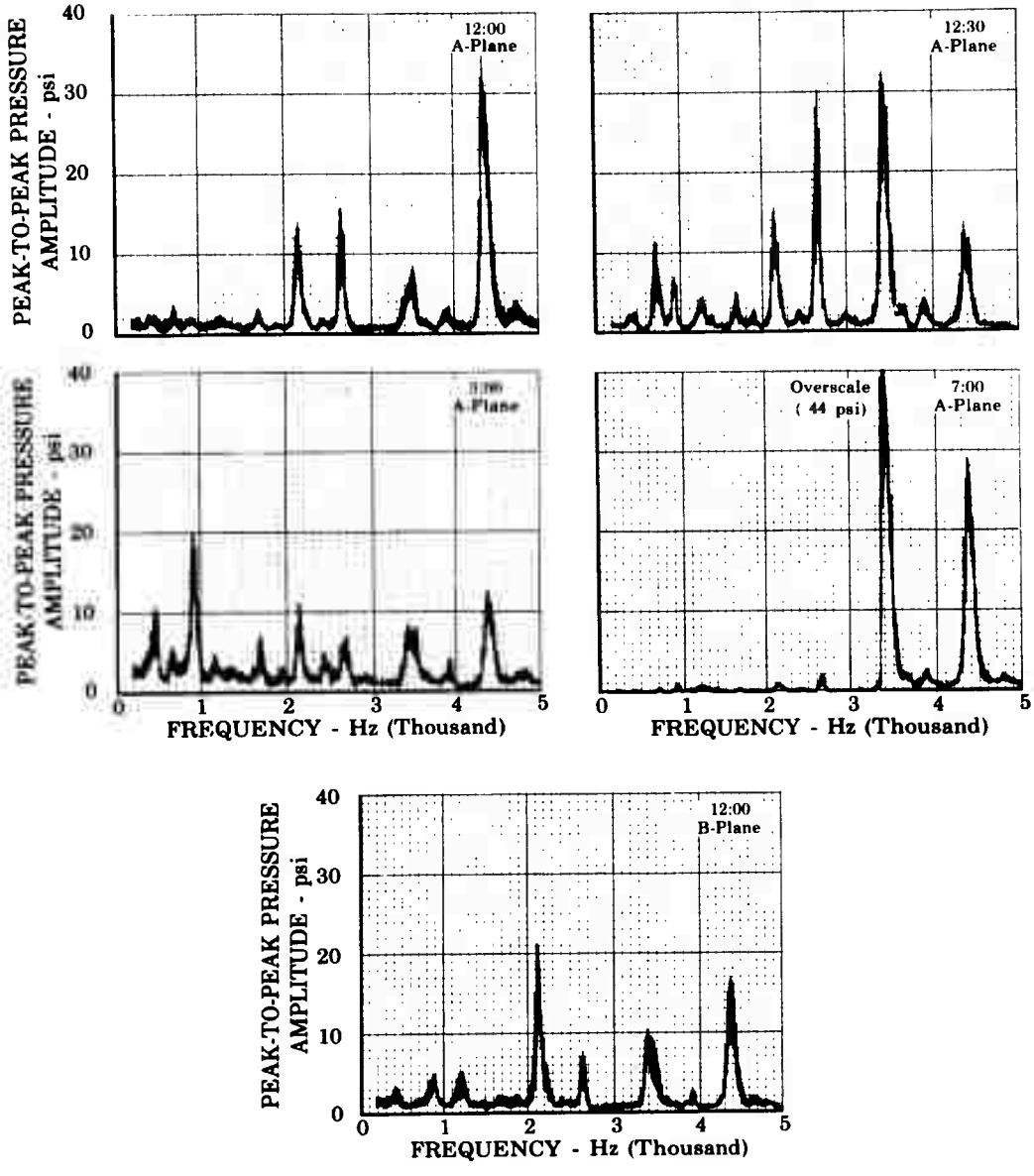

Figure 122. Pressure Amplitude Data for Ablative Liner Test No. 72.01 FD 24636

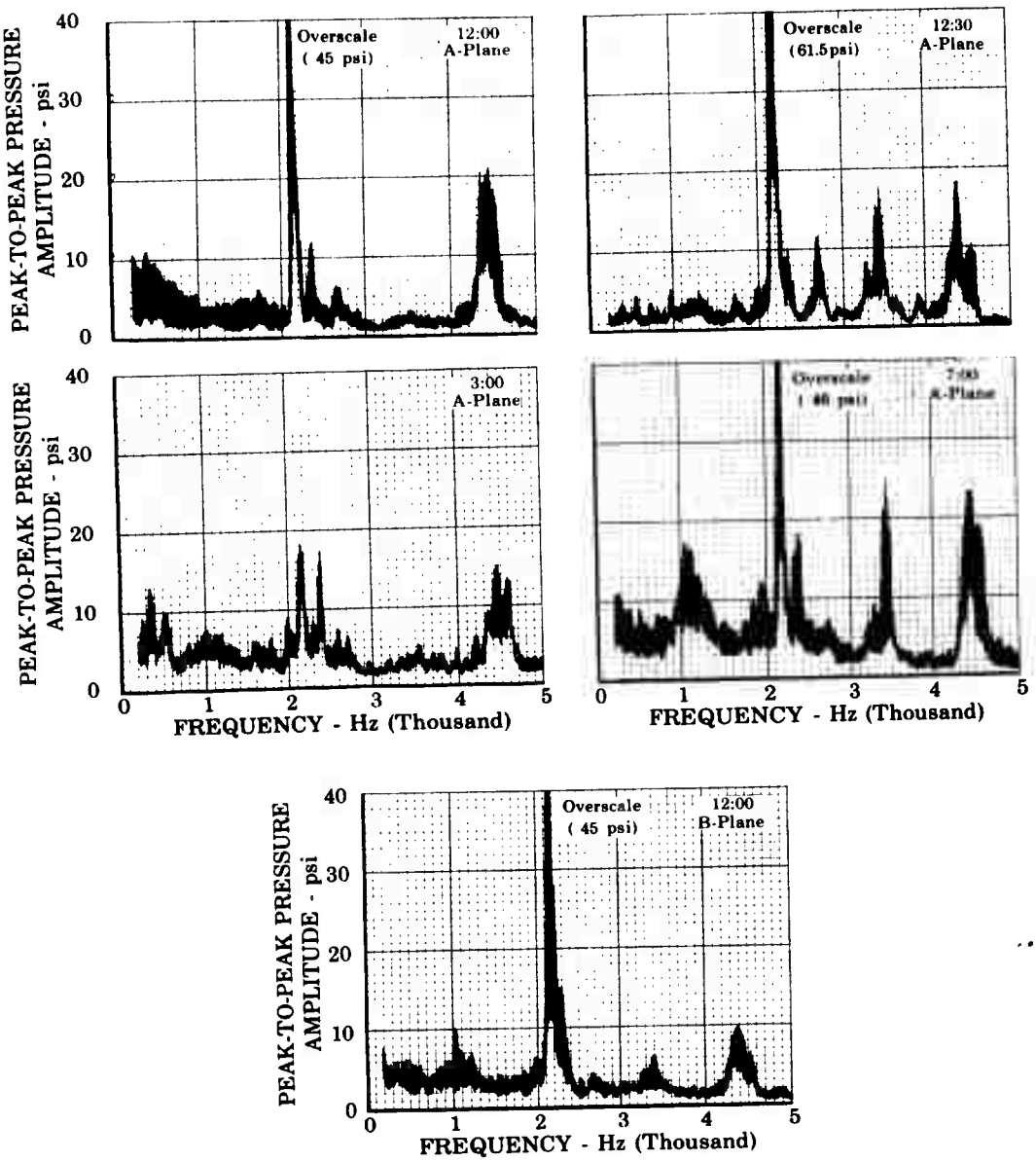

Figure 123. Pressure Amplitude Data for Ablative Liner Test No. 72.01

FD 24637

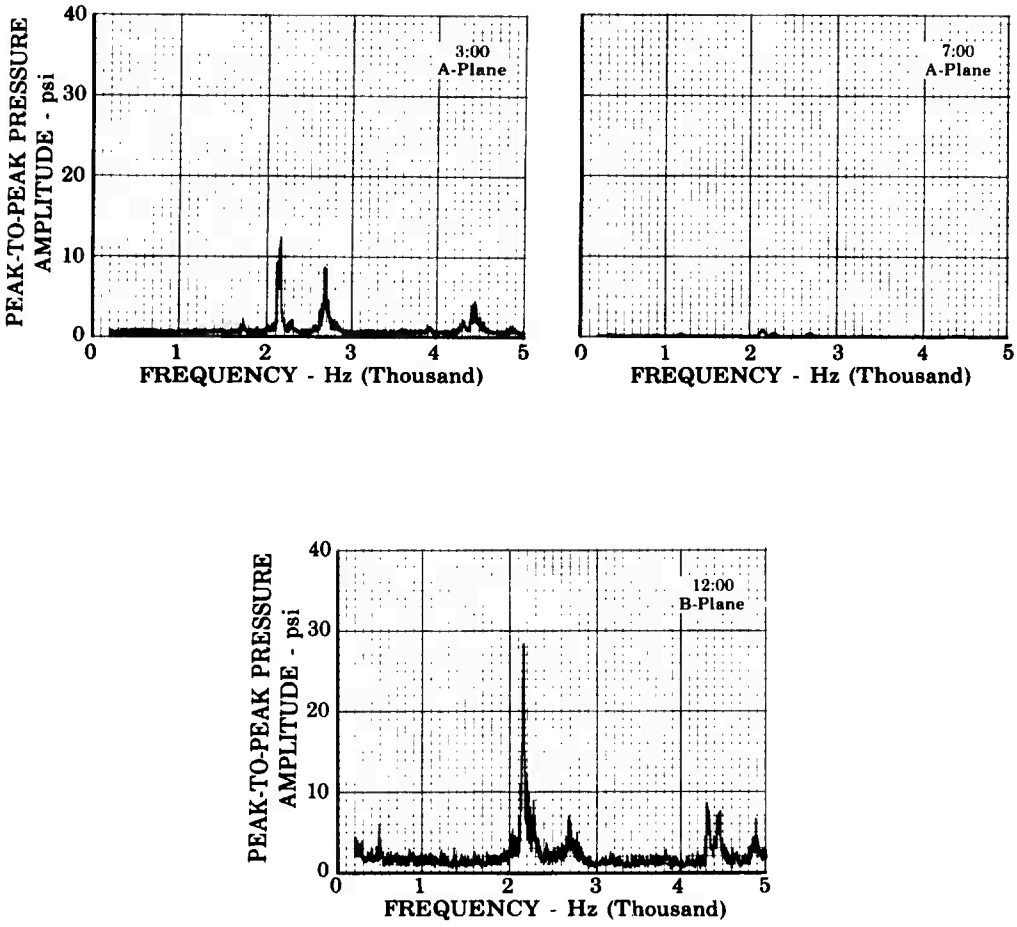

Figure 124. Pressure Amplitude Data for Ablative Liner Test No. 100.01 FD 24621

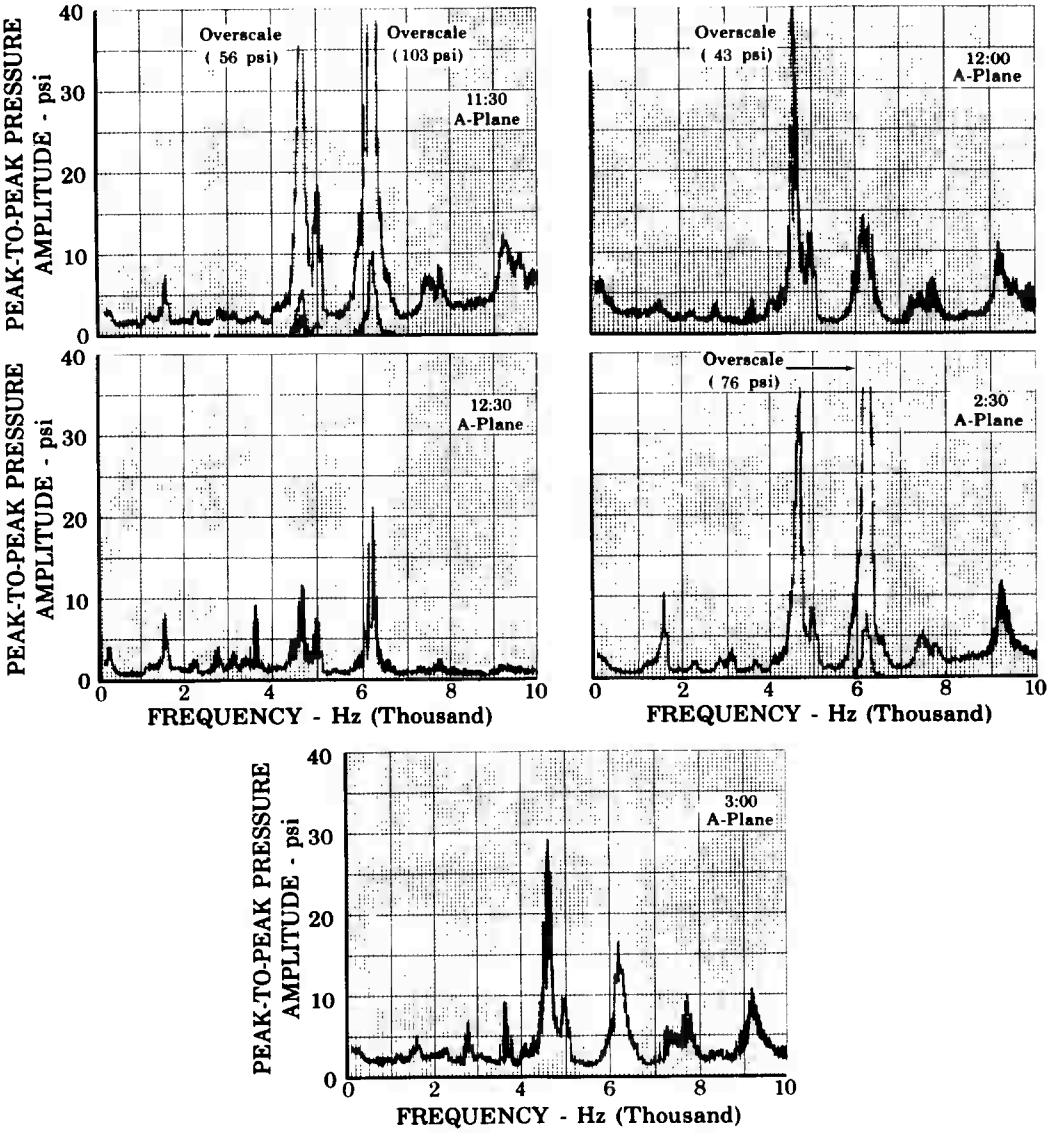

Figure 125. Pressure Amplitude Data for Individual Resonator Steel Liner Test No. 104.01

FD 24622

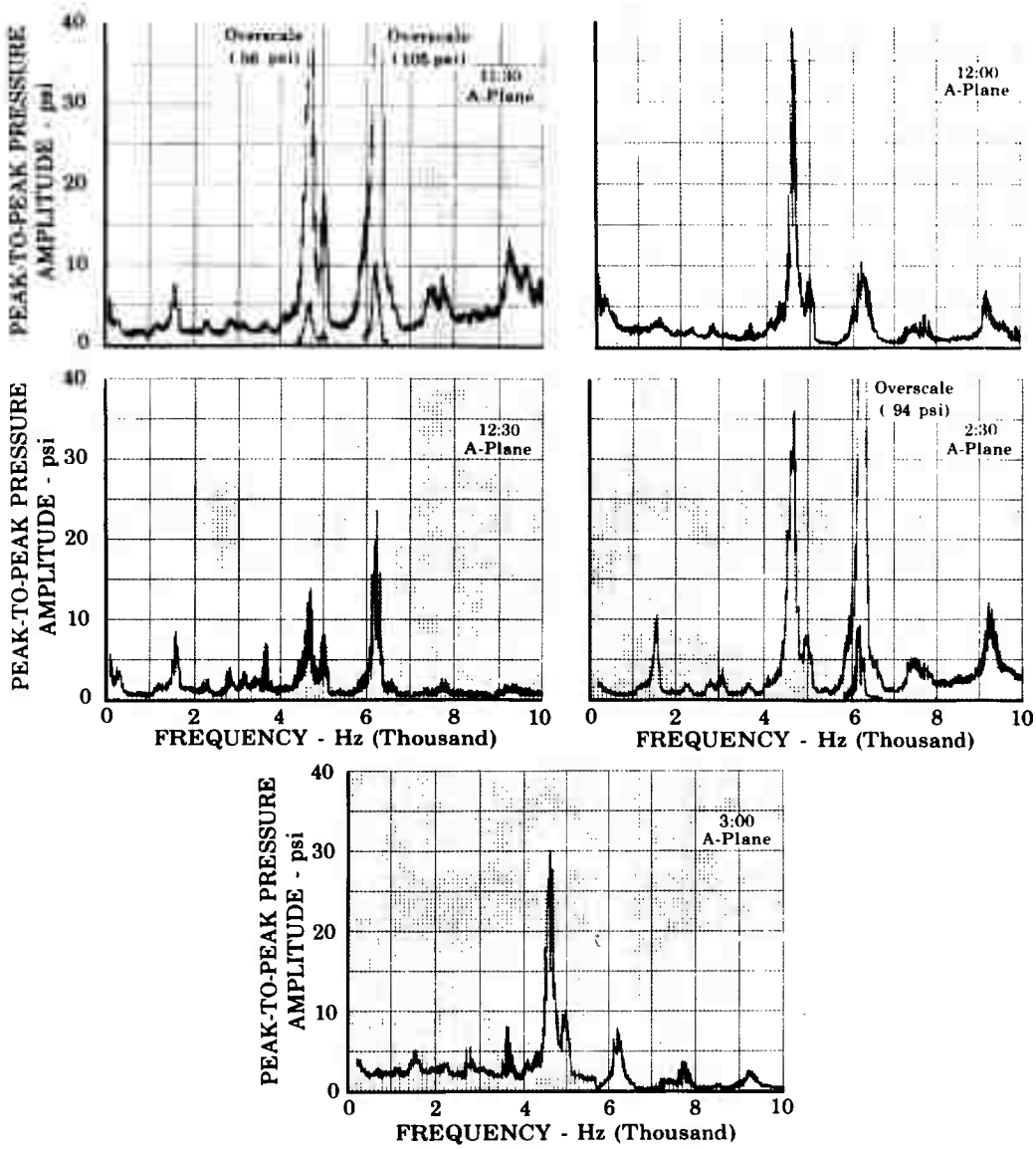

Figure 126. Pressure Amplitude Data for Individual Resonator Steel Liner Test No. 105.01

FD 24623

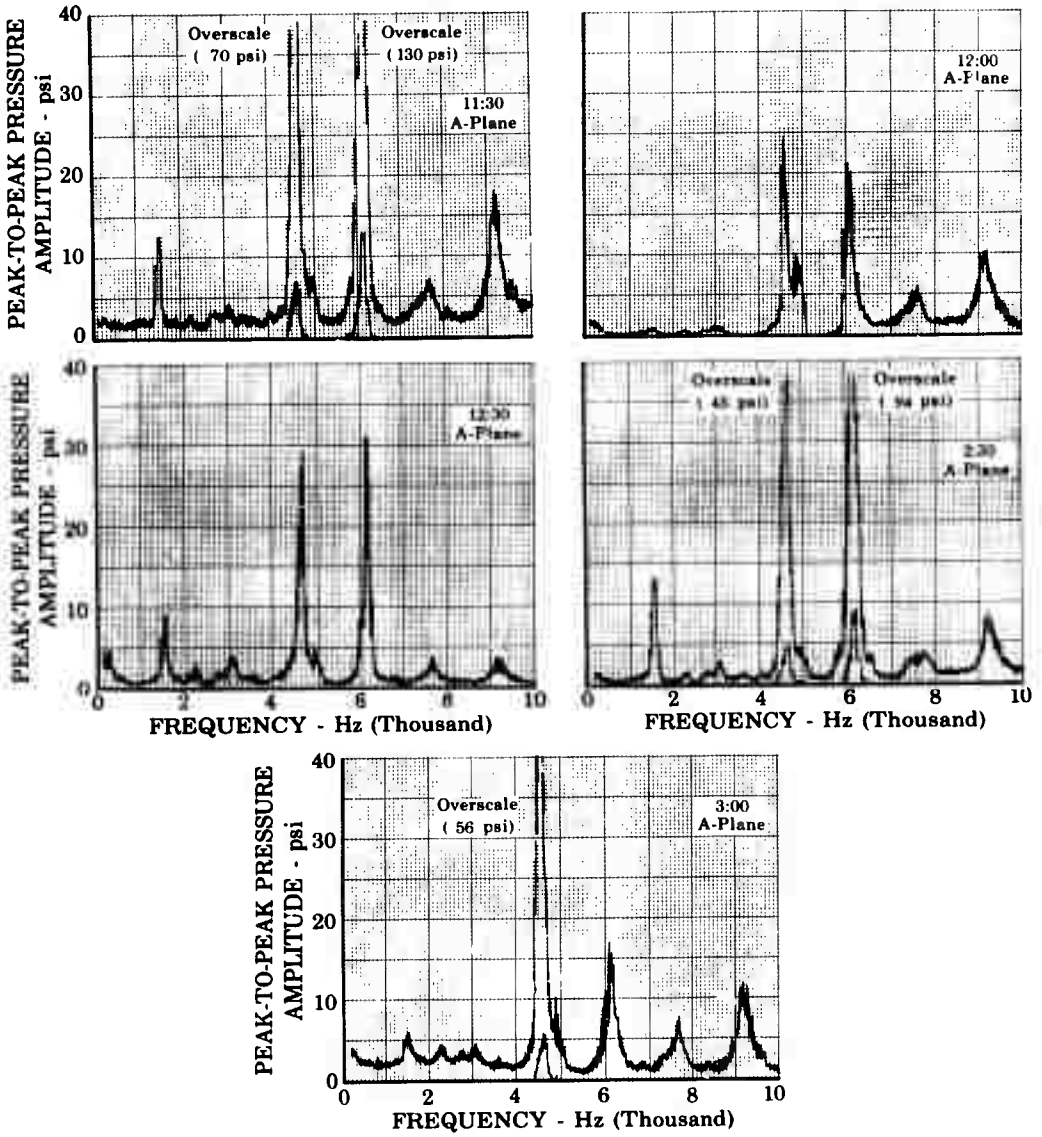

Figure 127. Pressure Amplitude Data for Individual Resonator Steel Liner Test No. 106.01

FD 24624

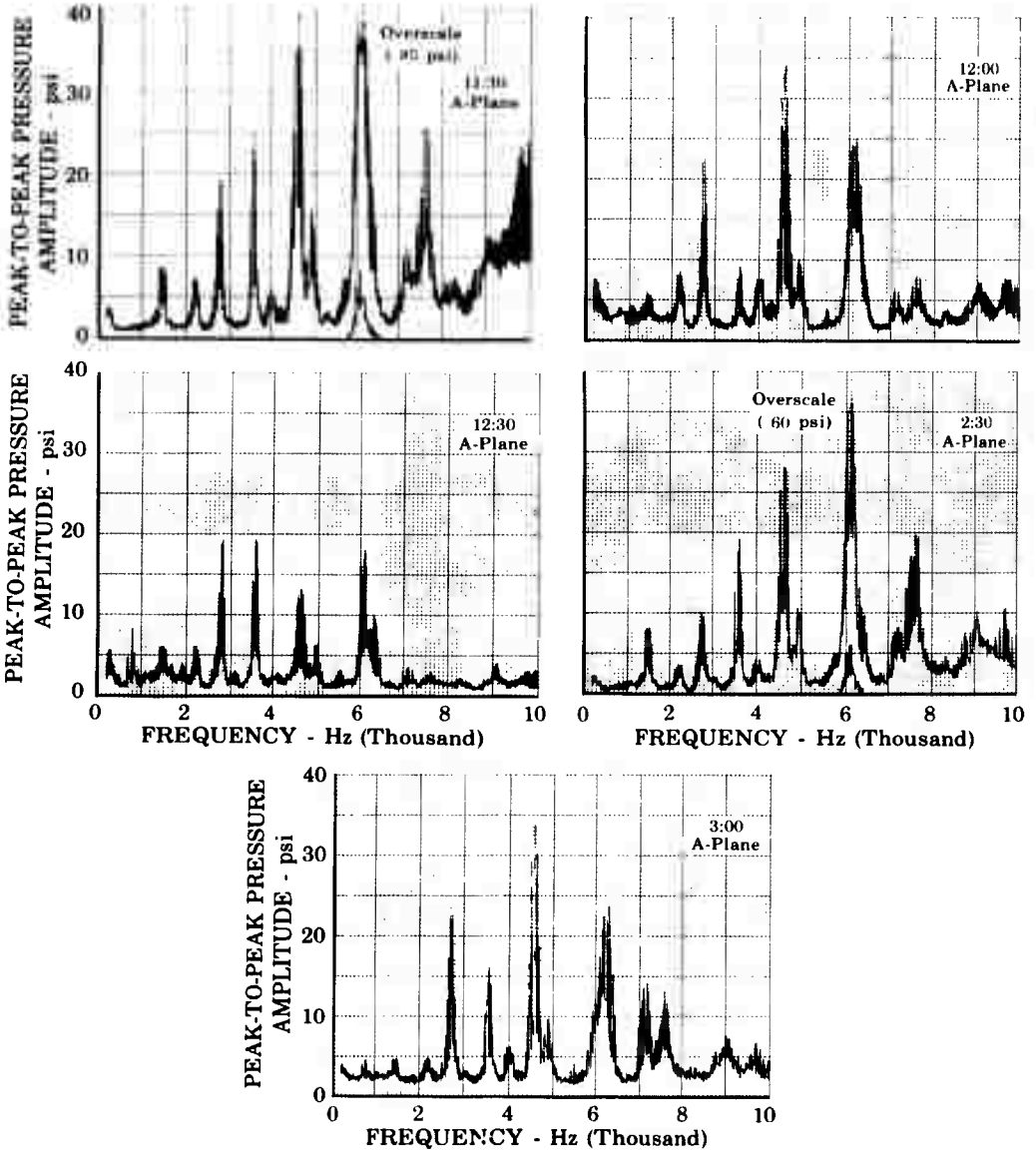

Figure 128. Pressure Amplitude Data for Individual Resonator Steel Liner Test No. 107.01

FD 24625

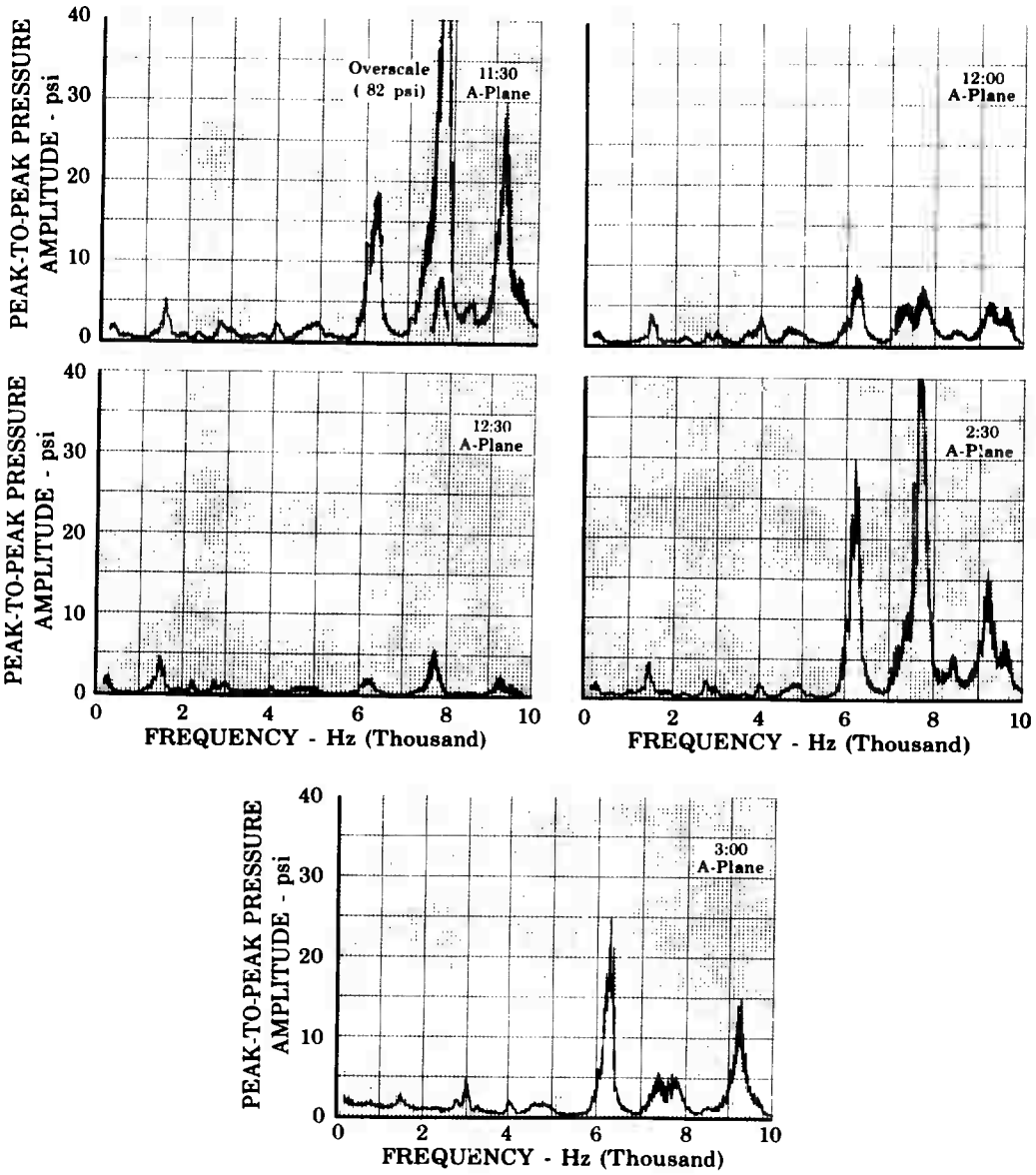

Figure 129. Pressure Amplitude Data for Parallel Array Steel Liner Test No. 110.01

FD 24626

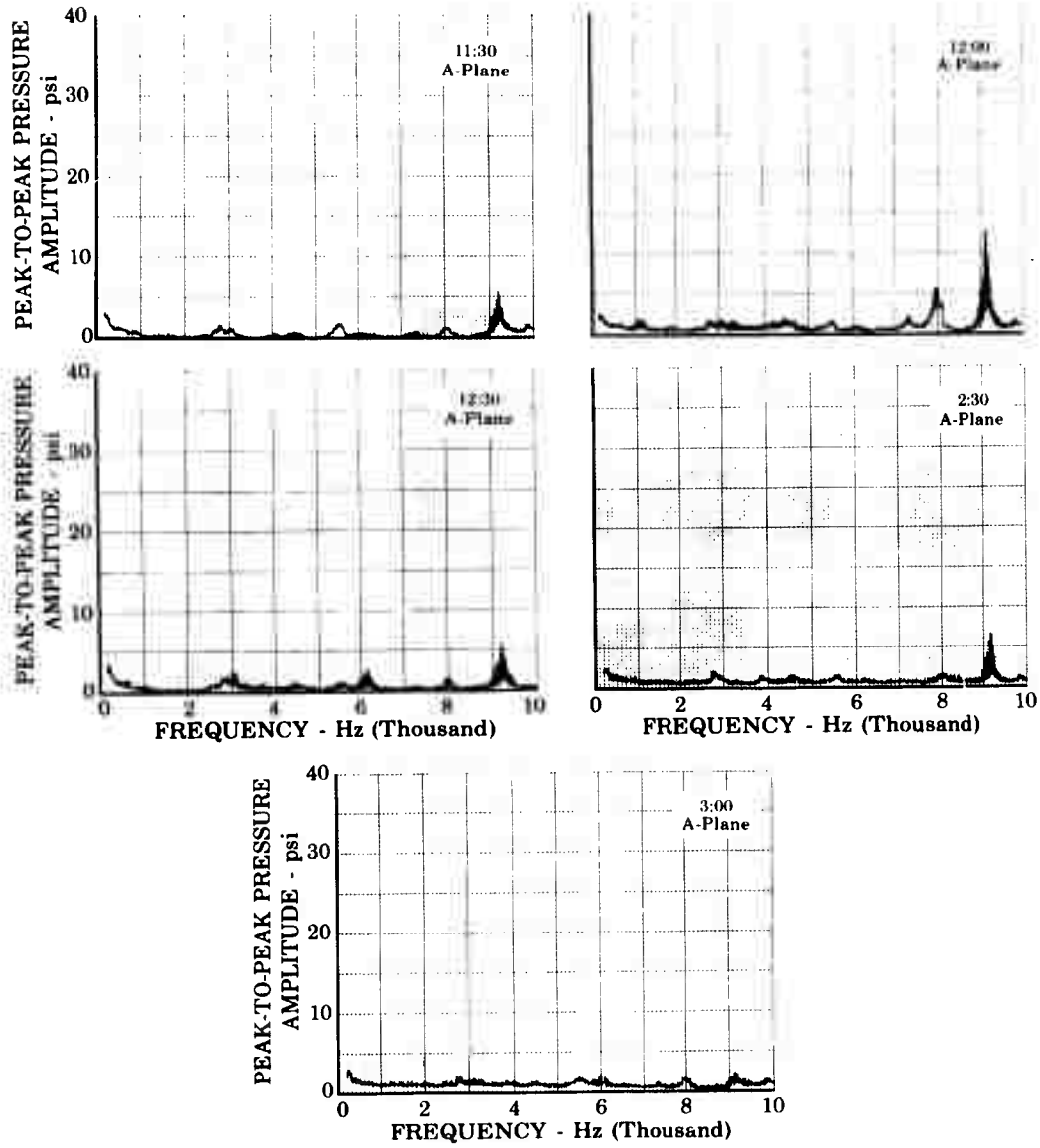

Figure 130. Pressure Amplitude Data for Parallel Array Steel Liner Test No. 111.01

FD 24627

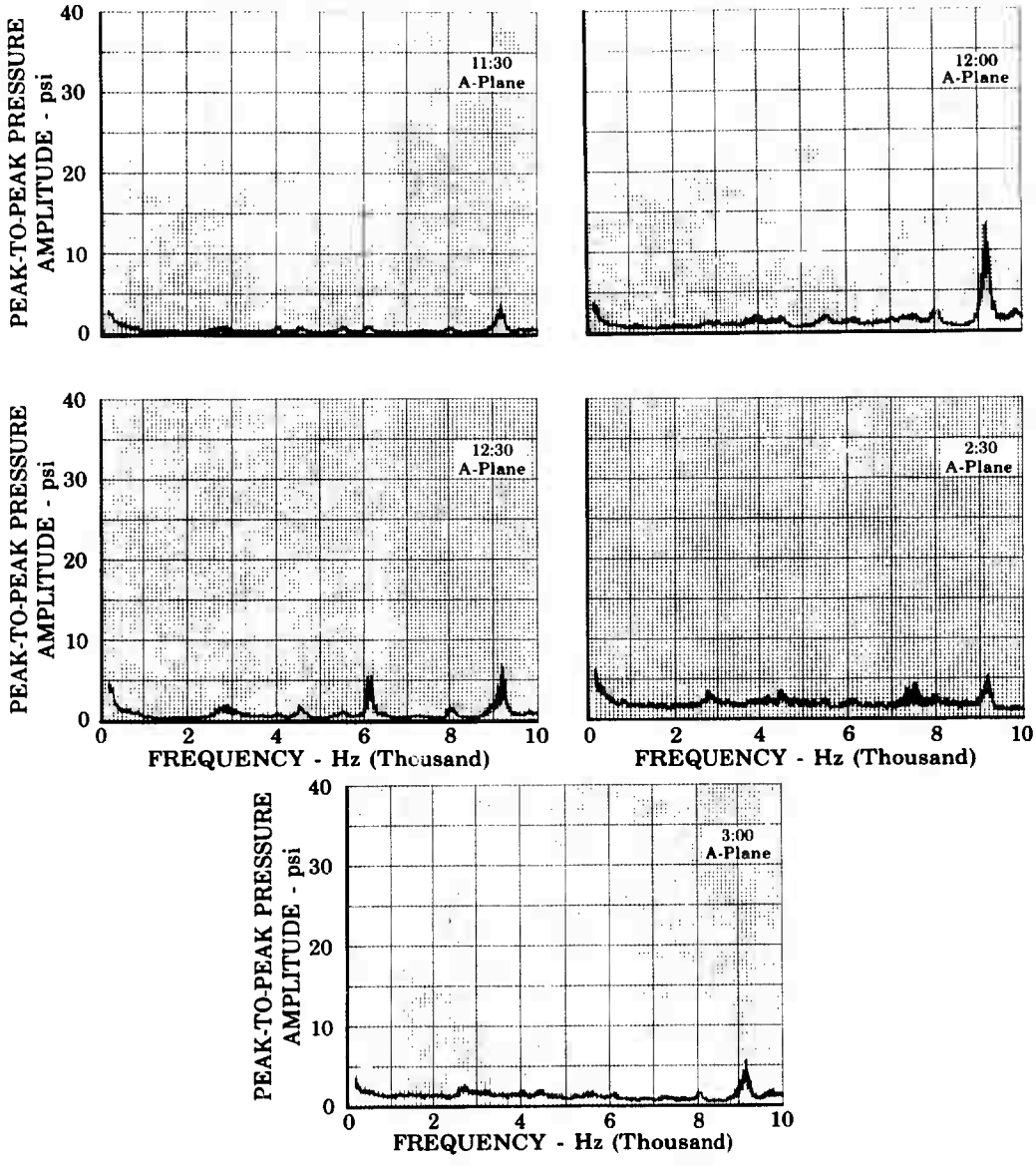

Figure 131. Pressure Amplitude Data for Parallel Array Steel Liner Test No. 112.01

FD 24628

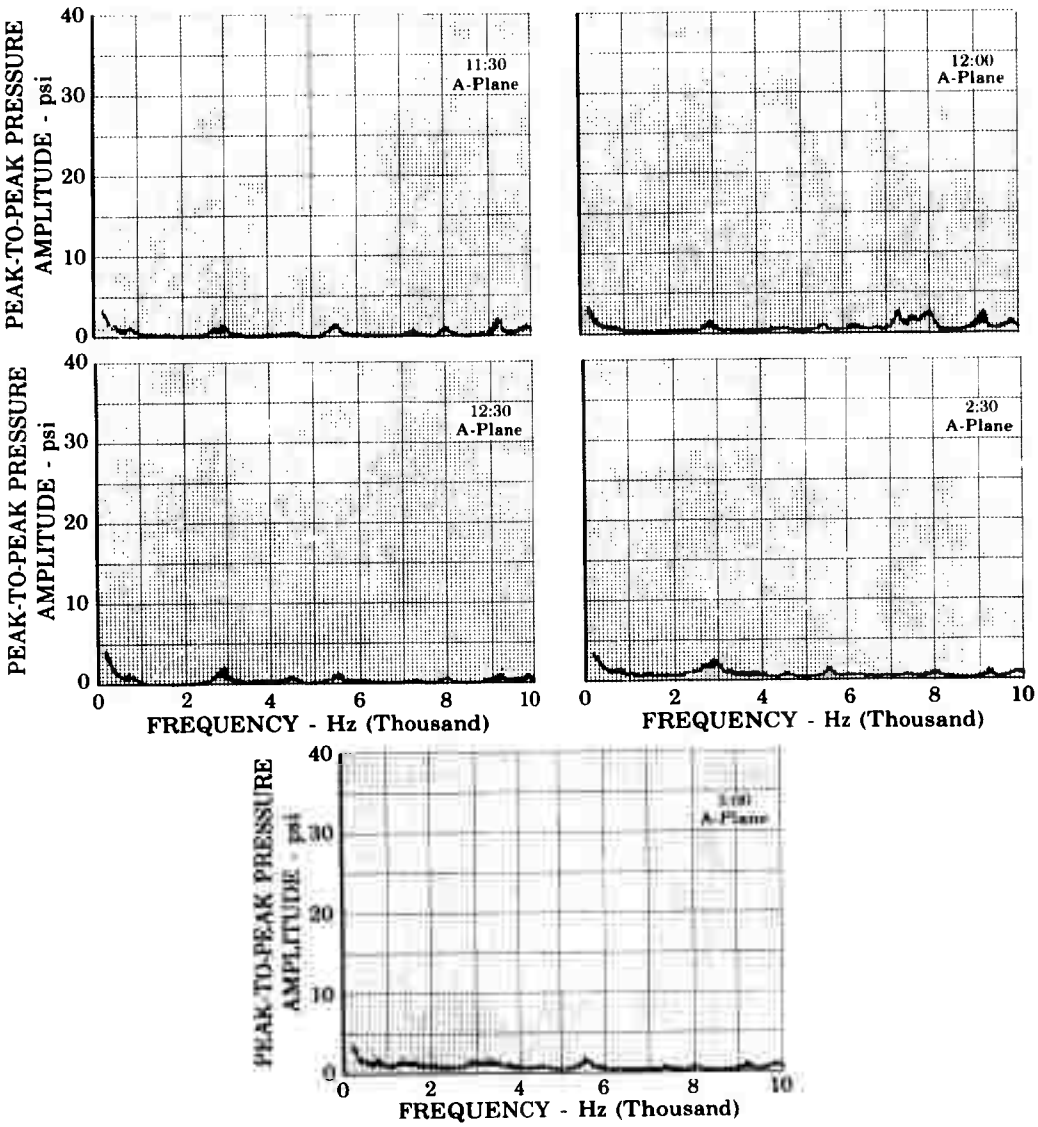

Figure 132. Pressure Amplitude Data for Parallel Array Steel Liner Test No. 112.01

FD 24629

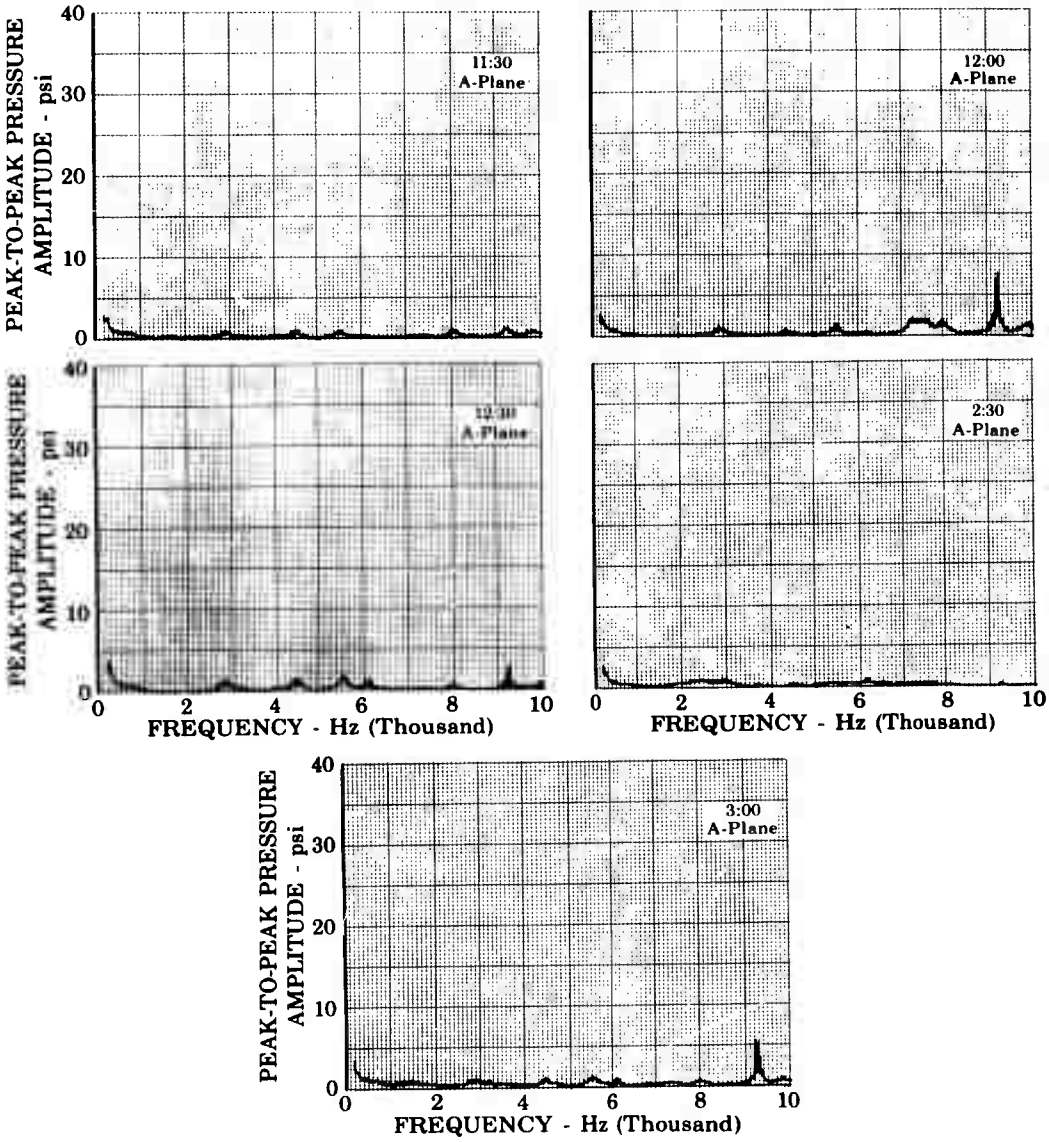

Figure 133. Pressure Amplitude Data for Parallel Array Steel Liner Test No. 113.01

FD 24630

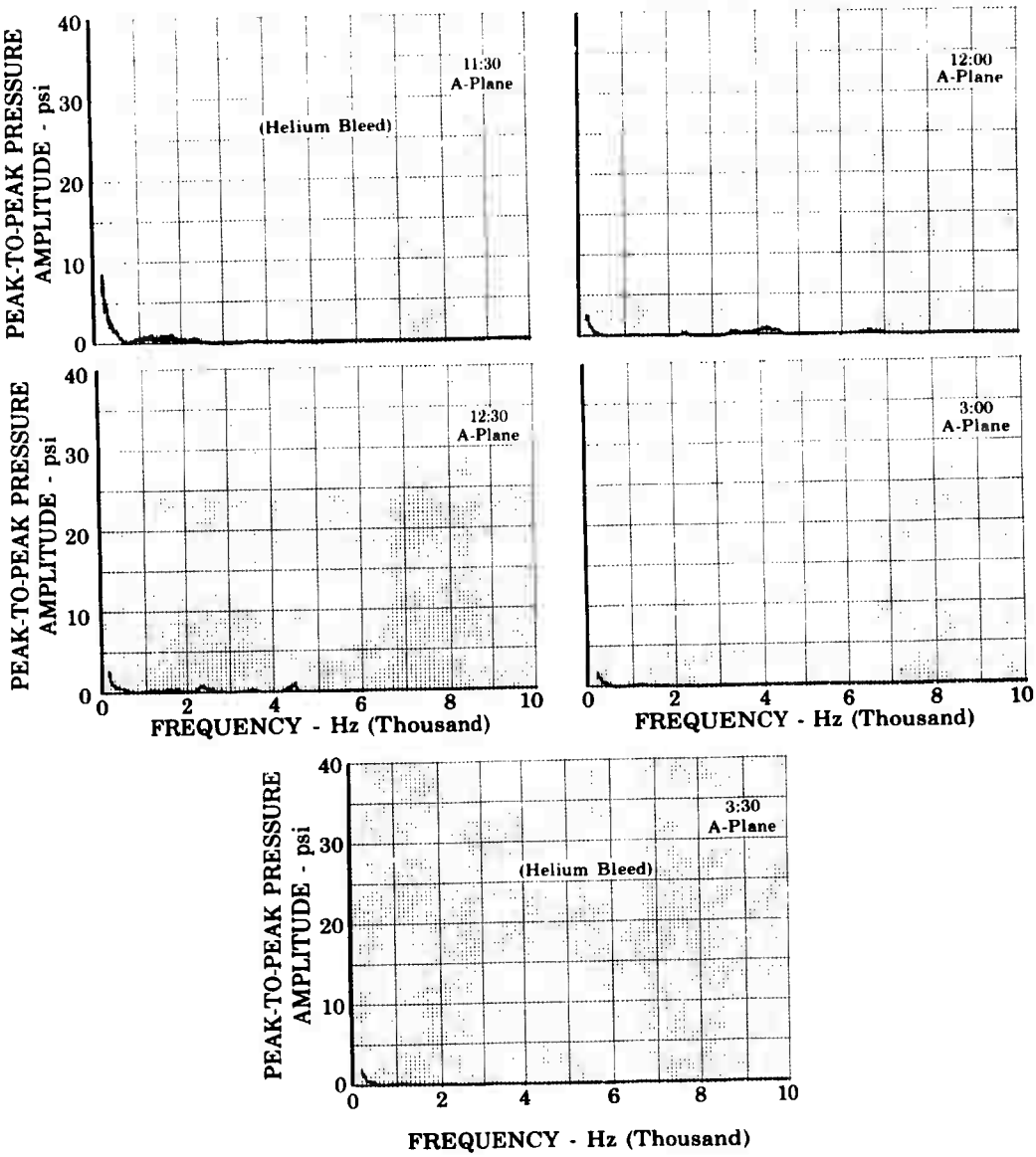

Figure 134. Pressure Amplitude Data for Parallel Array Ablative Liner Test No. 118.01

FD 24662

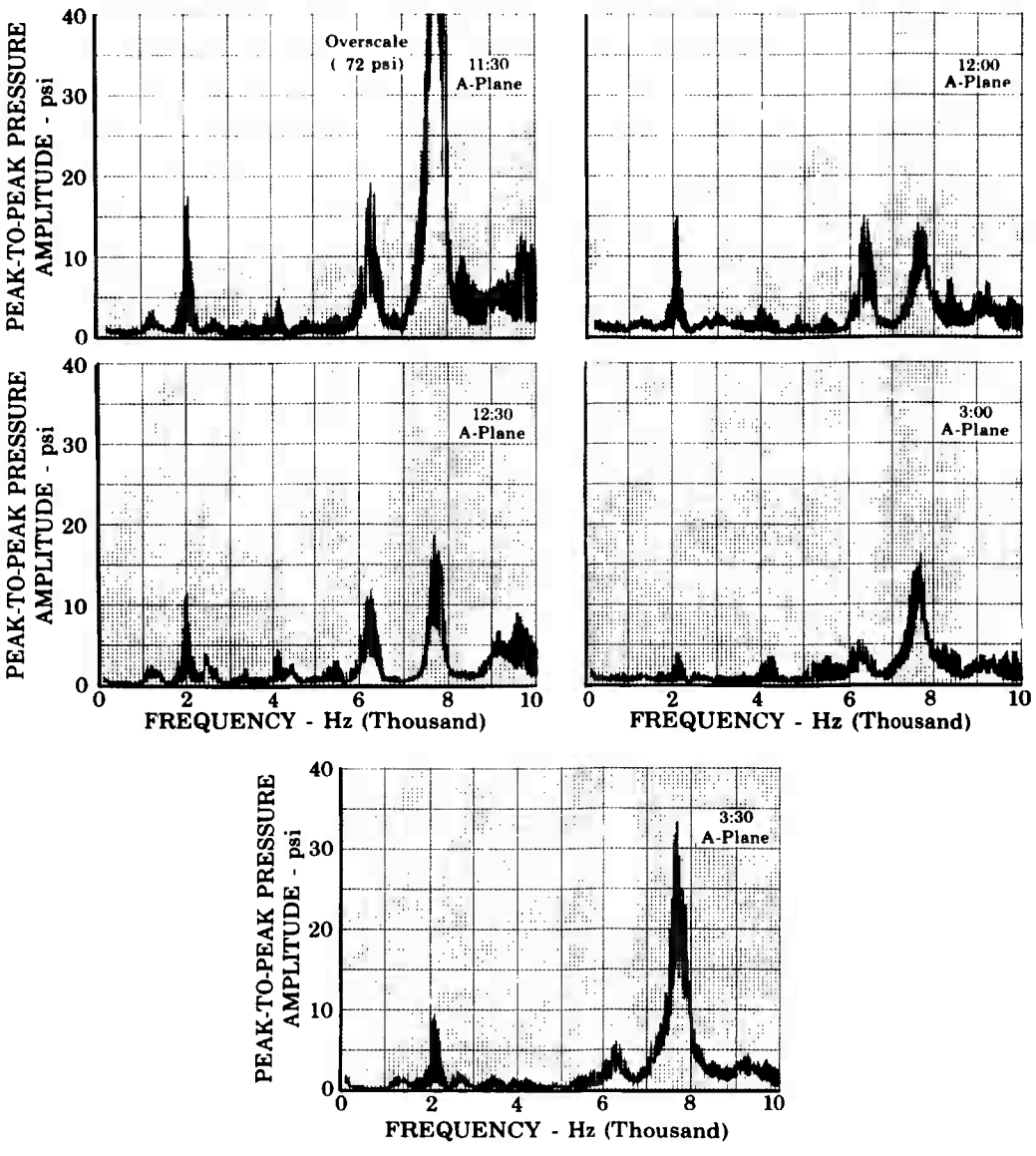

Figure 135. Pressure Amplitude Data for Dual Open Area Steel Liner Test No. 121.01

FD 24663

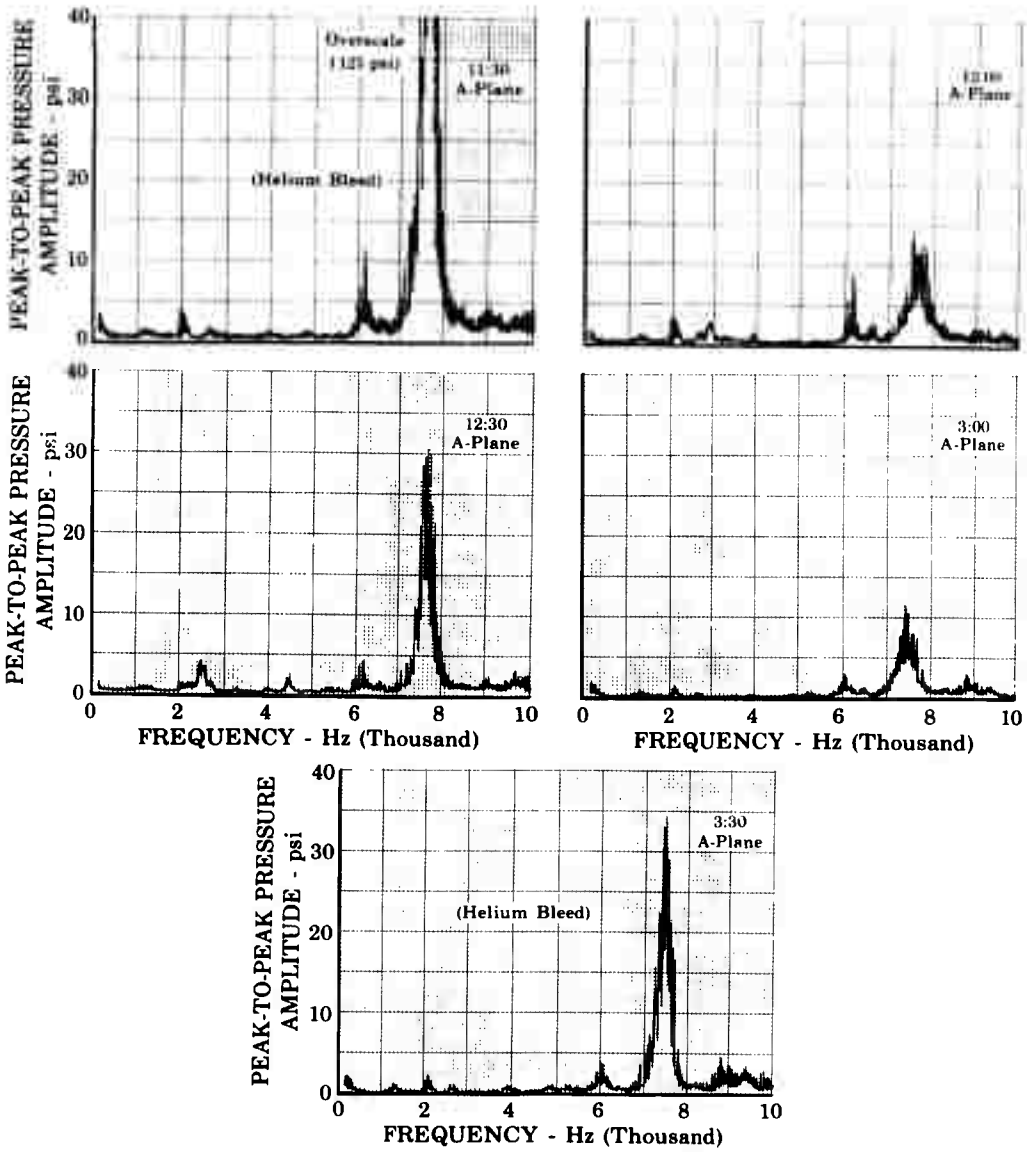

Figure 136. Pressure Amplitude Data for Dual Open Area Steel Liner Test No. 122.01

FD 24664

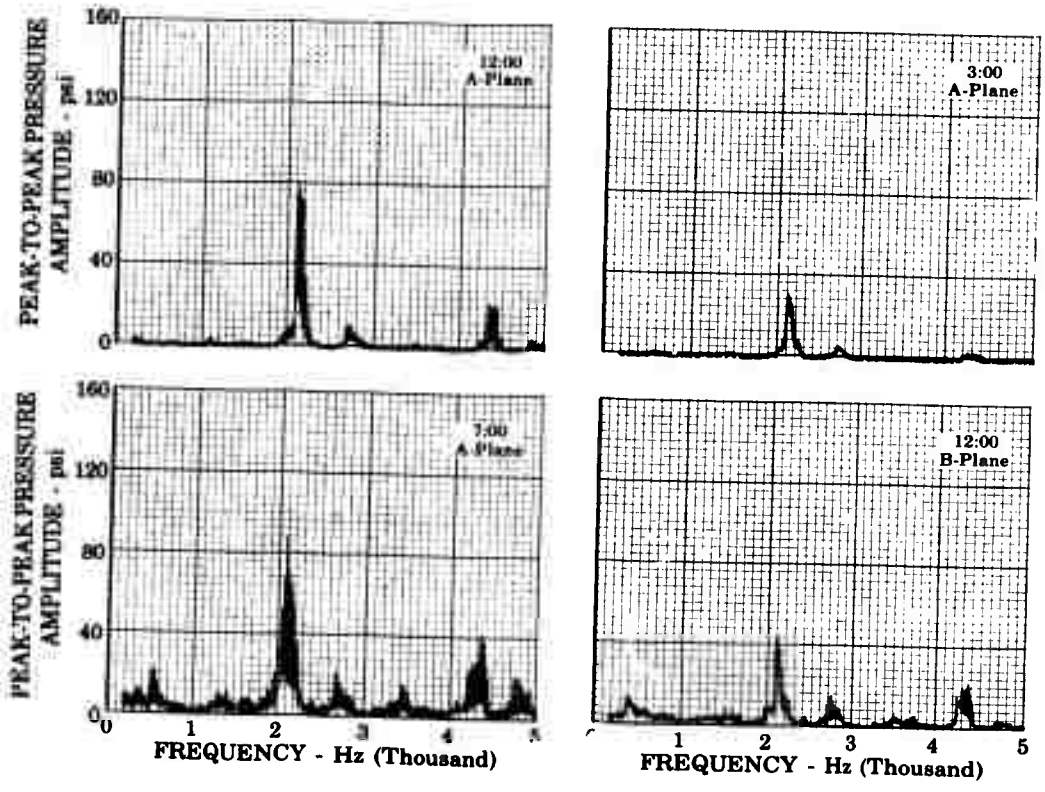

Figure 137. Pressure Amplitude Data for Wafer Liner Test No. 92.09 FD 24612

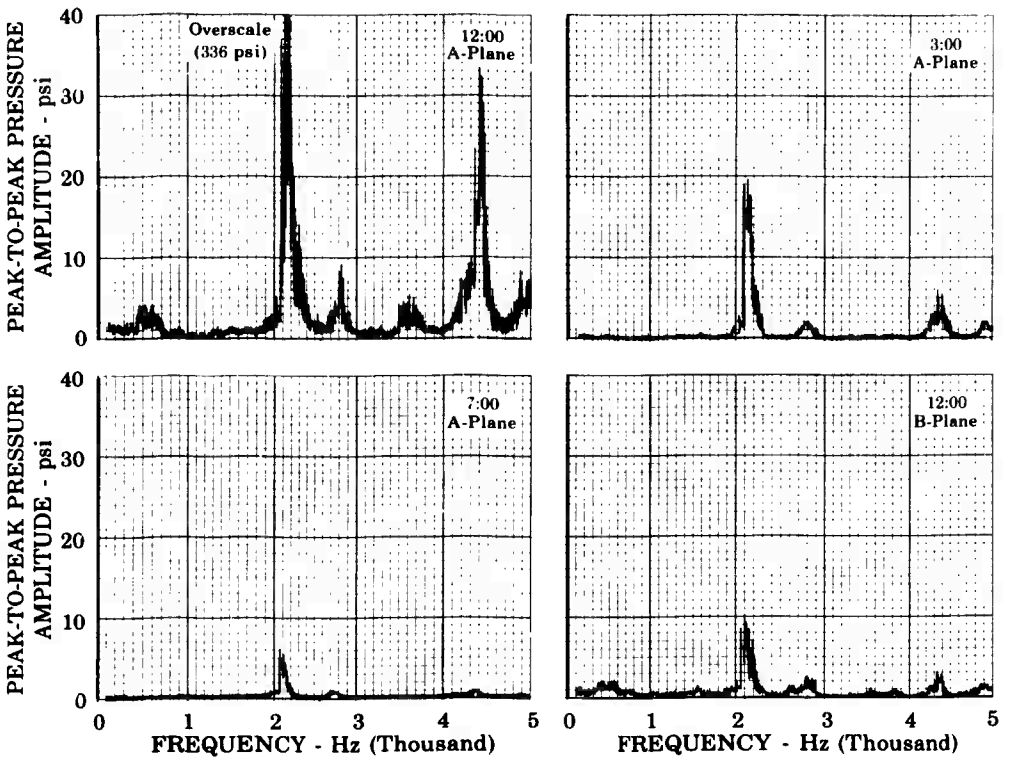

Figure 138. Pressure Amplitude Data for Wafer Liner Test No. 93.01 FD 24613

UNCLASSIFIED

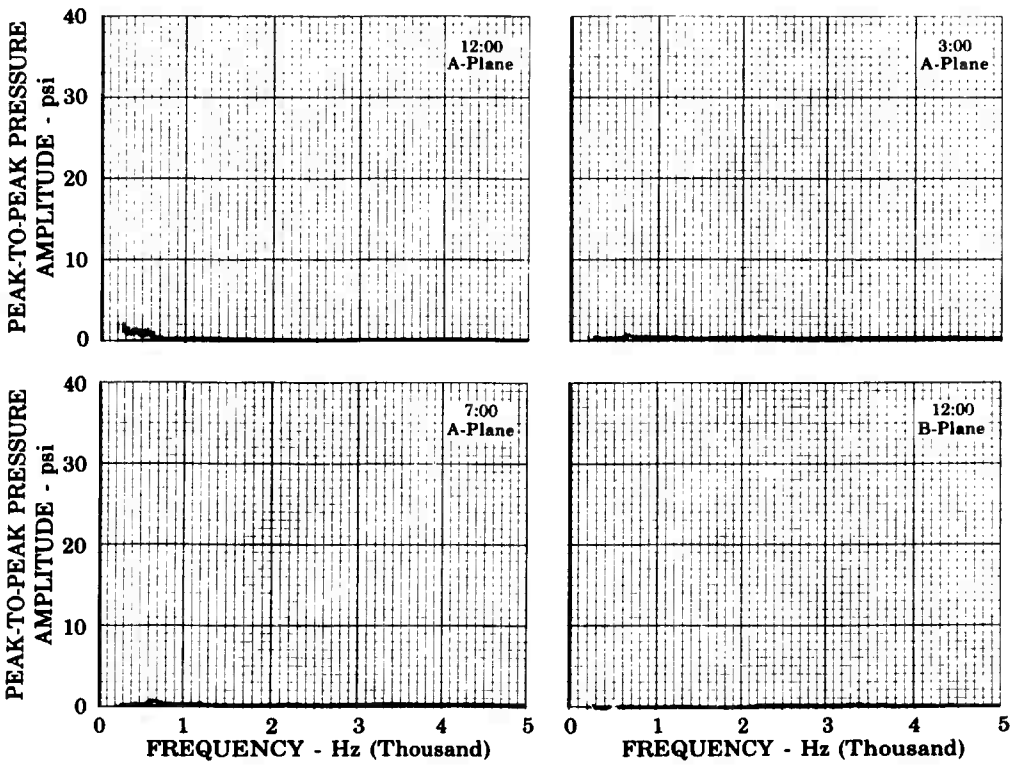

Figure 139. Pressure Amplitude Data for Wafer Liner Test No. 94.01 FD 24614

UNCLASSIFIED

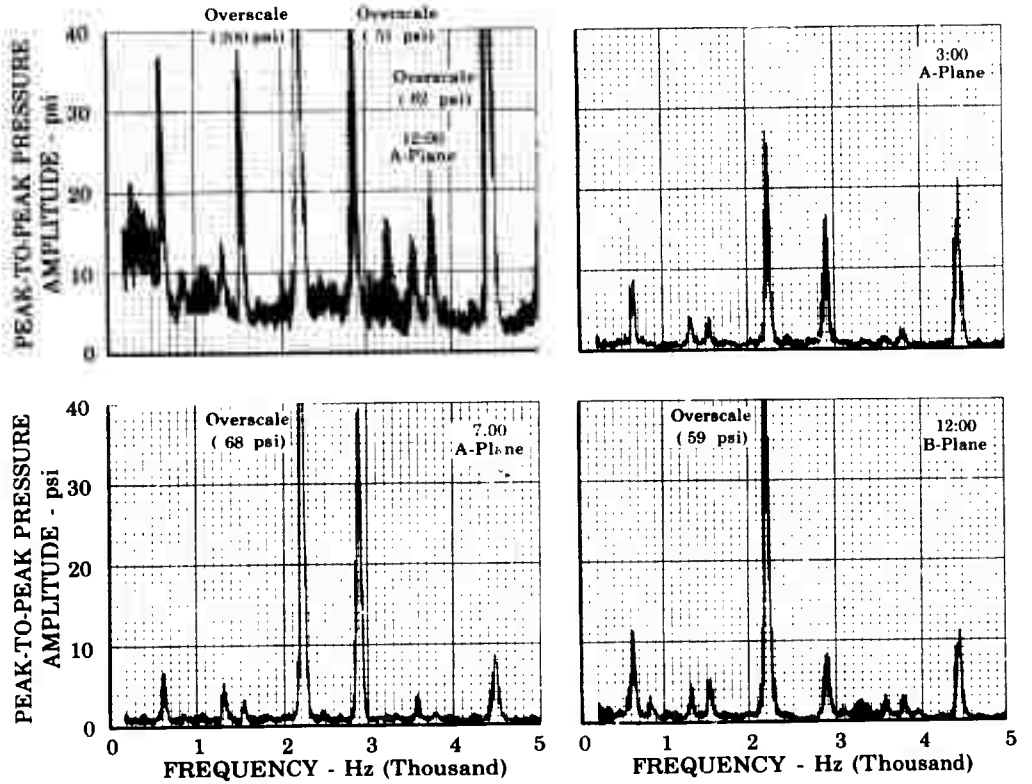

Figure 140. Pressure Amplitude Data for Wafer Liner Test No. 95.01

FD 24615

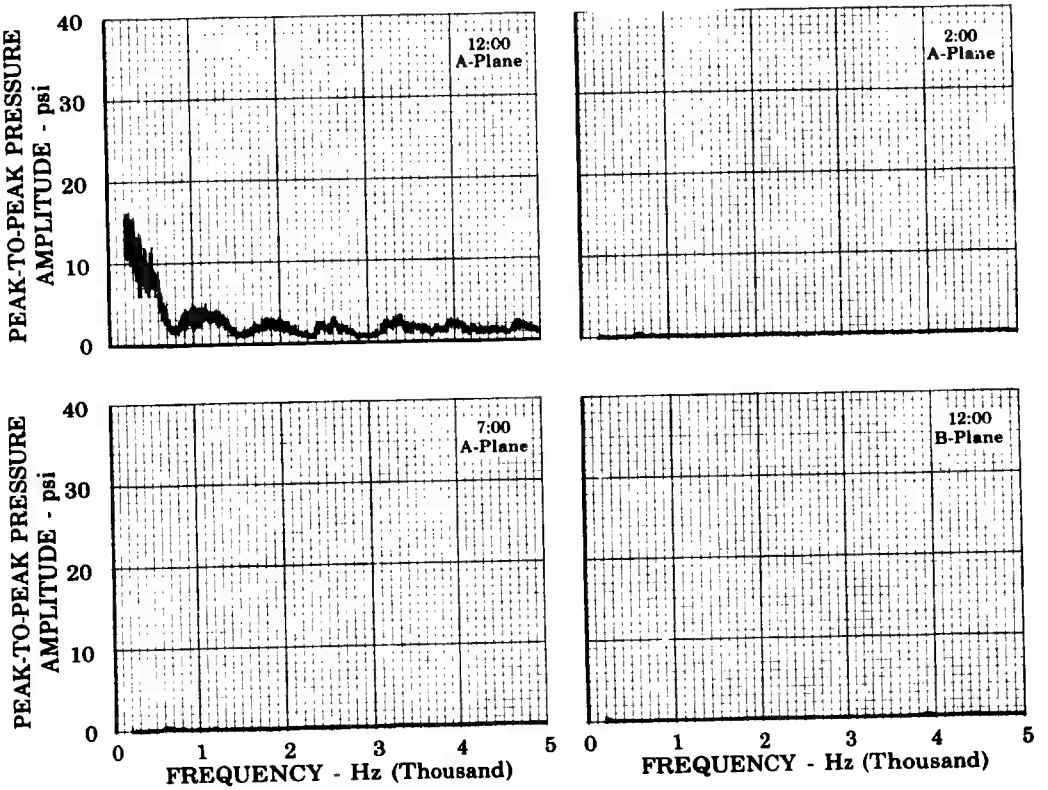

Figure 141. Pressure Amplitude Data for Wafer Liner Test No. 96.03

FD 24616

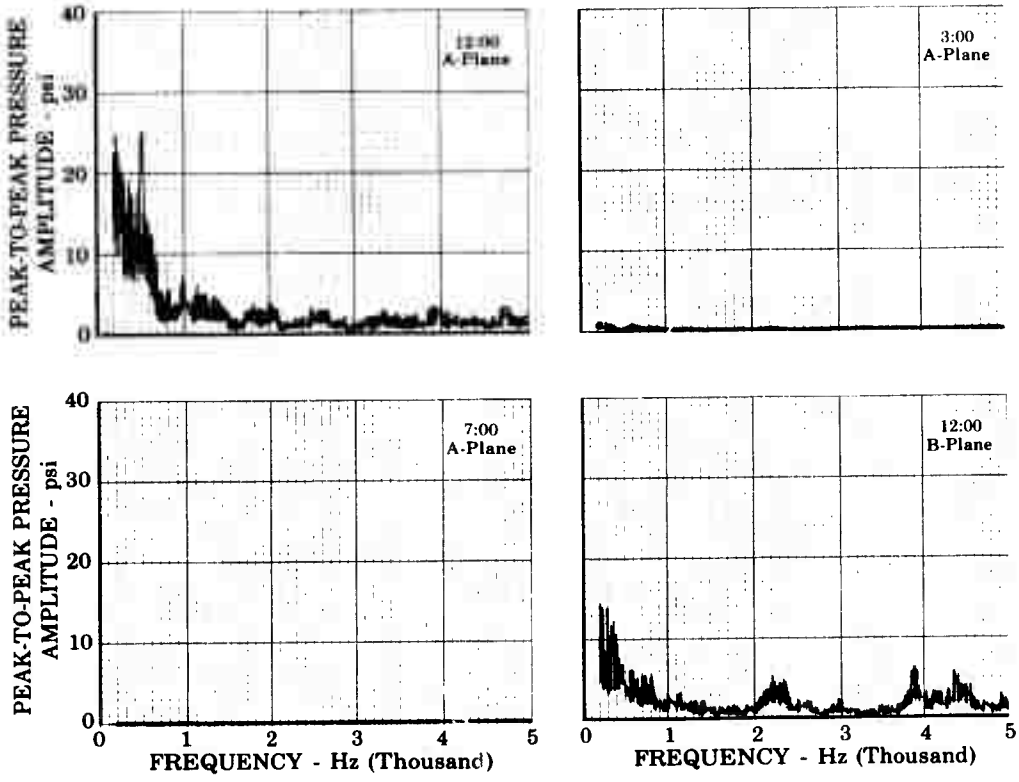

Figure 142. Pressure Amplitude Data for Wafer Liner Test No. 97.02

FD 24619

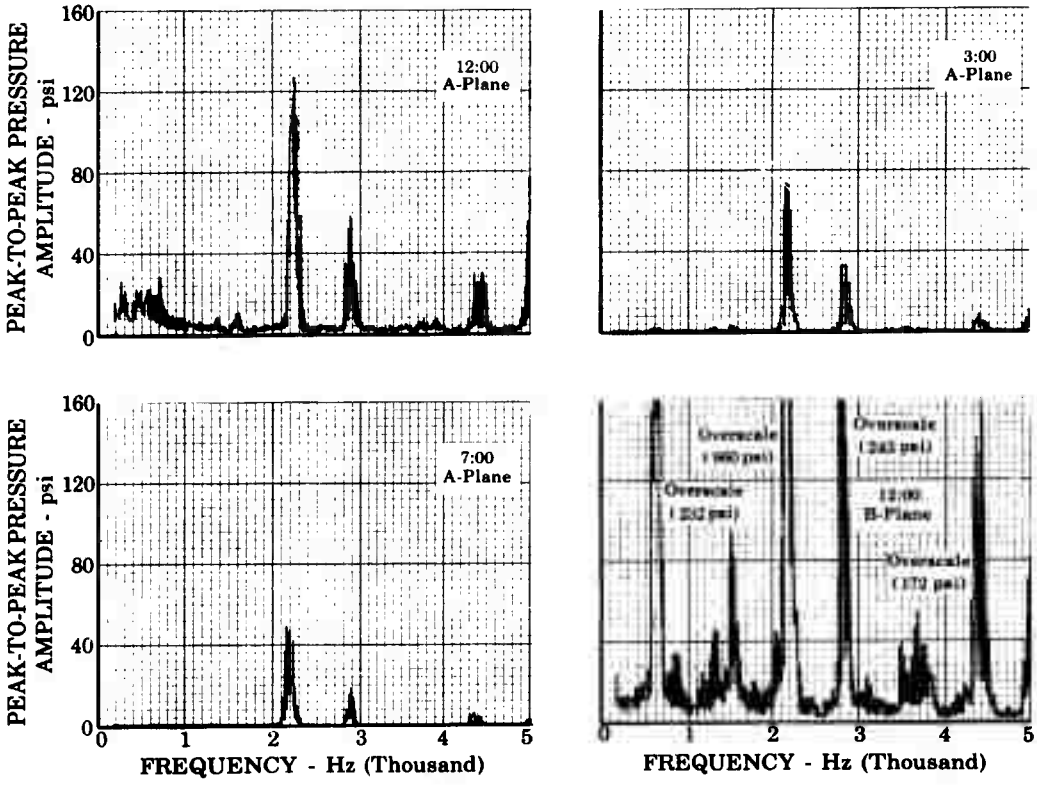

Figure 143. Pressure Amplitude Data for Wafer Liner Test No. 98.01 FD 24620

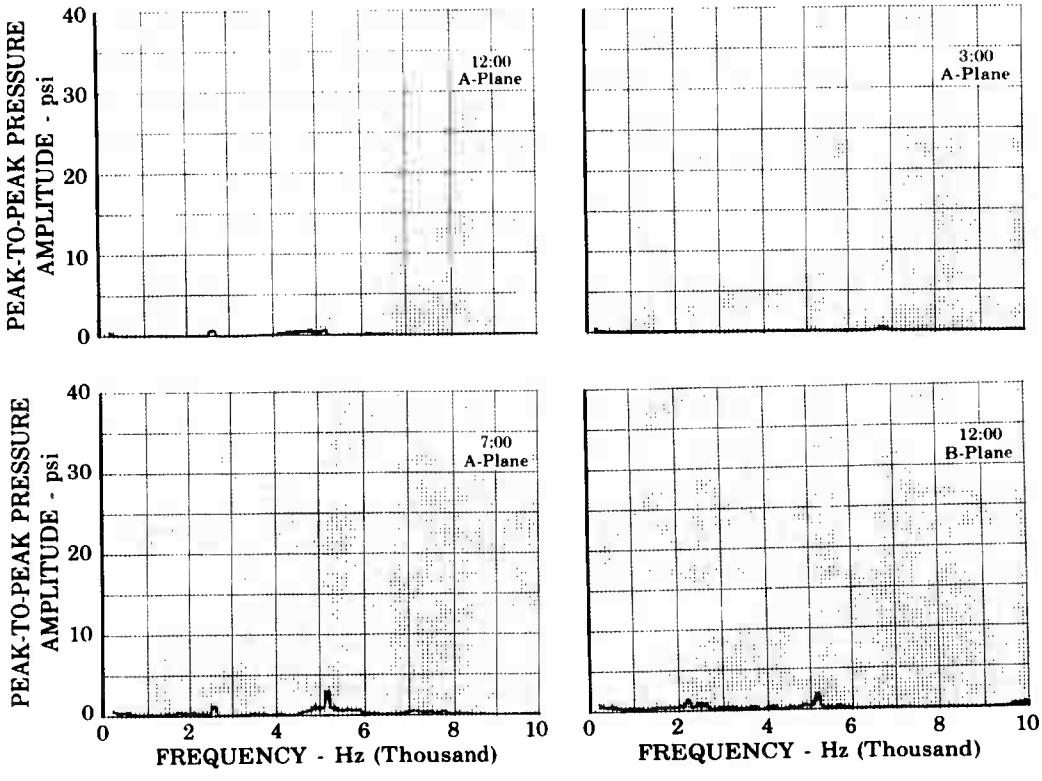

Figure 144. Pressure Amplitude Data for Wafer Liner Test No. 125.01 FD 24667

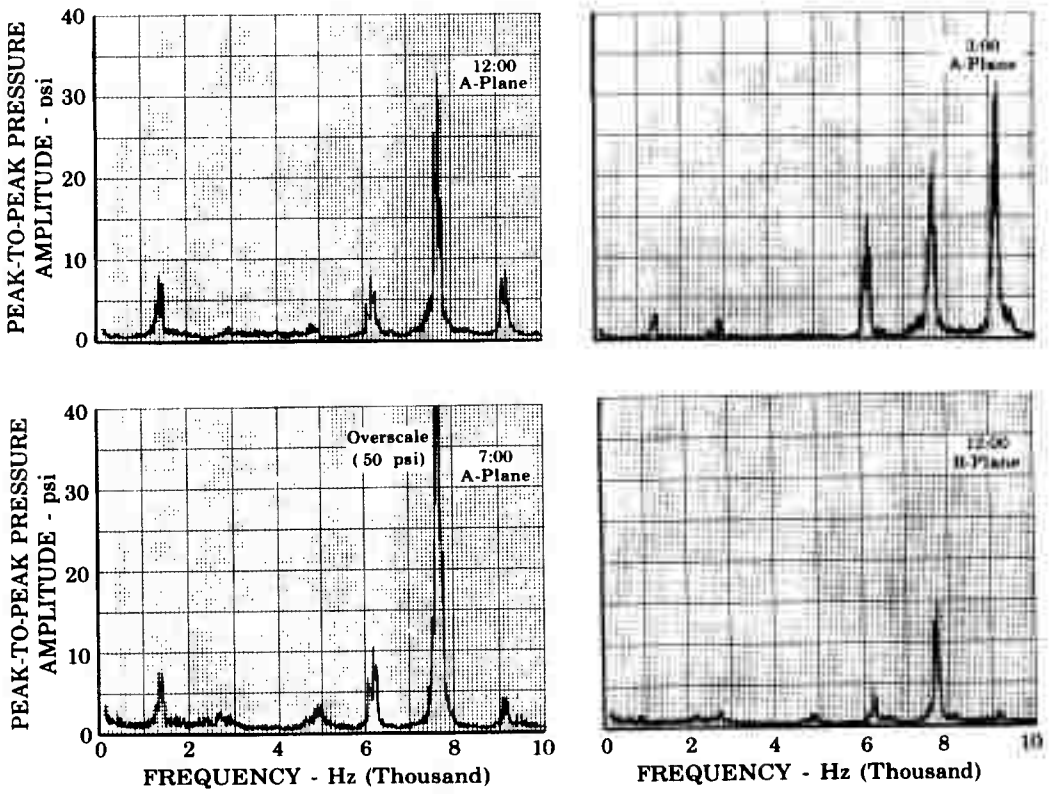

Figure 145. Pressure Amplitude Data for Wafer Liner Test No. 126.01 FD 24668

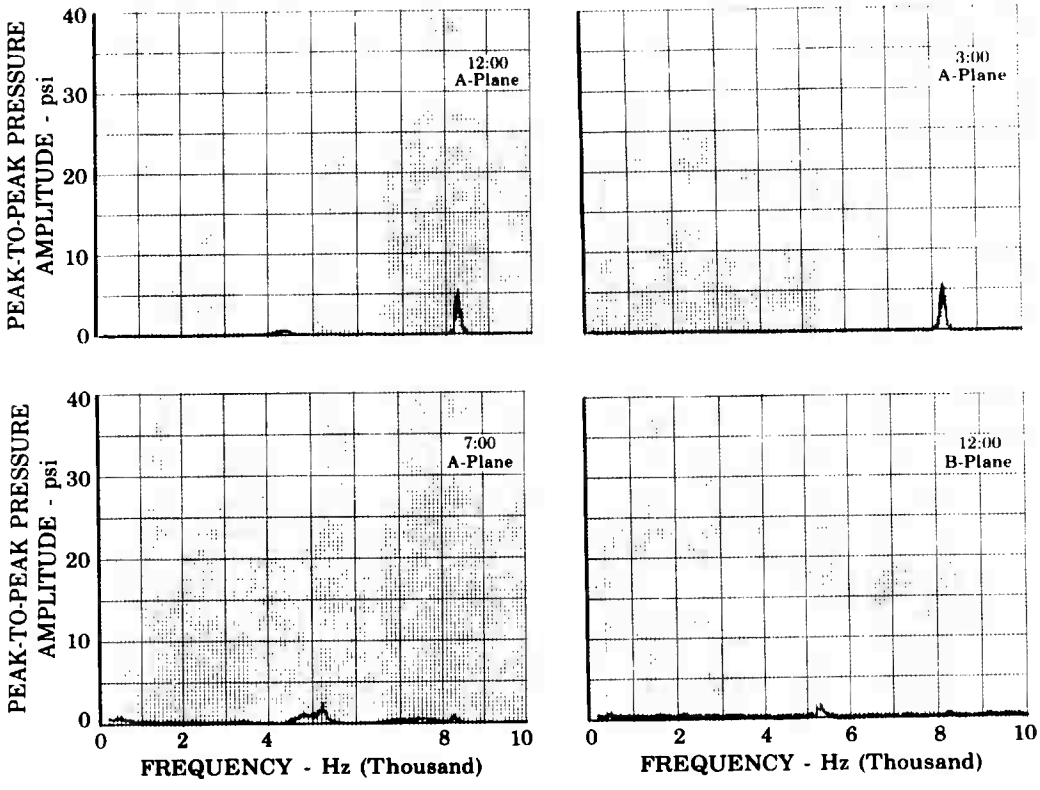

Figure 146. Pressure Amplitude Data for Wafer Liner Test No. 128.01 FD 24669

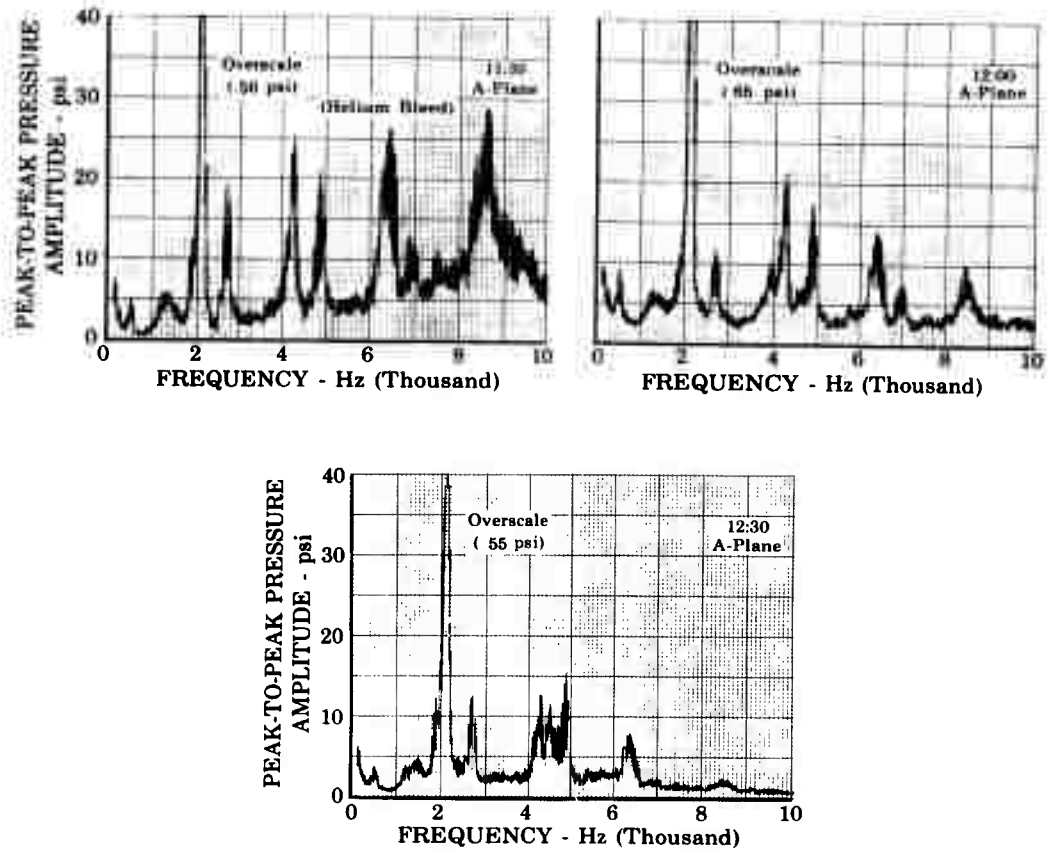

Figure 147. Pressure Amplitude Data for Wide Band Liner Test No. 123.01 FD 24665

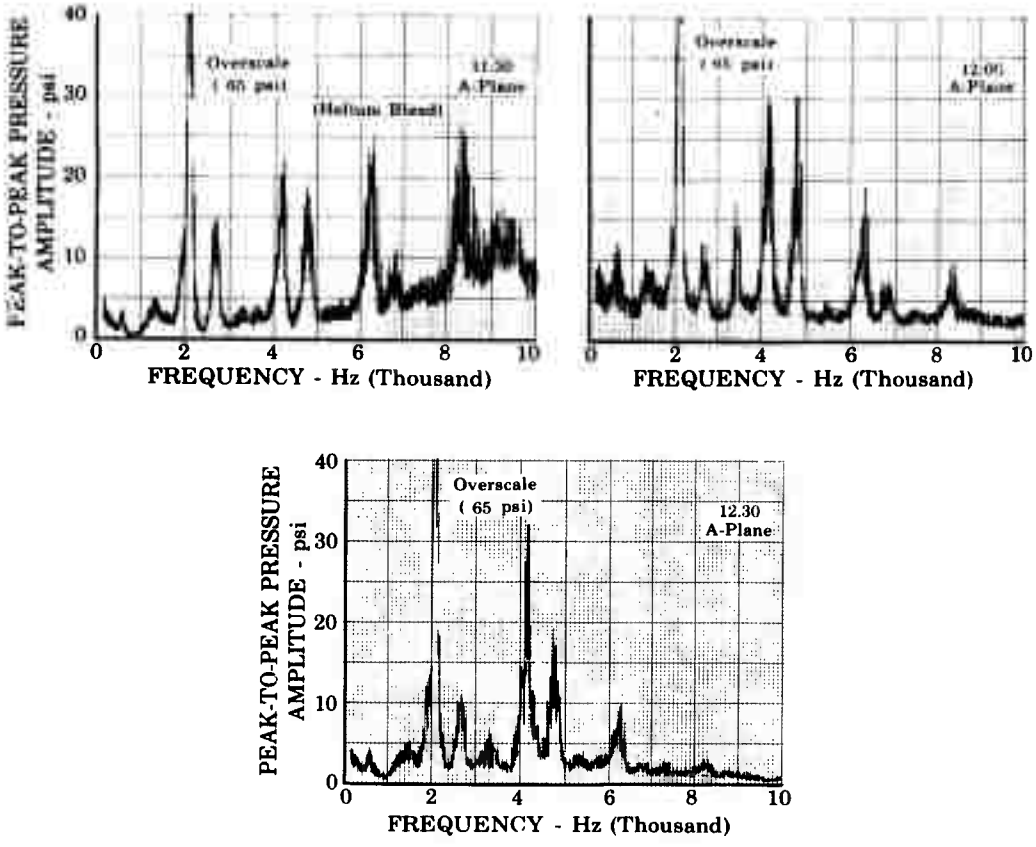

Figure 148. Pressure Amplitude Data for Wide Band Liner Test No. 124.01 FD 24666

APPENDIX C
FABRICATION DRAWINGS

Part Number	Part Description	Page No.
BKJ-9068	N_2O_4/Aerozine Chamber Assembly	172
BKJ-9098	Injector Face Pattern	173
BKJ-9099	Injector Face Pattern	174
BKJ-9172	Fuel Manifold Plate	175
BKJ-9174	Injector Backup Plate	176
BKJ-9176	Injector Assembly	177
CKJ-4554	Solid Ablative Liner for 200 psi F/C	178
CKJ-4581	Nozzle Insert Retaining Plate	179
CKJ-4582	Rear Nozzle Insert Retaining Plate	180
CKJ-4583	200-psi Graphite Nozzle Insert	181
CKJ-4584	100-psi Nozzle Rework	182
CKJ-4585	200-psi Storable Nozzle Assembly	183
CKJ-4744	200-psi Ablative Acoustic Liner	184
CKJ-4785	1000-psi F/C Liner Backing	185
CKJ-4786	1000-psi F/C Liner	186
CKJ-4787	1000-psi F/C Liner Assembly	187
CKJ-5212	Film-Cooled Nozzle Section C	188
CKJ-5213	Film-Cooled Nozzle Throat Section D	189
CKJ-5214	Film-Cooled Nozzle Flange Section A	190
CKJ-5215	Film-Cooled Nozzle Section B	191
CKJ-5419	1000-psi Film-Cooled Nozzle Assembly	192
CKJ-5494	Acoustic Wafer Plate	193
CKJ-5495	Front Wafer Plate	194
CKJ-5496	End Wafer Plate	195
CKJ-5497	Wafer Liner Shell	196
CKJ-5500	Wafer Liner Assembly	197
CKJ-5784	200-psi Film-Cooled Liner Assembly	198
CKJ-5785	200-psi Film-Cooled Liner Cooling Plate	199
CKJ-5786	200-psi Film-Cooled Liner No. 1	200
CKJ-5787	200-psi Film-Cooled Liner No. 2	201
CKJ-5788	200-psi Film-Cooled Liner Cooling Plate Plug	202
CKJ-7023	200-psi Individual Cavity Steel Acoustic Liner	203
CKJ-8297	200-psi Stainless Steel Liner (Rwk No. 1)	204
CKJ-8528	200-psi Ablative Liner No. 2	205
CKJ-8626	200-psi Ablative Liner No. 2B	206
CKJ-8666	Wide Band Absorption Liner	207
CKJ-8742	200-psi Dual Open Area Steel Liner	208
CKJ-9055	200-psi Rocket Motor Assembly	209
CKJ-9059	1000-psi Rocket Motor Assembly	210

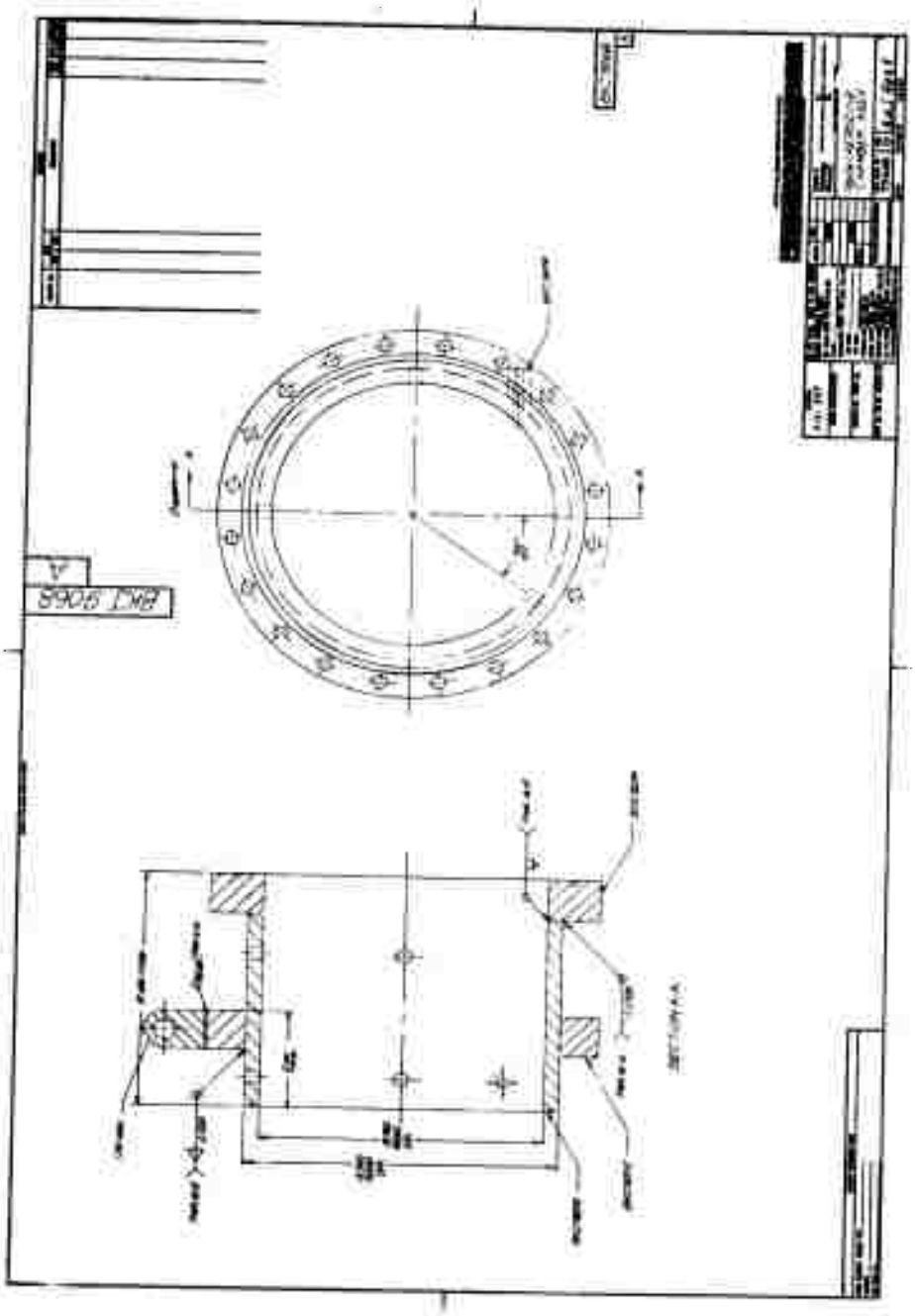

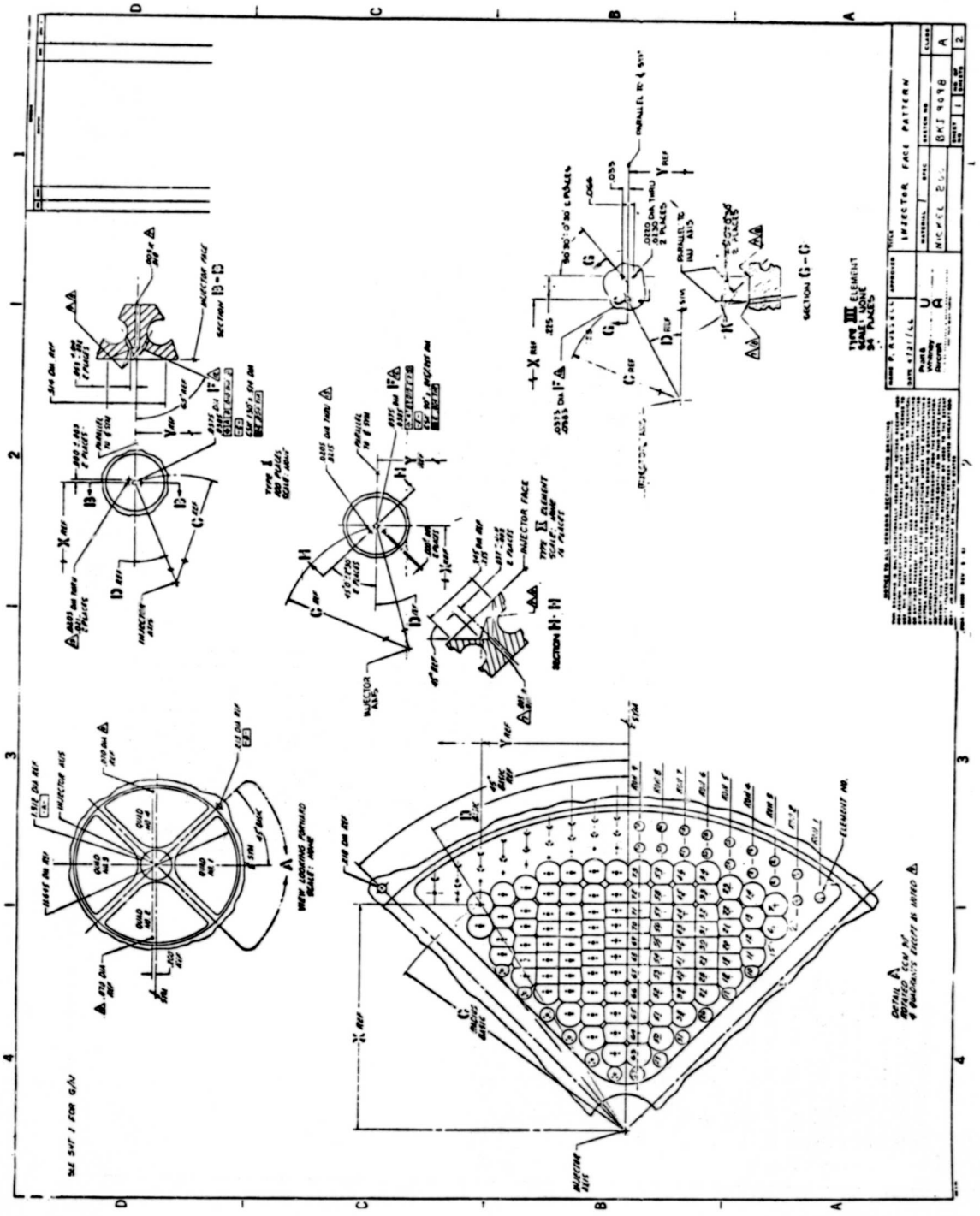
INJECTOR FACE PATTERN
SECTION B-B
SECTION H-H
SECTION G-G
TYPE III ELEMENT
SCALE: NONE
84 PLACES
TYPE II ELEMENT
SCALE: NONE
12 PLACES
TYPE I
SCALE: NONE
SEE SHT 1 FOR G/N

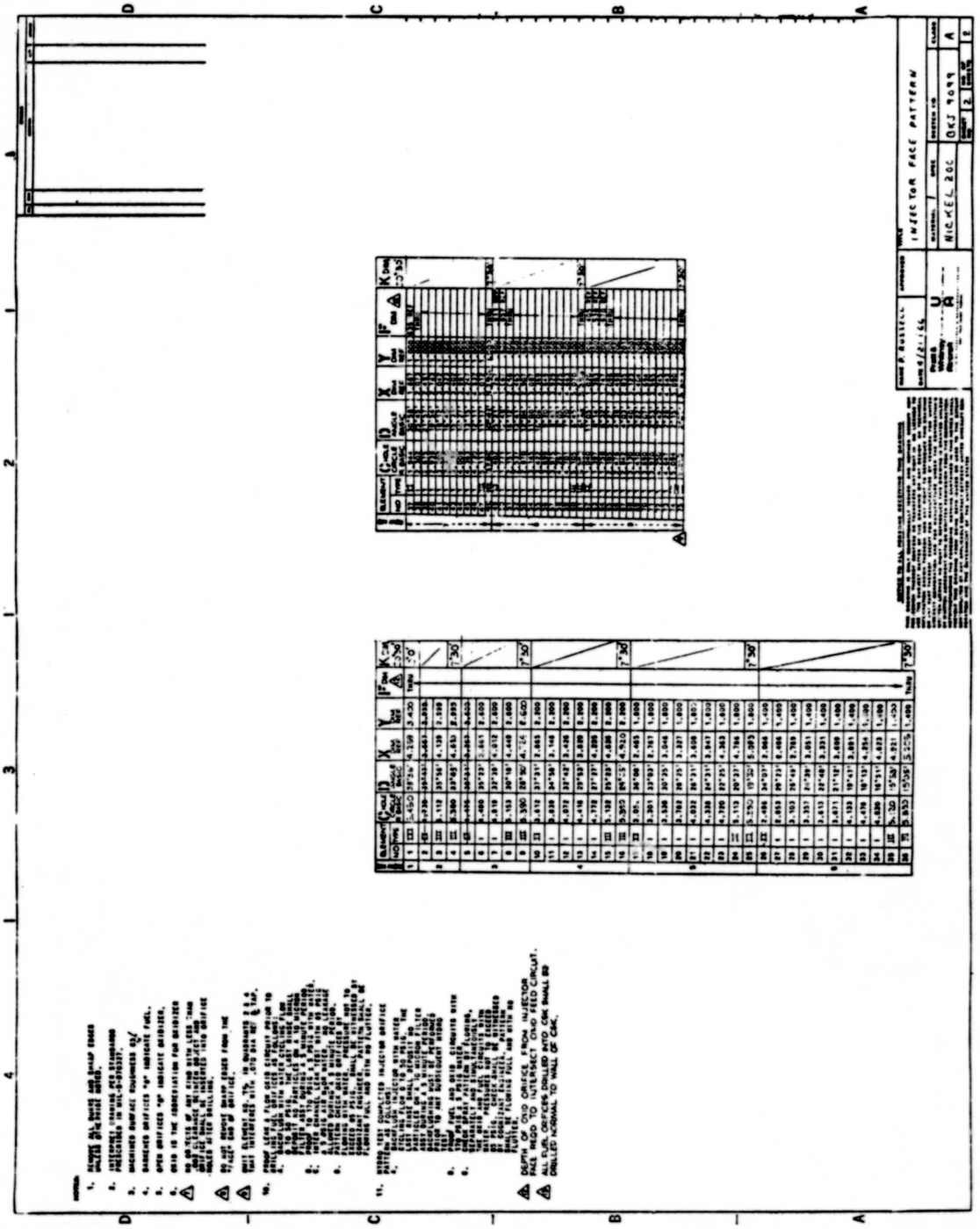

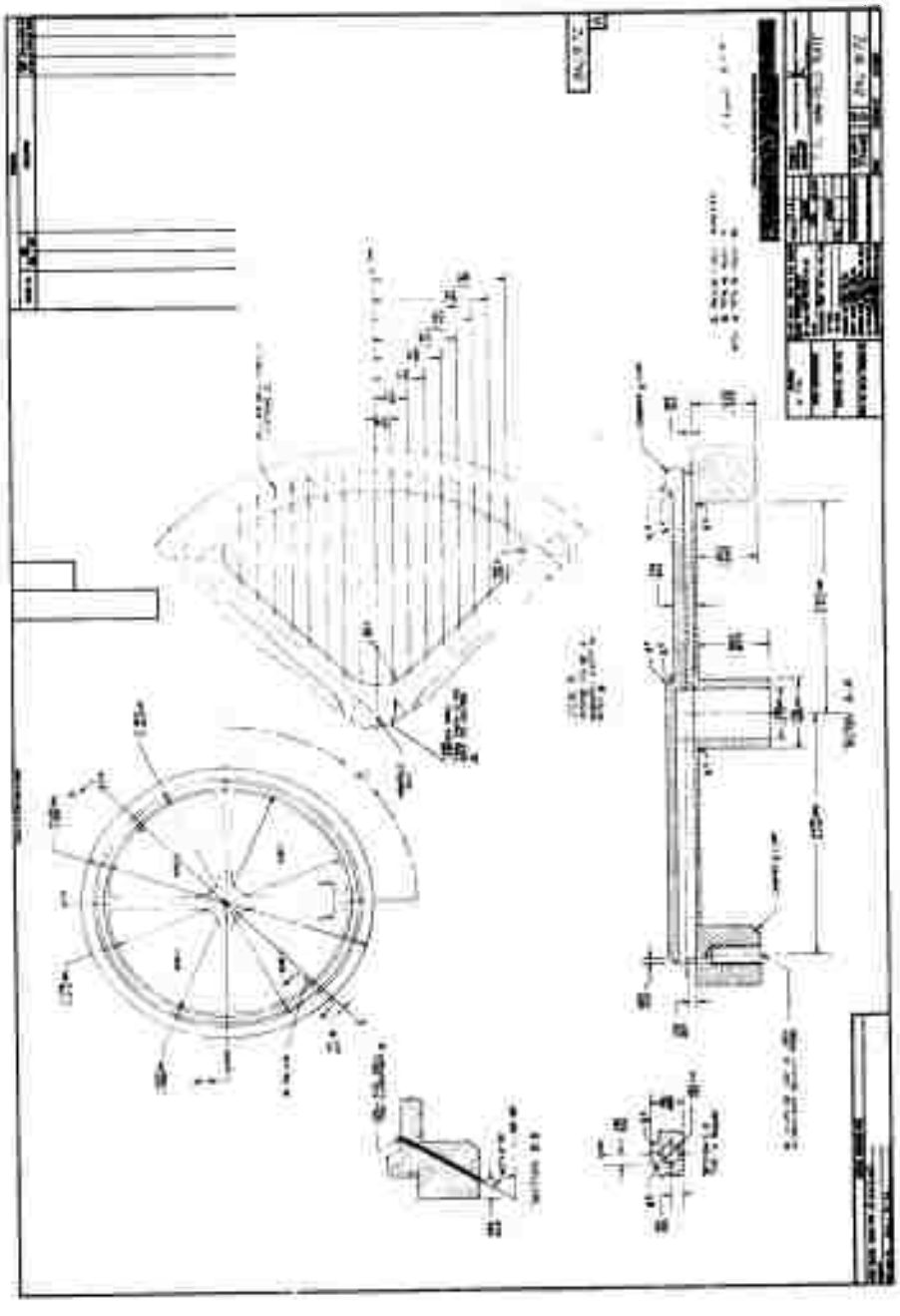

UNCLASSIFIED

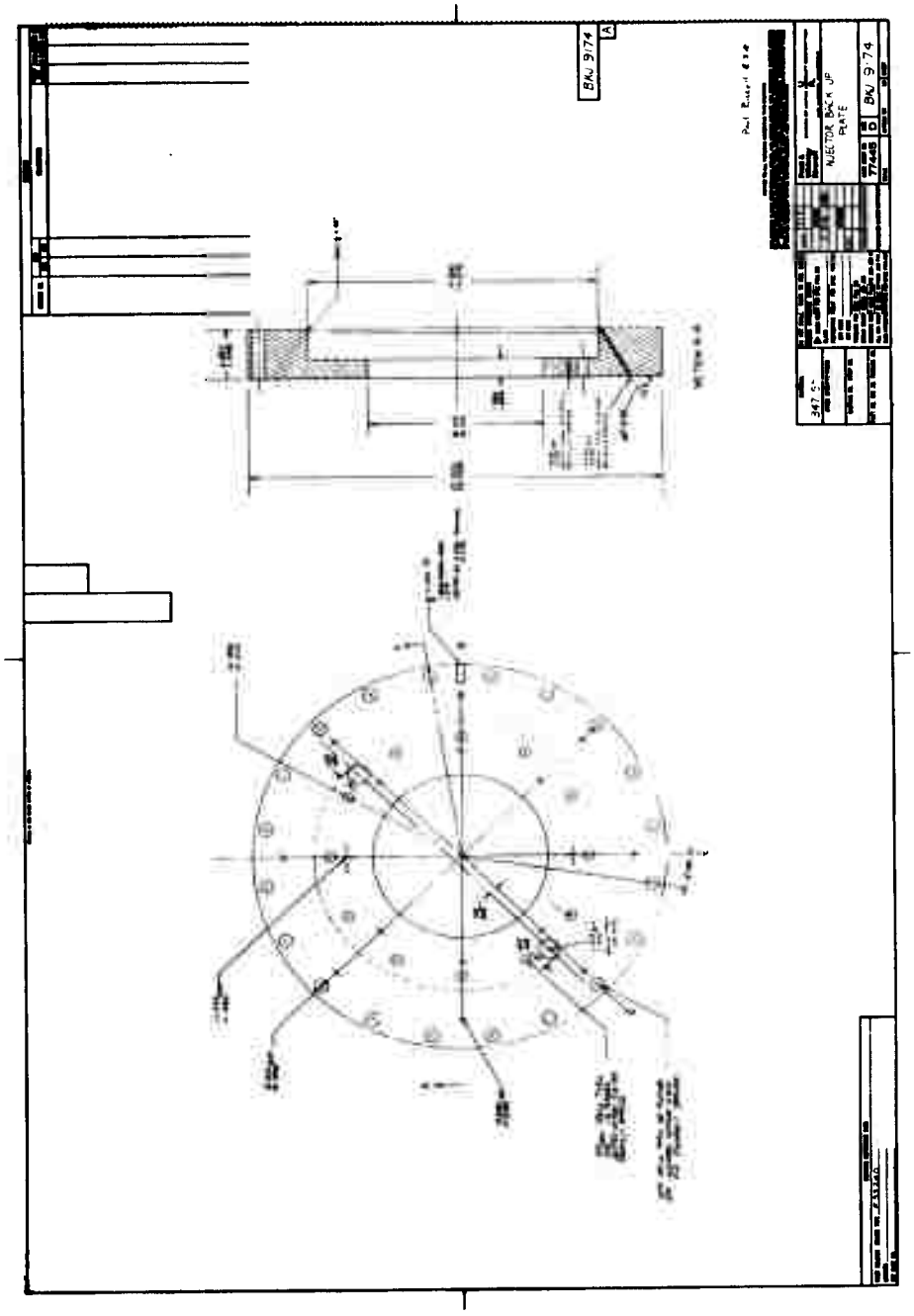

UNCLASSIFIED

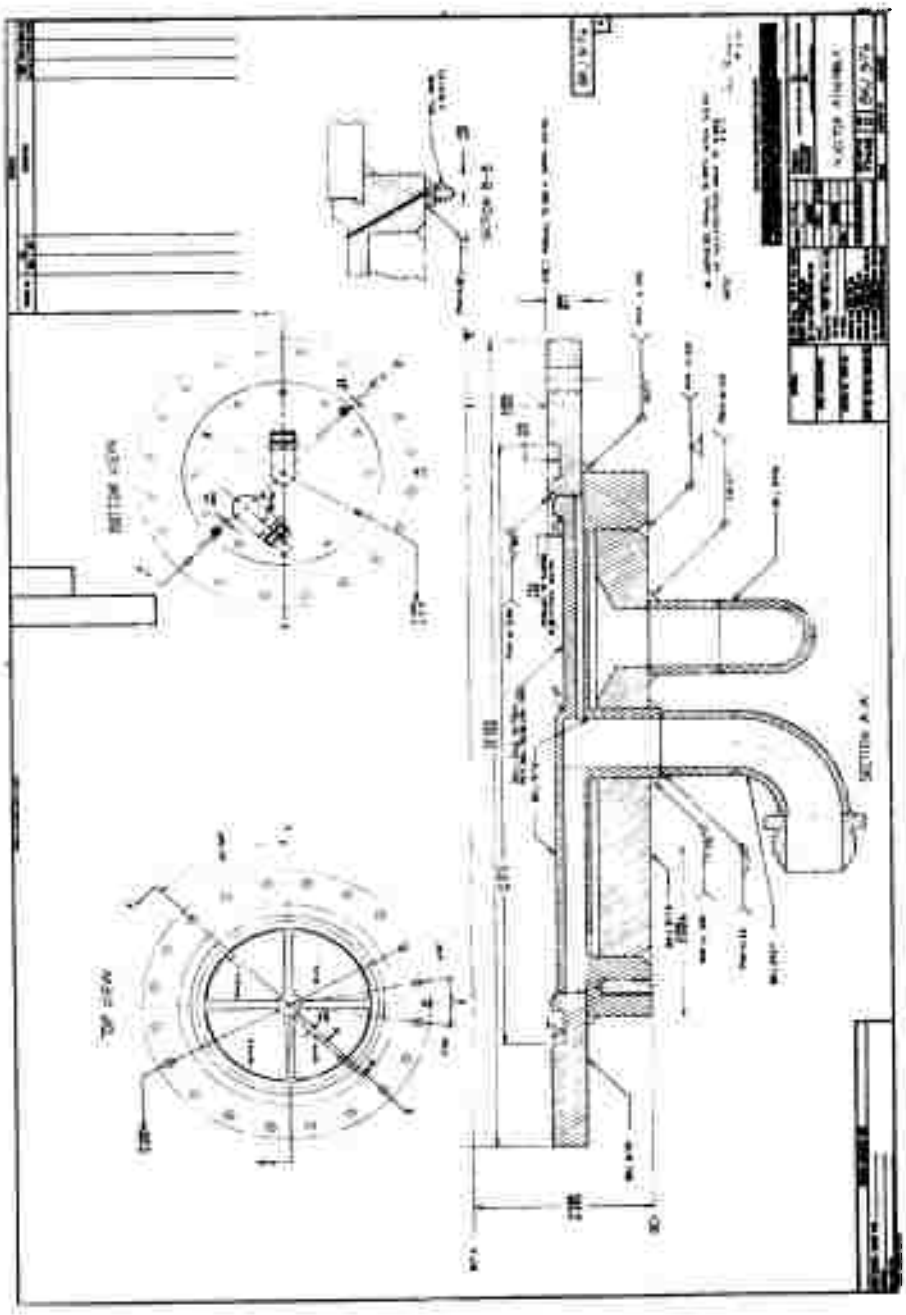

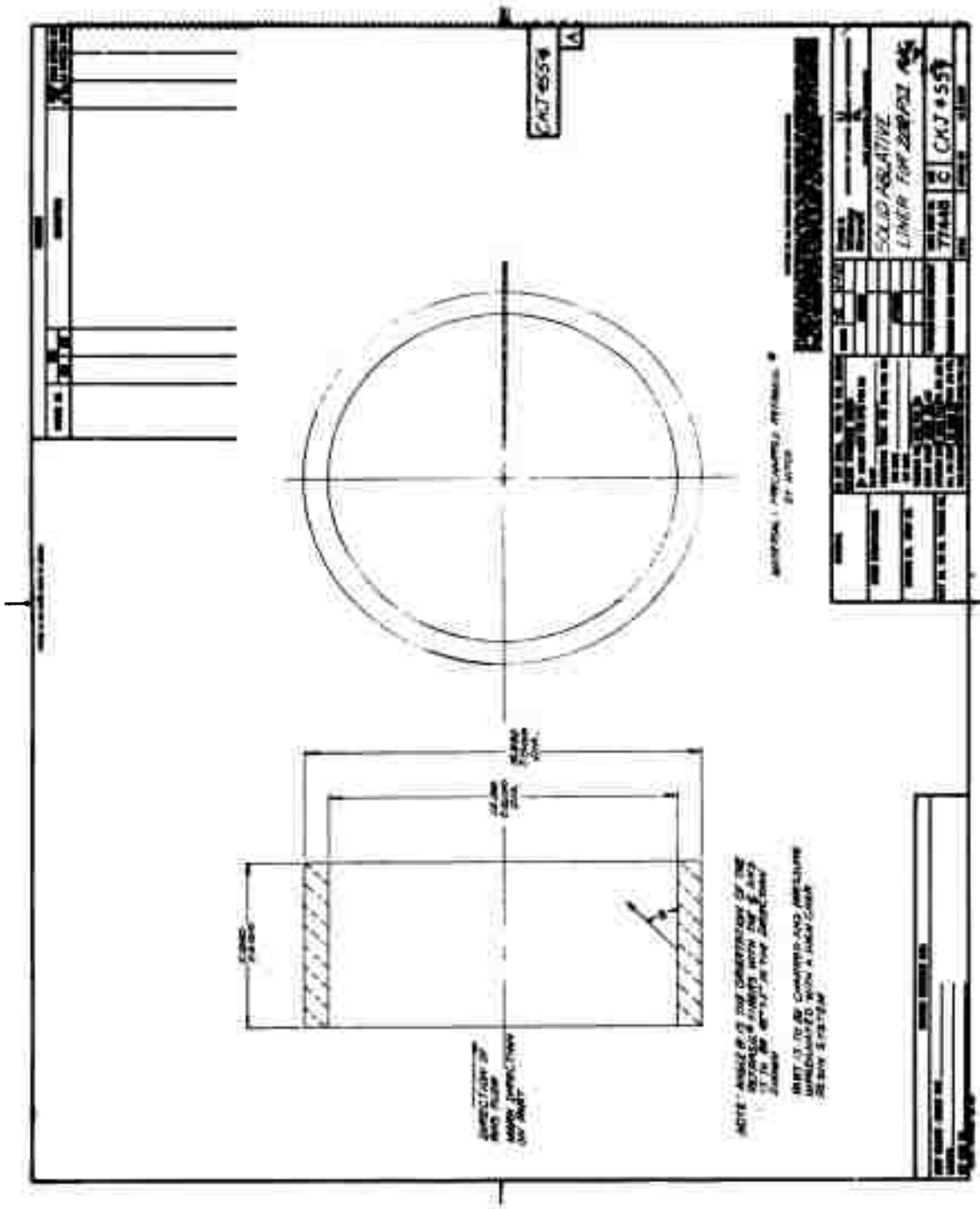
CKJ-655
SOLID ABLATIVE
LINER FOR 260PSI
CKJ-551

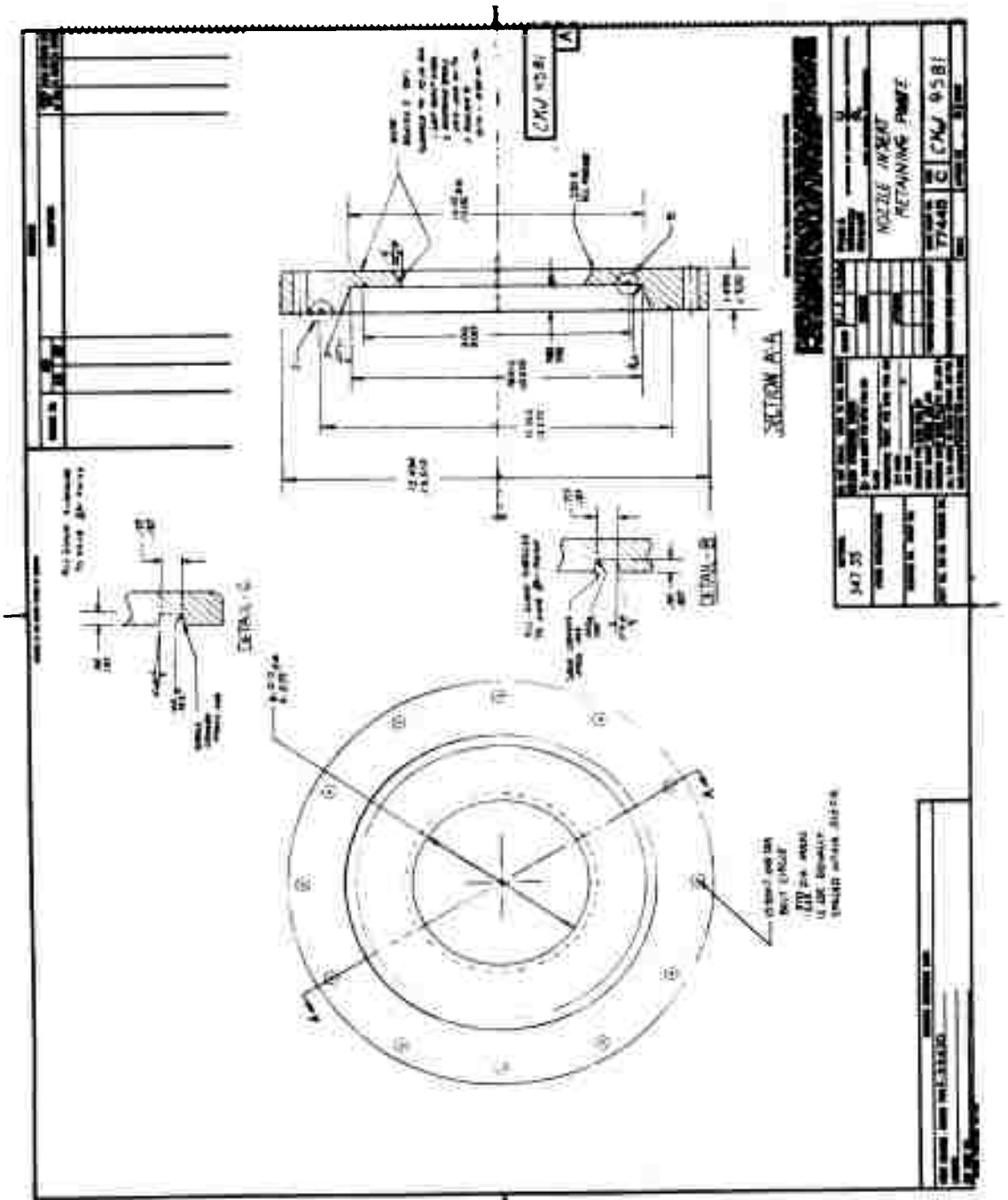
SECTION A-A
DETAIL-B
DETAIL-C
NOZZLE INSERT RETAINING RING
CRU 9581
77446

UNCLASSIFIED

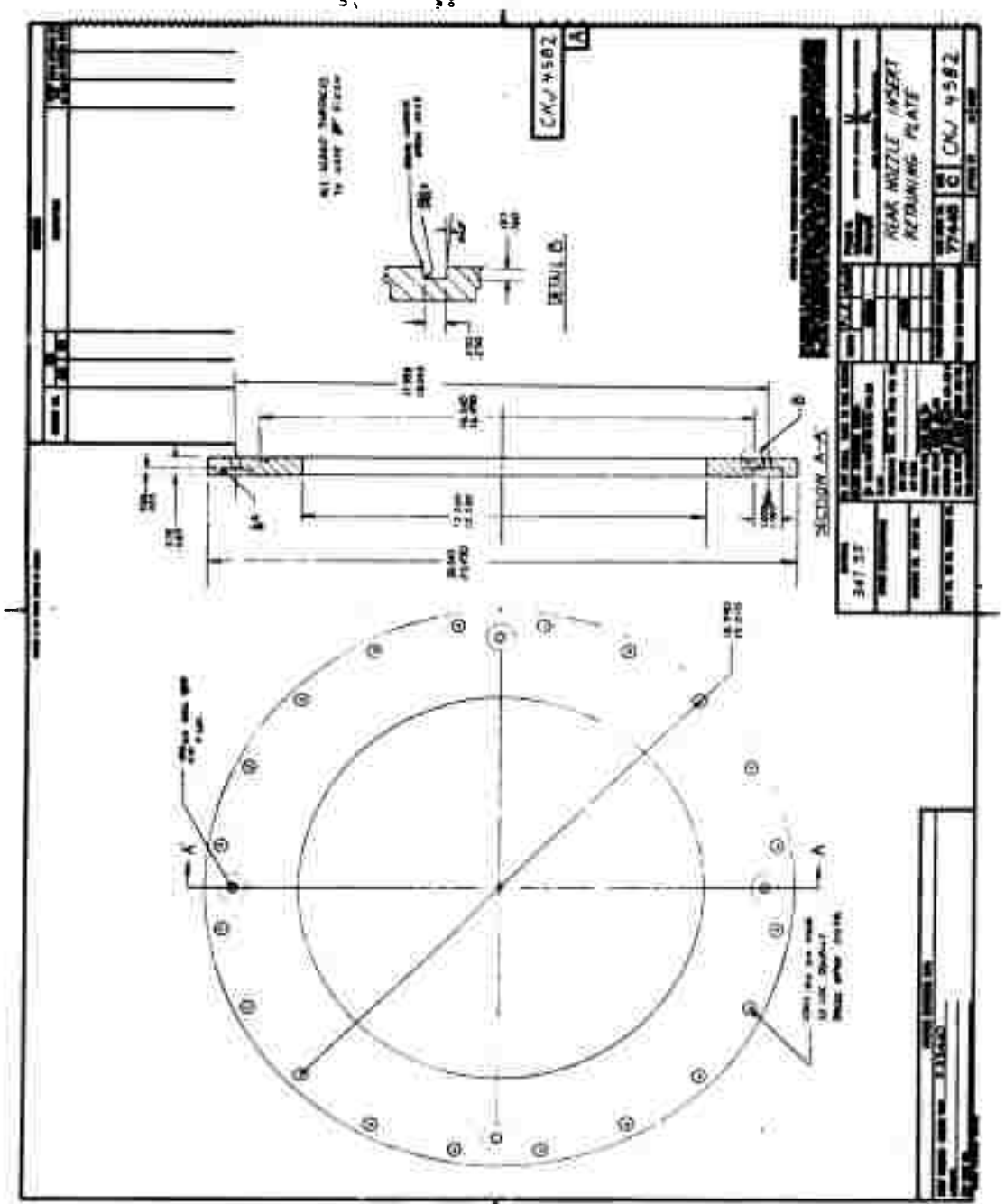

UNCLASSIFIED

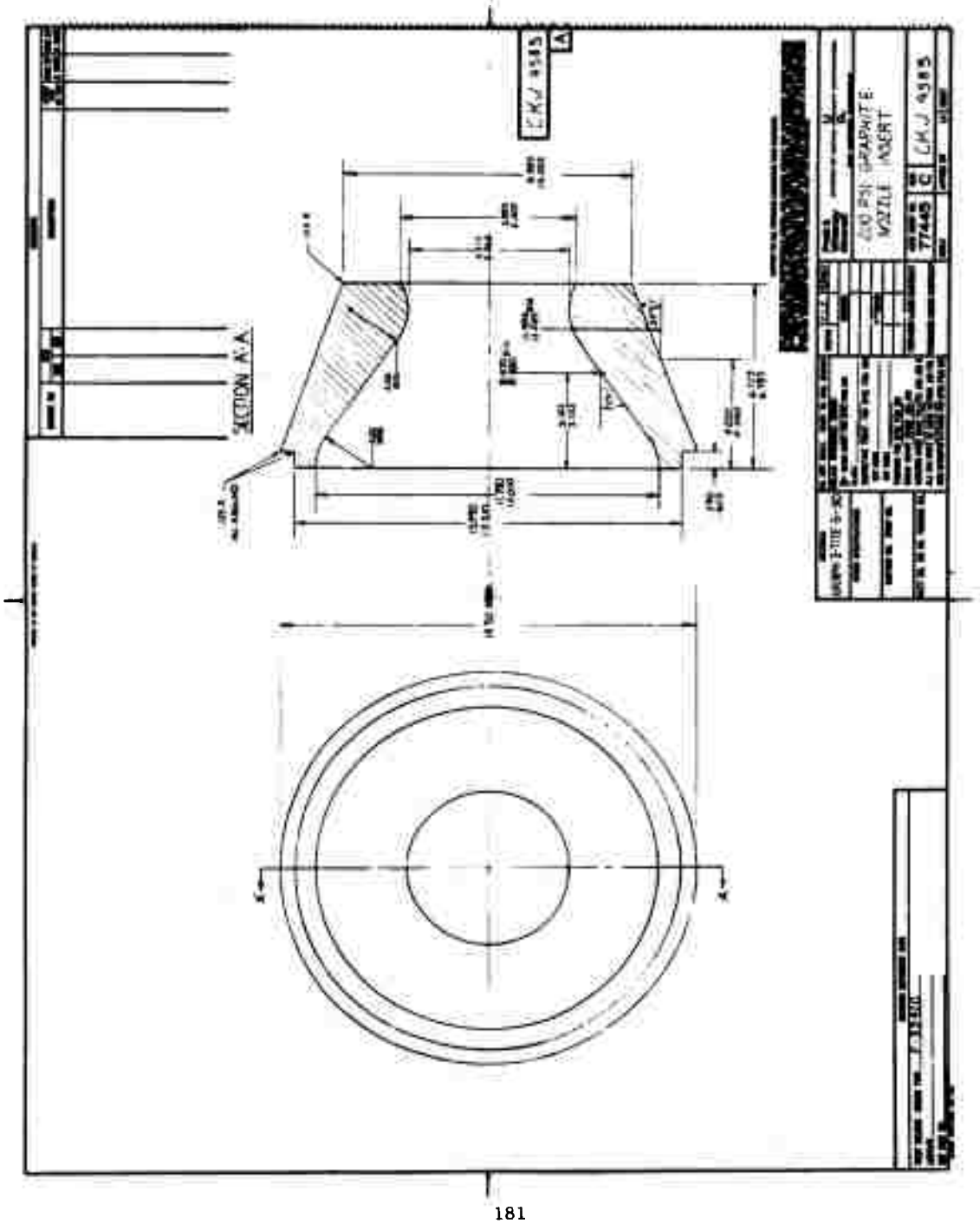

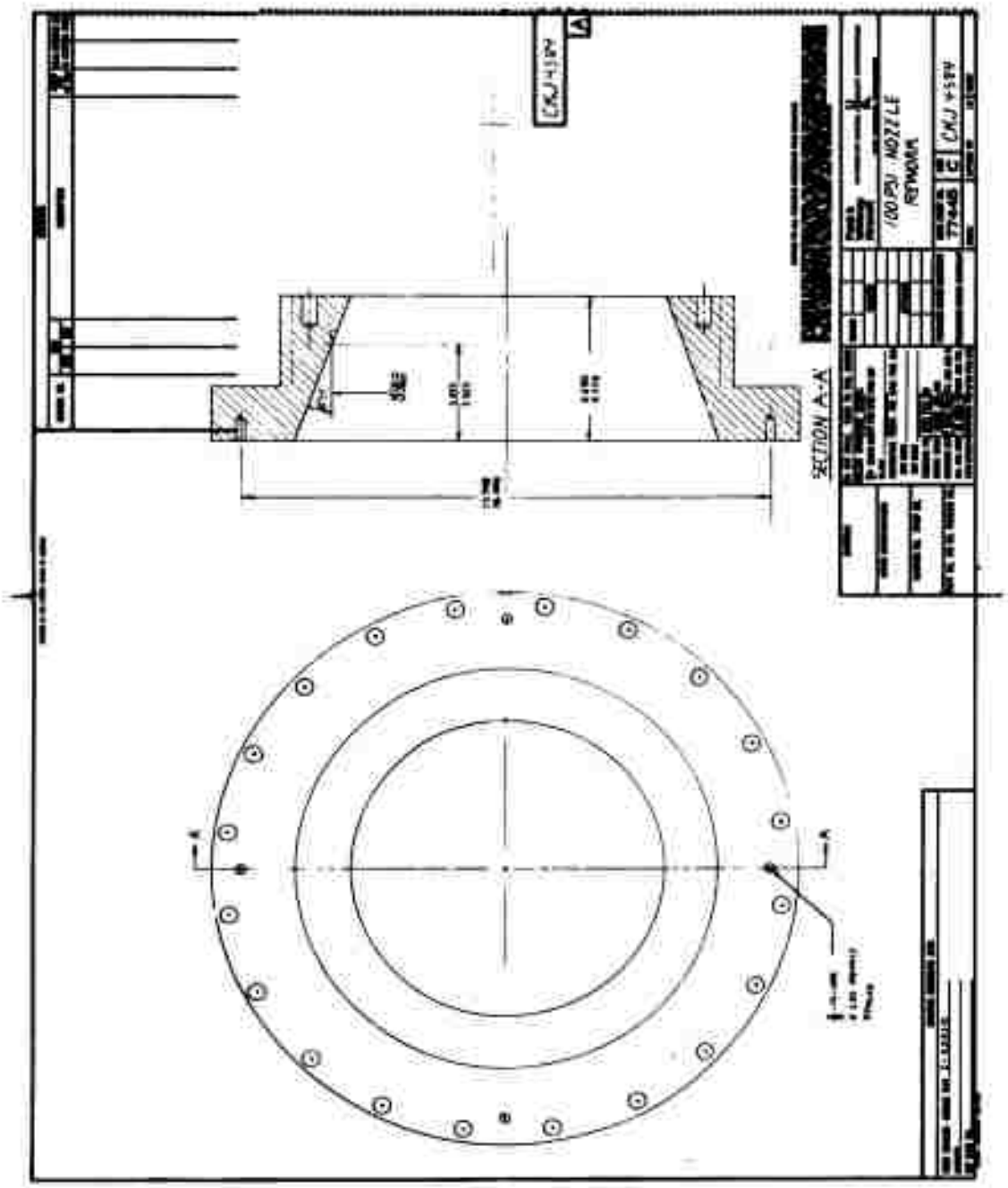
SECTION A-A

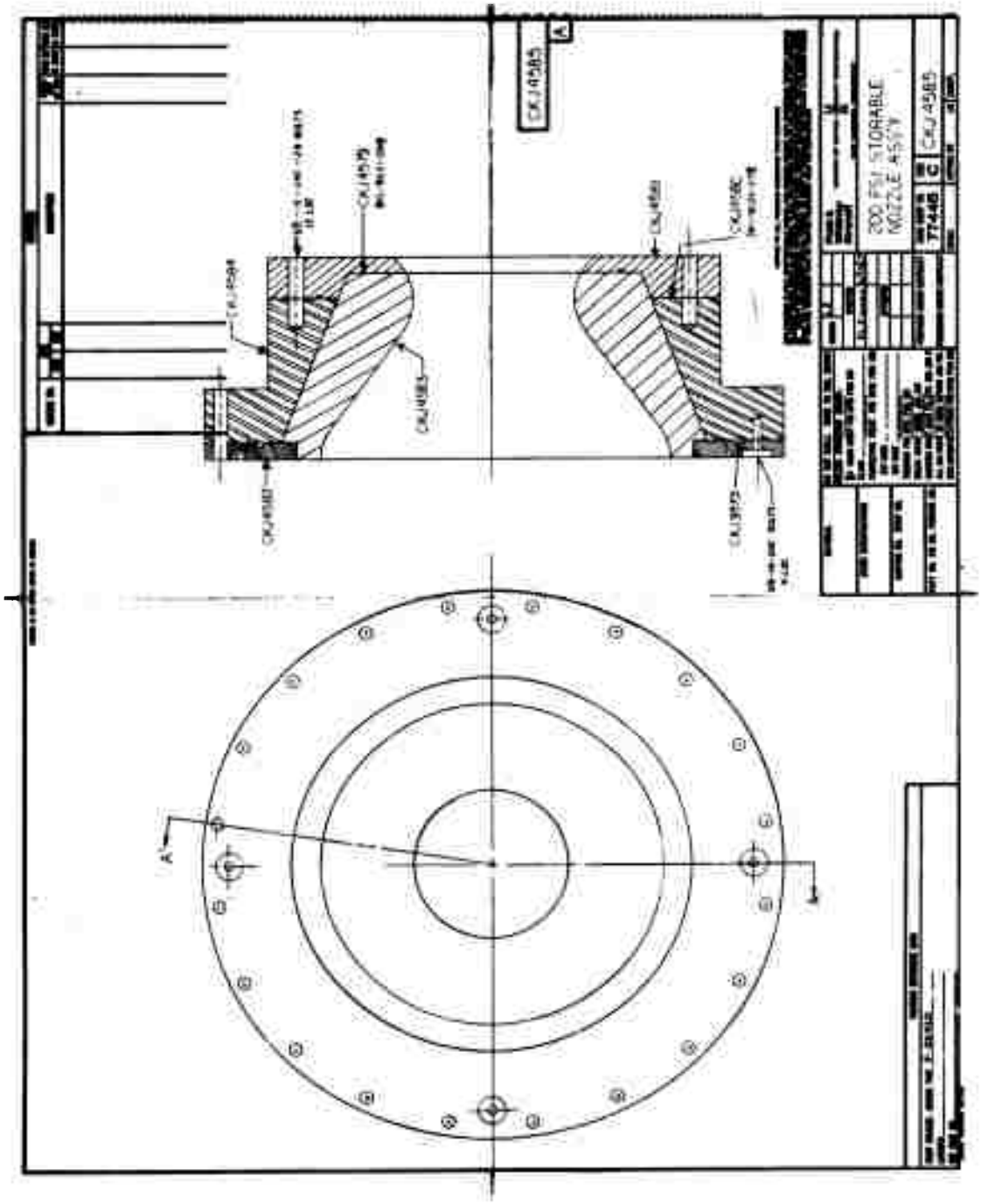
CKJ4585
A
CKJ4585
300 PSI STORABLE
NOZZLE ASSY
77448
C
CKJ4585
A
A

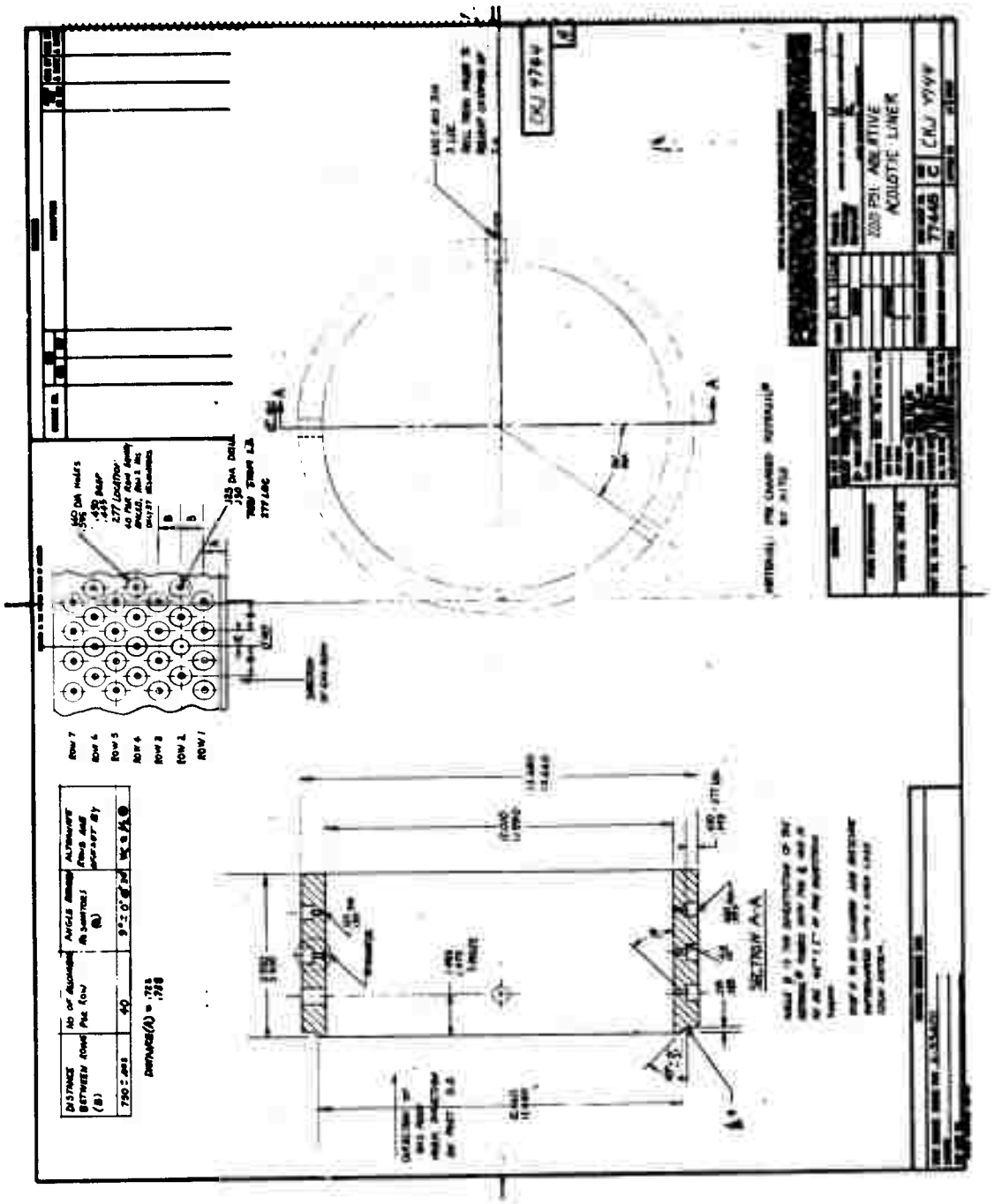

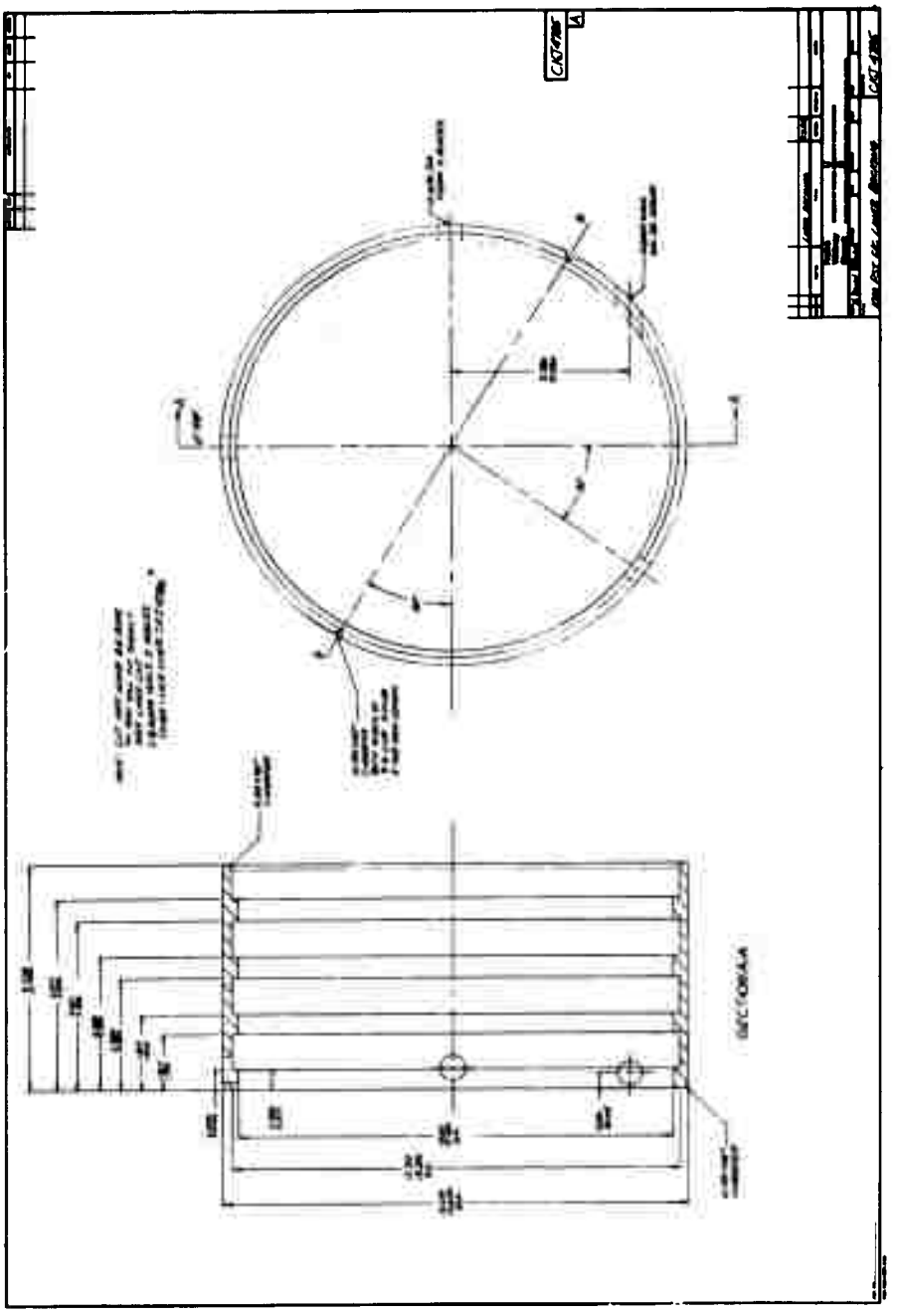

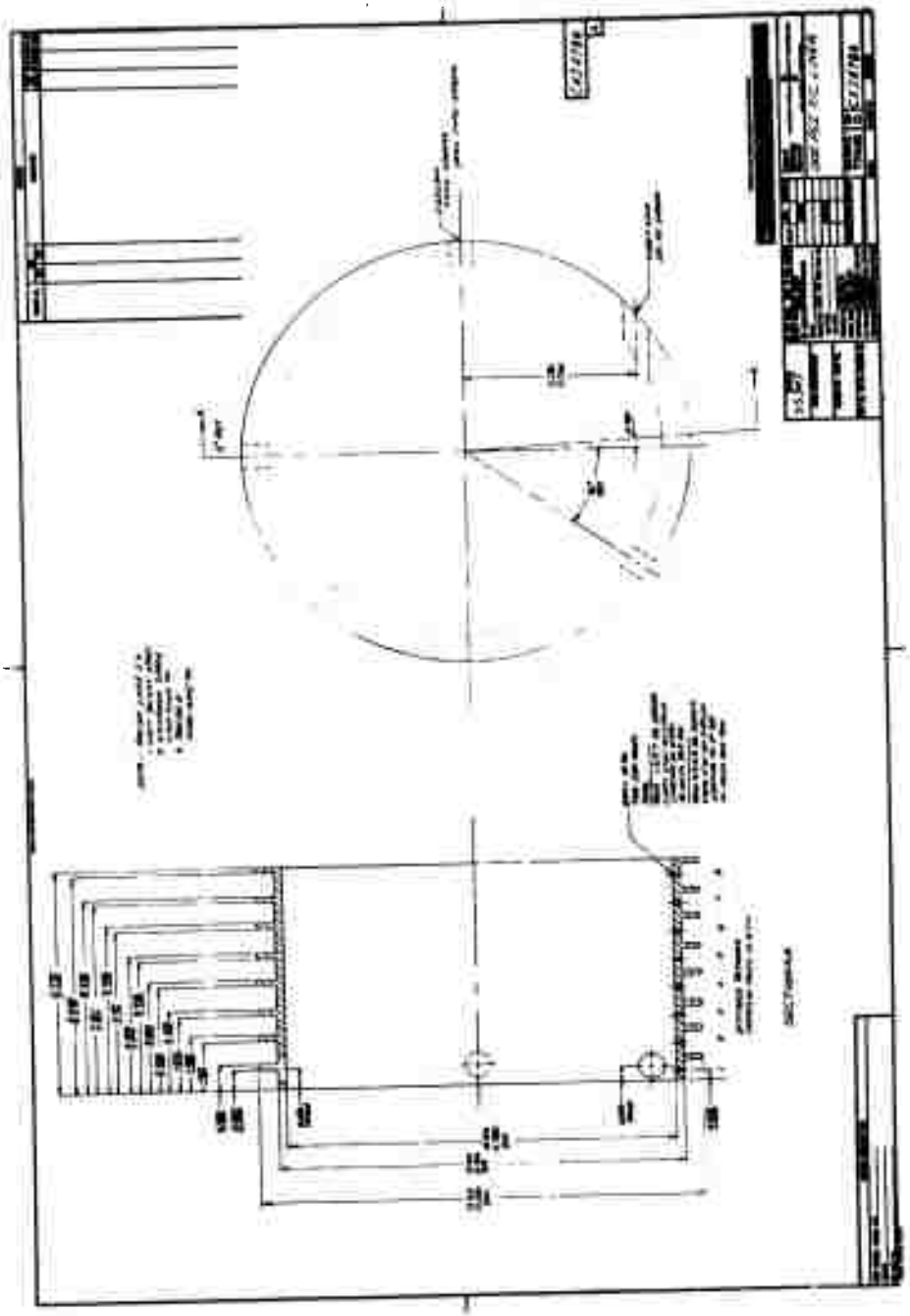

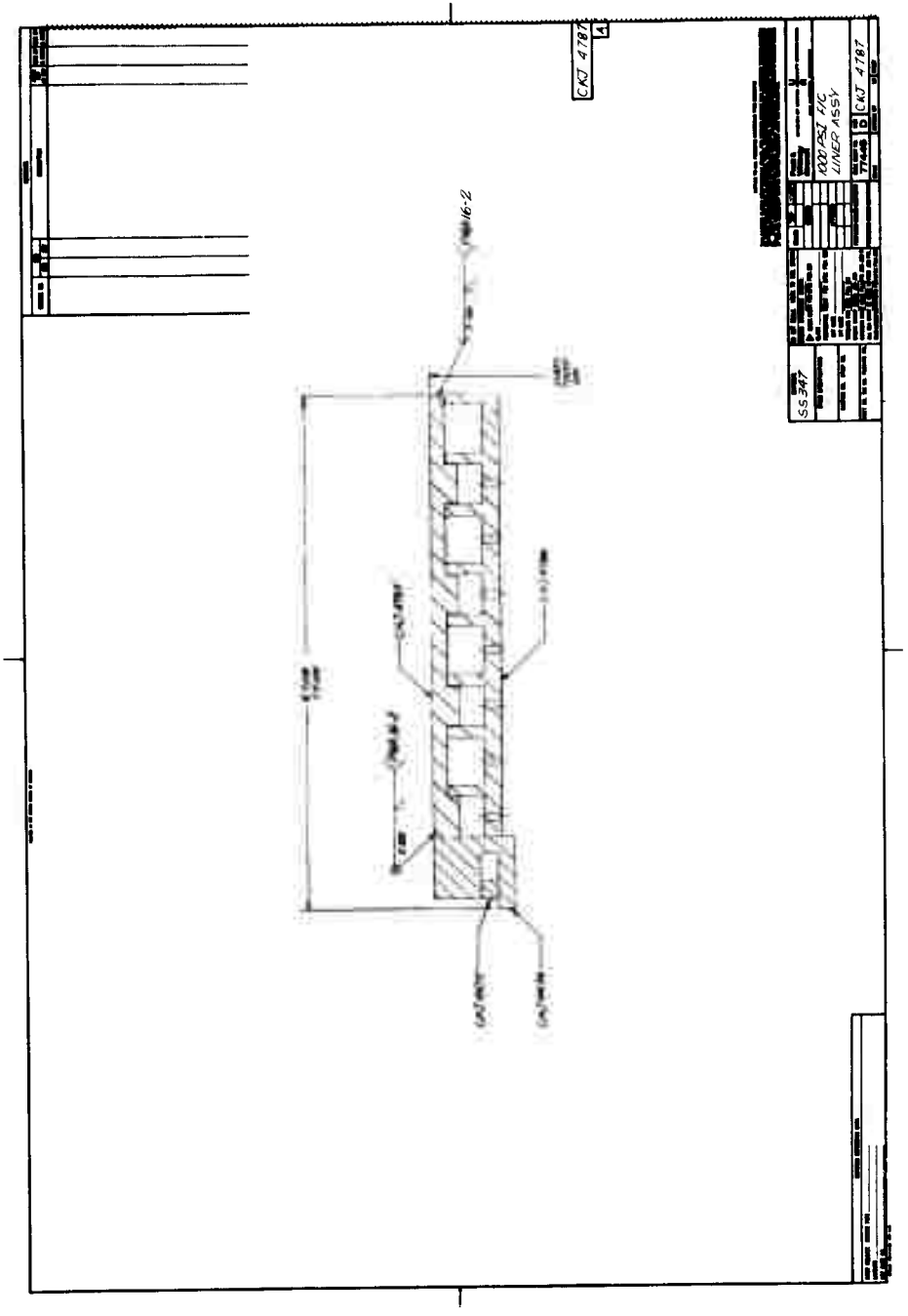
CKJ 4787
100 PSI H/C
LINER ASSY
CKJ 4787
SS 347

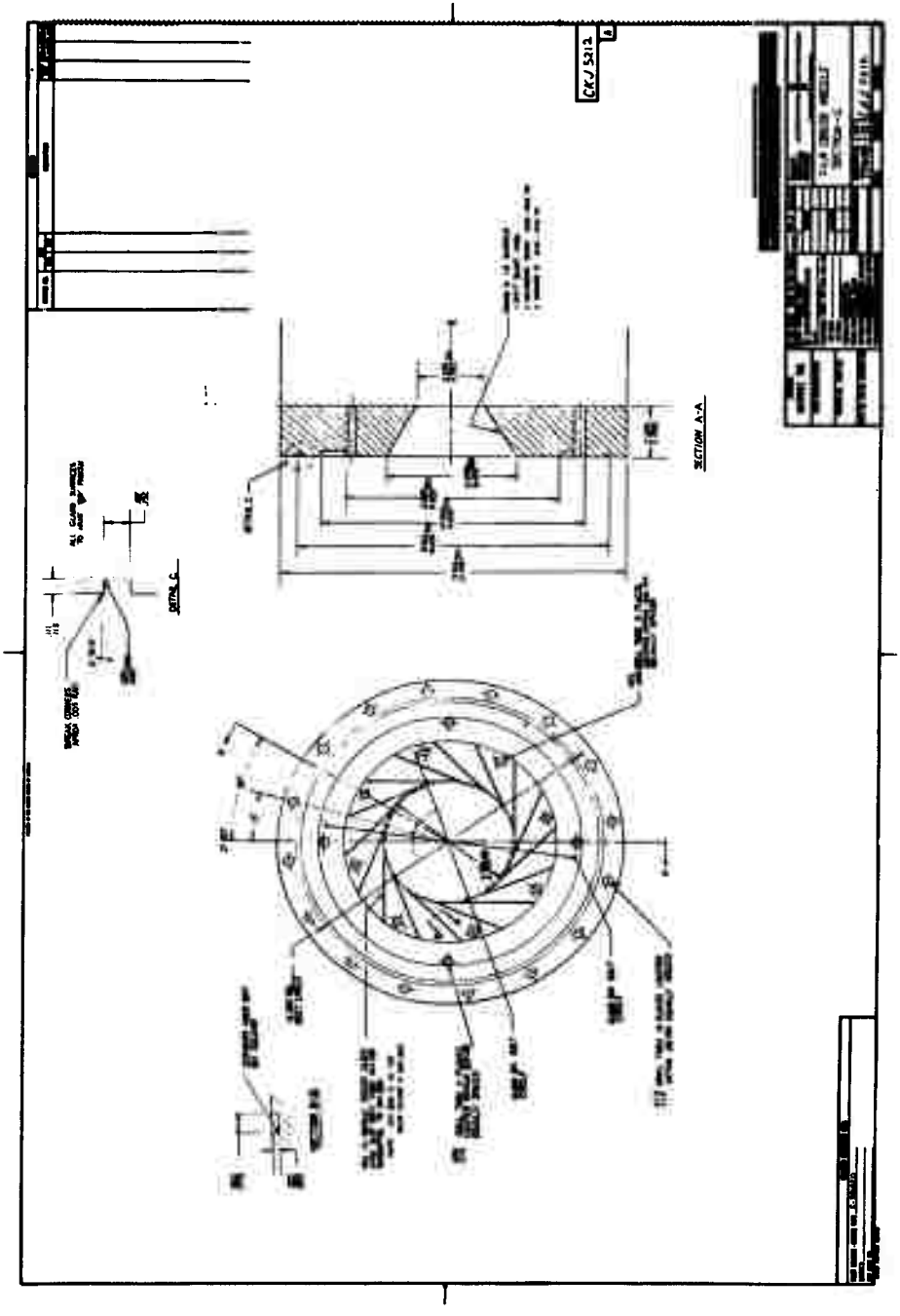
SECTION A-A

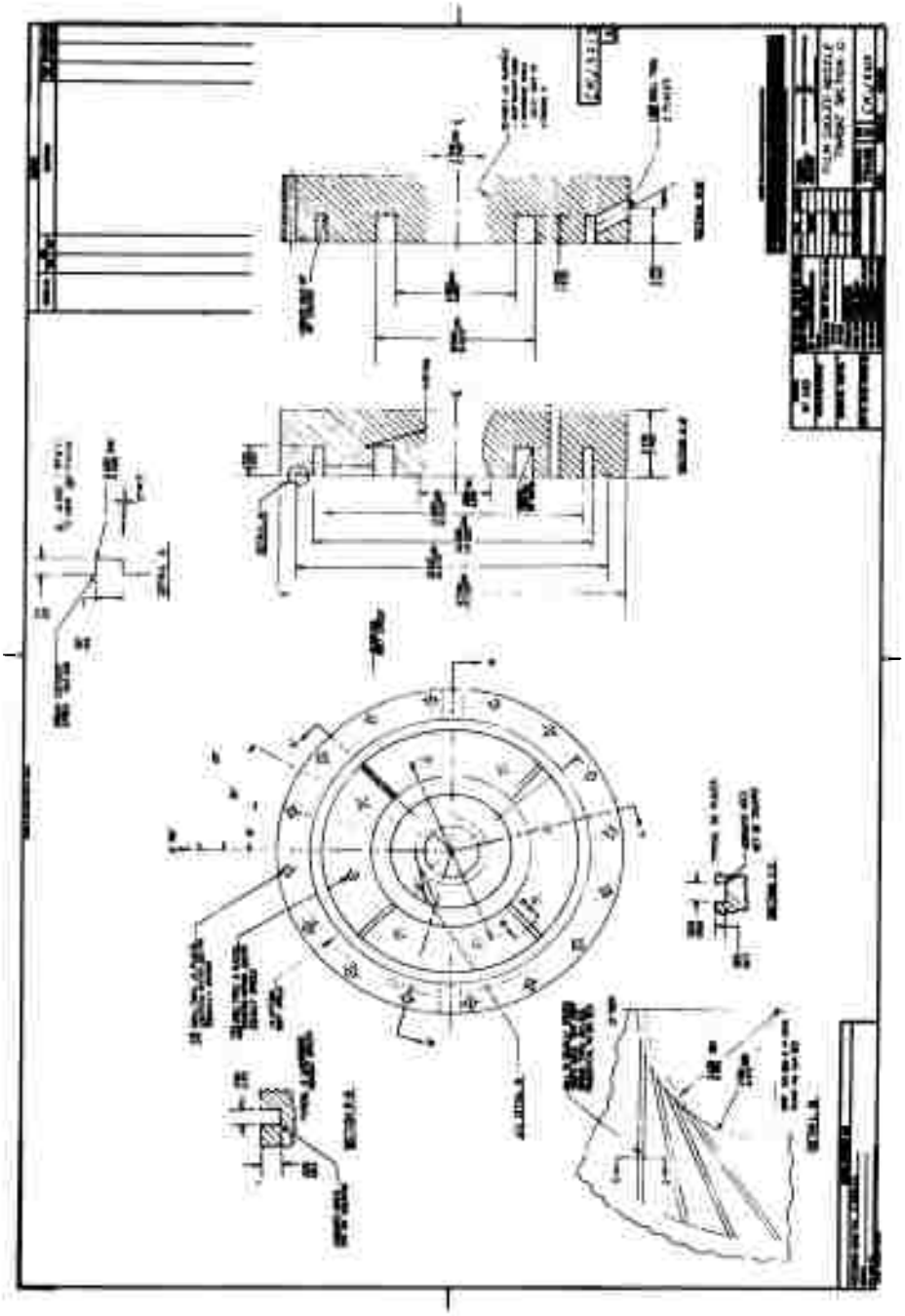

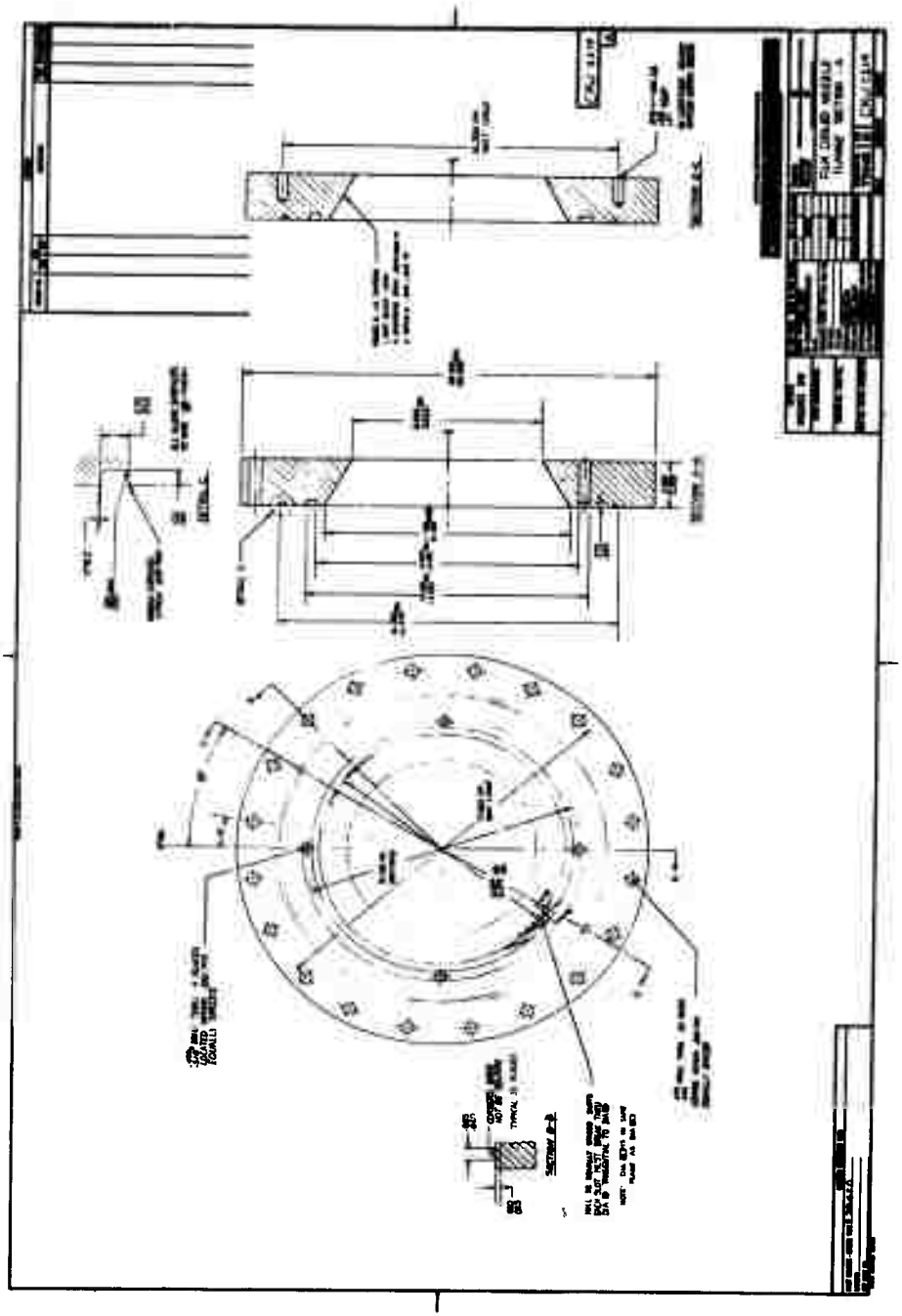

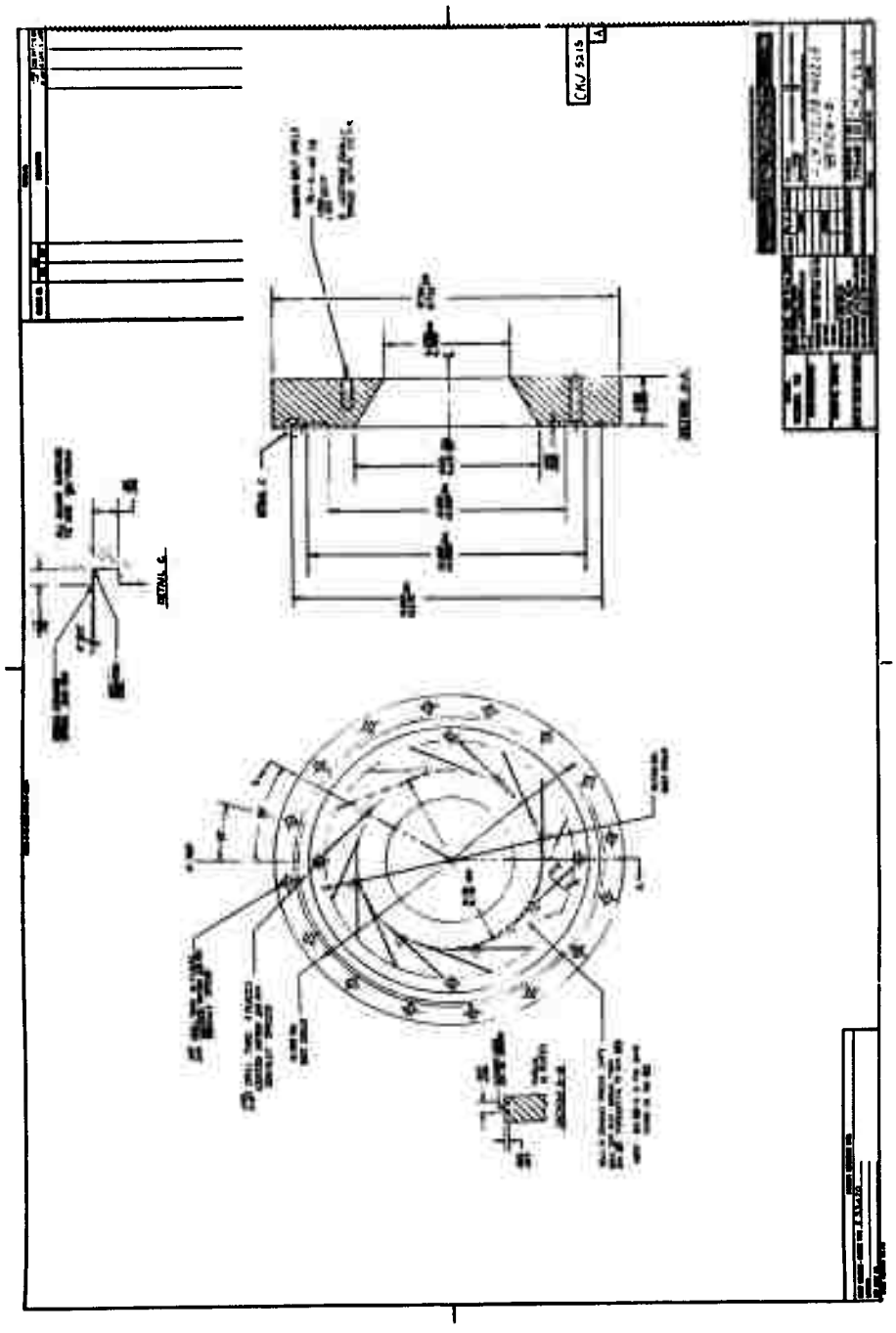

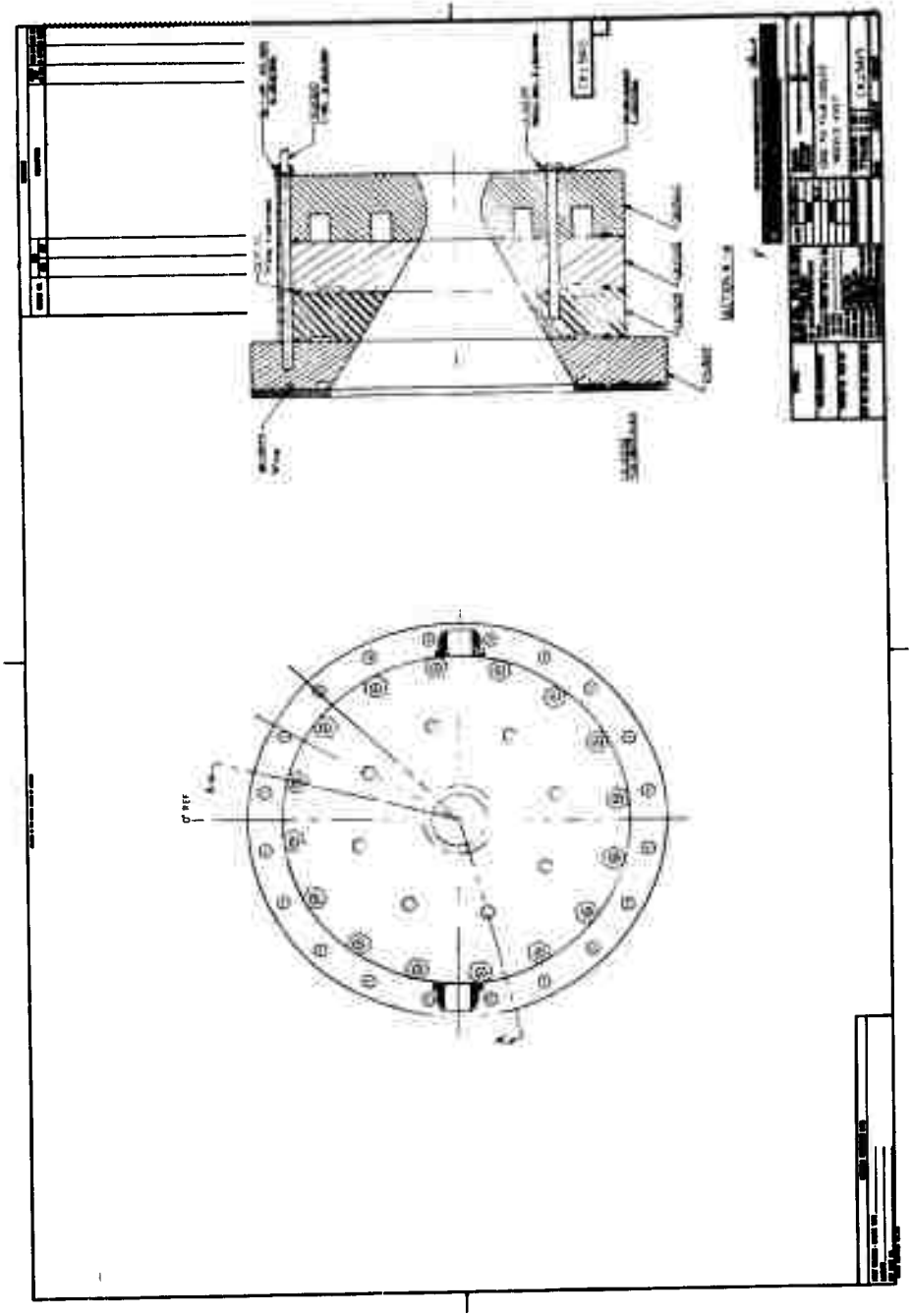

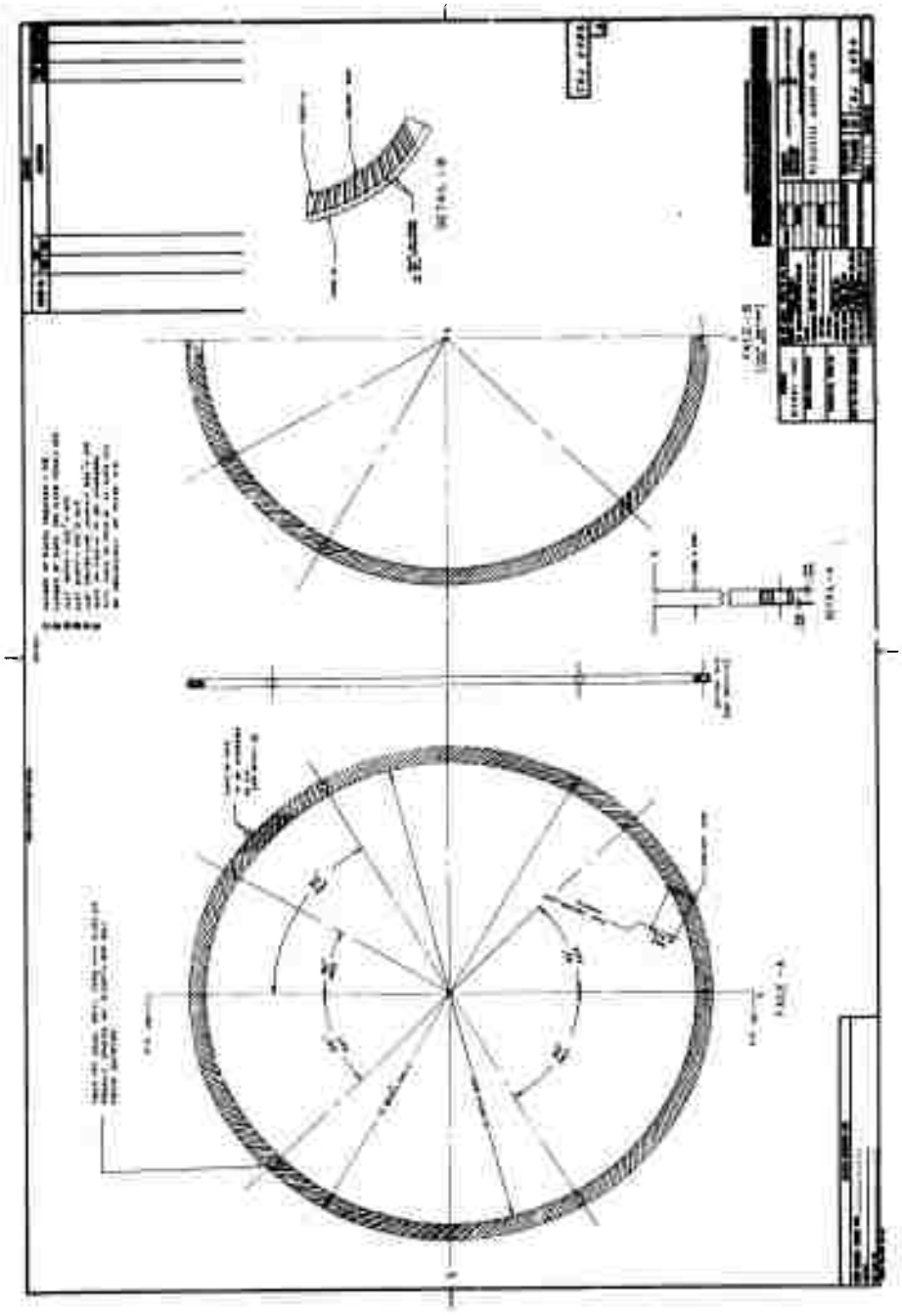

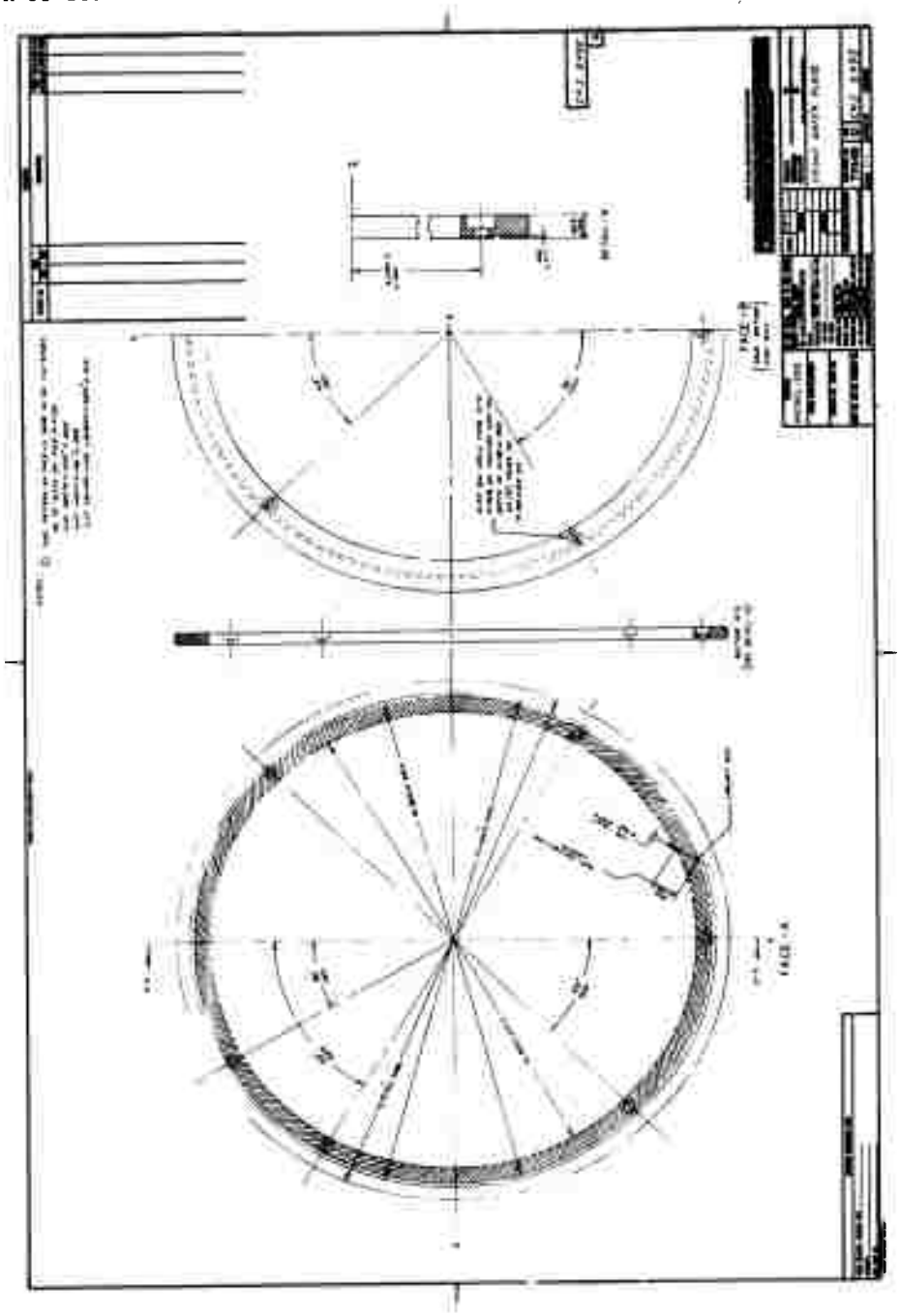

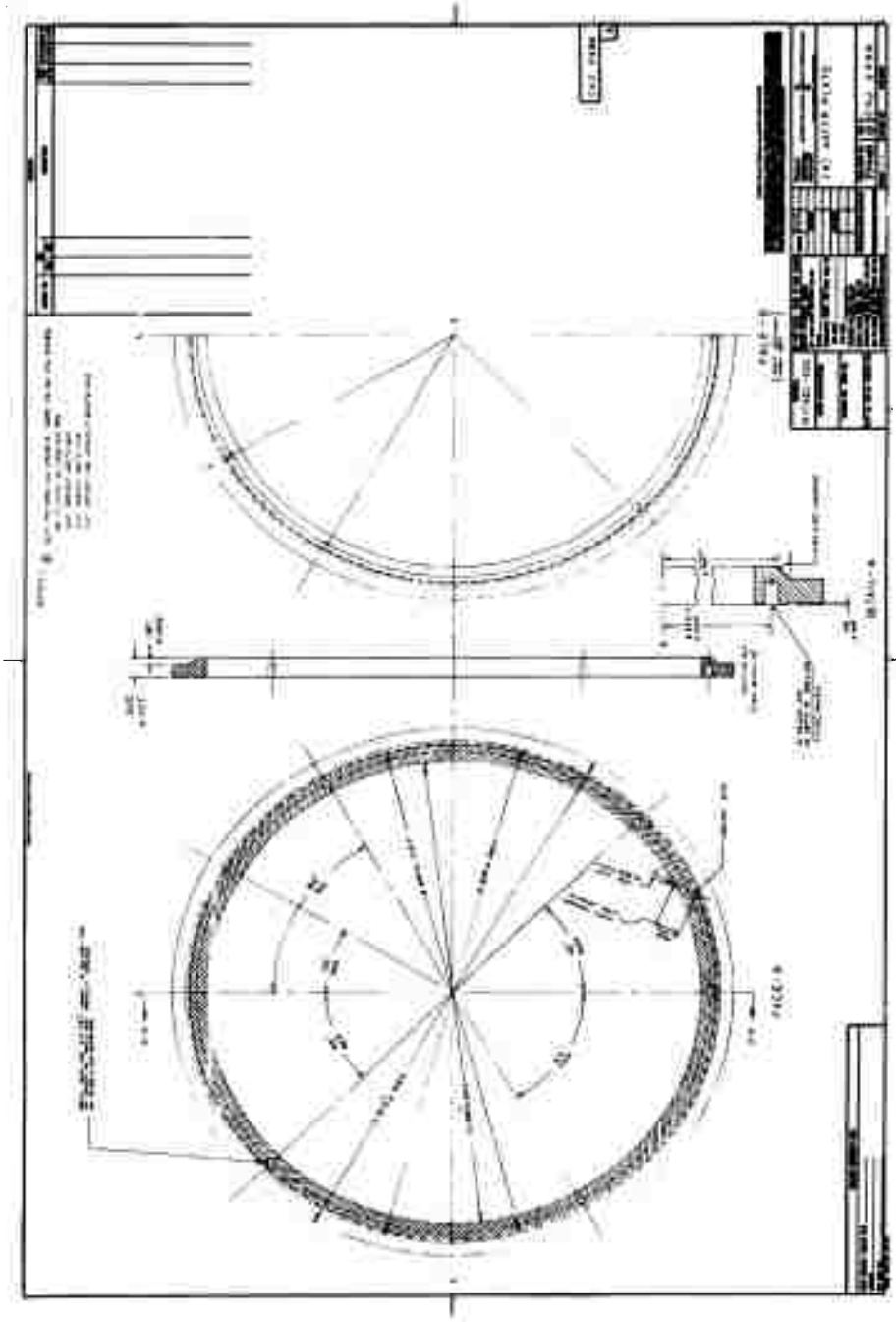

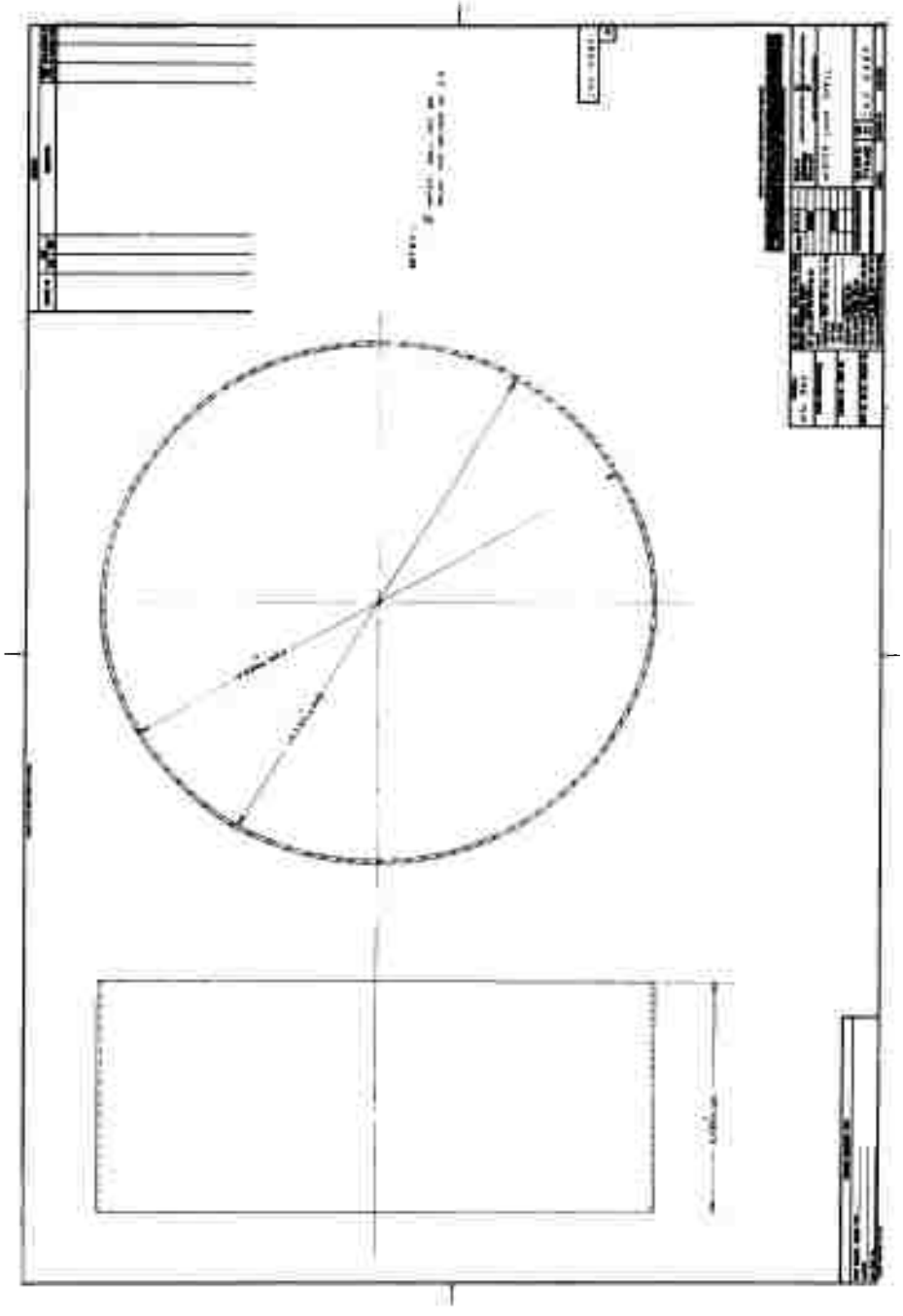

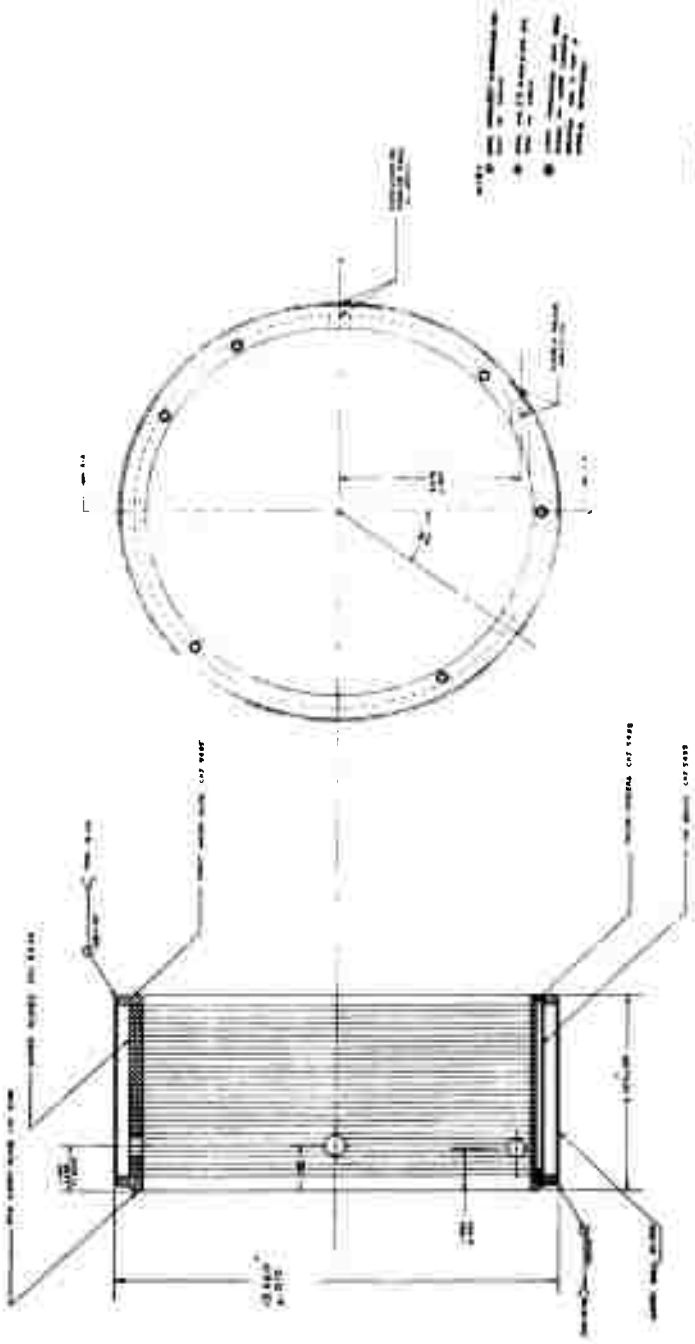

UNCLASSIFIED

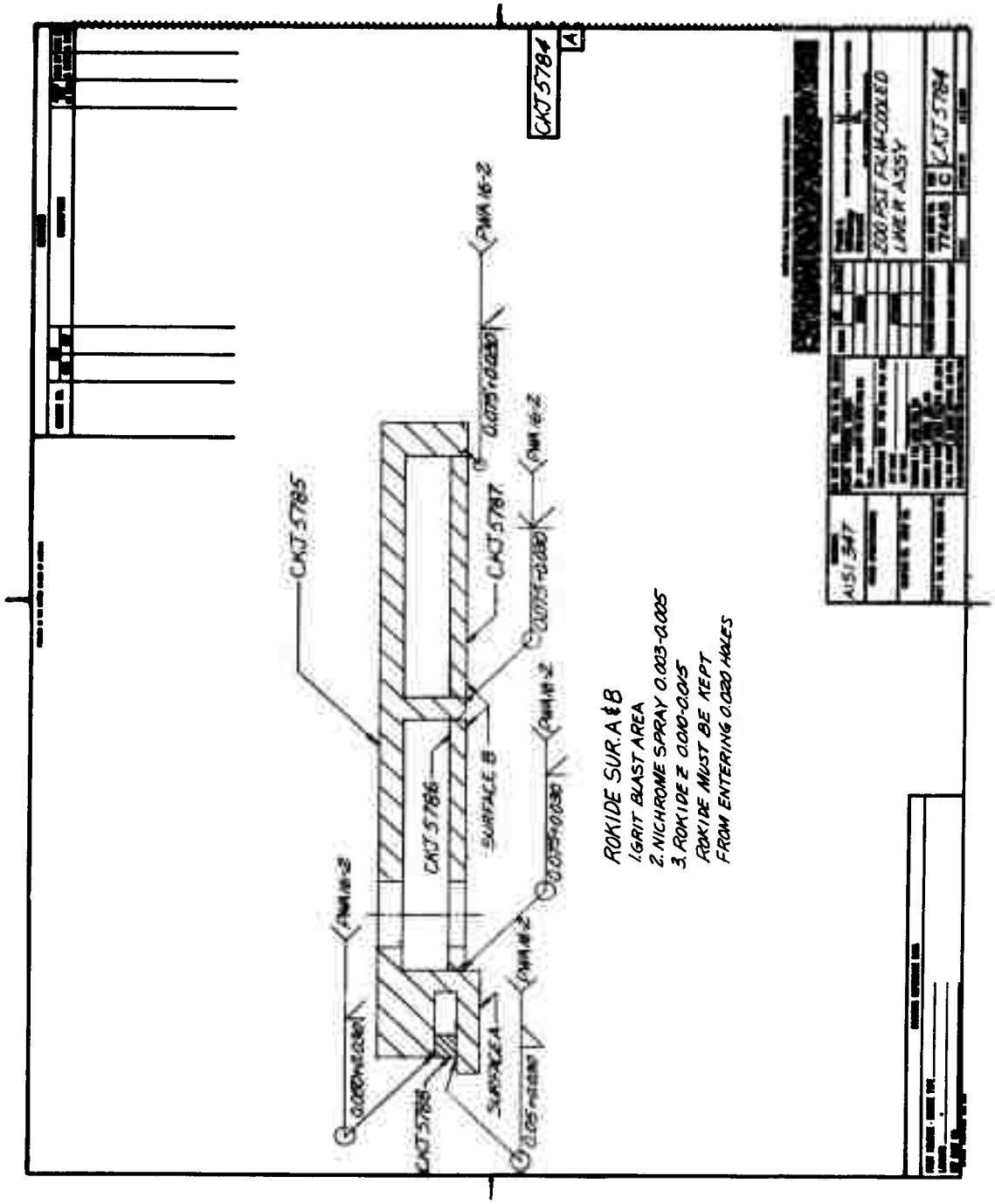

UNCLASSIFIED

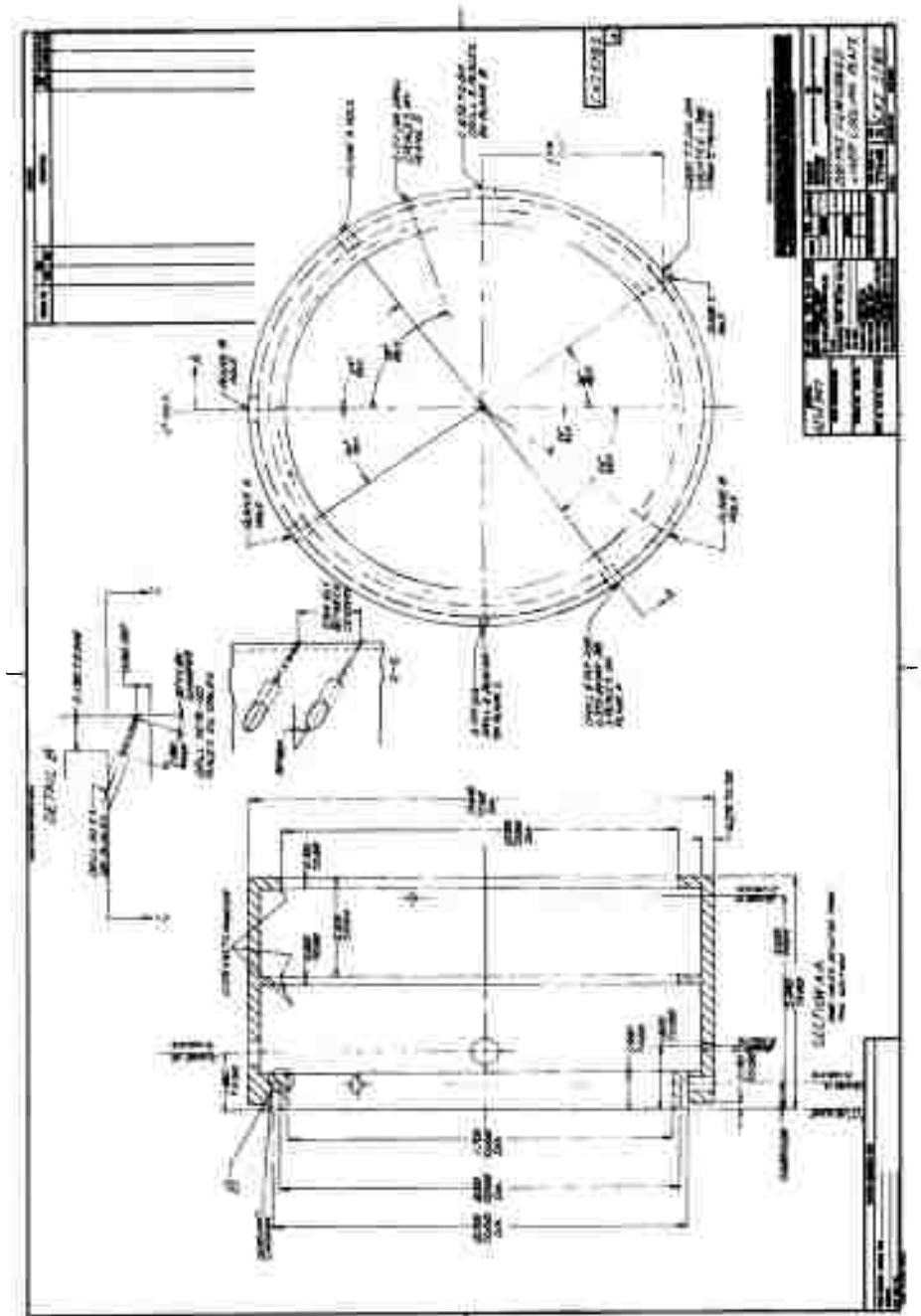

UNCLASSIFIED

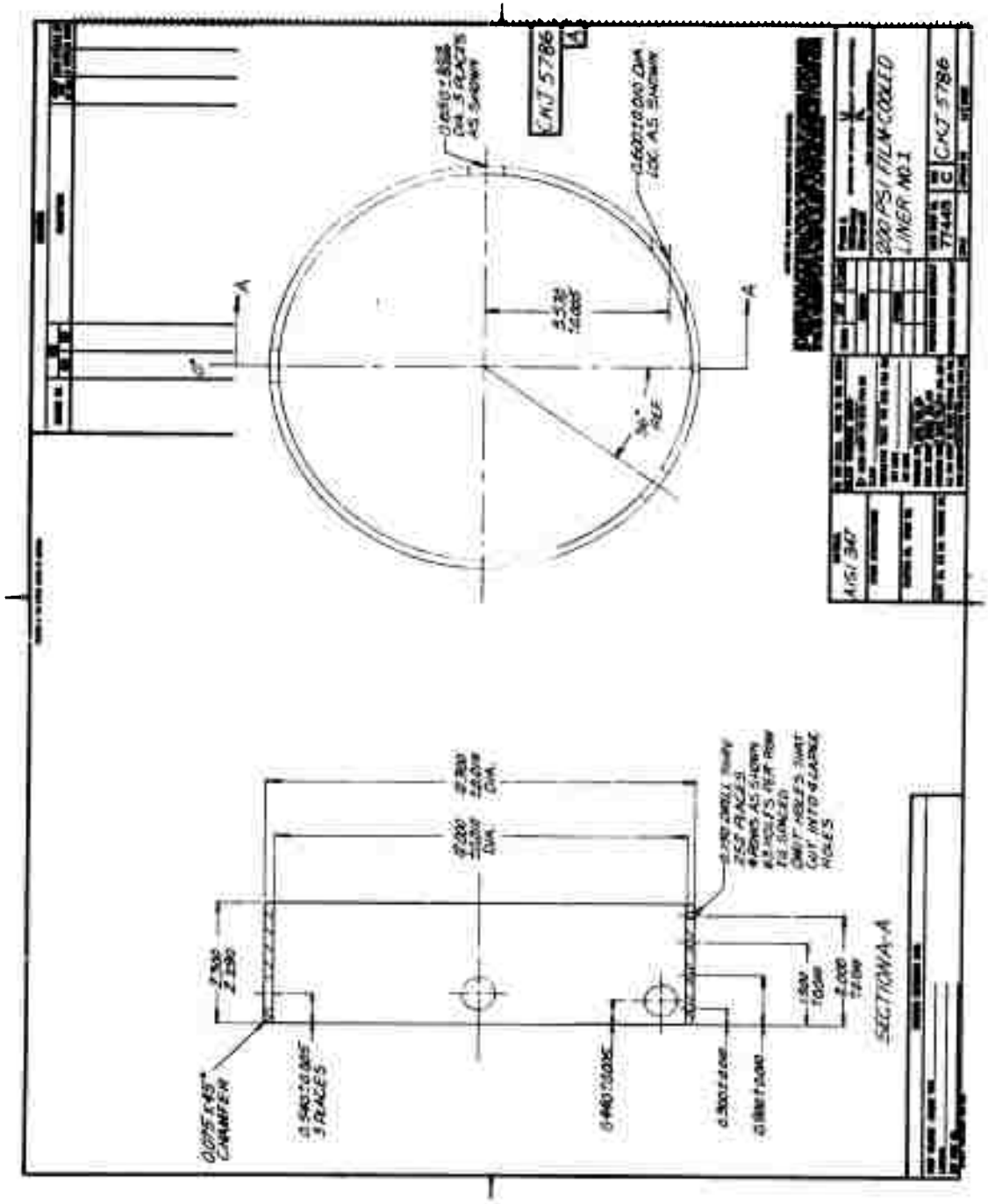

UNCLASSIFIED

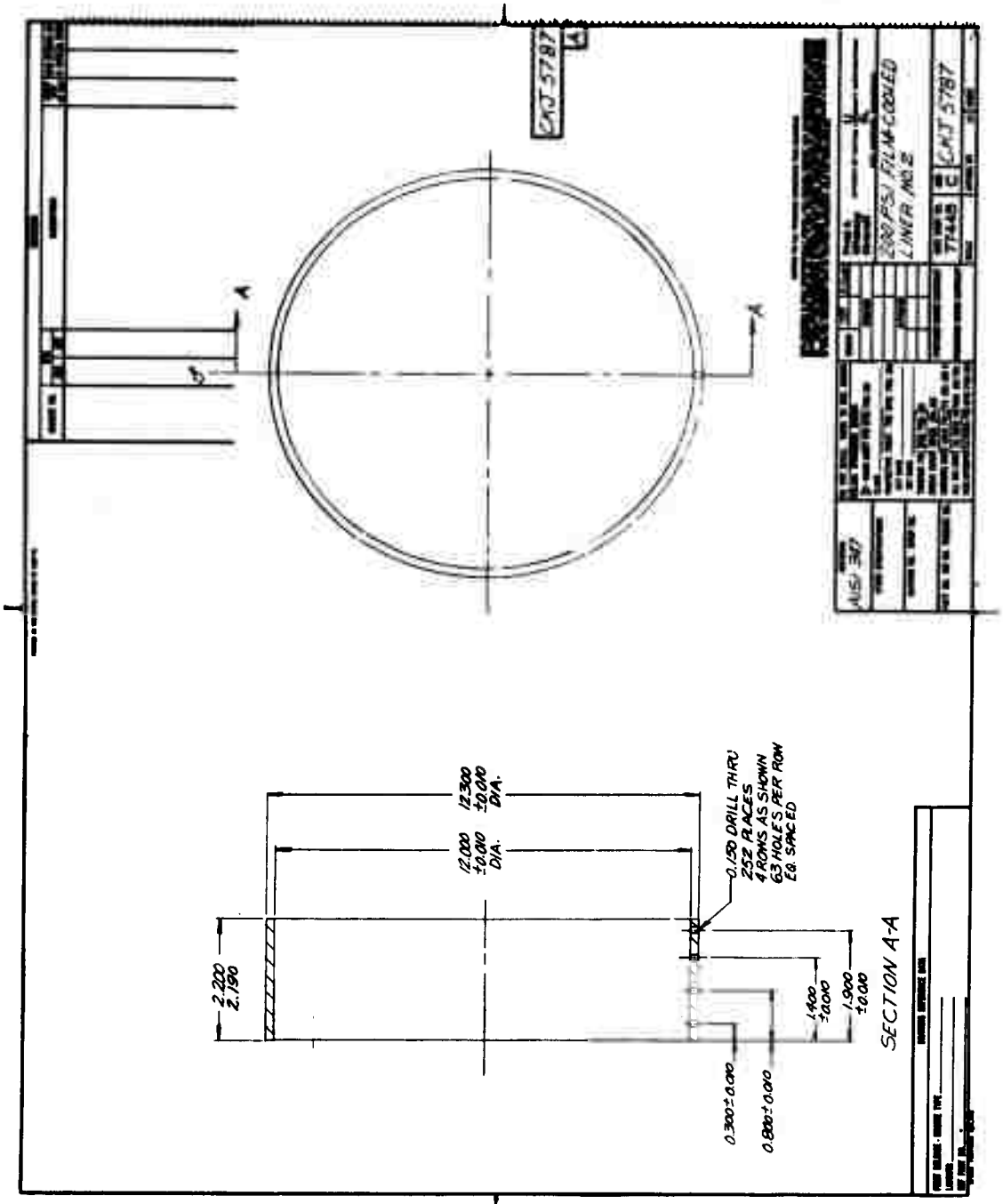
CMT 5787
A
A
200 PSI FILM COOLED
LINER MK 2
CMT 5787
AISI 347
12.300
±0.010
DIA.
12.000
±0.010
DIA.
0.150 DRILL THRU
252 PLACES
4 ROWS AS SHOWN
63 HOLES PER ROW
EQ. SPACED
2.200
2.190
1.400
±0.010
1.900
±0.010
0.300±0.010
0.800±0.010
SECTION A-A

UNCLASSIFIED

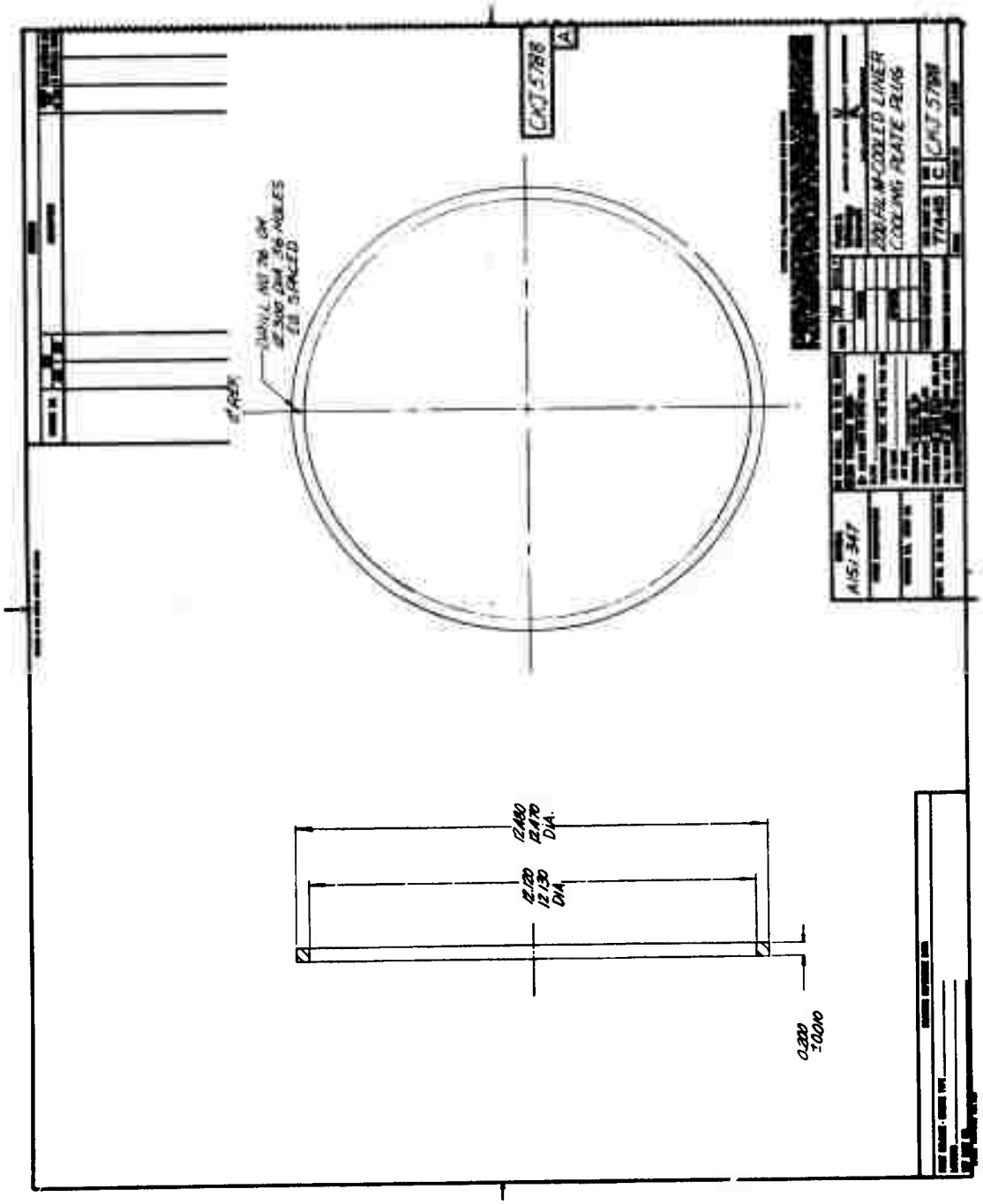

UNCLASSIFIED

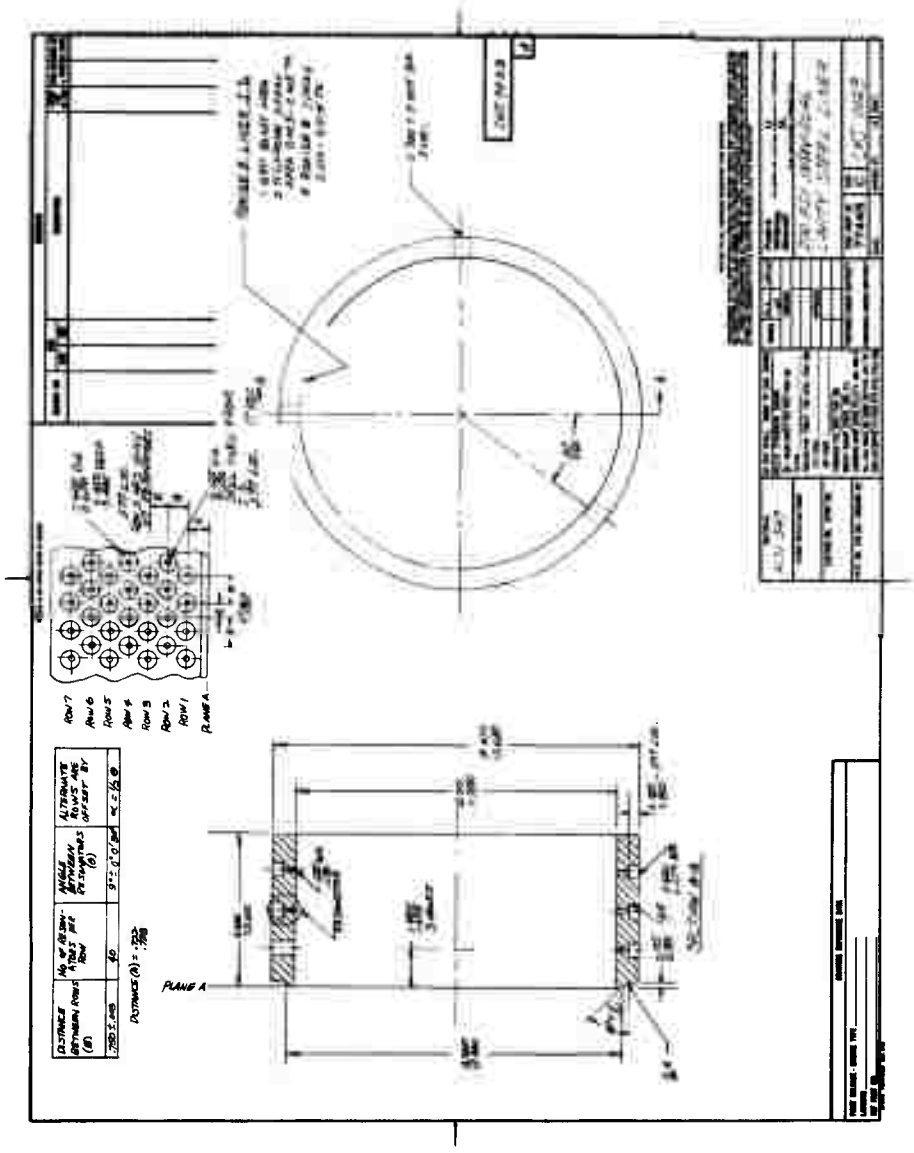
PLANE A
Row 7
Row 6
Row 5
Row 4
Row 3
Row 2
Row 1
PLANE A

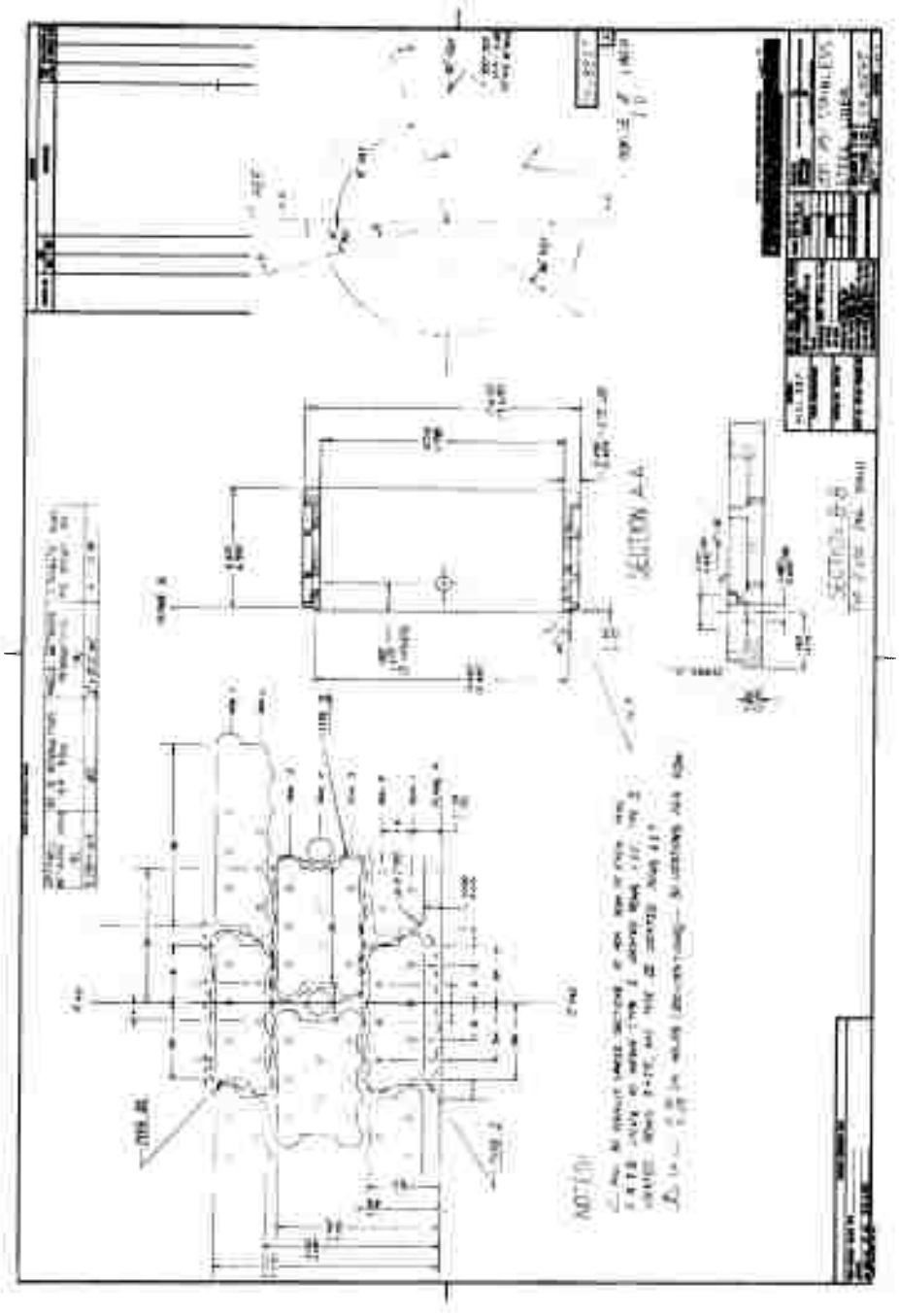

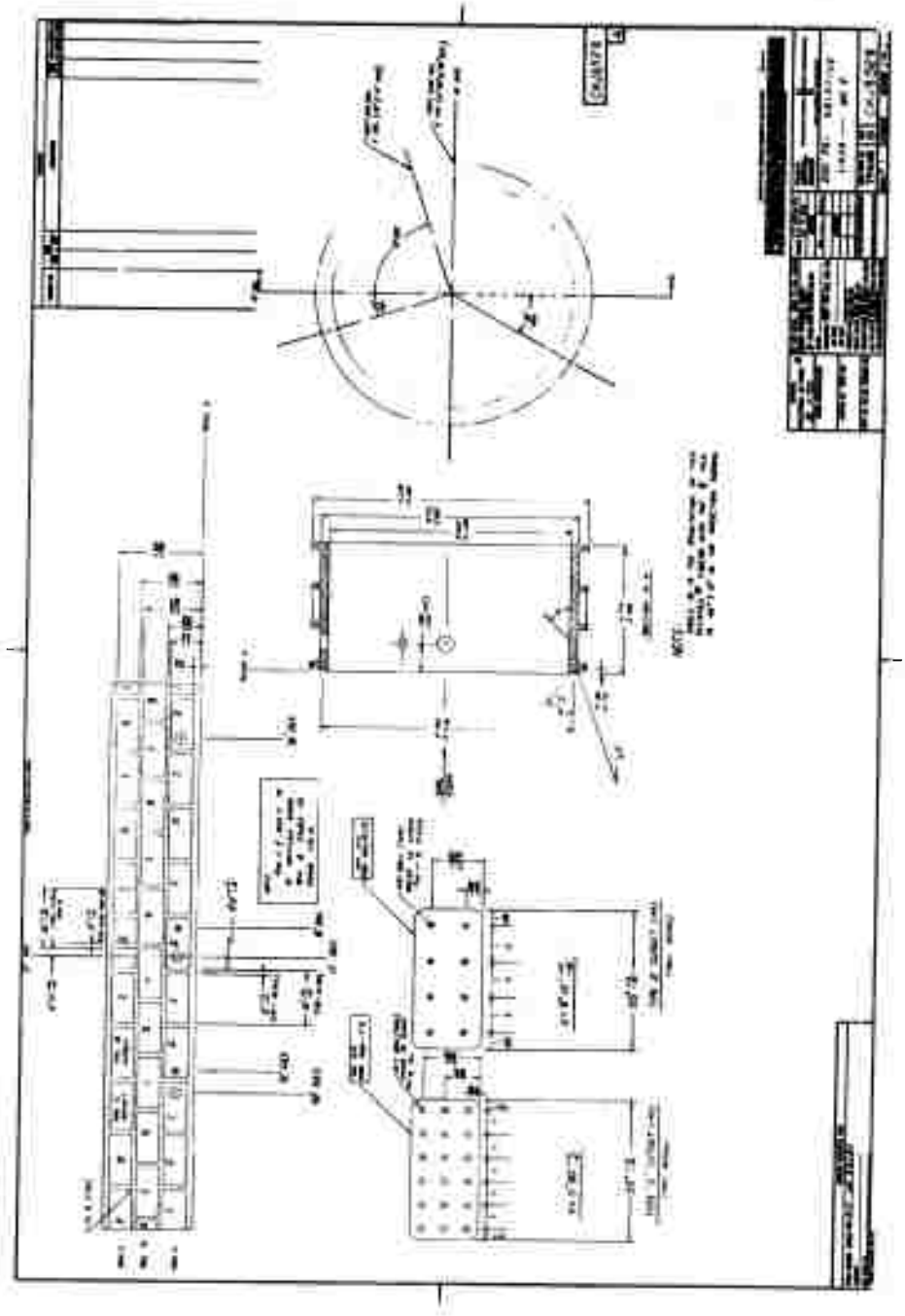

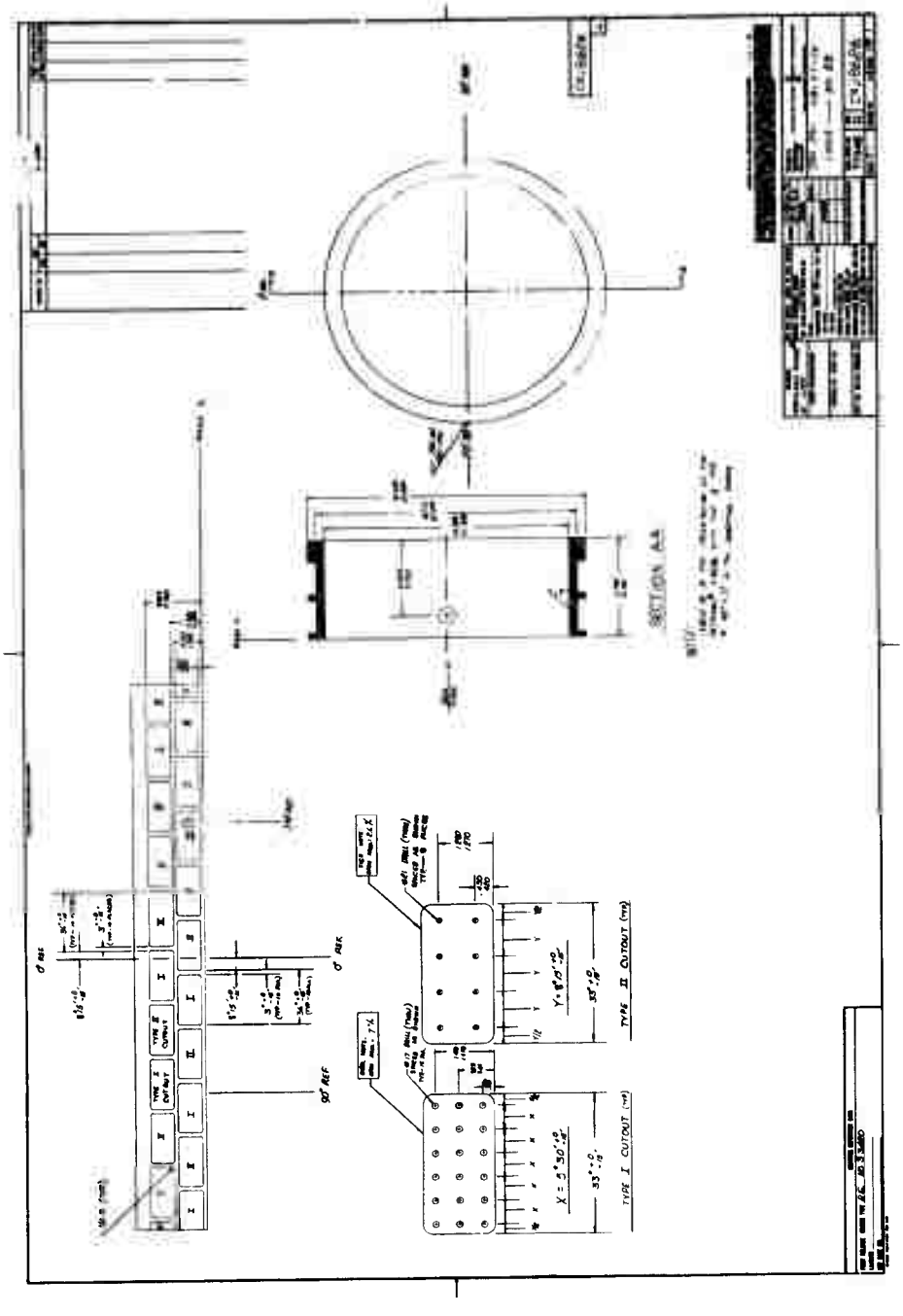
SECTION A-A
TYPE II CUTOUT (ref)
TYPE I CUTOUT (ref)
90° REF

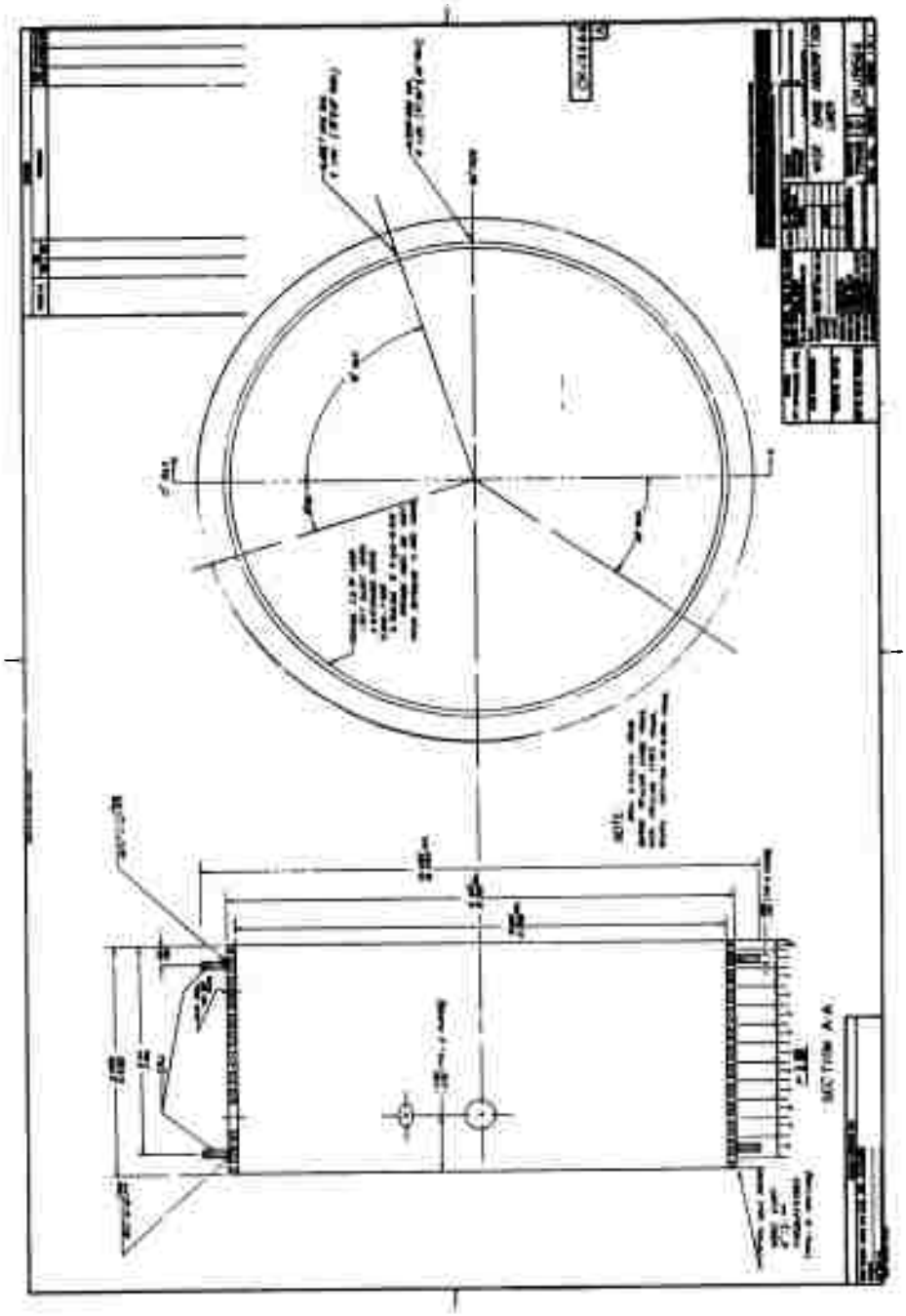

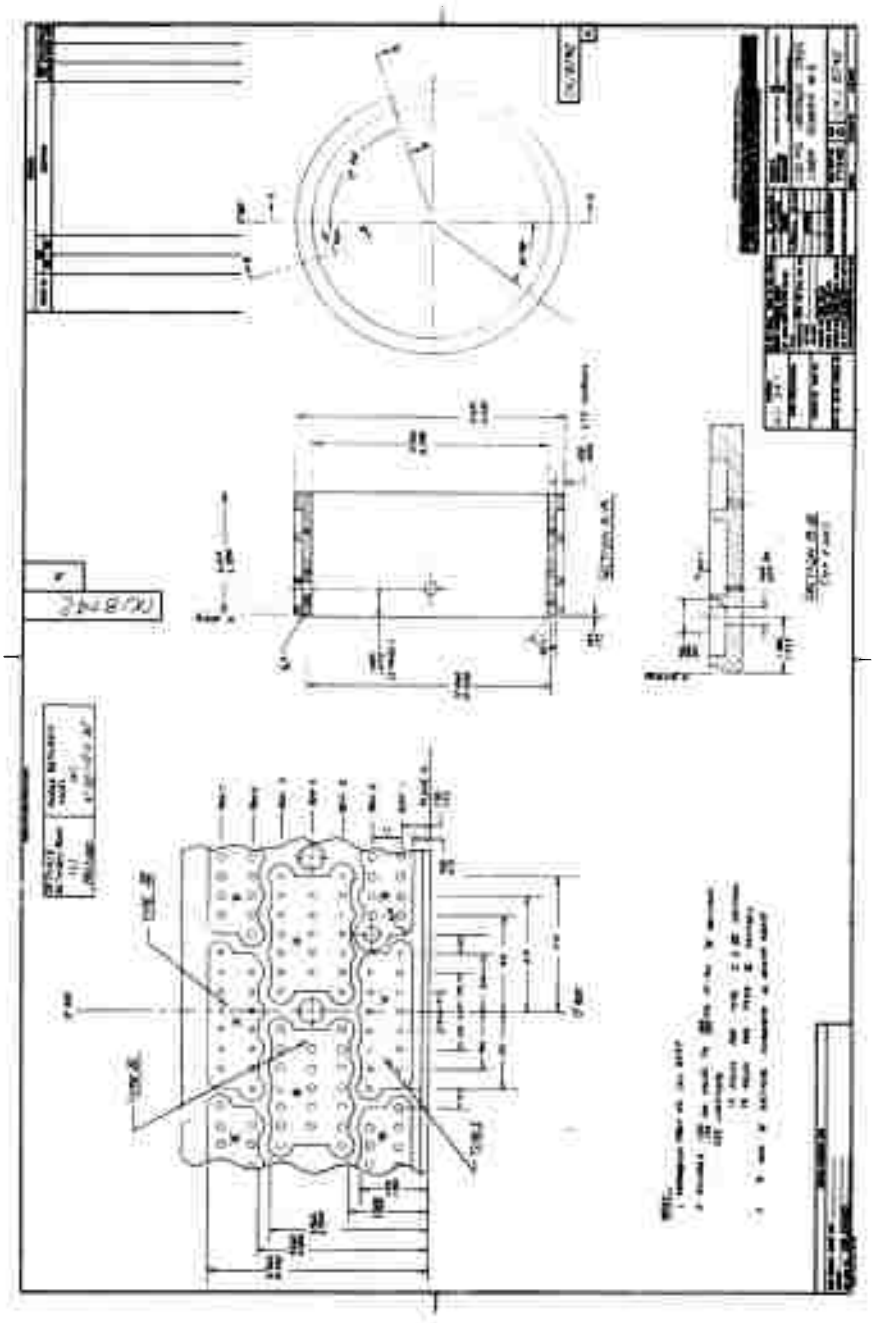

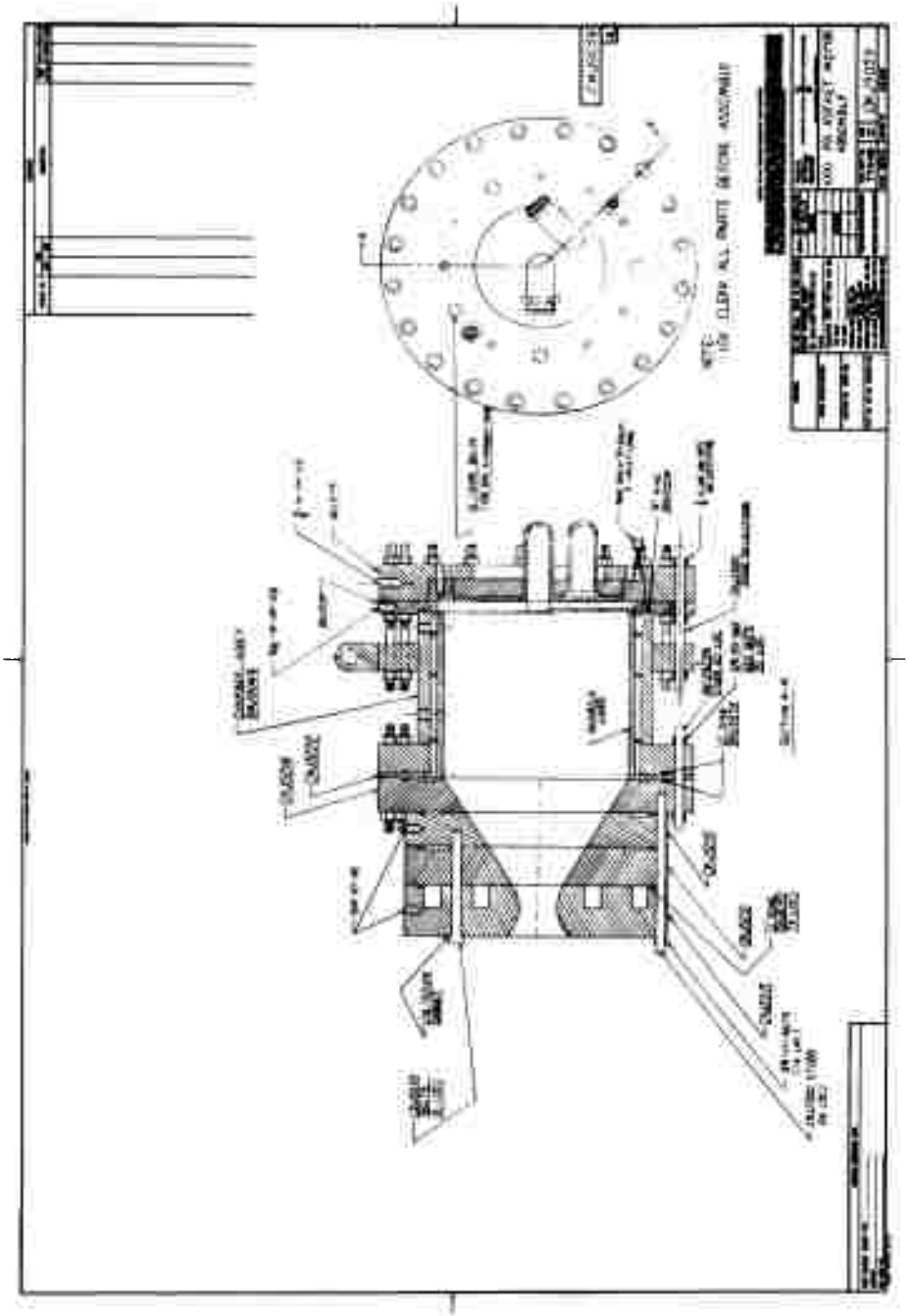

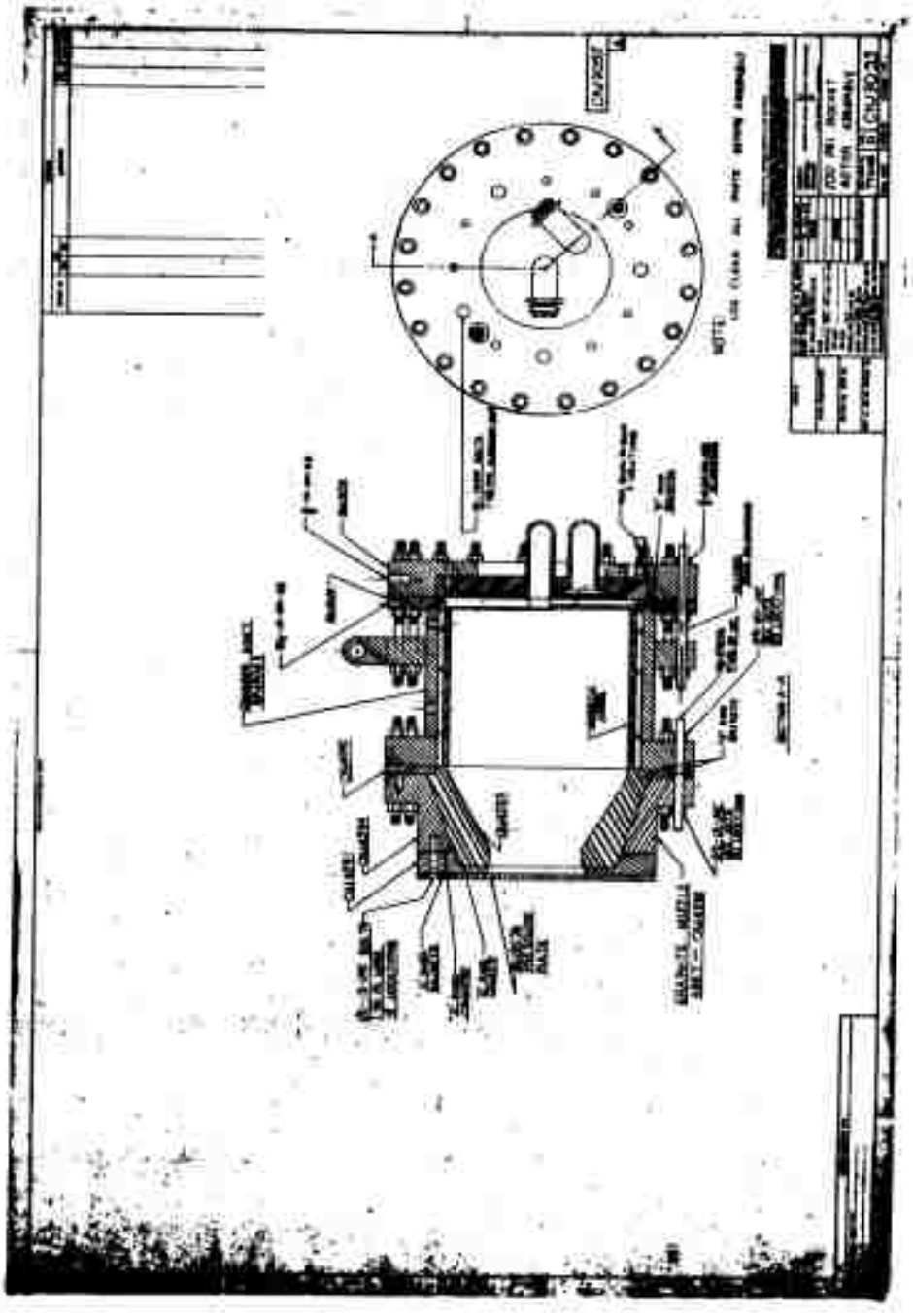

UNCLASSIFIED
Security Classification

CONFIDENTIAL

DOCUMENT CONTROL DATA - R&D
(Security classification of title, body of abstract and indexing annotation must be entered when the overall report is classified)

1 ORIGINATING ACTIVITY (Corporate author)
Pratt & Whitney Aircraft
Division of United Aircraft Corporation
Florida Research and Development Center

2a REPORT SECURITY CLASSIFICATION
Confidential

2b GROUP
4

3 REPORT TITLE
Acoustic Liners for Storable Propellant Rocket Chambers - Phase II Final Report

4 DESCRIPTIVE NOTES (Type of report and inclusive dates)
Phase II Final Report - 28 March 1967 Through 31 May 1968

5 AUTHOR(S) (Last name, first name, initial)
Garrison, G.D.

6. REPORT DATE	7a. TOTAL NO. OF PAGES	7b. NO. OF REFS
August 1968	217	5

8a. CONTRACT OR GRANT NO.
AF 04(611)-11387

b. PROJECT NO.
BPSN 623058

c.
Air Force Project No. 3058

d Program Structure No. A3B2

9a. ORIGINATOR'S REPORT NUMBER(S)
PWA FR-2812

9b. OTHER REPORT NO(S) (Any other numbers that may be assigned this report)
AFRPL-TR-68-118

10 AVAILABILITY/LIMITATION NOTICES
Qualified requestors may obtain copies of this report from DDC

11 SUPPLEMENTARY NOTES

12. SPONSORING MILITARY ACTIVITY
Air Force Rocket Propulsion Laboratory
Air Force Systems Command
Edwards Air Force Base, California

13 ABSTRACT The Phase II work of Contract AF 04(611)-11387 consisted of three interrelated tasks: (1) the establishment and testing of a theory and design procedure for nonresonant absorbers; (2) the evaluation of the effects on liner performance of coolant flow through and/or past the liner apertures; and (3) the evaluation of ablative liners. The types of cooled liners that were studied were transpiration liners (wafer and porous types), film-cooled, and ablative liners. Impedance data were obtained on transpiration and ablative-type liner samples and the results applied to liner design theory. Rocket test programs were conducted using film-cooled liners and a wafer liner at nominal chamber pressures of 200 and 800 psia; individual resonators and dual-open area ablative liners were tested at 200-psia chamber pressure. In addition, uncooled steel liners were tested to obtain data to support the ablative liner program. The film-cooled liners demonstrated stable combustion when no cooling and low cooling flows were used, but the combustion became progressively more unstable as cooling flow was increased. The wafer liner provided stable operation when no cooling was used but combustion was extremely unstable when hydrogen cooling was introduced. The test results show that when the chamber or liner wall is cooled externally with a film layer, or transpirationally, combustion stability varied inversely with the coolant flowrate. A dual-open area (parallel array) ablative liner was effective in suppressing combustion oscillations but an ablative liner with individual resonators failed to stabilize combustion. From the results of this program it was concluded that nonresonant absorbers are not as effective in suppressing combustion oscillations as are resonant absorbers and it is recommended that ablative or regenerative cooling be used in conjunction with an acoustic liner rather than external wall cooling.

DD FORM 1 JAN 64 1473

CONFIDENTIAL

UNCLASSIFIED
Security Classification

14. KEY WORDS	LINK A		LINK B		LINK C	
	ROLE	WT	ROLE	WT	ROLE	WT
Acoustic Liners						
Film-Cooled Liners						
Ablative Liners						
Transpiration-Cooled Liners						
Rocket Combustion Chambers						
Impedance Tube Data						
Combustion Stability						

INSTRUCTIONS

1. ORIGINATING ACTIVITY: Enter the name and address of the contractor, subcontractor, grantee, Department of Defense activity or other organization *(corporate author)* issuing the report.

2a. REPORT SECURITY CLASSIFICATION: Enter the overall security classification of the report. Indicate whether "Restricted Data" is included. Marking is to be in accordance with appropriate security regulations.

2b. GROUP: Automatic downgrading is specified in DoD Directive 5200.10 and Armed Forces Industrial Manual. Enter the group number. Also, when applicable, show that optional markings have been used for Group 3 and Group 4 as authorized.

3. REPORT TITLE: Enter the complete report title in all capital letters. Titles in all cases should be unclassified. If a meaningful title cannot be selected without classification, show title classification in all capitals in parenthesis immediately following the title.

4. DESCRIPTIVE NOTES: If appropriate, enter the type of report, e.g., interim, progress, summary, annual, or final. Give the inclusive dates when a specific reporting period is covered.

5. AUTHOR(S): Enter the name(s) of author(s) as shown on or in the report. Enter last name, first name, middle initial. If military, show rank and branch of service. The name of the principal author is an absolute minimum requirement.

6. REPORT DATE: Enter the date of the report as day, month, year; or month, year. If more than one date appears on the report, use date of publication.

7a. TOTAL NUMBER OF PAGES: The total page count should follow normal pagination procedures, i.e., enter the number of pages containing information.

7b. NUMBER OF REFERENCES: Enter the total number of references cited in the report.

8a. CONTRACT OR GRANT NUMBER: If appropriate, enter the applicable number of the contract or grant under which the report was written.

8b, 8c, & 8d. PROJECT NUMBER: Enter the appropriate military department identification, such as project number, subproject number, system numbers, task number, etc.

9a. ORIGINATOR'S REPORT NUMBER(S): Enter the official report number by which the document will be identified and controlled by the originating activity. This number must be unique to this report.

9b. OTHER REPORT NUMBER(S): If the report has been assigned any other report numbers *(either by the originator or by the sponsor)*, also enter this number(s).

10. AVAILABILITY/LIMITATION NOTICES: Enter any limitations on further dissemination of the report, other than those imposed by security classification, using standard statements such as:

(1) "Qualified requesters may obtain copies of this report from DDC."

(2) "Foreign announcement and dissemination of this report by DDC is not authorized."

(3) "U. S. Government agencies may obtain copies of this report directly from DDC. Other qualified DDC users shall request through _____."

(4) "U. S. military agencies may obtain copies of this report directly from DDC. Other qualified users shall request through _____."

(5) "All distribution of this report is controlled. Qualified DDC users shall request through _____."

If the report has been furnished to the Office of Technical Services, Department of Commerce, for sale to the public, indicate this fact and enter the price, if known.

11. SUPPLEMENTARY NOTES: Use for additional explanatory notes.

12. SPONSORING MILITARY ACTIVITY: Enter the name of the departmental project office or laboratory sponsoring *(paying for)* the research and development. Include address.

13. ABSTRACT: Enter an abstract giving a brief and factual summary of the document indicative of the report, even though it may also appear elsewhere in the body of the technical report. If additional space is required, a continuation sheet shall be attached.

It is highly desirable that the abstract of classified reports be unclassified. Each paragraph of the abstract shall end with an indication of the military security classification of the information in the paragraph, represented as *(TS), (S), (C), or (U)*.

There is no limitation on the length of the abstract. However, the suggested length is from 150 to 225 words.

14. KEY WORDS: Key words are technically meaningful terms or short phrases that characterize a report and may be used as index entries for cataloging the report. Key words must be selected so that no security classification is required. Identifiers, such as equipment model designation, trade name, military project code name, geographic location, may be used as key words but will be followed by an indication of technical context. The assignment of links, rules, and weights is optional.